

## Photometric analyses of Saturn's small moons: Aegaeon, Methone and Pallene are dark; Helene and Calypso are bright.

M. M. HEDMAN,<sup>1</sup> P. HELFENSTEIN,<sup>2</sup> R. O. CHANCIA,<sup>1,3</sup> P. THOMAS,<sup>2</sup> E. ROUSSOS,<sup>4</sup>  
C. PARANICAS,<sup>5</sup> AND A. J. VERBISCER<sup>6</sup>

<sup>1</sup>*Department of Physics, University of Idaho, Moscow, ID 83844*

<sup>2</sup>*Cornell Center for Astrophysics and Planetary Science, Cornell University, Ithaca NY 14853*

<sup>3</sup>*Center for Imaging Science, Rochester Institute of Technology, Rochester NY 14623*

<sup>4</sup>*Max Planck Institute for Solar System Research, Göttingen, Germany 37077*

<sup>5</sup>*APL, John Hopkins University, Laurel MD 20723*

<sup>6</sup>*Department of Astronomy, University of Virginia, Charlottesville, VA 22904*

### ABSTRACT

We examine the surface brightnesses of Saturn's smaller satellites using a photometric model that explicitly accounts for their elongated shapes and thus facilitates comparisons among different moons. Analyses of Cassini imaging data with this model reveals that the moons Aegaeon, Methone and Pallene are darker than one would expect given trends previously observed among the nearby mid-sized satellites. On the other hand, the trojan moons Calypso and Helene have substantially brighter surfaces than their co-orbital companions Tethys and Dione. These observations are inconsistent with the moons' surface brightnesses being entirely controlled by the local flux of E-ring particles, and therefore strongly imply that other phenomena are affecting their surface properties. The darkness of Aegaeon, Methone and Pallene is correlated with the fluxes of high-energy protons, implying that high-energy radiation is responsible for darkening these small moons. Meanwhile, Prometheus and Pandora appear to be brightened by their interactions with nearby dusty F ring, implying that enhanced dust fluxes are most likely responsible for Calypso's and Helene's excess brightness. However, there are no obvious structures in the E ring that would preferentially brighten these two moons, so there must either be something subtle in the E-ring particles' orbital properties that leads to asymmetries in the relevant fluxes, or something happened recently to temporarily increase these moons' brightnesses.

### 1. INTRODUCTION

Saturn's regular moons exhibit a very diverse range of spectral and photometric properties, with Enceladus having an extremely bright and ice-rich surface, while the leading side of Iapetus is exceptionally dark due to being covered with a layer of debris derived from Saturn's irregular satellites (for recent reviews, see Hendrix et al. 2018; Thomas et al. 2018; Verbiscer et al. 2018). For the mid-sized moons orbiting between Titan and the rings (i.e. Mimas, Enceladus, Tethys, Dione and Rhea), many of the observed spectral and photometric trends have been attributed to interactions with the E ring. This broad and diffuse ring consists of dust-sized, ice-rich particles generated by Enceladus' geological activity that impact the

surfaces of different moons at different rates. The brightness and density of the E ring is strongly correlated with the geometric albedos of these satellites at visible (Verbiscer et al. 2007) and radio wavelengths (Ostro et al. 2010; Le Gall et al. 2019), as well as spectral features like the depth of water-ice absorption bands (Filacchione et al. 2012, 2013). Furthermore, there are brightness asymmetries between the leading and trailing sides of these moons that can be attributed to differences in the fluxes of E-ring particles (Buratti et al. 1998; Schenk et al. 2011; Scipioni et al. 2013, 2014; Hendrix et al. 2018; Le Gall et al. 2019).

However, there are several smaller moons orbiting within the E ring whose surface scattering properties deviate from the trends observed among the larger moons. On the one hand, four extremely small moons (Aegaeon, Anthe, Methone and Pallene) are found within the E-ring's inner flank. Aegaeon is situated between Janus and Mimas in the G ring, while Methone, Anthe and Pallene orbit between Mimas and Enceladus. One might therefore expect these moons to follow the same trend as Janus, Mimas and Enceladus, but in fact they appear to be somewhat darker than this trend would predict (Thomas et al. 2018; Verbiscer et al. 2018). On the other hand, the small moons Telesto and Calypso share Tethys' orbit, while Helene and Polydeuces share Dione's orbit, but they do not all appear to have the same spectrophotometric properties as their larger companions (Verbiscer et al. 2007, 2018; Filacchione et al. 2012, 2013).

A major challenge in interpreting existing brightness estimates of these objects is that many of them are significantly elongated, and so their brightness varies substantially depending on their orientation relative to the observer and the Sun, leading to large scatter in the disk-integrated brightness estimates at any given phase angle. Fortunately, all these objects are spin-locked and so their orientation relative to the Sun and the spacecraft can be securely predicted. Furthermore, almost all of these moons were observed at high enough resolution to determine their shapes, and Aegaeon, Methone and Pallene in particular are very close to perfect ellipsoids. It should therefore be possible to model their shape-related brightness variations to a fair degree of accuracy, and thereby derive estimates of their surface brightnesses that can be compared to those of the larger moons.

This paper describes a new investigation of Saturn's moons that uses a photometric model to obtain precise and comparable measurements of the surface brightnesses for both the small and mid-sized moons orbiting interior to Titan. The brightness estimates for the mid-sized moons, along with the smaller moons Janus and Epimetheus, are consistent with previous studies in that they are clearly correlated with the local flux of E-ring particles. However, this work also confirms that many small moons deviate from this basic trend, implying that other processes influence the moons' surface brightnesses. Specifically, we find that (1) Aegaeon is exceptionally dark, (2) Methone and Pallene are darker than one would expect given their locations between Mimas and Enceladus, (3) Calypso and Helene are brighter than their larger companions, and (4) Prometheus and Pandora are brighter than moons orbiting nearby like Atlas, Janus and Epimetheus. Aegaeon, Methone, and Pallene are most likely dark because they occupy belts of high energy proton fluxes. While the mechanism by which this radiation darkens their surfaces is still obscure, we find that the overall brightnesses of these moons are probably determined by the ratio of the energetic proton flux to the E-ring particle flux. On the other hand, the excess brightness of Helene,

Calypso, Prometheus and Pandora is most likely due to some localized increase in the particle flux. For Prometheus and Pandora, the additional flux of particles from the F ring is probably responsible for increasing their brightness. However, there is no obvious particle source that would preferentially brighten Calypso and Helene more than their co-orbital companions, so the brightness of these moons either involves a previously-unknown asymmetry in the E-ring particle flux or is a transient phenomenon due to a recent event like an impact.

Section 2 below describes the Cassini imaging data used in this study, and how it is transformed into estimates of the disk-integrated brightness of Saturn's various moons. Section 3 then describes the photometric model we use to convert these disk-integrated brightness estimates into estimates of the moons' surface brightness while accounting for the moons' variably elongated shapes. Finally, Section 4 describes the trends among these shape-corrected brightness estimates and their implications, while Section 5 summarizes our findings.

## 2. OBSERVATIONS AND PRELIMINARY DATA REDUCTION

The disk-integrated brightness estimates considered in this study are derived from images obtained by the Narrow Angle Camera (NAC) of the Imaging Science Subsystem (ISS) on-board the Cassini Spacecraft (Porco et al. 2004). These images were all calibrated using version 3.9 of the Cisscal package to remove dark current and instrumental electronic noise, apply flat-field corrections, and convert the raw data numbers to values of radiance factors  $I/F$ , a standard dimensionless measure of reflectance that is unity for an illuminated Lambertian surface viewed at normal incidence and emission angles (Porco et al. 2004; West et al. 2010). Here  $I$  is the scattered intensity of light and  $\pi F$  is the specific solar flux over the camera filter bandpass.

While this analysis focuses on the photometry of the small moons, in order to facilitate comparisons with the mid-sized satellites we will consider data for all the satellites interior to Titan except for Daphnis (whose location within a narrow gap in the main rings would have required specialized algorithms). We searched for images containing all moons obtained by the NAC through its clear filters using the OPUS search tool on the PDS ring-moon system node (<https://pds-rings.seti.org/search>). For the small moons Aegaeon, Anthe, Methone and Pallene, as well as the trojan moons Telesto, Calypso, Helene and Polydueces we considered all images where the moon was observed at phase angles below  $80^\circ$  (at higher phase angles the signal-to-noise ratio for these moons was often too poor to be useful), while for Pan, Atlas, Prometheus, Pandora, Janus, Epimetheus, Mimas, Enceladus, Tethys, Dione and Rhea we only considered images where the moon was at phase angles between  $20^\circ$  and  $40^\circ$ . This more restricted phase range corresponds to conditions with the best signal-to-noise ratio data for the smaller moons, and reduces the number of images that needed to be analyzed to a manageable level.

Since nearly all of the images of the small moons were unresolved, this analysis will only consider disk-integrated brightness estimates for the moons, which were computed following approaches similar to those described in Hedman et al. (2010). This process begins by selecting a region within each image that contains the entire signal from the moon based on visual inspection. Then, instrumental and ring backgrounds are removed from this region using one of three different procedures depending on the moon:

- **Aegaeon and Pan** For these moons the dominant backgrounds come from the nearby rings (the A ring for Pan and the G ring for Aegaeon). Each image was therefore geometrically navigated based on the positions of stars in the field of view and the appropriate SPICE kernels (Acton 1996) using a variant of the CAVIAR software package (<https://www.imcce.fr/recherche/equipes/pegase/caviar>). We then used regions extending 10 pixels on either side of the selected region along the moon’s orbit to determine the mean background image brightness as a function of ringplane radius. This profile was then interpolated onto the pixels in the selected region containing the moon and removed from that region.
- **Atlas, Anthe, Methone, Pallene, Telesto, Calypso, Helene and Polydeuces.** For these moons, instrumental backgrounds dominate, and these are typically a stronger function of row than sample number (West et al. 2010). Hence we used regions 10 columns wide on either side of the region containing the moon to define a background brightness level as a function of row number which was then removed from all the pixels in the selected regions.
- **Prometheus, Pandora, Janus, Epimetheus, Mimas, Enceladus, Tethys, Dione and Rhea.** These larger moons were often resolved and so the signal-to-noise ratio was much higher than for the smaller moons. Hence we used regions 10 columns wide on either side of the region containing the moon to define a mean background brightness level that was removed from all the pixels in the selected regions.

After removing the backgrounds, the total brightness of the object in each image was computed and expressed in terms of an effective area,  $A_{\text{eff}}$ , which is the equivalent area of material with  $I/F = 1$  that would be required to account for the observed brightness:

$$A_{\text{eff}} = \sum_x \sum_y I/F_{x,y} \times \Omega_{\text{pixel}} \times D^2 \quad (1)$$

where  $x$  and  $y$  are the row and column numbers of the pixels in the selected region,  $I/F_{x,y}$  is the (background-subtracted) brightness in the  $x, y$  pixel,  $\Omega_{\text{pixel}} = (6 \mu\text{rad})^2$  is the assumed solid angle subtended by a NAC pixel, and  $D$  is the distance between the spacecraft and the object during the observation (designated as “Range” in Tables 8- 28 of Appendix C). The assumed values for  $D$  are derived from the appropriate SPICE kernels (Acton 1996). This approach deviates from traditional integrated disk measurement convention in that an effective whole-disk area is measured at each phase angle rather than the magnitude equivalent of an average whole-disk reflectance. Two advantages of this approach for our study are that (1) it requires no *a priori* knowledge of the object’s average size and (2) it easily accommodates target blur in which subpixel-sized objects are smeared across several pixels due to spacecraft motion and/or long camera exposures. We also estimate the statistical uncertainty on  $A_{\text{eff}}$  based on the standard deviation of the brightness levels in the second region after any radial trends have been removed. Note that this procedure underestimates the true uncertainty in the measurements, but is still a useful way to identify images with low signal-to-noise ratios. For the smaller objects, we also computed their mean position in

the field of view by computing the coordinates (in pixels) of the streaks center of light  $x_c$  and  $y_c$ :

$$x_c = \frac{\sum_x \sum_y x \times I/F_{x,y}}{\sum_x \sum_y I/F_{x,y}} \quad (2)$$

$$y_c = \frac{\sum_x \sum_y y \times I/F_{x,y}}{\sum_x \sum_y I/F_{x,y}} \quad (3)$$

These numbers are not used directly for any part of this study. However, they are useful for identifying images where the background levels were not removed properly, since in those images the computed center of light would fall outside the image of the moon.

For the larger moons, the signal-to-noise ratio for every image was sufficiently high that all unsaturated images yielded useful estimates of  $A_{\text{eff}}$ . After excluding any moons with saturated pixels, we had the following numbers of data points for these moons: 40 for Prometheus, 40 for Pandora, 53 for Janus, 47 for Epimetheus, 76 for Mimas, 82 for Enceladus, 67 for Tethys, 67 for Dione and 74 for Rhea (see Tables 18- 26 in Appendix C). For the smaller moons, we visually inspected the regions containing the moons and excluded any images where these regions were obviously corrupted by bad pixels or cosmic rays, or where the computed center of light was noticeably displaced from the bright pixels containing the signal from the moon. For Aegaeon, Anthe, Methone and Pallene, we also excluded any images where  $A_{\text{eff}}$  was negative or more than 10 times the median value among all the images, as well as any images where the brightest pixel in the relevant region was more than 10 times the median pixel brightness times the number of pixels in the region (this removed images contaminated by a bad pixel or cosmic ray that was not obvious upon visual inspection). Finally, we excluded any images of Aegaeon, Anthe, Methone and Pallene with exposures less than 0.5 seconds because these usually had poor signal-to-noise ratios, and any images of Anthe, Methone and Pallene with exposures longer than 2 seconds, where unresolved images could be saturated. Similarly, we excluded images of Polydeuces with exposures longer than 0.68 seconds and any images of Telesto, Calypso and Helene with exposures longer than 0.15 seconds. After these selections, the final number of measurements for the small moons were: 168 for Aegaeon, 167 for Anthe, 187 for Methone, 159 for Pallene, 41 for Pan, 71 for Atlas, 142 for Telesto, 157 for Calypso, 122 for Helene and 136 for Polydeuces (see Tables 8- 17 in Appendix C). Estimates of  $A_{\text{eff}}$  for these images, along with relevant geometric parameters like the sub-solar and sub-observer latitudes and longitudes, are provided in Tables 8- 26 in Appendix C.

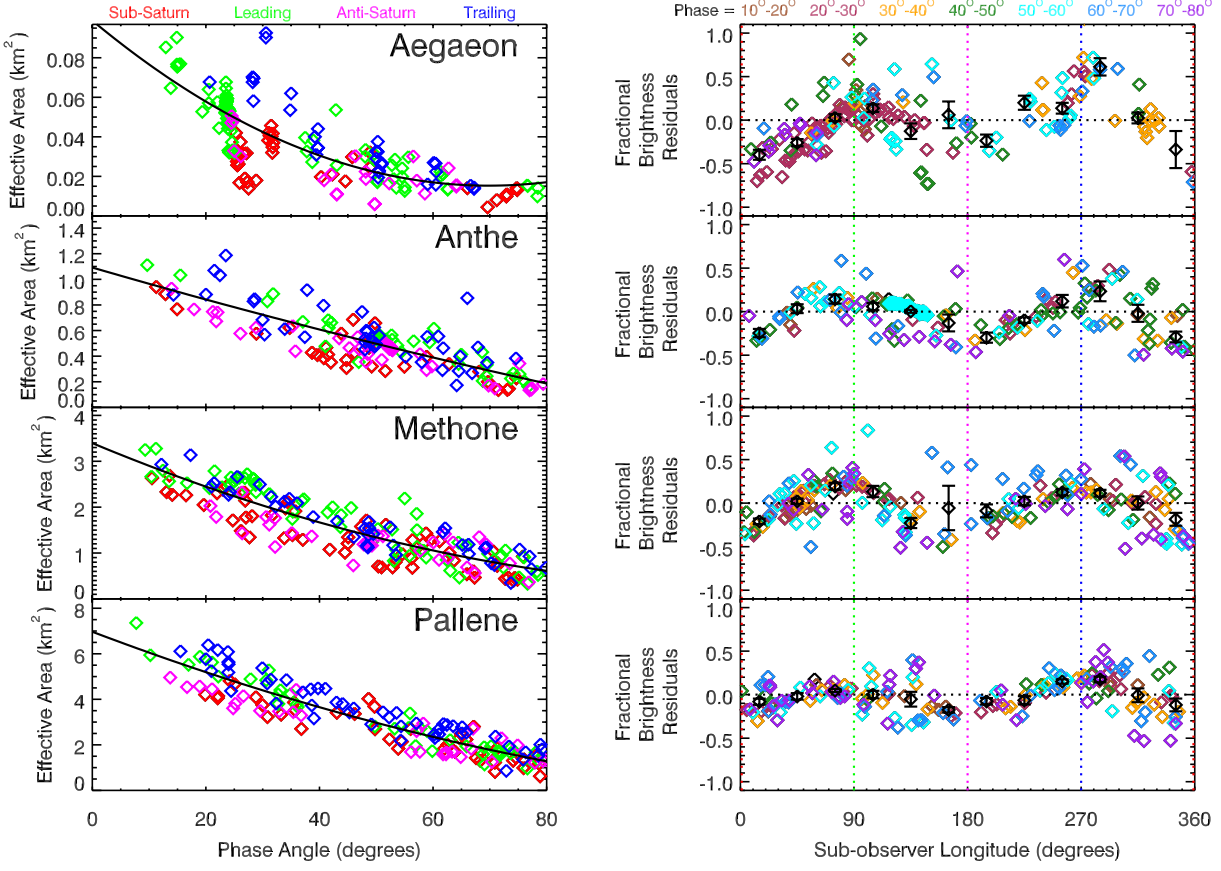


**Figure 1.** Summary of the brightness measurements for Aegaeon, Anthe, Methone and Pallene. The left-hand plots show the effective areas  $A_{\text{eff}}$  of the moons as a function of phase angle, with the data points color coded by the quadrant viewed by the spacecraft. The right-hand plots show the fractional residuals of the brightness estimates relative to the quadratic trend shown as a solid line in the left-hand plots. Note that all these objects are consistently brighter when their leading or trailing sides are viewed than when their sub-Saturn or anti-Saturn sides are viewed.

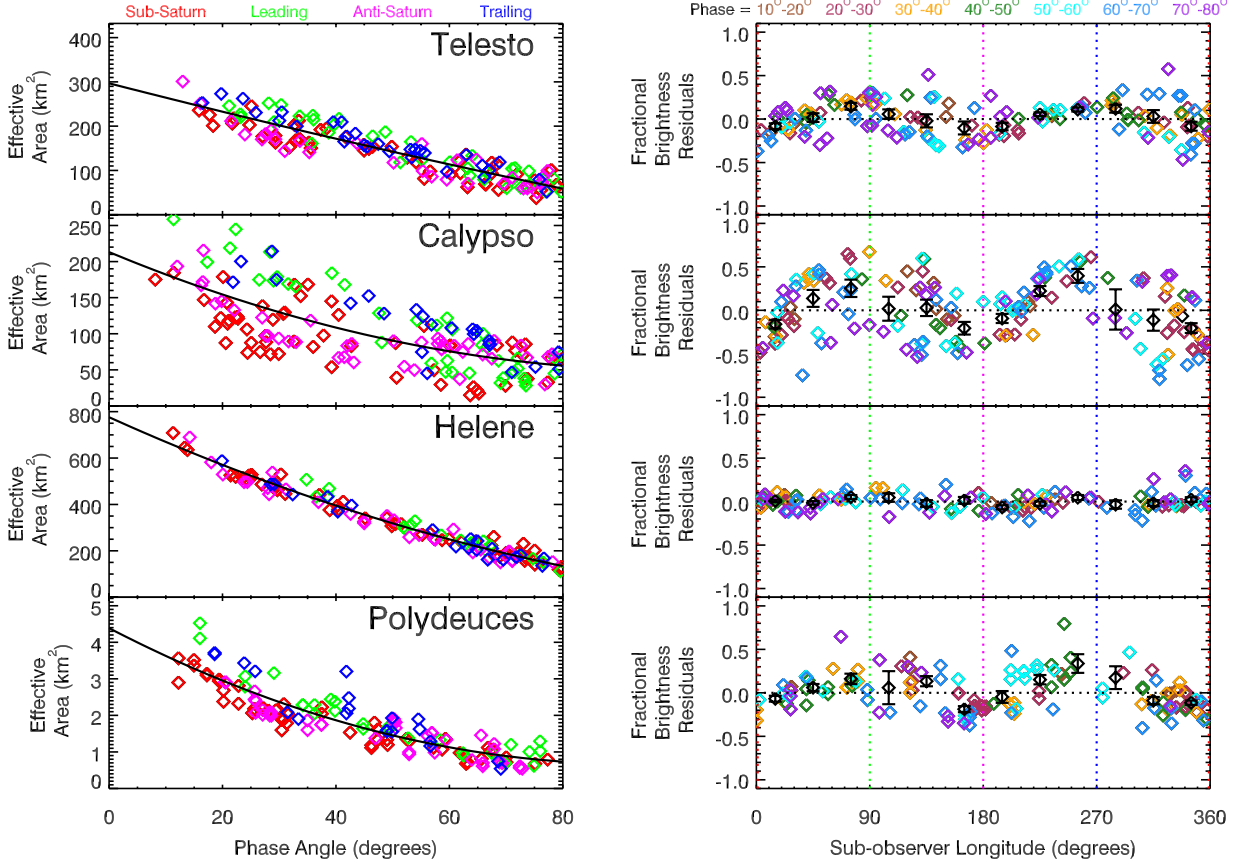


**Figure 2.** Summary of the brightness measurements for the trojan moons Telesto, Calypso, Helene and Polydeuces. The left-hand plots show the effective areas  $A_{\text{eff}}$  of the moons as a function of phase angle, with the data points color coded by the quadrant viewed by the spacecraft. The right-hand plots show the fractional residuals of the brightness estimates relative to the quadratic trend shown as a solid line in the left-hand plots. Note that these objects are consistently brighter when their leading or trailing sides are viewed than they are when their sub-Saturn or anti-Saturn sides are viewed.

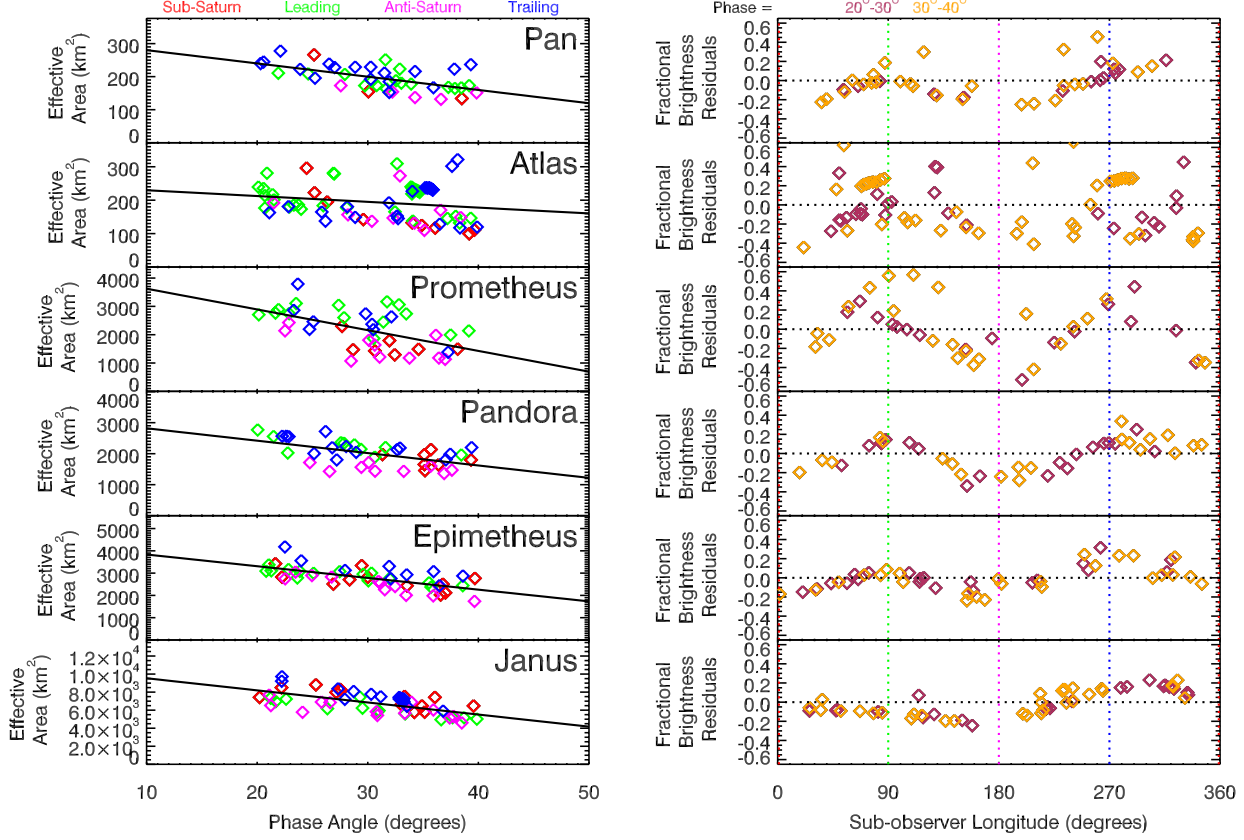


**Figure 3.** Summary of the brightness measurements for the ring moons. The left-hand plots show the effective areas  $A_{\text{eff}}$  of the moons as a function of phase angle, with the data points color coded by the quadrant viewed by the spacecraft. The right-hand plots show the fractional residuals of the brightness estimates relative to the linear trend shown as a solid line in the left-hand plots. Note that these objects are often brighter when their leading or trailing sides are viewed than they are when their sub-Saturn or anti-Saturn sides are viewed.

**Table 1.** Satellite shapes from resolved images (Thomas 2010; Thomas et al. 2013; Thomas and Helfenstein 2019, and Appendix B)

Object	$a$ (km)	$b$ (km)	$c$ (km)	$b/a$	$c/b$	$R_m$ (km)
Aegaeon	$0.70 \pm 0.05$	$0.25 \pm 0.06$	$0.20 \pm 0.08$	$0.36 \pm 0.09$	$0.80 \pm 0.37$	$0.33 \pm 0.06$
Methone	$1.94 \pm 0.02$	$1.29 \pm 0.04$	$1.21 \pm 0.02$	$0.66 \pm 0.02$	$0.94 \pm 0.03$	$1.45 \pm 0.03$
Pallene	$2.88 \pm 0.07$	$2.08 \pm 0.07$	$1.84 \pm 0.07$	$0.72 \pm 0.03$	$0.89 \pm 0.04$	$2.23 \pm 0.07$
Mimas	$207.8 \pm 0.5$	$196.7 \pm 0.5$	$190.6 \pm 0.3$	$0.947 \pm 0.003$	$0.969 \pm 0.003$	$198.2 \pm 0.4$
Enceladus	$256.6 \pm 0.3$	$251.4 \pm 0.2$	$248.3 \pm 0.2$	$0.980 \pm 0.002$	$0.988 \pm 0.001$	$252.1 \pm 0.2$
Tethys	$538.4 \pm 0.3$	$528.3 \pm 1.1$	$526.3 \pm 0.6$	$0.981 \pm 0.002$	$0.996 \pm 0.002$	$531.0 \pm 0.6$
Dione	$563.4 \pm 0.6$	$561.3 \pm 0.5$	$559.6 \pm 0.4$	$0.996 \pm 0.001$	$0.997 \pm 0.001$	$561.4 \pm 0.4$
Rhea	$765.0 \pm 0.7$	$763.1 \pm 0.6$	$762.4 \pm 0.6$	$0.998 \pm 0.001$	$0.999 \pm 0.001$	$763.5 \pm 0.6$
Pan	$17.3 \pm 0.2$	$14.1 \pm 0.2$	$10.5 \pm 0.5$	$0.815 \pm 0.015$	$0.745 \pm 0.037$	$13.7 \pm 0.3$
Atlas	$20.4 \pm 0.1$	$17.7 \pm 0.2$	$9.3 \pm 0.3$	$0.868 \pm 0.011$	$0.525 \pm 0.018$	$14.9 \pm 0.2$
Prometheus	$68.5 \pm 0.5$	$40.5 \pm 1.4$	$28.1 \pm 0.4$	$0.591 \pm 0.021$	$0.694 \pm 0.026$	$42.8 \pm 0.7$
Pandora	$51.5 \pm 0.3$	$39.5 \pm 0.3$	$31.5 \pm 0.2$	$0.767 \pm 0.007$	$0.797 \pm 0.008$	$40.0 \pm 0.3$
Epimetheus	$64.8 \pm 0.3$	$58.1 \pm 0.2$	$53.5 \pm 0.2$	$0.897 \pm 0.005$	$0.921 \pm 0.005$	$58.6 \pm 0.3$
Janus	$101.7 \pm 0.9$	$92.9 \pm 0.3$	$74.5 \pm 0.3$	$0.913 \pm 0.009$	$0.802 \pm 0.004$	$89.0 \pm 0.5$
Telesto	$16.6 \pm 0.3$	$11.7 \pm 0.3$	$9.6 \pm 0.2$	$0.705 \pm 0.022$	$0.821 \pm 0.027$	$12.3 \pm 0.3$
Calypso	$14.7 \pm 0.3$	$9.3 \pm 0.9$	$6.4 \pm 0.3$	$0.632 \pm 0.062$	$0.688 \pm 0.073$	$9.5 \pm 0.4$
Helene	$22.6 \pm 0.2$	$19.6 \pm 0.3$	$13.3 \pm 0.2$	$0.867 \pm 0.015$	$0.679 \pm 0.015$	$18.1 \pm 0.2$
Polydeuces	$1.75 \pm 0.2$	$1.55 \pm 0.2$	$1.31 \pm 0.2$	$0.89 \pm 0.15$	$0.85 \pm 0.17$	$1.53 \pm 0.2$

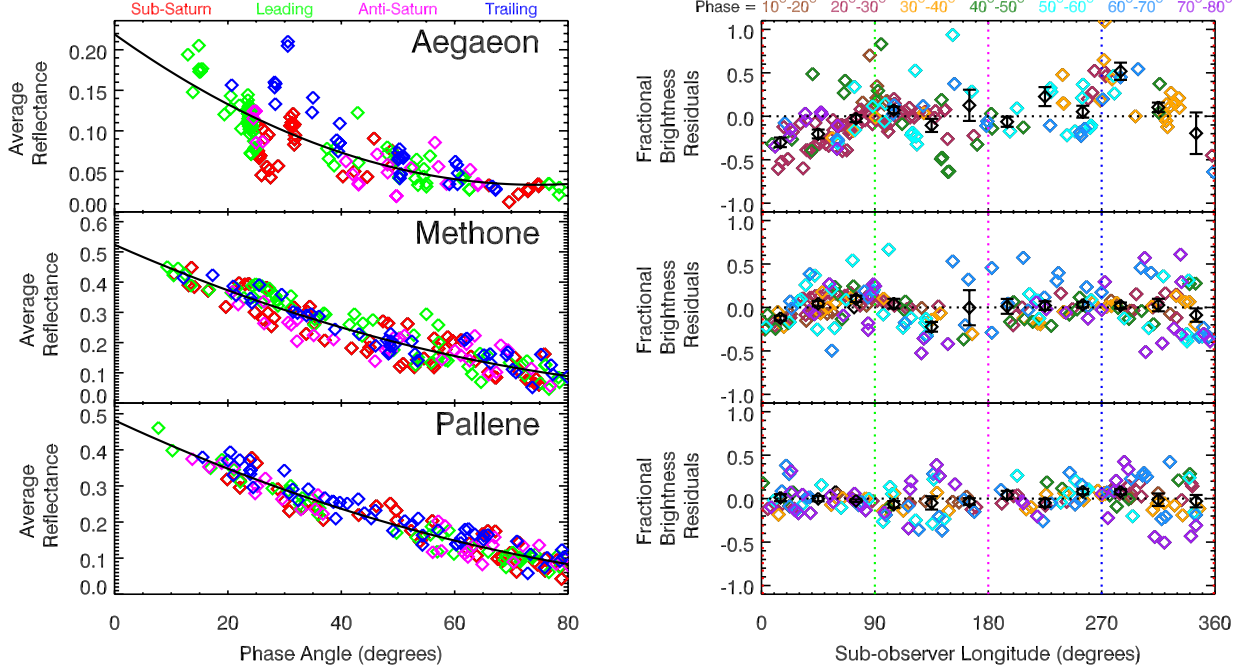


**Figure 4.** Average reflectances of Aegaeon, Methone and Pallene. The left-hand plots show the average reflectances of the moons as a function of phase angle, with the data points color coded by the quadrant viewed by the spacecraft. The right-hand plots show the fractional residuals of the brightness estimates relative to the quadratic trend shown as a solid line in the left-hand plots. While the longitudinal brightness variations are reduced compared to the effective areas shown in Figure 1, they are not completely removed, especially at higher phase angles.

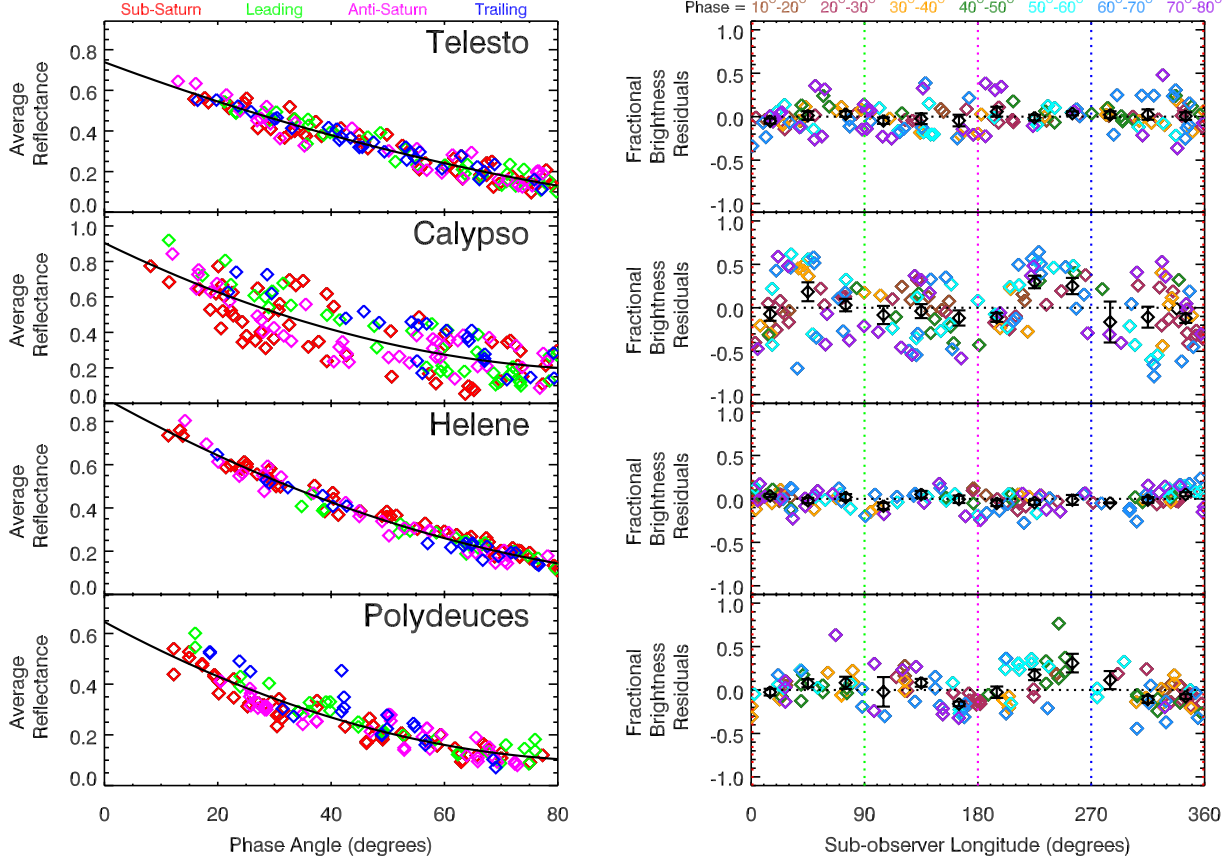


**Figure 5.** Average reflectances of of Telesto, Calypso, Helene and Polydeuces with their nominal shapes. The left-hand plots show the average reflectances of the moons as a function of phase angle, with the data points color coded by the quadrant viewed by the spacecraft. The right-hand plots show the fractional residuals of the average reflectances relative to the quadratic trend shown as a solid line in the left-hand plots. While the longitudinal brightness variations are reduced compared to the effective areas shown in Figure 2, they are not completely removed, especially at higher phase angles.

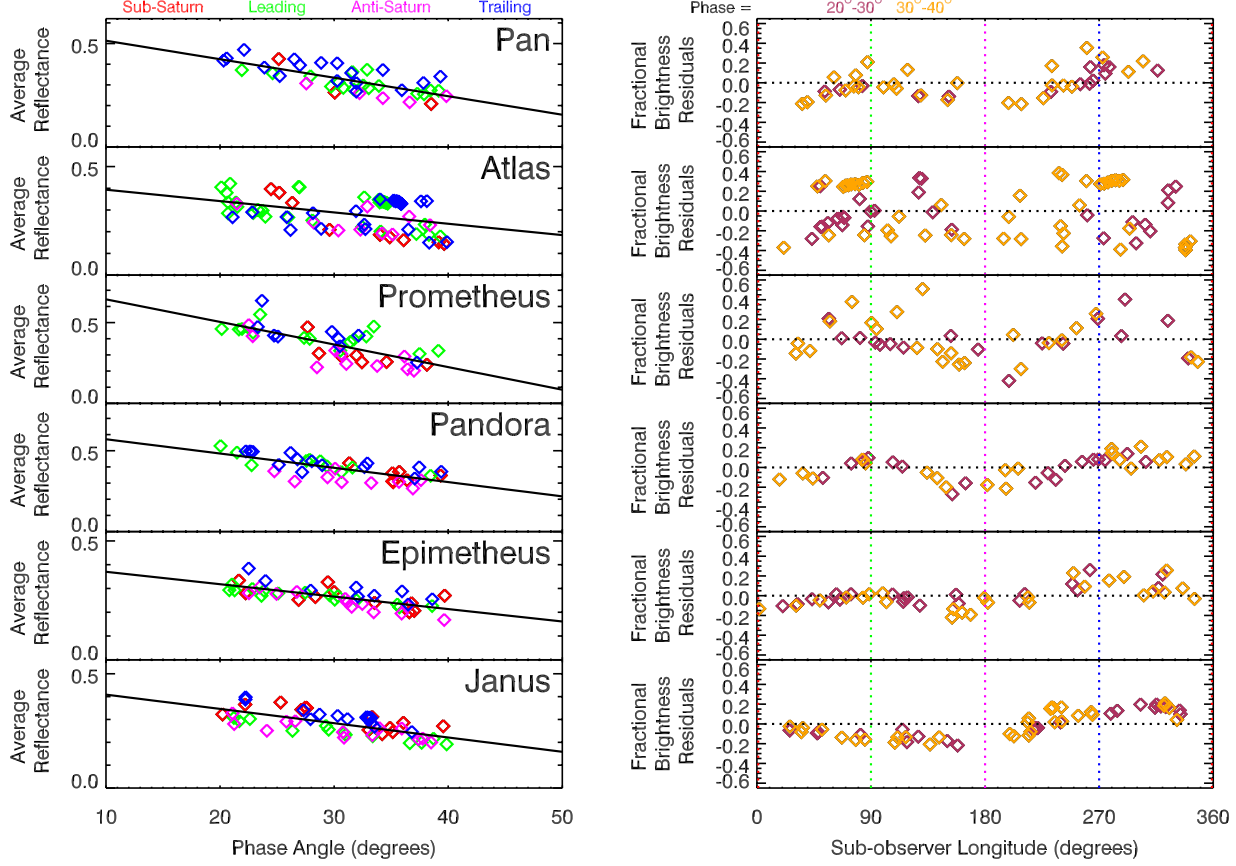


**Figure 6.** Average reflectances of the ring moons with their nominal shapes. The left-hand plots show the average reflectances of the moons as a function of phase angle, with the data points color coded by the quadrant viewed by the spacecraft. The right-hand plots show the fractional residuals of the brightness estimates relative to the linear trend shown as a solid line in the left-hand plots. Again, while the longitudinal brightness variations are slightly reduced compared to the effective areas shown in Figure 3, they are not completely removed.

### 3. A PHOTOMETRIC MODEL FOR ELONGATED BODIES

The challenges associated with photometric analyses of small moons are best seen in the left-hand panels of Figures 1-3, which show the effective area estimates for these moons as functions of the observed phase angle. While there is a clear trend of decreasing brightness with increasing phase angle, the data points also show a relatively large amount of scatter around this basic trend. This scatter cannot be entirely attributed to measurement errors because it is strongly correlated with the viewing geometry. In particular, the moons' sub-Saturn and anti-Saturn quadrants are systematically lower in  $A_{\text{eff}}$  than their leading and trailing quadrants. These variations can be more clearly documented by plotting the fractional residuals from the mean trend (where  $A_{\text{eff}}$  is assumed to be a linear or quadratic function of phase angle) as functions of the sub-observer longitude. With the exception of Helene, Pan and Atlas, these plots all show clear sinusoidal patterns with maxima around  $90^\circ$  and  $270^\circ$  and minima around  $0^\circ$  and  $180^\circ$ .

These trends with sub-observer longitude arise because these small moons have ellipsoidal shapes and are tidally locked so that their long axes point towards Saturn. Resolved images of these moons show that they are all significantly elongated (see Table 1, note that Anthe was never observed with sufficient resolution to determine its shape and size accurately). Furthermore, the relative magnitudes of the longitudinal brightness variations shown in Figures 1-3 are generally consistent with the relative  $a/b$  ratios of these different moons, with Aegaeon being the most elongated object and the one with the largest longitudinal brightness variations, followed by Calypso, Prometheus and Methone.

#### 3.1. *Variations in projected area do not adequately account for the moons' photometric properties*

The simplest way to account for these shape-related brightness variations is to divide the observed  $A_{\text{eff}}$  by the plane-projected area of the object  $A_{\text{phys}}$ , which for an ellipsoidal object is given by the following formula (Vickers 1996):

$$A_{\text{phys}} = \pi [b^2 c^2 \cos^2 \lambda_O \cos^2 \phi_O + a^2 c^2 \cos^2 \lambda_O \sin^2 \phi_O + a^2 b^2 \sin^2 \lambda_O]^{1/2} \quad (4)$$

where  $a$ ,  $b$ , and  $c$  are the dimensions of the ellipsoid, while  $\lambda_O$  and  $\phi_O$  are the sub-observer latitude and longitude for the object. The resulting ratio then yields the disk-averaged reflectance of the object:

$$\langle I/F \rangle = \frac{A_{\text{eff}}}{A_{\text{phys}}} \quad (5)$$

Tables 8-28 include estimates of  $A_{\text{phys}}$  computed assuming that these bodies have the shape parameters given in Table 1, and Figures 4-6 show the resulting estimates of  $\langle I/F \rangle$  as functions of phase and sub-observer longitude. While the fractional brightness residuals around the mean phase curve are somewhat smaller for  $\langle I/F \rangle$  than they are for  $A_{\text{eff}}$ , the dispersion is still rather large. For Aegaeon, Prometheus and Pandora there are still clear maxima at  $90^\circ$  and  $270^\circ$ , while for Methone, Pallene, Telesto and Calypso the dispersion at larger phase angles has a similar magnitude for the two parameters.

### 3.2. A Generic Ellipsoid Photometric Model (GEPM)

The major problem with using  $\langle I/F \rangle$  is that this parameter only accounts for the viewing geometry, but not how the moon is illuminated by the Sun, which for very elongated bodies can strongly affect the observed brightness (Helfenstein and Veverka 1989). Muinonen and Lumme (2015) provide analytical formula for elongated bodies assuming the surface follows a Lommel-Seeliger scattering law, which is appropriate for dark surfaces. However, the applicability of such a model for bright objects like many of Saturn's moons is less clear. We therefore use a more generic numerical method to translate whole-disk brightness data into information about the object's global average reflectance behavior, which we call the *Generic Ellipsoid Photometric Model (GEPM)*.

The GEPM predicts an ellipsoidal object's  $A_{\text{eff}}$  in any given image assuming its surface reflectance  $R$  follows a generic scattering law that is a function of the cosines of the incidence and emission angles  $\cos i$  and  $\cos e$ . The predicted effective area of an object whose surface obeys these scattering laws is given by the following integral:

$$A_{\text{pred}} = \int_{++} (\cos e) R r_{\text{eff}}^2 \cos \lambda d\lambda d\phi \quad (6)$$

where  $\lambda$  and  $\phi$  are the latitude and longitude on the object, the  $++$  sign indicates that the integral is performed only over the part of the object that is both illuminated and visible (i.e. where  $\cos i$  and  $\cos e$  are both positive), the factor of  $\cos e$  in this integral accounts for variations in the projected size of the area element, and  $r_{\text{eff}}$  is the effective radius of the object at a given latitude and longitude, which is given by the following expression:

$$r_{\text{eff}}^2 = [b^2 c^2 \cos^2 \lambda \cos^2 \phi + a^2 c^2 \cos^2 \lambda \sin^2 \phi + a^2 b^2 \sin^2 \lambda]^{1/2}. \quad (7)$$

The factors of  $\cos i$  and  $\cos e$  in the above integral are also functions of  $\lambda$  and  $\phi$  that depend upon the viewing and illumination geometry, as well as the object's shape. To obtain these functions, we first use the sub-observer latitude  $\lambda_O$  and longitude  $\phi_O$  to define a unit vector pointing from the center of the body towards the spacecraft:

$$\hat{\mathbf{o}} = \cos \lambda_O \cos \phi_O \hat{\mathbf{x}} + \cos \lambda_O \sin \phi_O \hat{\mathbf{y}} + \sin \lambda_O \hat{\mathbf{z}} \quad (8)$$

where  $\hat{\mathbf{x}}$  points from the moon towards Saturn,  $\hat{\mathbf{y}}$  points in the direction of orbital motion and  $\hat{\mathbf{z}}$  points along the object's rotation axis. Similarly, we use the sub-solar latitude  $\lambda_S$  and longitude  $\phi_S$  to define a unit vector pointing from the center of the body towards the Sun:

$$\hat{\mathbf{s}} = \cos \lambda_S \cos \phi_S \hat{\mathbf{x}} + \cos \lambda_S \sin \phi_S \hat{\mathbf{y}} + \sin \lambda_S \hat{\mathbf{z}} \quad (9)$$

Finally, for each latitude  $\lambda$  and longitude  $\phi$  on the surface, we compute the surface normal for the body, which depends on the shape parameters  $a$ ,  $b$  and  $c$ .

$$\hat{\mathbf{n}} = \frac{\frac{\cos \lambda \cos \phi}{a} \hat{\mathbf{x}} + \frac{\cos \lambda \sin \phi}{b} \hat{\mathbf{y}} + \frac{\sin \lambda}{c} \hat{\mathbf{z}}}{\sqrt{\frac{\cos^2 \lambda \cos^2 \phi}{a^2} + \frac{\cos^2 \lambda \sin^2 \phi}{b^2} + \frac{\sin^2 \lambda}{c^2}}} \quad (10)$$

The cosines of the incidence and emission angles are then given by the standard expressions  $\cos i = \hat{\mathbf{n}} \cdot \hat{\mathbf{s}}$  and  $\cos e = \hat{\mathbf{n}} \cdot \hat{\mathbf{o}}$ .

The above expressions allow us to evaluate  $A_{\text{pred}}$  for any given scattering law  $R$ , including Lunar-Lambert functions or Akimov functions (McEwen 1991; Shkuratov et al. 2011; Schröder et al. 2014). However, for the sake of concreteness, we will here assume that  $R$  is given by the Minnaert function (Minnaert 1941):

$$R_M = B(\cos i)^k(\cos e)^{1-k}, \quad (11)$$

where the quantities  $k$  and  $B$  will be assumed to be constants for each image. Note that if we assume that  $k = 1$  the above expression reduces to the Lambert photometric function:

$$R_L = B \cos i. \quad (12)$$

For a generic Minnaert function, Equation 6 becomes:

$$A_{\text{pred}} = B \int_{++} (\cos i)^k(\cos e)^{2-k} r_{\text{eff}}^2 \cos \lambda d\lambda d\phi = Ba_{\text{pred}} \quad (13)$$

The factor of  $B$  moves outside the integral, and the remaining factor  $a_{\text{pred}}$  can be numerically evaluated for any specified viewing and illumination geometry, so long as we also assume values for the object's shape parameters  $a$ ,  $b$  and  $c$ , as well as the photometric parameter  $k$ . A Python function which evaluates  $a_{\text{pred}}$  given these parameters is provided in Appendix A. From this, we can estimate the “brightness coefficient” parameter  $B$  to be simply the ratio  $A_{\text{eff}}/a_{\text{pred}}$ . Note that  $B$  is not equal to the mean reflectance  $\langle I/F \rangle$ , even for spherical bodies, because it includes corrections for the varying incidence and emission angles across the disk.

Of course, the estimated value of  $B$  depends on the assumed values of  $a$ ,  $b$ ,  $c$  and  $k$ , which are typically estimated from resolved images. While only a few images are needed to obtain useful estimates of  $a$ ,  $b$  and  $c$ , the parameter  $k$  can depend on the observed phase angle and location on the object, and so  $k$  is far harder to estimate reliably for the full range of observation geometries. Previous studies of resolved Voyager images of the mid-sized moons found that Mimas, Enceladus, Tethys, Dione and Rhea had  $k = 0.65, 0.78, 0.63, 0.53 - 0.56$  and  $0.52-0.54$  respectively at phase angles between  $5^\circ$  and  $17^\circ$  (Buratti 1984), while a study of resolved Cassini images of Methone found that  $k = 0.887 - 0.003\alpha$  ( $\alpha$  being the solar phase angle) based on images obtained at phase angles between  $45^\circ$  and  $65^\circ$  (Thomas et al. 2013). Thus this parameter likely varies among these moons and with observation geometry and terrain for each moon.

Figure 7 shows the fractional differences in the predicted values of  $a_{\text{pred}}$  between a model where  $k = 0.5$  and a model where  $k = 1$  (that is, a Lambertian surface). Each data point corresponds to a different combination of sub-observer and sub-solar locations scattered over the entire object. For the spherical object there is a trend where the  $k = 0.5$  model becomes 15% brighter than the Lambertian model at high phase angles. Very prolate and oblate objects show a similar overall trend, but with considerably more scatter depending on the exact viewing and illumination geometry. This suggests that one could constrain  $k$  by minimizing the *rms* scatter in the estimated brightness coefficients from unresolved images of elongated bodies at each phase angle. In practice, the *rms* scatter in the brightness

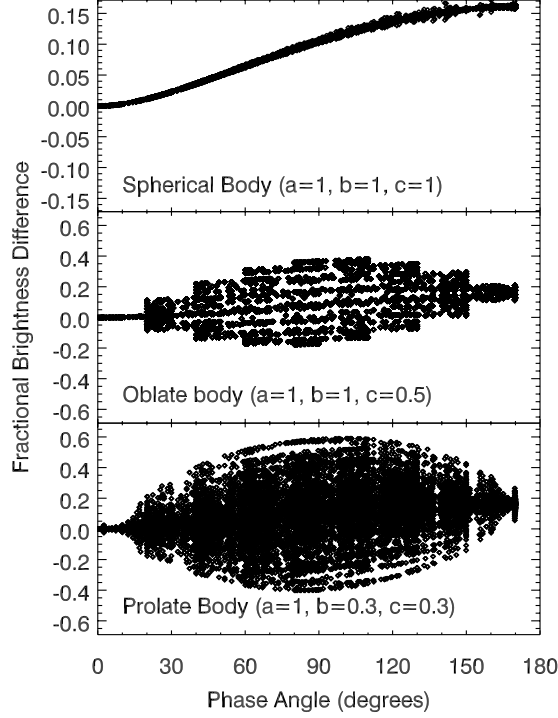


**Figure 7.** The fractional difference between the predicted values of  $a_{\text{pred}}$  between a Minnaert model with  $k = 0.5$  and a Lambertian model for three different shapes. Each point corresponds to a different combination of viewing and illuminate geometries scattered uniformly over the objects' surface.

coefficients for the various moons are very weak functions of  $k$ , most likely because real surface albedo variations and/or instrumental noise dominate the dispersion in the brightness coefficients. We therefore expect that a thorough analysis of resolved images would be needed to constrain  $k$  reliably for each of the moons, and such an analysis is well beyond the scope of this paper.

Fortunately, it turns out that the results presented below are insensitive to the exact value of  $k$ . We bracket the range of possible  $k$ -values by considering cases where  $k = 0.5, 0.75$  and  $1.0$  when estimating the brightnesses of the various moons. Estimates of  $a_{\text{pred}}$  derived from all three cases are provided in Tables 8- 28. However, since the brightness differences among these different scenarios are subtle, we will normally only plot brightness coefficients computed assuming the surface follows a Lambertian scattering law (i.e.  $k = 1$ ).

### 3.3. Validation of General Ellipsoid Photometric Model with Saturn's small moons

The utility of this model can be most clearly demonstrated by taking a closer look at the data for Aegaeon. Aegaeon is not only the most elongated moon, it was also observed in multiple ARCORBIT sequences where the spacecraft repeatedly imaged the moon as it moved around a significant fraction of its orbit, yielding true rotational light curves. The images from eight of these sequences are listed in Table 2, while the values of  $A_{\text{eff}}$  are shown in Figure 8, plotted as a function of the sub-observer longitude. All show clear brightness variations that can be attributed to the changing viewing geometry of the moon, with the

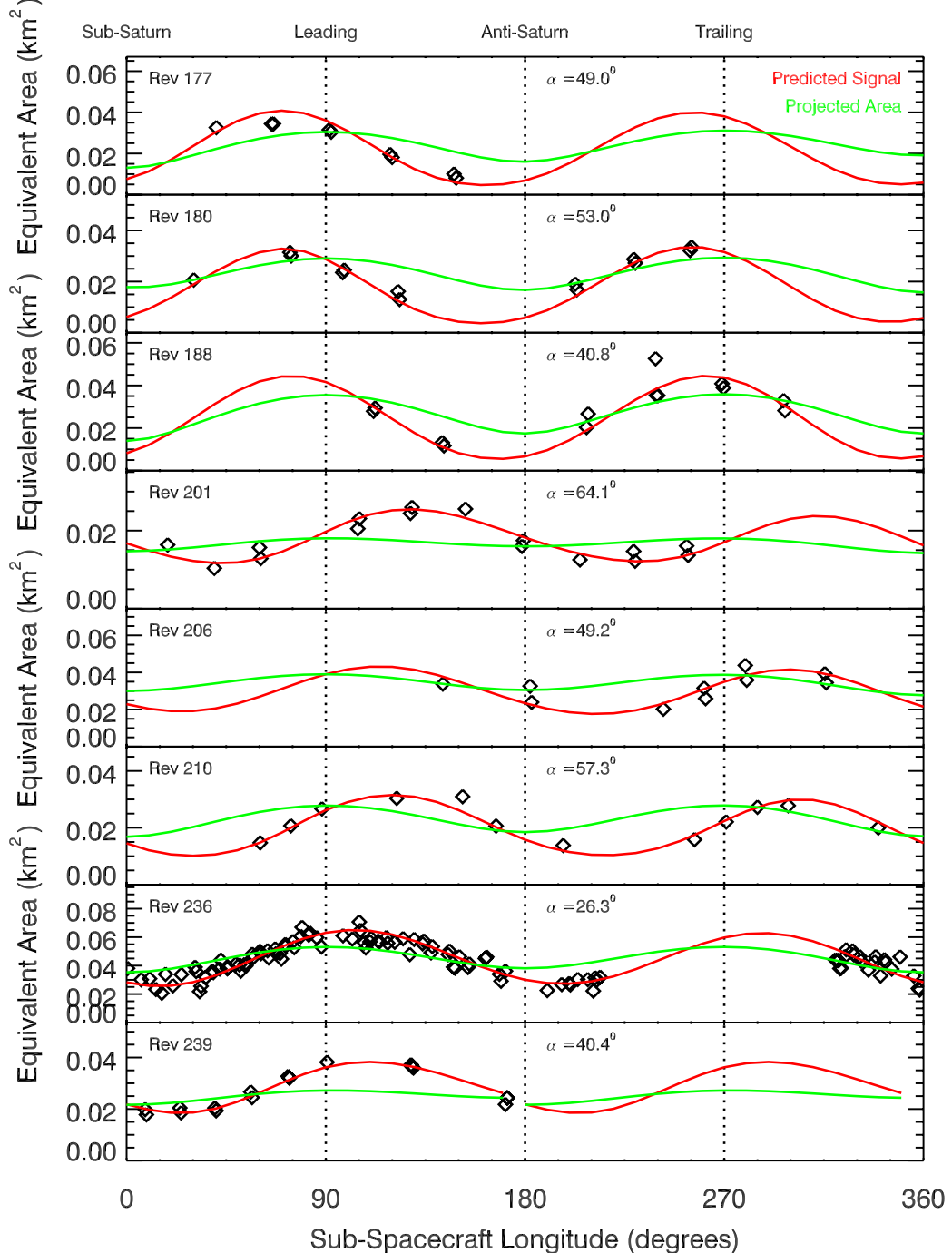


**Figure 8.** Observed and predicted rotation light curves for Aegaeon. Each plot shows data from one particular ARCORBIT observation of Aegaeon, which measured the brightness of Aegaeon as a function of sub-observer longitude. The data points are the measured data, while the green curves show the variations in the projected area of the moon, and the red curves show the predicted variations in  $a_{\text{pred}}$  for a Lambertian model with Aegaeon's nominal shape (Minnaert models with  $k = 0.5$  and  $k = 0.75$  show nearly the same trends). The predicted curves are both scaled to best match the median observed signal. The GEPM model predictions clearly match the data much better than the effective areas.

**Table 2.** Cassini ISS NAC images belonging to the various ARCORBIT sequences

Sequence	Images
Rev 177	N1735282418 N1735287671 N1735287895 N1735292924 N1735293148 N1735298177 N1735298401 N1735303430 N1735303654
Rev 180	N1738781138 N1738781312 N1738785881 N1738786055 N1738790624 N1738790798 N1738804853 N1738805027 N1738809596 N1738809770 N1738814339 N1738814513 N1738842971
Rev 188	N1746467285 N1746467459 N1746472918 N1746473092 N1746484184 N1746484358 N1746489747 N1746489817 N1746489991 N1746495450 N1746495624 N1746501083 N1746501257
Rev 201	N1769540993 N1769545670 N1769549999 N1769550173 N1769559005 N1769559179 N1769563508 N1769563682 N1769568011 N1769572514 N1769572688 N1769577191 N1769581520 N1769581694 N1769586023 N1769586197
Rev 206	N1783325708 N178332836 N178333010 N1783343963 N1783347440 N1783347614 N1783351091 N1783351265 N1783358393 N1783358567
Rev 210	N1796027549 N1796033113 N1796035895 N1796041459 N1796052587 N1796055369 N1796058151 N1796060933 N1796069279 N1796085971 N1796088753 N1796091535
Rev 236	N1843274411 N1843274619 N1843274723 N1843274810 N1843274984 N1843275331 N1843275435 N1843276039 N1843276143 N1843276747 N1843276851 N1843277559 N1843278163 N1843278267 N1843278379 N1843279092 N1843279196 N1843279800 N1843280612 N1843281924 N1843282326 N1843282500 N1843282957 N1843284269 N1843285081 N1843285685 N1843286261 N1843286614 N1843287322 N1843288134 N1843289446 N1843289550 N1843289848 N1843290022 N1843290479 N1843291083 N1843291187 N1843291791 N1843291895 N1843292499 N1843292603 N1843293311 N1843293609 N1843293783 N1843294136 N1843294240 N1843294844 N1843294948 N1843295552 N1843295656 N1843296260 N1843296364 N1843296968 N1843297072 N1843297370 N1843297544 N1843297897 N1843298001 N1843298605 N1843298709 N1843299313 N1843299417 N184330021 N1843300125 N1843300729 N1843301131 N1843303074 N1843303886 N1843304490 N1843304594 N1843304892 N1843305066 N1843305419 N1843305523 N1843306127 N1843306231 N1843306835 N1843306939 N1843307543 N1843308251 N1843308827 N1843309180 N1843309888 N1843309992 N1843310596 N1843310700 N1843312012 N1843312116 N1843312414 N1843312588 N1843312941 N1843313649 N1843313753 N1843315065 N1843315169 N1843316175 N1843316349 N1843316702 N1843320110 N1843321275 N1843321879 N1843321983 N1843322587 N1843323399 N1843323864 N1843324006 N1843324110 N1843324422
Rev 239	N1848936800 N1848936974 N1848940466 N1848940640 N1848944132 N1848944306 N1848947798 N1848947972 N1848951464 N1848951638 N1848955130 N1848962392 N1848962462 N1848962636 N1848969794 N1848969968 N184896996

lowest signals seen when the sub-observer longitude is near  $0^\circ$  or  $180^\circ$ , and the highest signals seen when the sub-observer longitude is close to  $90^\circ$  or  $270^\circ$ . However, it is also clear that the maxima and minima are not precisely aligned with these four longitudes (this is most clearly seen in the Rev 201, 210 and 236 data). This result clearly demonstrates that the projected area is not the only thing affecting the moon's projected brightness. Indeed, the green curves show the variations in the projected area, scaled to match the mean signal in the data. These variations are both too subtle to match the observations, and the observed and predicted peaks and troughs do not line up. By contrast, the GEPM predictions are a much better fit to the data in all cases. This demonstrates that accounting for the lighting geometry not only causes the predicted locations of peaks and troughs to shift into alignment with the data, but also increases the predicted fractional brightness variations.

More generally, Figures 9-11 show the estimated brightness coefficients for the small moons derived assuming that they have the nominal shapes given in Table 1 and surfaces that follow a Lambertian scattering law (assuming the surfaces follow Minnaert scattering laws with  $k=0.5$  and  $0.75$  yield nearly identical results). Compared with Figures 4-6, the scatter around the mean trends with phase angle are much tighter for almost all of the moons. The exceptions to this trend are Helene, Polydeuces, Janus and Epimetheus, for which the dispersions in  $B$  and  $< I/F >$  are comparable. These exceptions are likely because these four moons are the most spherical in shape, so the corrections included in the GEPM are less important. There are some outlying data points for Aegaeon, Atlas and Prometheus, but these can be attributed to the low signals from Aegaeon and misestimated background levels for Atlas and Prometheus.

Besides the reduction in dispersion, the fractional brightness residuals no longer show double-peaked trends with co-rotating longitude. Instead, the most obvious remaining longitudinal trends are that the leading sides of Pallene, Epimetheus and Janus are 10-20%

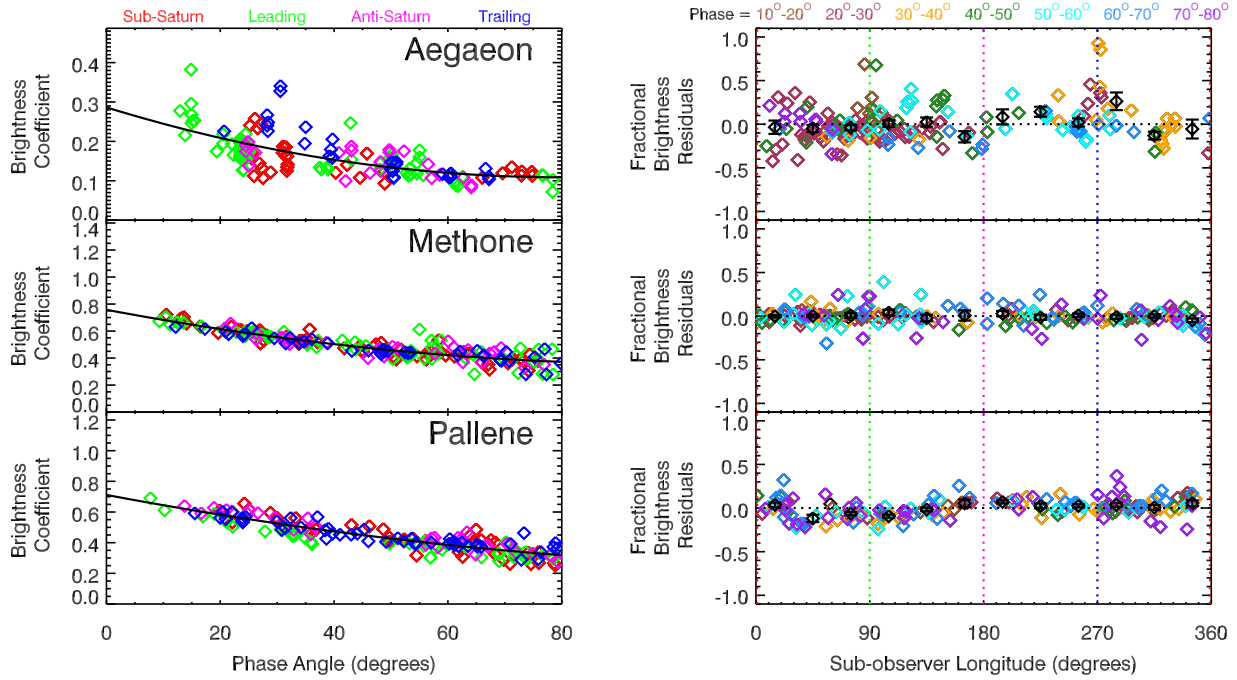


**Figure 9.** Estimated brightness coefficients for Lambertian models of Aegaeon, Methone and Pallene with their nominal shapes. The left plots show the brightness coefficients of the moons as a function of phase angle, with the data points color coded by the quadrant viewed by the spacecraft. The right-hand plots show the fractional residuals of the brightness estimates relative to the quadratic trend shown as a solid line in the left-hand plots. The longitude dependent brightness variations are almost completely removed, and those that remain, like Pallene’s leading-trailing asymmetry, are probably real surface features.

darker than their trailing sides. Such leading-trailing asymmetries are reminiscent of the longitudinal brightness variations seen in ground-based, Voyager and Cassini images of the mid-sized icy moons (Noland et al. 1974; Franz and Millis 1975; Buratti and Veverka 1984; Verbiscer and Veverka 1989; Buratti et al. 1990; Verbiscer and Veverka 1992, 1994; Buratti et al. 1998; Pitman et al. 2010; Schenk et al. 2011). Figure 12 shows the brightness coefficients for these larger moons derived assuming the same Lambertian model as was used for the smaller moons.<sup>1</sup> Consistent with prior work (Buratti et al. 1998; Schenk et al. 2011; Hendrix et al. 2018; Verbiscer et al. 2018), we find that Tethys, Dione and Rhea have brighter leading sides, while Mimas has a brighter trailing side. This overall trend is thought to arise because the particles in the E ring preferentially strike the leading sides of moons orbiting exterior to Enceladus and the trailing sides of moons orbiting interior to Enceladus (Hamilton and Burns 1994). The longitudinal brightness asymmetries observed on Pallene, Janus and Epimetheus are consistent with this pattern, but it is worth noting that Aegaeon, Methone and the trojan moons do not appear to have such asymmetries. The implications of these findings will be discussed further in Section 4 below.

<sup>1</sup> Due to the nearly spherical shape of these moons, the dispersions around the mean trends in these cases do not change much between  $A_{\text{eff}}$ ,  $\langle I/F \rangle$  and  $B$ .

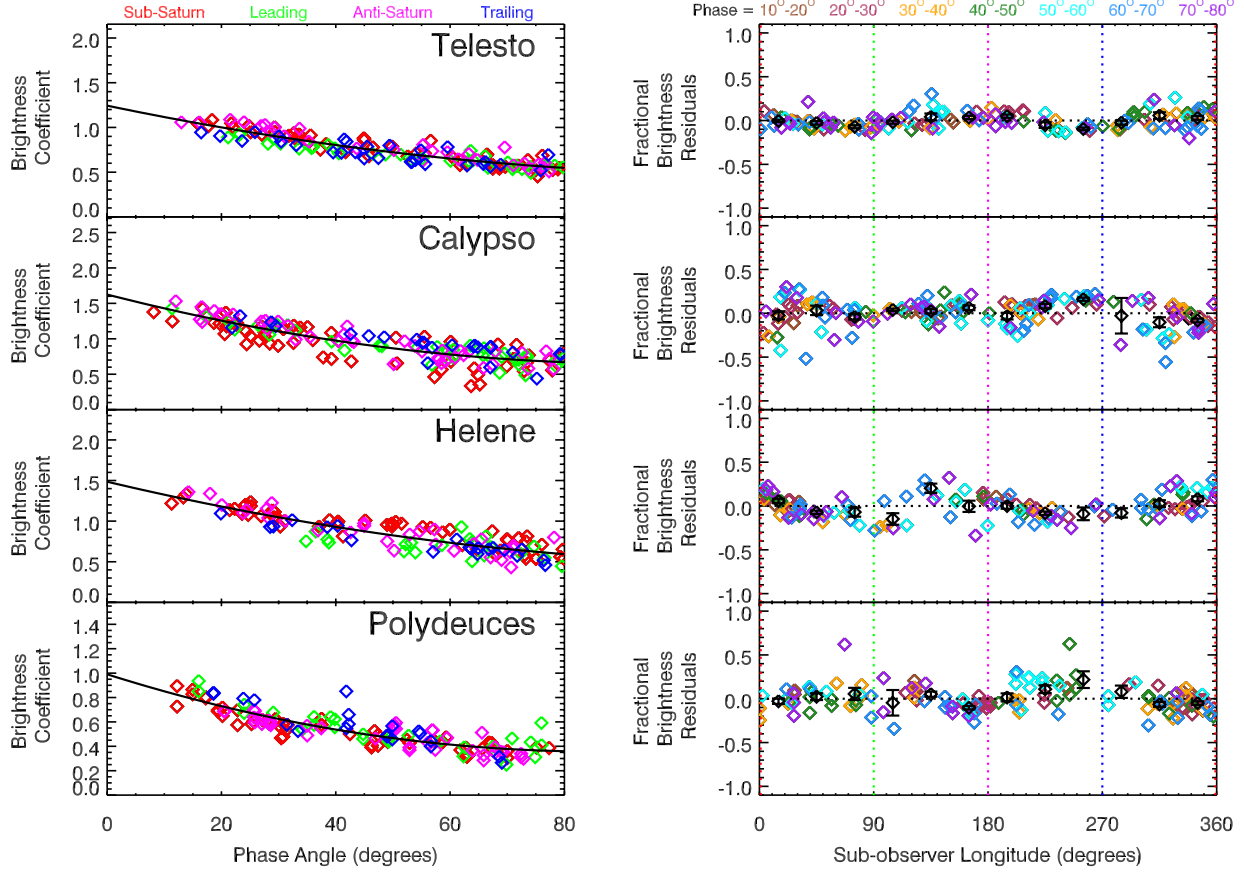


**Figure 10.** Estimated brightness coefficients for Lambertian models of Telesto, Calypso, Helene and Polydeuces with their nominal shapes. The left plots show the brightness coefficients of the moons as a function of phase angle, with the data points color coded by the quadrant viewed by the spacecraft. The right-hand plots show the fractional residuals of the brightness estimates relative to the quadratic trend shown as a solid line in the left-hand plots. For Telesto, Calypso and Polydeuces, this model yields reduces the dispersion associated with the viewing geometry. However, for Helene the dispersion of the measurements around the mean trend has actually increased.

Finally, we may consider what happens if we relax the assumption that the shapes of these moons equal the best-fit values from resolved images. Figures 13 and 14 show the *rms* residuals as functions of the aspect ratios  $b/a$  and  $c/b$  for Aegaeon, Anthe, Methone, Pallene and the trojan moons, along with the aspect ratios derived from the resolved images. For the smaller moons shown in Figure 13, the two methods for determining the shape agree fairly well. The best-fit solution for Aegeon falls where  $b \simeq c$  and  $b \simeq 0.3a$ , consistent with the constraints from the resolved images. For Methone, the two methods yield best-fit solutions with the same value of  $c/b \simeq 0.95$  and  $b/a \simeq 0.65$ , although the photometry favors a slightly higher value for  $b/a$ . Similarly, for Pallene we find both methods give  $c/b \simeq 0.9$ , but the resolved images favor  $b/a \simeq 0.7$ , while the photometry prefers 0.8. This discrepancy is likely related to the variations in the surface brightness with longitude mentioned above. More sophisticated photometric models could potentially resolve this difference, but even this level of consistency gives us some confidence in this method. Also, the photometric data

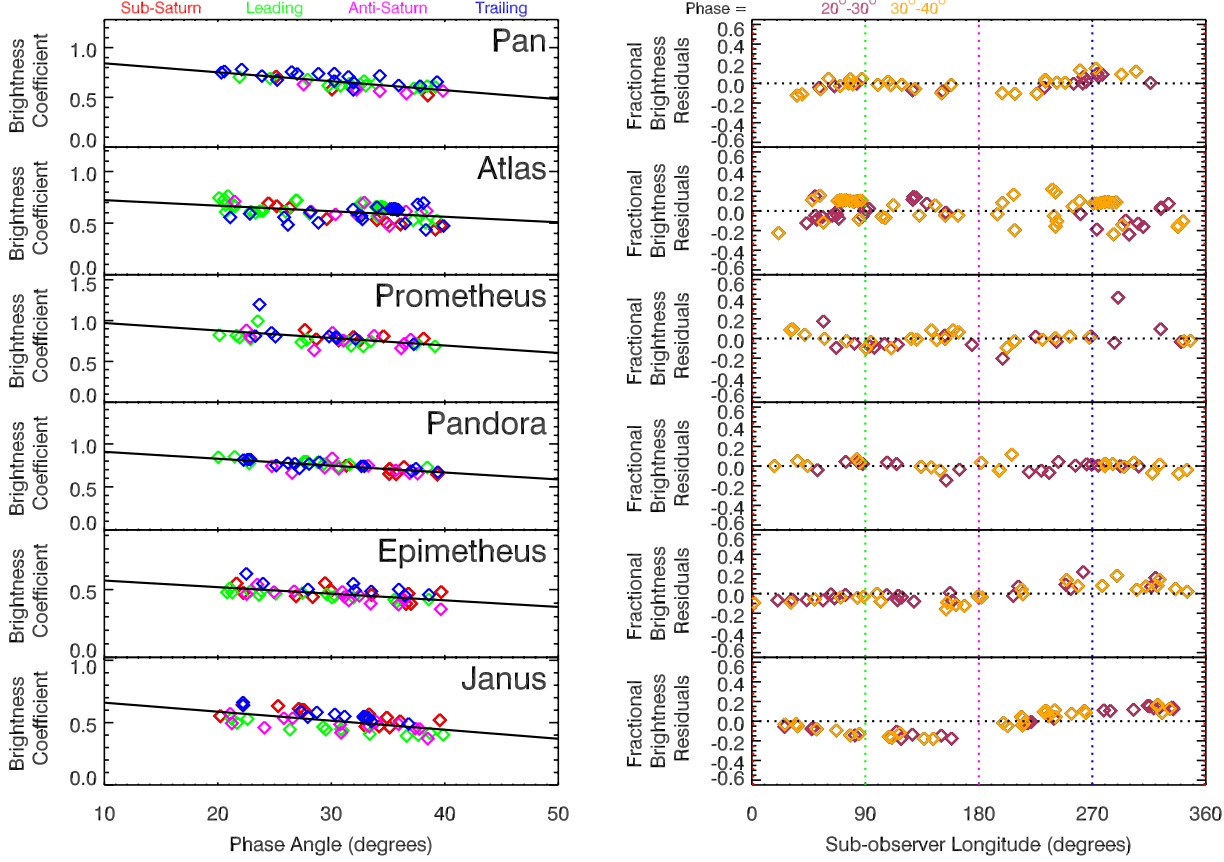


**Figure 11.** Estimated brightness coefficients for Lambertian models of the ring moons with their nominal shapes. The left plots show the brightness coefficients of the moons as a function of phase angle, with the data points color coded by the quadrant viewed by the spacecraft. The right-hand plots show the fractional residuals of the brightness estimates relative to the linear trend shown as a solid line in the left-hand plots. This model again reduces the dispersion around the phase trend, although for Atlas the dispersion is rather high compared to the other moons. Also note that for Janus and Epimetheus the leading hemisphere is clearly darker than the trailing hemisphere.

for Anthe clearly favor a shape with  $b/a \simeq 0.7$  and  $c/b \simeq 0.95$ , which implies that Anthe has a shape similar to Methone.

The shapes of the trojan moons derived from the photometry and resolved images are somewhat more discrepant. For Polydeuces, both methods yield  $b/a \simeq 0.8$  and  $c/b \simeq 1$  with rather large uncertainties. For Calypso, both methods agree that  $b/a \simeq 0.6$ , but the photometry favors  $c/b \simeq 0.9$  while the resolved images prefer  $c/b \simeq 0.7$ . For Telesto, both methods agree that  $c/b \simeq 0.8$ , but the photometry favors  $b/a \simeq 0.8$  while the resolved images prefer  $b/a \simeq 0.7$ . The biggest discrepancies are found with Helene, where the photometry prefers a much more spherical shape than found with the resolved images. These differences most likely arise because the shapes of these objects are not simple ellipsoids like the smaller moons appear to be. Again, a more sophisticated photometric model that could accommodate more complex shapes would likely reduce these discrepancies. Even so, the relatively simple GEPM clearly reduces the dispersion in the brightness estimates for

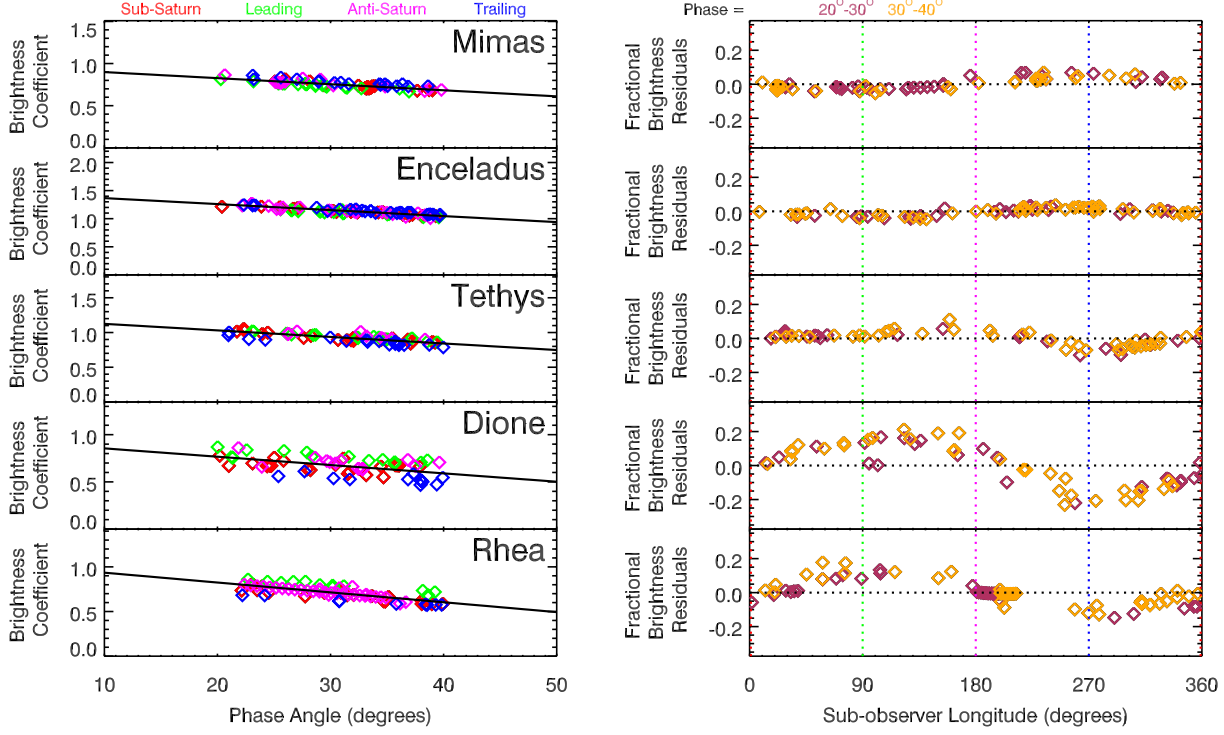


**Figure 12.** Estimated brightness coefficients for Lambertian models of the mid-sized moons with their nominal shapes. The left plot show the brightness coefficients of the moons as a function of phase angle, with the data points color coded by the quadrant viewed by the spacecraft. The right-hand plots show the fractional residuals of the brightness estimates relative to the linear trend shown as a solid line in the left-hand plots. Since all of these moons are close to spherical, the model does not affect the trends with longitude very much. Instead, this model simply enables the data for these moons to be compared with that from smaller moons. Note the longitudinal brightness asymmetries seen in these data are consistent with previous measurements and are mostly due to asymmetries in the E-ring flux.

Telesto, Polydeuces, and especially Calypso, and so it provides a useful basis for comparing the brightnesses of all these satellites.

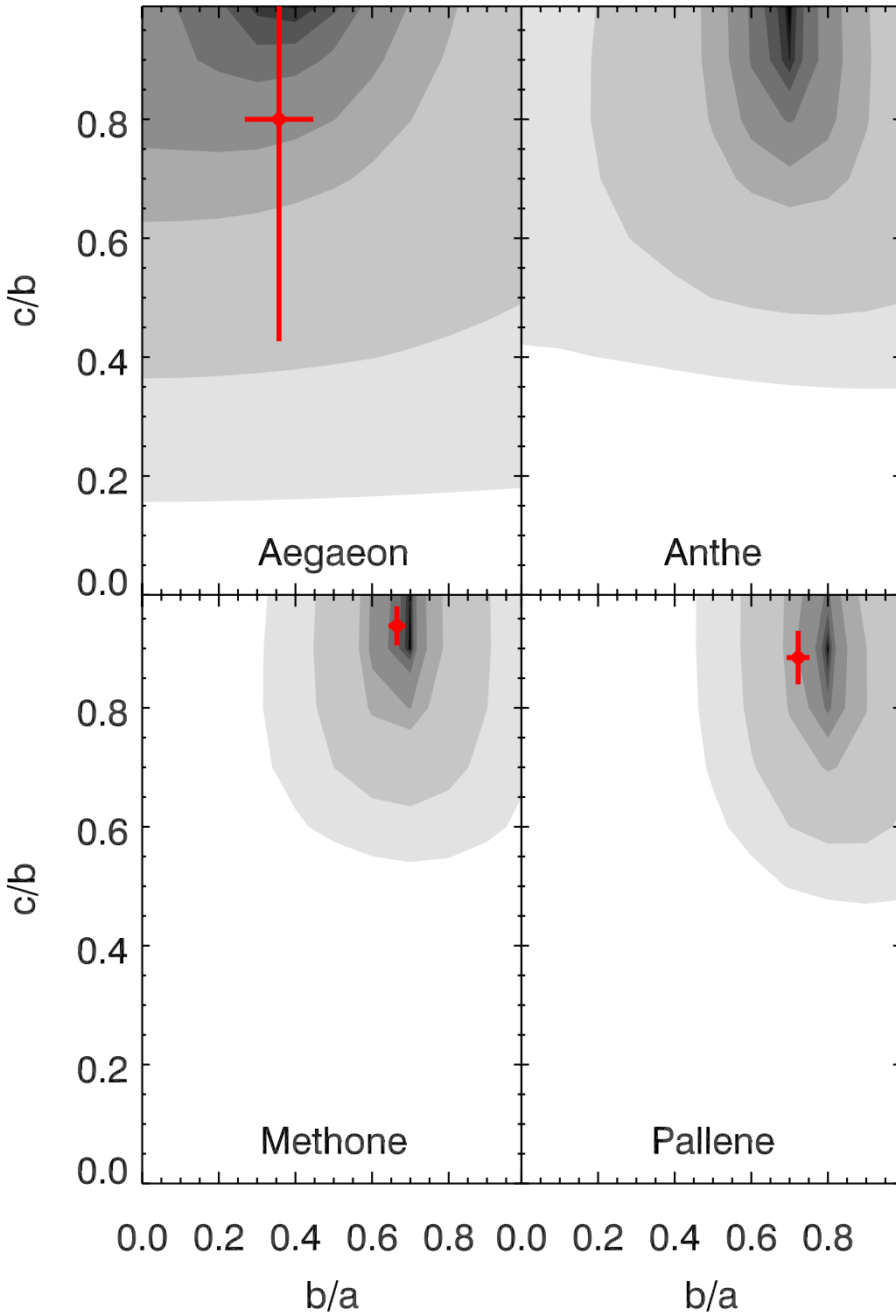


**Figure 13.** Photometric analysis of the shapes of Aegaeon, Anthe, Methone and Pallene. Each panel shows the *rms* dispersion of the residuals between the photometric data and a Lambertian GEPM model with different shape parameters  $a/b$  and  $b/c$  and a quadratic  $B(\alpha)$  function. The red data points are the estimates of these parameters derived from resolved images. For Aegaeon, Methone and Pallene the best-fit photometric models are reasonably consistent with the observed shapes. For Pallene, the best-fit model has a slightly higher  $b/a$  than was observed, but this can probably be attributed to the longitudinal brightness variations in this moon. These data also indicate that Methone and Anthe have very similar aspect ratios.

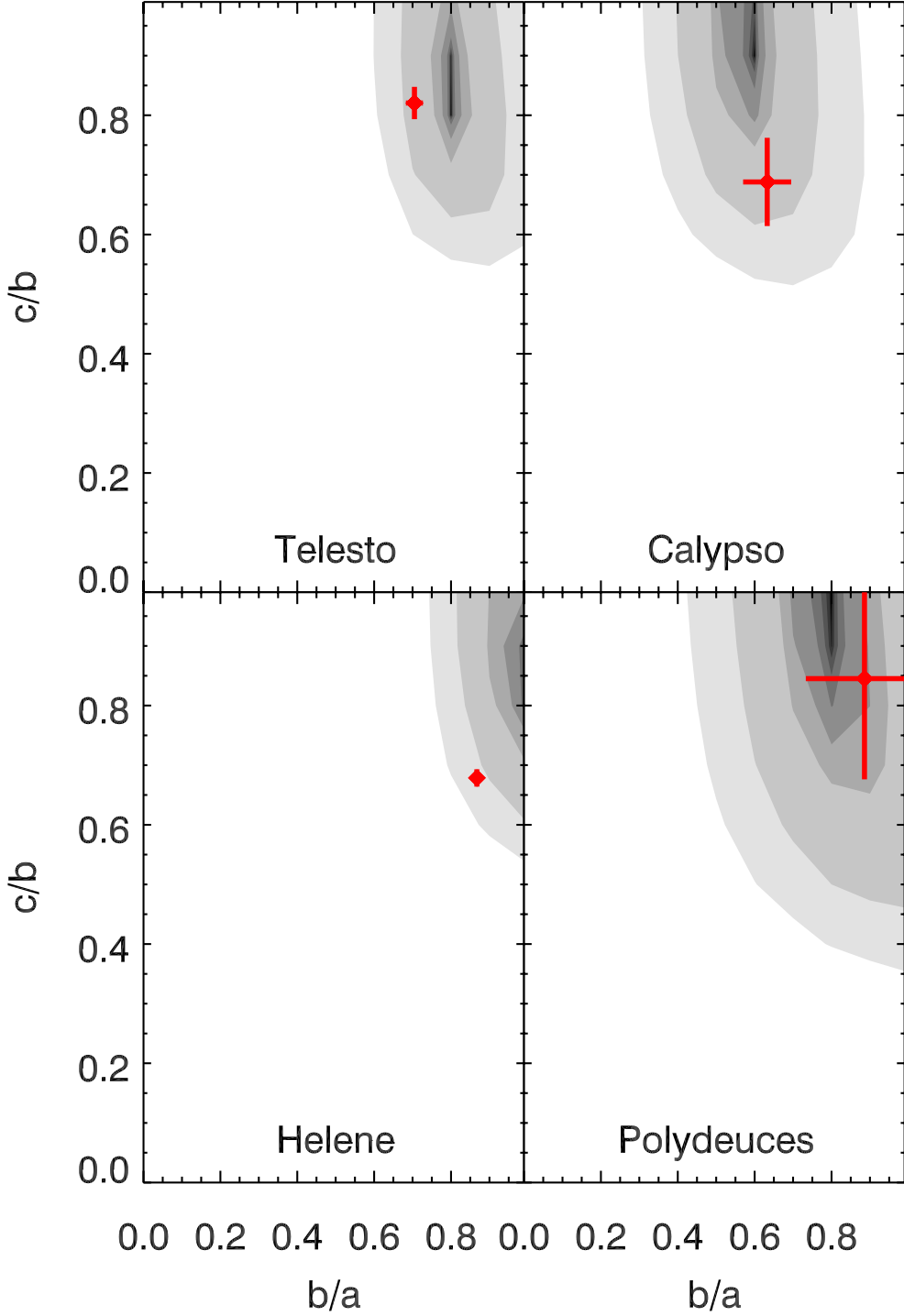


**Figure 14.** Photometric analysis of the shapes of Telesto, Calypso, Helene and Polydeuces. Each panel shows the *rms* dispersion of the residuals between the photometric data and a Lambertian GEPM model with different shape parameters  $a/b$  and  $b/c$  and a quadratic  $B(\alpha)$  function. The red data points are the estimates of these parameters derived from resolved images. For Calypso and Polydeuces the best-fit photometric models are reasonably consistent with the observed shapes. For Telesto, the best-fit model has a slightly higher  $b/a$  than was observed, and for Helene the best-fit model has a  $b/a = 1$ .

**Table 3.** Brightness Coefficients for Saturn’s Moons based on data between  $20^\circ$  and  $40^\circ$  phase assuming a Lambertian surface scattering law. The first error bars are statistical, second are systematic errors due to uncertainties in the object’s average size.

$B$ at $\alpha = 30^\circ$ $C_B = dB/d\alpha$ (per degree)	All Data	Sub-Saturn Quadrant	Leading Quadrant	Anti-Saturn Quadrant	Trailing Quadrant
Pan	0.6492 $\pm$ 0.0058 $\pm$ 0.0142 -0.0071 $\pm$ 0.0011 $\pm$ 0.0002	0.6398 $\pm$ 0.0233 $\pm$ 0.0140 -0.0135 $\pm$ 0.0041 $\pm$ 0.0003	0.6314 $\pm$ 0.0056 $\pm$ 0.0138 -0.0066 $\pm$ 0.0011 $\pm$ 0.0001	0.6293 $\pm$ 0.0126 $\pm$ 0.0138 -0.0056 $\pm$ 0.0022 $\pm$ 0.0001	0.6744 $\pm$ 0.0089 $\pm$ 0.0148 -0.0042 $\pm$ 0.0016 $\pm$ 0.0001
Atlas	0.6254 $\pm$ 0.0084 $\pm$ 0.0084 -0.0055 $\pm$ 0.0014 $\pm$ 0.0001	0.5960 $\pm$ 0.0092 $\pm$ 0.0080 -0.0151 $\pm$ 0.0015 $\pm$ 0.0002	0.6475 $\pm$ 0.0100 $\pm$ 0.0087 -0.0051 $\pm$ 0.0016 $\pm$ 0.0001	0.6334 $\pm$ 0.0242 $\pm$ 0.0085 -0.0070 $\pm$ 0.0046 $\pm$ 0.0001	0.5898 $\pm$ 0.0180 $\pm$ 0.0079 0.0026 $\pm$ 0.0031 $\pm$ 0.0000
Prometheus	0.7928 $\pm$ 0.0127 $\pm$ 0.0130 -0.0083 $\pm$ 0.0025 $\pm$ 0.0001	0.8153 $\pm$ 0.0184 $\pm$ 0.0133 -0.0038 $\pm$ 0.0048 $\pm$ 0.0001	0.7550 $\pm$ 0.0164 $\pm$ 0.0123 -0.0084 $\pm$ 0.0027 $\pm$ 0.0001	0.7924 $\pm$ 0.0236 $\pm$ 0.0130 -0.0062 $\pm$ 0.0047 $\pm$ 0.0001	0.8129 $\pm$ 0.0420 $\pm$ 0.0133 -0.0168 $\pm$ 0.0090 $\pm$ 0.0003
Pandora	0.7600 $\pm$ 0.0053 $\pm$ 0.0057 -0.0072 $\pm$ 0.0010 $\pm$ 0.0001	0.7638 $\pm$ 0.0320 $\pm$ 0.0057 -0.0089 $\pm$ 0.0054 $\pm$ 0.0001	0.7704 $\pm$ 0.0052 $\pm$ 0.0058 -0.0069 $\pm$ 0.0009 $\pm$ 0.0001	0.7570 $\pm$ 0.0225 $\pm$ 0.0057 -0.0049 $\pm$ 0.0049 $\pm$ 0.0000	0.7550 $\pm$ 0.0052 $\pm$ 0.0057 -0.0073 $\pm$ 0.0009 $\pm$ 0.0001
Janus	0.5305 $\pm$ 0.0082 $\pm$ 0.0027 -0.0075 $\pm$ 0.0015 $\pm$ 0.0000	0.5726 $\pm$ 0.0138 $\pm$ 0.0029 -0.0081 $\pm$ 0.0024 $\pm$ 0.0000	0.4654 $\pm$ 0.0055 $\pm$ 0.0024 -0.0069 $\pm$ 0.0009 $\pm$ 0.0000	0.4989 $\pm$ 0.0120 $\pm$ 0.0026 -0.0057 $\pm$ 0.0020 $\pm$ 0.0000	0.5814 $\pm$ 0.0043 $\pm$ 0.0030 -0.0104 $\pm$ 0.0010 $\pm$ 0.0001
Epimetheus	0.4628 $\pm$ 0.0060 $\pm$ 0.0026 -0.0049 $\pm$ 0.0010 $\pm$ 0.0000	0.4665 $\pm$ 0.0141 $\pm$ 0.0026 -0.0041 $\pm$ 0.0024 $\pm$ 0.0000	0.4480 $\pm$ 0.0038 $\pm$ 0.0025 -0.0042 $\pm$ 0.0006 $\pm$ 0.0000	0.4422 $\pm$ 0.0080 $\pm$ 0.0025 -0.0079 $\pm$ 0.0015 $\pm$ 0.0000	0.5188 $\pm$ 0.0103 $\pm$ 0.0029 -0.0076 $\pm$ 0.0019 $\pm$ 0.0000
Aegaeon	0.1793 $\pm$ 0.0050 $\pm$ 0.0326 -0.0009 $\pm$ 0.0009 $\pm$ 0.0002	0.1648 $\pm$ 0.0084 $\pm$ 0.0300 -0.0019 $\pm$ 0.0008 $\pm$ 0.0003	0.1582 $\pm$ 0.0042 $\pm$ 0.0288 -0.0034 $\pm$ 0.0006 $\pm$ 0.0006	0.1352 $\pm$ 0.0921 $\pm$ 0.0246 -0.0086 $\pm$ 0.0183 $\pm$ 0.0016	0.2437 $\pm$ 0.0145 $\pm$ 0.0443 -0.0056 $\pm$ 0.0022 $\pm$ 0.0010
Mimas	0.7546 $\pm$ 0.0028 $\pm$ 0.0015 -0.0072 $\pm$ 0.0006 $\pm$ 0.0000	0.7533 $\pm$ 0.0040 $\pm$ 0.0015 -0.0093 $\pm$ 0.0009 $\pm$ 0.0000	0.7340 $\pm$ 0.0016 $\pm$ 0.0015 -0.0081 $\pm$ 0.0004 $\pm$ 0.0000	0.7622 $\pm$ 0.0073 $\pm$ 0.0015 -0.0079 $\pm$ 0.0012 $\pm$ 0.0000	0.7862 $\pm$ 0.0034 $\pm$ 0.0016 -0.0075 $\pm$ 0.0007 $\pm$ 0.0000
Methone	0.5558 $\pm$ 0.0033 $\pm$ 0.0115 -0.0058 $\pm$ 0.0006 $\pm$ 0.0001	0.5631 $\pm$ 0.0081 $\pm$ 0.0117 -0.0048 $\pm$ 0.0003 $\pm$ 0.0001	0.5529 $\pm$ 0.0042 $\pm$ 0.0114 -0.0060 $\pm$ 0.0009 $\pm$ 0.0001	0.5542 $\pm$ 0.0083 $\pm$ 0.0115 -0.0073 $\pm$ 0.0015 $\pm$ 0.0002	0.5498 $\pm$ 0.0066 $\pm$ 0.0114 -0.0049 $\pm$ 0.0011 $\pm$ 0.0001
Pallene	0.5228 $\pm$ 0.0066 $\pm$ 0.0164 -0.0071 $\pm$ 0.0011 $\pm$ 0.0002	0.5556 $\pm$ 0.0126 $\pm$ 0.0174 -0.0051 $\pm$ 0.0005 $\pm$ 0.0002	0.4660 $\pm$ 0.0057 $\pm$ 0.0146 -0.0076 $\pm$ 0.0012 $\pm$ 0.0002	0.5519 $\pm$ 0.0114 $\pm$ 0.0173 -0.0085 $\pm$ 0.0021 $\pm$ 0.0003	0.5267 $\pm$ 0.0078 $\pm$ 0.0165 -0.0052 $\pm$ 0.0012 $\pm$ 0.0002
Enceladus	1.1530 $\pm$ 0.0029 $\pm$ 0.0009 -0.0107 $\pm$ 0.0005 $\pm$ 0.0000	1.1451 $\pm$ 0.0034 $\pm$ 0.0009 -0.0104 $\pm$ 0.0006 $\pm$ 0.0000	1.1215 $\pm$ 0.0043 $\pm$ 0.0009 -0.0095 $\pm$ 0.0010 $\pm$ 0.0000	1.1580 $\pm$ 0.0049 $\pm$ 0.0009 -0.0126 $\pm$ 0.0009 $\pm$ 0.0000	1.1711 $\pm$ 0.0034 $\pm$ 0.0009 -0.0103 $\pm$ 0.0006 $\pm$ 0.0000
Tethys	0.9363 $\pm$ 0.0046 $\pm$ 0.0011 -0.0094 $\pm$ 0.0008 $\pm$ 0.0000	0.9408 $\pm$ 0.0050 $\pm$ 0.0011 -0.0103 $\pm$ 0.0008 $\pm$ 0.0000	0.9550 $\pm$ 0.0035 $\pm$ 0.0011 -0.0087 $\pm$ 0.0007 $\pm$ 0.0000	0.9704 $\pm$ 0.0106 $\pm$ 0.0011 -0.0086 $\pm$ 0.0022 $\pm$ 0.0000	0.8903 $\pm$ 0.0067 $\pm$ 0.0010 -0.0081 $\pm$ 0.0011 $\pm$ 0.0000
Telesto	0.9028 $\pm$ 0.0100 $\pm$ 0.0220 -0.0125 $\pm$ 0.0019 $\pm$ 0.0003	0.9365 $\pm$ 0.0148 $\pm$ 0.0228 -0.0088 $\pm$ 0.0006 $\pm$ 0.0002	0.8383 $\pm$ 0.0087 $\pm$ 0.0204 -0.0084 $\pm$ 0.0014 $\pm$ 0.0002	0.9671 $\pm$ 0.0147 $\pm$ 0.0236 -0.0151 $\pm$ 0.0034 $\pm$ 0.0004	0.8494 $\pm$ 0.0216 $\pm$ 0.0207 -0.0112 $\pm$ 0.0042 $\pm$ 0.0003
Calypso	1.0999 $\pm$ 0.0176 $\pm$ 0.0463 -0.1444 $\pm$ 0.0032 $\pm$ 0.0006	1.0628 $\pm$ 0.0224 $\pm$ 0.0448 -0.0123 $\pm$ 0.0011 $\pm$ 0.0005	1.1331 $\pm$ 0.0239 $\pm$ 0.0477 -0.0107 $\pm$ 0.0045 $\pm$ 0.0004	1.1645 $\pm$ 0.0240 $\pm$ 0.0490 -0.0251 $\pm$ 0.0061 $\pm$ 0.0011	1.2138 $\pm$ 0.0712 $\pm$ 0.0511 -0.0028 $\pm$ 0.0134 $\pm$ 0.0001
Dione	0.6785 $\pm$ 0.0099 $\pm$ 0.0005 -0.0088 $\pm$ 0.0017 $\pm$ 0.0000	0.6669 $\pm$ 0.0105 $\pm$ 0.0005 -0.0039 $\pm$ 0.0020 $\pm$ 0.0000	0.7634 $\pm$ 0.0094 $\pm$ 0.0005 -0.0064 $\pm$ 0.0015 $\pm$ 0.0000	0.7027 $\pm$ 0.0151 $\pm$ 0.0005 -0.0062 $\pm$ 0.0033 $\pm$ 0.0000	0.5561 $\pm$ 0.0144 $\pm$ 0.0004 -0.0049 $\pm$ 0.0021 $\pm$ 0.0000
Helene	1.0251 $\pm$ 0.0148 $\pm$ 0.0113 -0.0196 $\pm$ 0.0027 $\pm$ 0.0002	1.0807 $\pm$ 0.0187 $\pm$ 0.0119 -0.0086 $\pm$ 0.0007 $\pm$ 0.0001	0.8373 $\pm$ 0.1644 $\pm$ 0.0093 -0.0074 $\pm$ 0.0224 $\pm$ 0.0001	1.0544 $\pm$ 0.0308 $\pm$ 0.0117 -0.0169 $\pm$ 0.0058 $\pm$ 0.0002	0.9522 $\pm$ 0.0289 $\pm$ 0.0105 -0.0001 $\pm$ 0.0064 $\pm$ 0.0000
Polydeuces	0.6075 $\pm$ 0.0089 $\pm$ 0.0794 -0.0071 $\pm$ 0.0016 $\pm$ 0.0009	0.6034 $\pm$ 0.0120 $\pm$ 0.0789 -0.0073 $\pm$ 0.0006 $\pm$ 0.0010	0.6476 $\pm$ 0.0205 $\pm$ 0.0846 -0.0072 $\pm$ 0.0030 $\pm$ 0.0009	0.5945 $\pm$ 0.0090 $\pm$ 0.0777 -0.0094 $\pm$ 0.0017 $\pm$ 0.0012	0.6266 $\pm$ 0.0121 $\pm$ 0.0819 -0.0300 $\pm$ 0.0029 $\pm$ 0.0039
Rhea	0.7144 $\pm$ 0.0057 $\pm$ 0.0006 -0.0110 $\pm$ 0.0011 $\pm$ 0.0000	0.6967 $\pm$ 0.0066 $\pm$ 0.0005 -0.0109 $\pm$ 0.0011 $\pm$ 0.0000	0.7937 $\pm$ 0.0046 $\pm$ 0.0006 -0.0093 $\pm$ 0.0009 $\pm$ 0.0000	0.7146 $\pm$ 0.0042 $\pm$ 0.0006 -0.0120 $\pm$ 0.0011 $\pm$ 0.0000	0.6321 $\pm$ 0.0031 $\pm$ 0.0005 -0.0065 $\pm$ 0.0004 $\pm$ 0.0000

**Table 4.** Brightness Coefficients for Saturn’s Moons based on data between  $20^\circ$  and  $40^\circ$  phase assuming a Minnaert surface scattering law with  $k = 0.75$ . The first error bars are statistical, second are systematic errors due to uncertainties in the object’s average size.

$B$ at $\alpha = 30^\circ$ $C_B = dB/d\alpha$ (per degree)	All Data	Sub-Saturn Quadrant	Leading Quadrant	Anti-Saturn Quadrant	Trailing Quadrant
Pan	0.6379 $\pm$ 0.0061 $\pm$ 0.0140 -0.0080 $\pm$ 0.0011 $\pm$ 0.0002	0.6289 $\pm$ 0.0284 $\pm$ 0.0138 -0.0152 $\pm$ 0.0050 $\pm$ 0.0003	0.6190 $\pm$ 0.0060 $\pm$ 0.0136 -0.0072 $\pm$ 0.0012 $\pm$ 0.0002	0.6166 $\pm$ 0.0144 $\pm$ 0.0135 -0.0063 $\pm$ 0.0025 $\pm$ 0.0001	0.6633 $\pm$ 0.0091 $\pm$ 0.0145 -0.0053 $\pm$ 0.0016 $\pm$ 0.0001
Atlas	0.6122 $\pm$ 0.0088 $\pm$ 0.0082 -0.0064 $\pm$ 0.0015 $\pm$ 0.0001	0.5863 $\pm$ 0.0108 $\pm$ 0.0079 -0.0174 $\pm$ 0.0018 $\pm$ 0.0002	0.6347 $\pm$ 0.0110 $\pm$ 0.0085 -0.0058 $\pm$ 0.0017 $\pm$ 0.0001	0.6126 $\pm$ 0.0215 $\pm$ 0.0082 -0.0074 $\pm$ 0.0041 $\pm$ 0.0001	0.5787 $\pm$ 0.0187 $\pm$ 0.0078 0.0016 $\pm$ 0.0032 $\pm$ 0.0000
Prometheus	0.7702 $\pm$ 0.0127 $\pm$ 0.0126 -0.0108 $\pm$ 0.0025 $\pm$ 0.0002	0.8051 $\pm$ 0.0208 $\pm$ 0.0132 -0.0114 $\pm$ 0.0054 $\pm$ 0.0002	0.7404 $\pm$ 0.0184 $\pm$ 0.0121 -0.0089 $\pm$ 0.0031 $\pm$ 0.0001	0.7668 $\pm$ 0.0236 $\pm$ 0.0125 -0.0108 $\pm$ 0.0047 $\pm$ 0.0002	0.7848 $\pm$ 0.0398 $\pm$ 0.0128 -0.0198 $\pm$ 0.0086 $\pm$ 0.0003
Pandora	0.7498 $\pm$ 0.0052 $\pm$ 0.0056 -0.0075 $\pm$ 0.0010 $\pm$ 0.0001	0.7639 $\pm$ 0.0299 $\pm$ 0.0057 -0.0102 $\pm$ 0.0051 $\pm$ 0.0001	0.7577 $\pm$ 0.0061 $\pm$ 0.0057 -0.0073 $\pm$ 0.0011 $\pm$ 0.0001	0.7397 $\pm$ 0.0220 $\pm$ 0.0055 -0.0048 $\pm$ 0.0048 $\pm$ 0.0000	0.7481 $\pm$ 0.0059 $\pm$ 0.0056 -0.0078 $\pm$ 0.0011 $\pm$ 0.0001
Janus	0.5257 $\pm$ 0.0084 $\pm$ 0.0027 -0.0077 $\pm$ 0.0015 $\pm$ 0.0000	0.5692 $\pm$ 0.0142 $\pm$ 0.0029 -0.0085 $\pm$ 0.0025 $\pm$ 0.0000	0.4595 $\pm$ 0.0054 $\pm$ 0.0024 -0.0070 $\pm$ 0.0009 $\pm$ 0.0000	0.4924 $\pm$ 0.0115 $\pm$ 0.0025 -0.0058 $\pm$ 0.0019 $\pm$ 0.0000	0.5777 $\pm$ 0.0051 $\pm$ 0.0030 -0.0107 $\pm$ 0.0012 $\pm$ 0.0001
Epimetheus	0.4588 $\pm$ 0.0060 $\pm$ 0.0026 -0.0051 $\pm$ 0.0011 $\pm$ 0.0000	0.4651 $\pm$ 0.0145 $\pm$ 0.0026 -0.0043 $\pm$ 0.0024 $\pm$ 0.0000	0.4433 $\pm$ 0.0039 $\pm$ 0.0025 -0.0045 $\pm$ 0.0006 $\pm$ 0.0000	0.4375 $\pm$ 0.0078 $\pm$ 0.0025 -0.0083 $\pm$ 0.0015 $\pm$ 0.0000	0.5136 $\pm$ 0.0105 $\pm$ 0.0029 -0.0078 $\pm$ 0.0019 $\pm$ 0.0000
Aegaeon	0.1758 $\pm$ 0.0049 $\pm$ 0.0320 -0.0008 $\pm$ 0.0008 $\pm$ 0.0001	0.1620 $\pm$ 0.0079 $\pm$ 0.0295 -0.0016 $\pm$ 0.0008 $\pm$ 0.0003	0.1512 $\pm$ 0.0042 $\pm$ 0.0275 -0.0037 $\pm$ 0.0006 $\pm$ 0.0007	0.1323 $\pm$ 0.0939 $\pm$ 0.0241 -0.0099 $\pm$ 0.0186 $\pm$ 0.0018	0.2386 $\pm$ 0.0138 $\pm$ 0.0434 -0.0054 $\pm$ 0.0021 $\pm$ 0.0010
Mimas	0.7498 $\pm$ 0.0028 $\pm$ 0.0015 -0.0073 $\pm$ 0.0006 $\pm$ 0.0000	0.7506 $\pm$ 0.0038 $\pm$ 0.0015 -0.0094 $\pm$ 0.0008 $\pm$ 0.0000	0.7285 $\pm$ 0.0015 $\pm$ 0.0015 -0.0082 $\pm$ 0.0004 $\pm$ 0.0000	0.7576 $\pm$ 0.0076 $\pm$ 0.0015 -0.0082 $\pm$ 0.0013 $\pm$ 0.0000	0.7796 $\pm$ 0.0037 $\pm$ 0.0016 -0.0076 $\pm$ 0.0008 $\pm$ 0.0000
Methone	0.5508 $\pm$ 0.0035 $\pm$ 0.0114 -0.0070 $\pm$ 0.0007 $\pm$ 0.0001	0.5663 $\pm$ 0.0087 $\pm$ 0.0117 -0.0050 $\pm$ 0.0003 $\pm$ 0.0001	0.5488 $\pm$ 0.0043 $\pm$ 0.0114 -0.0064 $\pm$ 0.0009 $\pm$ 0.0001	0.5423 $\pm$ 0.0073 $\pm$ 0.0112 -0.0090 $\pm$ 0.0014 $\pm$ 0.0002	0.5415 $\pm$ 0.0074 $\pm$ 0.0112 -0.0064 $\pm$ 0.0013 $\pm$ 0.0001
Pallene	0.5181 $\pm$ 0.0064 $\pm$ 0.0163 -0.0077 $\pm$ 0.0011 $\pm$ 0.0002	0.5537 $\pm$ 0.0127 $\pm$ 0.0174 -0.0052 $\pm$ 0.0005 $\pm$ 0.0002	0.4622 $\pm$ 0.0050 $\pm$ 0.0145 -0.0078 $\pm$ 0.0010 $\pm$ 0.0002	0.5468 $\pm$ 0.0097 $\pm$ 0.0172 -0.0095 $\pm$ 0.0018 $\pm$ 0.0003	0.5210 $\pm$ 0.0065 $\pm$ 0.0164 -0.0058 $\pm$ 0.0010 $\pm$ 0.0002
Enceladus	1.1462 $\pm$ 0.0029 $\pm$ 0.0009 -0.0110 $\pm$ 0.0005 $\pm$ 0.0000	1.1391 $\pm$ 0.0035 $\pm$ 0.0009 -0.0108 $\pm$ 0.0006 $\pm$ 0.0000	1.1146 $\pm$ 0.0043 $\pm$ 0.0009 -0.0099 $\pm$ 0.0010 $\pm$ 0.0000	1.1511 $\pm$ 0.0048 $\pm$ 0.0009 -0.0130 $\pm$ 0.0009 $\pm$ 0.0000	1.1639 $\pm$ 0.0035 $\pm$ 0.0009 -0.0106 $\pm$ 0.0006 $\pm$ 0.0000
Tethys	0.9311 $\pm$ 0.0046 $\pm$ 0.0011 -0.0096 $\pm$ 0.0008 $\pm$ 0.0000	0.9360 $\pm$ 0.0049 $\pm$ 0.0011 -0.0105 $\pm$ 0.0008 $\pm$ 0.0000	0.9494 $\pm$ 0.0035 $\pm$ 0.0011 -0.0090 $\pm$ 0.0007 $\pm$ 0.0000	0.9645 $\pm$ 0.0108 $\pm$ 0.0011 -0.0087 $\pm$ 0.0023 $\pm$ 0.0000	0.8849 $\pm$ 0.0065 $\pm$ 0.0010 -0.0083 $\pm$ 0.0010 $\pm$ 0.0000
Telesto	0.8915 $\pm$ 0.0103 $\pm$ 0.0217 -0.0134 $\pm$ 0.0019 $\pm$ 0.0003	0.9298 $\pm$ 0.0150 $\pm$ 0.0227 -0.0085 $\pm$ 0.0006 $\pm$ 0.0002	0.8245 $\pm$ 0.0067 $\pm$ 0.0201 -0.0094 $\pm$ 0.0011 $\pm$ 0.0002	0.9545 $\pm$ 0.0162 $\pm$ 0.0233 -0.0169 $\pm$ 0.0037 $\pm$ 0.0004	0.8341 $\pm$ 0.0185 $\pm$ 0.0203 -0.0107 $\pm$ 0.0036 $\pm$ 0.0003
Calypso	1.0928 $\pm$ 0.0196 $\pm$ 0.0460 -0.0143 $\pm$ 0.0035 $\pm$ 0.0006	1.0672 $\pm$ 0.0257 $\pm$ 0.0449 -0.0125 $\pm$ 0.0012 $\pm$ 0.0005	1.1091 $\pm$ 0.0336 $\pm$ 0.0467 -0.0126 $\pm$ 0.0064 $\pm$ 0.0005	1.1360 $\pm$ 0.0286 $\pm$ 0.0478 -0.0226 $\pm$ 0.0073 $\pm$ 0.0010	1.2102 $\pm$ 0.0790 $\pm$ 0.0510 -0.0026 $\pm$ 0.0148 $\pm$ 0.0001
Dione	0.6747 $\pm$ 0.0098 $\pm$ 0.0005 -0.0090 $\pm$ 0.0017 $\pm$ 0.0000	0.6631 $\pm$ 0.0104 $\pm$ 0.0005 -0.0041 $\pm$ 0.0020 $\pm$ 0.0000	0.7591 $\pm$ 0.0093 $\pm$ 0.0005 -0.0066 $\pm$ 0.0015 $\pm$ 0.0000	0.6987 $\pm$ 0.0151 $\pm$ 0.0005 -0.0063 $\pm$ 0.0032 $\pm$ 0.0000	0.5530 $\pm$ 0.0142 $\pm$ 0.0004 -0.0051 $\pm$ 0.0020 $\pm$ 0.0000
Helene	1.0163 $\pm$ 0.0150 $\pm$ 0.0112 -0.0201 $\pm$ 0.0027 $\pm$ 0.0002	1.0758 $\pm$ 0.0184 $\pm$ 0.0119 -0.0088 $\pm$ 0.0007 $\pm$ 0.0001	0.8208 $\pm$ 0.02026 $\pm$ 0.0091 -0.0081 $\pm$ 0.0276 $\pm$ 0.0001	1.0479 $\pm$ 0.0289 $\pm$ 0.0116 -0.0153 $\pm$ 0.0054 $\pm$ 0.0002	0.9473 $\pm$ 0.0256 $\pm$ 0.0105 -0.0012 $\pm$ 0.0057 $\pm$ 0.0000
Polydeuces	0.6016 $\pm$ 0.0090 $\pm$ 0.0786 -0.0074 $\pm$ 0.0016 $\pm$ 0.0010	0.6016 $\pm$ 0.0121 $\pm$ 0.0786 -0.0075 $\pm$ 0.0006 $\pm$ 0.0010	0.6375 $\pm$ 0.0212 $\pm$ 0.0833 -0.0071 $\pm$ 0.0031 $\pm$ 0.0009	0.5867 $\pm$ 0.0087 $\pm$ 0.0767 -0.0099 $\pm$ 0.0017 $\pm$ 0.0013	0.6201 $\pm$ 0.0090 $\pm$ 0.0811 -0.0310 $\pm$ 0.0022 $\pm$ 0.0041
Rhea	0.7104 $\pm$ 0.0056 $\pm$ 0.0006 -0.0112 $\pm$ 0.0011 $\pm$ 0.0000	0.6928 $\pm$ 0.0066 $\pm$ 0.0005 -0.0111 $\pm$ 0.0011 $\pm$ 0.0000	0.7894 $\pm$ 0.0046 $\pm$ 0.0006 -0.0094 $\pm$ 0.0008 $\pm$ 0.0000	0.7106 $\pm$ 0.0042 $\pm$ 0.0006 -0.0121 $\pm$ 0.0011 $\pm$ 0.0000	0.6286 $\pm$ 0.0031 $\pm$ 0.0005 -0.0067 $\pm$ 0.0004 $\pm$ 0.0000

**Table 5.** Brightness Coefficients for Saturn’s Moons based on data between  $20^\circ$  and  $40^\circ$  phase assuming a Minnaert surface scattering law with  $k = 0.50$ . The first error bars are statistical, second are systematic errors due to uncertainties in the object’s average size.

$B$ at $\alpha = 30^\circ$ $C_B = dB/d\alpha$ (per degree)	All Data	Sub-Saturn Quadrant	Leading Quadrant	Anti-Saturn Quadrant	Trailing Quadrant
Pan	0.6181 $\pm$ 0.0066 $\pm$ 0.0135 -0.0093 $\pm$ 0.0012 $\pm$ 0.0002	0.6099 $\pm$ 0.0346 $\pm$ 0.0134 -0.0174 $\pm$ 0.0061 $\pm$ 0.0004	0.5976 $\pm$ 0.0068 $\pm$ 0.0131 -0.0079 $\pm$ 0.0013 $\pm$ 0.0002	0.5935 $\pm$ 0.0172 $\pm$ 0.0130 -0.0072 $\pm$ 0.0030 $\pm$ 0.0002	0.6444 $\pm$ 0.0099 $\pm$ 0.0141 -0.0067 $\pm$ 0.0018 $\pm$ 0.0001
Atlas	0.5903 $\pm$ 0.0095 $\pm$ 0.0079 -0.0075 $\pm$ 0.0016 $\pm$ 0.0001	0.5682 $\pm$ 0.0141 $\pm$ 0.0076 -0.0202 $\pm$ 0.0024 $\pm$ 0.0003	0.6134 $\pm$ 0.0124 $\pm$ 0.0082 -0.0066 $\pm$ 0.0019 $\pm$ 0.0001	0.5808 $\pm$ 0.0207 $\pm$ 0.0078 -0.0080 $\pm$ 0.0039 $\pm$ 0.0001	0.5595 $\pm$ 0.0201 $\pm$ 0.0075 0.0006 $\pm$ 0.0034 $\pm$ 0.0000
Prometheus	0.7362 $\pm$ 0.0130 $\pm$ 0.0120 -0.0138 $\pm$ 0.0025 $\pm$ 0.0002	0.7796 $\pm$ 0.0255 $\pm$ 0.0128 -0.0192 $\pm$ 0.0066 $\pm$ 0.0003	0.7167 $\pm$ 0.0207 $\pm$ 0.0117 -0.0096 $\pm$ 0.0035 $\pm$ 0.0002	0.7280 $\pm$ 0.0242 $\pm$ 0.0119 -0.0160 $\pm$ 0.0048 $\pm$ 0.0003	0.7486 $\pm$ 0.0375 $\pm$ 0.0122 -0.0225 $\pm$ 0.0081 $\pm$ 0.0004
Pandora	0.7299 $\pm$ 0.0057 $\pm$ 0.0055 -0.0082 $\pm$ 0.0010 $\pm$ 0.0001	0.7540 $\pm$ 0.0330 $\pm$ 0.0057 -0.0118 $\pm$ 0.0056 $\pm$ 0.0001	0.7349 $\pm$ 0.0072 $\pm$ 0.0055 -0.0082 $\pm$ 0.0013 $\pm$ 0.0001	0.7105 $\pm$ 0.0217 $\pm$ 0.0053 -0.0051 $\pm$ 0.0047 $\pm$ 0.0000	0.7329 $\pm$ 0.0074 $\pm$ 0.0055 -0.0086 $\pm$ 0.0013 $\pm$ 0.0001
Janus	0.5143 $\pm$ 0.0086 $\pm$ 0.0026 -0.0082 $\pm$ 0.0015 $\pm$ 0.0000	0.5589 $\pm$ 0.0146 $\pm$ 0.0029 -0.0091 $\pm$ 0.0026 $\pm$ 0.0000	0.4478 $\pm$ 0.0055 $\pm$ 0.0023 -0.0074 $\pm$ 0.0009 $\pm$ 0.0000	0.4791 $\pm$ 0.0110 $\pm$ 0.0025 -0.0061 $\pm$ 0.0018 $\pm$ 0.0000	0.5672 $\pm$ 0.0060 $\pm$ 0.0029 -0.0112 $\pm$ 0.0014 $\pm$ 0.0001
Epimetheus	0.4494 $\pm$ 0.0061 $\pm$ 0.0025 -0.0056 $\pm$ 0.0011 $\pm$ 0.0000	0.4579 $\pm$ 0.0149 $\pm$ 0.0026 -0.0047 $\pm$ 0.0025 $\pm$ 0.0000	0.4336 $\pm$ 0.0040 $\pm$ 0.0024 -0.0050 $\pm$ 0.0007 $\pm$ 0.0000	0.4272 $\pm$ 0.0075 $\pm$ 0.0024 -0.0088 $\pm$ 0.0014 $\pm$ 0.0000	0.5027 $\pm$ 0.0108 $\pm$ 0.0028 -0.0082 $\pm$ 0.0020 $\pm$ 0.0000
Aegaeon	0.1712 $\pm$ 0.0048 $\pm$ 0.0311 -0.0007 $\pm$ 0.0008 $\pm$ 0.0001	0.1578 $\pm$ 0.0077 $\pm$ 0.0287 -0.0015 $\pm$ 0.0008 $\pm$ 0.0003	0.1440 $\pm$ 0.0044 $\pm$ 0.0262 -0.0040 $\pm$ 0.0007 $\pm$ 0.0007	0.1245 $\pm$ 0.0952 $\pm$ 0.0226 -0.0119 $\pm$ 0.0189 $\pm$ 0.0022	0.2322 $\pm$ 0.0132 $\pm$ 0.0422 -0.0053 $\pm$ 0.0020 $\pm$ 0.0010
Mimas	0.7362 $\pm$ 0.0028 $\pm$ 0.0015 -0.0077 $\pm$ 0.0006 $\pm$ 0.0000	0.7391 $\pm$ 0.0036 $\pm$ 0.0015 -0.0099 $\pm$ 0.0008 $\pm$ 0.0000	0.7147 $\pm$ 0.0015 $\pm$ 0.0014 -0.0085 $\pm$ 0.0004 $\pm$ 0.0000	0.7438 $\pm$ 0.0079 $\pm$ 0.0015 -0.0088 $\pm$ 0.0013 $\pm$ 0.0000	0.7640 $\pm$ 0.0041 $\pm$ 0.0015 -0.0080 $\pm$ 0.0008 $\pm$ 0.0000
Methone	0.5396 $\pm$ 0.0043 $\pm$ 0.0112 -0.0085 $\pm$ 0.0008 $\pm$ 0.0002	0.5621 $\pm$ 0.0102 $\pm$ 0.0116 -0.0054 $\pm$ 0.0004 $\pm$ 0.0001	0.5395 $\pm$ 0.0056 $\pm$ 0.0112 -0.0072 $\pm$ 0.0011 $\pm$ 0.0001	0.5228 $\pm$ 0.0073 $\pm$ 0.0108 -0.0109 $\pm$ 0.0013 $\pm$ 0.0002	0.5282 $\pm$ 0.0086 $\pm$ 0.0109 -0.0080 $\pm$ 0.0015 $\pm$ 0.0002
Pallene	0.5070 $\pm$ 0.0063 $\pm$ 0.0159 -0.0086 $\pm$ 0.0011 $\pm$ 0.0003	0.5436 $\pm$ 0.0134 $\pm$ 0.0171 -0.0055 $\pm$ 0.0036 $\pm$ 0.0002	0.4538 $\pm$ 0.0049 $\pm$ 0.0142 -0.0080 $\pm$ 0.0010 $\pm$ 0.0003	0.5336 $\pm$ 0.0087 $\pm$ 0.0168 -0.0107 $\pm$ 0.0016 $\pm$ 0.0003	0.5098 $\pm$ 0.0057 $\pm$ 0.0160 -0.0066 $\pm$ 0.0009 $\pm$ 0.0002
Enceladus	1.1264 $\pm$ 0.0029 $\pm$ 0.0009 -0.0120 $\pm$ 0.0005 $\pm$ 0.0000	1.1200 $\pm$ 0.0036 $\pm$ 0.0009 -0.0118 $\pm$ 0.0007 $\pm$ 0.0000	1.0949 $\pm$ 0.0044 $\pm$ 0.0009 -0.0107 $\pm$ 0.0010 $\pm$ 0.0000	1.1310 $\pm$ 0.0048 $\pm$ 0.0009 -0.0139 $\pm$ 0.0008 $\pm$ 0.0000	1.1433 $\pm$ 0.0036 $\pm$ 0.0009 -0.0115 $\pm$ 0.0006 $\pm$ 0.0000
Tethys	0.9152 $\pm$ 0.0045 $\pm$ 0.0010 -0.0103 $\pm$ 0.0008 $\pm$ 0.0000	0.9205 $\pm$ 0.0048 $\pm$ 0.0010 -0.0112 $\pm$ 0.0008 $\pm$ 0.0000	0.9330 $\pm$ 0.0034 $\pm$ 0.0011 -0.0097 $\pm$ 0.0006 $\pm$ 0.0000	0.9474 $\pm$ 0.0109 $\pm$ 0.0011 -0.0093 $\pm$ 0.0023 $\pm$ 0.0000	0.8694 $\pm$ 0.0063 $\pm$ 0.0010 -0.0089 $\pm$ 0.0010 $\pm$ 0.0000
Telesto	0.8680 $\pm$ 0.0107 $\pm$ 0.0212 -0.0144 $\pm$ 0.0020 $\pm$ 0.0004	0.9083 $\pm$ 0.0154 $\pm$ 0.0222 -0.0086 $\pm$ 0.0006 $\pm$ 0.0002	0.8019 $\pm$ 0.0064 $\pm$ 0.0196 -0.0106 $\pm$ 0.0010 $\pm$ 0.0003	0.9258 $\pm$ 0.0201 $\pm$ 0.0226 -0.0193 $\pm$ 0.0047 $\pm$ 0.0005	0.8096 $\pm$ 0.0149 $\pm$ 0.0197 -0.0103 $\pm$ 0.0029 $\pm$ 0.0003
Calypso	1.0692 $\pm$ 0.0227 $\pm$ 0.0450 -0.0142 $\pm$ 0.0041 $\pm$ 0.0006	1.0550 $\pm$ 0.0296 $\pm$ 0.0444 -0.0128 $\pm$ 0.0014 $\pm$ 0.0005	1.0738 $\pm$ 0.0437 $\pm$ 0.0452 -0.0150 $\pm$ 0.0083 $\pm$ 0.0006	1.0868 $\pm$ 0.0374 $\pm$ 0.0458 -0.0196 $\pm$ 0.0095 $\pm$ 0.0008	1.1901 $\pm$ 0.0861 $\pm$ 0.0501 -0.0032 $\pm$ 0.0162 $\pm$ 0.0001
Dione	0.6632 $\pm$ 0.0097 $\pm$ 0.0005 -0.0094 $\pm$ 0.0017 $\pm$ 0.0000	0.6517 $\pm$ 0.0103 $\pm$ 0.0005 -0.0046 $\pm$ 0.0019 $\pm$ 0.0000	0.7462 $\pm$ 0.0092 $\pm$ 0.0005 -0.0072 $\pm$ 0.0014 $\pm$ 0.0000	0.6868 $\pm$ 0.0149 $\pm$ 0.0005 -0.0069 $\pm$ 0.0032 $\pm$ 0.0000	0.5435 $\pm$ 0.0139 $\pm$ 0.0004 -0.0055 $\pm$ 0.0020 $\pm$ 0.0000
Helene	0.9935 $\pm$ 0.0151 $\pm$ 0.0110 -0.0204 $\pm$ 0.0028 $\pm$ 0.0002	1.0543 $\pm$ 0.0174 $\pm$ 0.0116 -0.0094 $\pm$ 0.0007 $\pm$ 0.0001	0.7958 $\pm$ 0.2351 $\pm$ 0.0088 -0.0090 $\pm$ 0.0320 $\pm$ 0.0001	1.0264 $\pm$ 0.0275 $\pm$ 0.0113 -0.0139 $\pm$ 0.0052 $\pm$ 0.0002	0.9315 $\pm$ 0.0215 $\pm$ 0.0103 -0.0029 $\pm$ 0.0048 $\pm$ 0.0000
Polydeuces	0.5879 $\pm$ 0.0090 $\pm$ 0.0769 -0.0079 $\pm$ 0.0016 $\pm$ 0.0010	0.5925 $\pm$ 0.0123 $\pm$ 0.0774 -0.0079 $\pm$ 0.0006 $\pm$ 0.0010	0.6206 $\pm$ 0.0215 $\pm$ 0.0811 -0.0073 $\pm$ 0.0032 $\pm$ 0.0010	0.5705 $\pm$ 0.0084 $\pm$ 0.0746 -0.0106 $\pm$ 0.0016 $\pm$ 0.0014	0.6065 $\pm$ 0.0060 $\pm$ 0.0793 -0.0322 $\pm$ 0.0014 $\pm$ 0.0042
Rhea	0.6984 $\pm$ 0.0055 $\pm$ 0.0005 -0.0116 $\pm$ 0.0011 $\pm$ 0.0000	0.6811 $\pm$ 0.0065 $\pm$ 0.0005 -0.0115 $\pm$ 0.0011 $\pm$ 0.0000	0.7760 $\pm$ 0.0044 $\pm$ 0.0006 -0.0100 $\pm$ 0.0008 $\pm$ 0.0000	0.6985 $\pm$ 0.0041 $\pm$ 0.0005 -0.0126 $\pm$ 0.0011 $\pm$ 0.0000	0.6179 $\pm$ 0.0031 $\pm$ 0.0005 -0.0071 $\pm$ 0.0004 $\pm$ 0.0000

#### 4. BRIGHTNESS TRENDS AMONG SATURN'S SMALL MOONS

The GEPM appears to provide reasonably consistent surface brightness estimates for moons with a range of sizes and shapes, so we will now compare these brightness estimates for the different moons and identify trends that might clarify the processes responsible for determining the moons' visible surface brightness. We begin by describing the specific brightness values we will use for this project in Section 4.1. Section 4.2 then shows how these brightness parameters for the mid-sized moons correlate with the local flux of E-ring particles, which is consistent with prior work. Next, Section 4.3 examines why some of the small moons are darker than expected given their locations within the E ring, and shows that high-energy proton radiation probably also influences the moons' surface brightness. Finally, Section 4.4 discusses the small moons that are brighter than one might expect given their locations.

##### 4.1. Comparable brightness estimates for Saturn's moons

The calculations described in Section 3 demonstrate that our model is a sensible way to quantify the surface brightness of elongated moons. However, the absolute values of  $B$  derived by this method are not directly comparable to traditional parameters like geometric or Bond albedos previously reported in the literature. In principle, the derived values of  $B$  as functions of phase angle could be extrapolated to zero, and then we could translate that value of  $B$  to a geometric albedo for an equivalent spherical object. However, in practice performing such an extrapolation would be problematic because the small moons were rarely observed by Cassini at phase angles below 10°, so we have no information about the magnitude or shape of the opposition surges for these bodies. Also, since these objects are not spherical, the amount of light scattered will depend on the orientation of the body, which complicates the classical definition of albedo. On the other hand, it is relatively straightforward to estimate  $B$  for Saturn's other moons, and so we have chosen that approach for this analysis.

In order to compare the reflectances of these objects, we only consider the data obtained between phase angles of 20° and 40°, and fit the brightness coefficients in this phase range to a linear function of phase angle  $\alpha$ :

$$B(\alpha) = B_0 + (\alpha - 30^\circ)C_B \quad (14)$$

Note that  $B_0$  is the brightness coefficient at 30° phase, which is in the middle of the range of observed phase angles and so does not depend on any questionable extrapolations. For a spherical object of radius  $r$  observed at 0° and 30° phase,  $a_{\text{pred}} = 2.12r^2$  and  $1.86r^2$  respectively for a Lambertian scattering law (for a Minnaert scattering law with  $k = 0.5$ , these numbers become  $a_{\text{pred}} = 2.12r^2$  and  $1.91r^2$ , respectively). Hence the average reflectance the object would have at 30° if it were a sphere is  $\langle I/F \rangle_{\text{sphere}} = 0.59B_0$  for a Lambertian scattering law (or  $\langle I/F \rangle_{\text{sphere}} = 0.61B_0$  for a Minnaert  $k = 0.5$  scattering law). The corresponding geometric albedo of the object assuming that the linear phase function could be extrapolated to an appropriately small phase angle  $\alpha_0$  would be<sup>2</sup>

$$\mathcal{A}_{\text{sphere}} = 0.67[B_0 + (\alpha_0 - 30^\circ)C_B] \quad (15)$$

<sup>2</sup> Note that at small phase angles the brightness differences for Minnaert and Lambertian scattering laws are negligible since the incidence and emission angles are nearly identical.

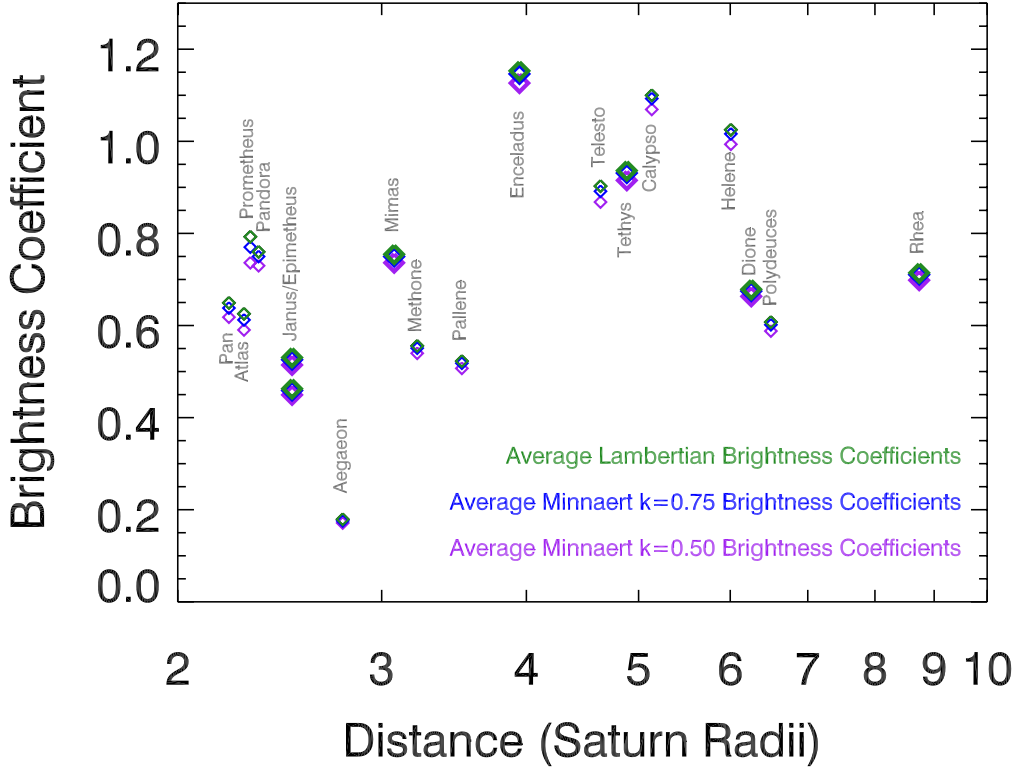


**Figure 15.** Comparisons of the average brightness coefficients of the various moons derived assuming different Minnaert scattering laws (see also Tables 3- 5). While models assuming lower values of  $k$  do yield systematically lower brightness coefficients, the differences between the different models are fairly subtle and do not alter the trends among the different moons.

For the mid-sized moons Mimas, Enceladus, Tethys, Dione and Rhea, this expression yields  $\mathcal{A}_{\text{sphere}} = 0.60, 0.92, 0.75, 0.57$  and  $0.63$ , respectively for  $\alpha_0 = 10^\circ$ , which are  $0.97, 0.92, 0.90, 0.87$  and  $1.00$  times the central values reported by Thomas et al. (2018), so at this phase angle the calculations are reasonably consistent. However, if we extrapolate to zero degrees phase we obtain  $\mathcal{A}_{\text{sphere}} = 0.65, 0.99, 0.82, 0.63$  and  $0.55$ , which are  $0.68, 0.72, 0.67, 0.63$  and  $0.74$  times the geometric albedos measured by Verbiest et al. (2007). This discrepancy most likely reflects the fact that this formula does not account for the opposition surges associated with these moons.

For the sake of simplicity we will just use the parameters  $B_0$  in our analyses below. Tables 3- 5 tabulate  $B_0$  and  $C_B$  for all of Saturn's moons examined here assuming either a Lambertian scattering law or a Minnaert scattering law with  $k = 0.75$  or  $k = 0.50$ . These tables also includes statistical errors based on the scatter of the points around the mean trend, and a systematic error which is based on the uncertainty in the mean size of the object. Additional systematic uncertainties associated with the size of the pixel response function are of order 5% and are not included here because these systematic uncertainties are common to all the brightness estimates and so do not affect the moons' relative brightness. Figure 15 compares the values of  $B_0$  derived assuming the different scattering laws for each of the

moons. This plot shows that models assuming lower values of the Minnaert  $k$  parameter yield systematically lower estimates of  $B_0$ , but that these differences are rather subtle and have little effect on the relative brightnesses of the various moons. Hence, for the sake of simplicity we will only consider the estimates of  $B_0$  computed assuming a Lambertian scattering law from here on. Figure 16 plots these central brightness values as a function of distance from the center of Saturn, along with estimates of the relative E-ring particle density and fluxes derived from images, as well as the relative energetic proton and electron fluxes (see below).

#### 4.2. Correlations between the moons' brightnesses and the E ring particle flux

Figure 16 shows that the brightness coefficients for the largest moons (Janus, Epimetheus, Mimas, Tethys, Dione and Rhea) follow the same basic trends as previously reported for these moon's geometric albedos (Verbiscer et al. 2007, 2018). The brightness of these larger moons falls off with distance from Enceladus' orbit, which strongly suggests that the E-ring plays an important role in determining these moons' surface brightness. Furthermore, the leading-trailing asymmetries in these moons' surface brightness are also consistent with how E-ring particles are expected to strike the moons (Buratti et al. 1998; Schenk et al. 2011). Most of the visible E ring particles have orbital semi-major axes close to Enceladus and a range of eccentricities (Horanyi et al. 1992; Hamilton and Burns 1994). The E-ring particles outside Enceladus' orbit are therefore closer to the apocenter of their eccentric orbits and so are moving slower around the planet than the moons are. Hence Tethys, Dione and Rhea mostly overtake the E-ring particles and the corresponding flux onto these moons is larger on their leading sides. On the other hand, the E-ring particles inside Enceladus' orbit are closer to their orbital pericenters, and so tend to move faster around the planet than the moons. Hence the E-ring particles tend to preferentially strike the trailing sides of Janus, Epimetheus and Mimas. For all of these moons, the side that is preferentially struck by E-ring particles is brighter, as one would expect if the E-ring flux was responsible for brightening the moons.

The connection between the E-ring and the moons' brightness can be made more quantitative by estimating the flux of E-ring particles onto each of the moons. The E ring consists of particles with a wide range of orbital elements, so detailed numerical simulations will likely be needed to accurately compute the fluxes onto each moon. Such simulations are beyond the scope of this report, and so we will here simply approximate the particle flux based on simplified analytical models of the E ring motivated by the available remote-sensing and in-situ observations.

Prior analyses of E-ring images obtained by the Cassini spacecraft provided maps of the local brightness density within this ring as functions of radius and height above Saturn's equatorial plane. These brightness densities are proportional to the local number density of particles times the size-dependent scattering efficiency for those particles, so these maps provide relatively direct estimates of the particle density in the vicinity of the moons. For this particular study, we will focus on the E-ring density profile shown in Figure 16, which is derived from the E130MAP observation made on day 137 of 2006, and is described in detail in Hedman et al. (2012). This observation included a set of wide-angle camera images that provided an extensive and high signal-to-noise edge-on map of the E ring at phase angles

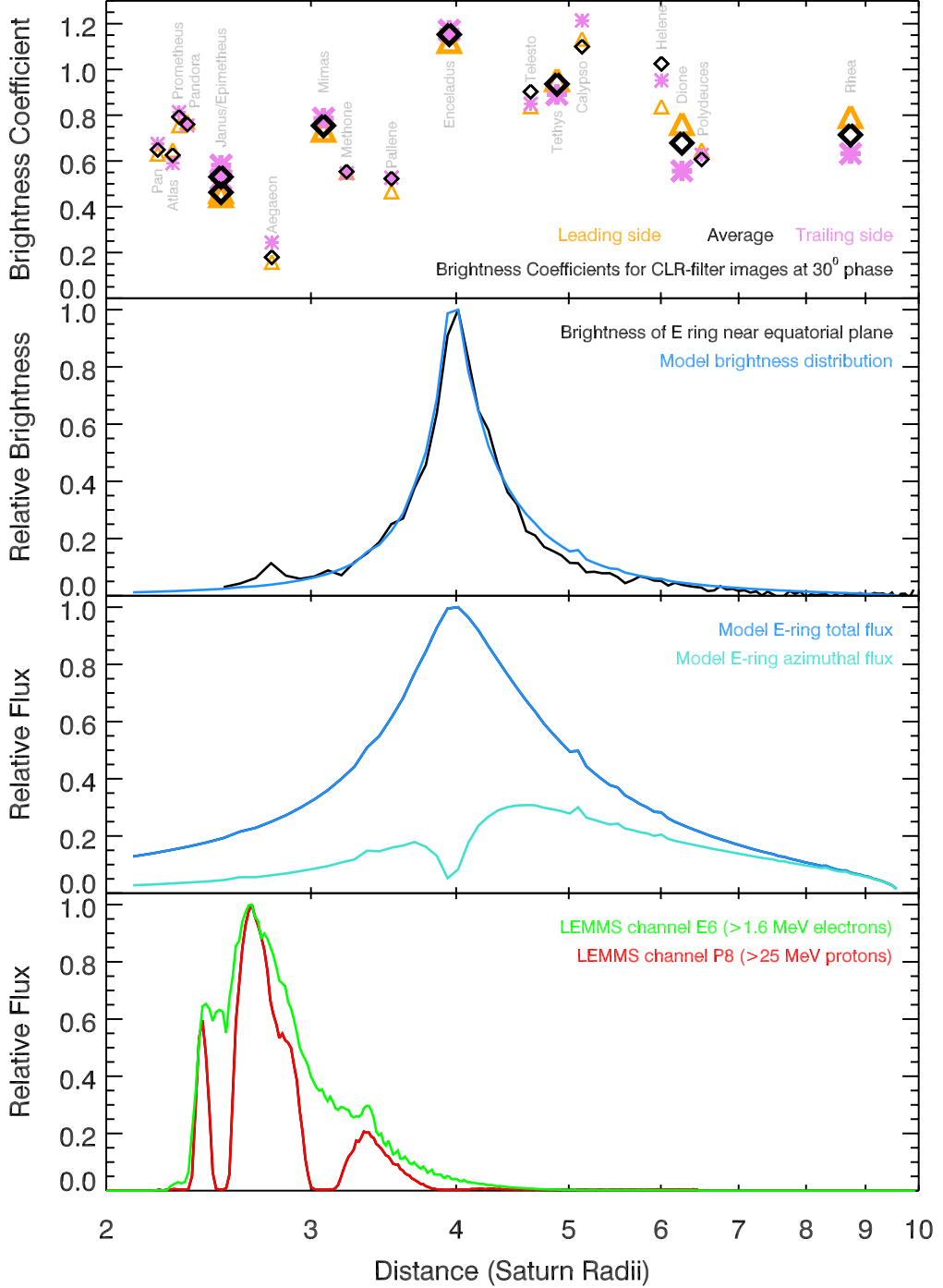


**Figure 16.** Correlations between the moon’s brightness and their environment. The top panel shows the brightness coefficients of the moons computed assuming a Lambertian scattering law as a function of distance from the planet’s center. Note that the locations of the trojan moons Telesto, Calypso, Polydeuces and Helene are offset slightly for the sake of clarity. The next two panels show the E-ring’s relative brightness density and the relative flux of E-ring particles into the moons (i.e. the parameters  $F$  and  $|\delta F_\lambda|$  see text). The bottom panel shows the flux of high-energy protons and electrons derived by the MIMI LEMMS instrument from one early pass through this entire region.

around  $130^\circ$  (W1526532467, W1526536067, W1526539667, W1526543267, W1526546867, W1526550467 and W1526554067). These images were assembled into a single mosaic of the edge-on ring, and then onion-peeled to transform the observed integrated brightness map into a map of the local ring brightness density in a vertical cut through the ring (Hedman et al. 2012). The profile of the brightness density near Saturn's equatorial plane was extracted from this map as the average brightness in regions between 1000 and 2000 km from Saturn's equator plane after removing a background level based on the average brightness 20,000-30,000 km away from that plane. Note the region used here deliberately excluded the region within 1000 km of the equator plane to minimize contamination from the G ring interior to 175,000 km. The vertical scale height of the E ring is sufficiently large that including data in the 1000-2000 km range should provide a reasonable estimate of the density in the plane containing all these moons.

Consistent with previous studies, the E-ring brightness density is strongly peaked around Enceladus' orbit. However, this profile also differs from the profiles reported elsewhere in the literature. For example, this profile is much more strongly peaked than that the profile used by Verbiscer et al. (2007). This is because the Verbiscer et al. (2007) profile was of the E-ring's vertically integrated brightness, rather than the brightness density close to the equatorial plane. The latter quantity is more sharply peaked because the E-ring's vertical thickness increases with distance from Enceladus' orbit, and because the ring is warped so that its peak brightness shifts away from Saturn's equator plane far from Enceladus' orbit (Kempf et al. 2008; Hedman et al. 2012; Ye et al. 2016). Since all the moons orbit close to the planet's equator plane, the profile shown in Figure 16 is a better representation of the relative dust density surrounding the moons. On the other hand, the profile shown in Figure 16 is also a bit broader than in-situ measurements would predict. These data have generally been fit to models where the particle density falls off with distance from Enceladus' orbit like power laws with very large indices (Kempf et al. 2008; Ye et al. 2016). Assuming that the brightness density is proportional to the particle number density, these models tend to underpredict the signals seen exterior to  $5 R_S$  and interior to  $3 R_S$ . These discrepancies arise in part because the in-situ instruments are only sensitive to grains with radii larger than 0.9 microns, while the images are sensitive to somewhat smaller particles that probably have a broader spatial distribution (Horányi et al. 2008; Hedman et al. 2012). The profile shown in Figure 16 therefore should provide a reasonable estimate of the relative densities of the particles larger than  $0.5 \mu\text{m}$  across within this ring.

However, for the purposes of understanding how the E-ring affects the moons' surface properties, we are primarily interested in the E-ring particle flux into the moons, which depends not only on the particle density, but also on the particles' velocity distribution. Since a detailed investigation of the E-ring's orbital element distribution is beyond the scope of this paper, we will here consider a simple analytical model of the E-ring particles' orbital properties that can provide useful rough estimates of the particle flux into the various moons.

Prior analyses of E-ring images indicate that most of the visible particles in this ring have semi-major axes close to Enceladus' orbit, and that the large size of this ring is because the particles have a wide range of eccentricities and inclinations. Furthermore, the images indicate that mean eccentricities, inclinations and semi-major axes were strongly correlated

with each other (Hedman et al. 2012). We therefore posit that the E-ring density distribution seen in Figure 16 primarily reflects a distribution of eccentricities  $\mathcal{F}(e)$ . We also allow the semi-major axes of the particles to vary, but for the sake of simplicity we assume that the semi-major axes of these particles  $a$  is a strict function of  $e$ :  $a = [240,000 + (e/0.1) \times 5000]$  km, which is consistent with the imaging data (Hedman et al. 2012). Since we are only concerned with particles near Saturn's equatorial plane, we will not consider the inclination distributions here.

For a given eccentricity distribution  $\mathcal{F}(e)$ , the particle density as a function of radius  $d(r)$  should be given by the following integral:

$$d(r) = \int_{e_{min}}^1 \frac{2}{|v_r|T} \mathcal{F}(e) de, \quad (16)$$

where  $v_r$  is the radial velocity of the particles and  $T$  is their orbital period, and the factor of two arises because particles with a finite eccentricity passes through each radius twice. The integral's lower limit is  $e_{min} = |1 - r/a|$  because only particles with eccentricities greater than this can reach the observed  $r$ . Similarly, the average flux of particles onto a body on a circular orbit at a given radius is given by the integral.

$$F(r) = \int_{e_{min}}^1 \frac{1}{2|v_r|T} \mathcal{F}(e) \sqrt{v_r^2 + \delta v_\lambda^2} de, \quad (17)$$

where  $v_r$  is the particle's radial velocity as defined above, and  $\delta v_\lambda$  is the particle's azimuthal velocity measured relative to the local circular orbital velocity. Note that a factor of  $1/4$  arises from averaging over the moon's surface. Since the radial motions of particles on any given orbit are symmetric inwards and outwards, in this model there are no differences in the fluxes on the sub-Saturn and anti-Saturn sides of the moon. However, because the particles at a given radius can have different average azimuthal velocities, there can be asymmetries in the fluxes on the moon's leading and trailing sides. These asymmetries can be parametrized by the following integral:

$$\delta F_\lambda(r) = \int_{e_{min}}^1 \frac{1}{2|v_r|T} \mathcal{F}(e) \delta v_\lambda de, \quad (18)$$

which is **half** the difference between the fluxes on the leading and trailing points.

In order to evaluate these integrals, recall the standard expressions for  $v_r$  and  $\delta v_\lambda$  in terms of orbital elements (Murray and Dermott 1999):

$$v_r = \frac{na}{\sqrt{1-e^2}} e \sin f \quad (19)$$

$$\delta v_\lambda = \frac{na}{\sqrt{1-e^2}} (1 + e \cos f) - na \sqrt{a/r} \quad (20)$$

where  $n = 2\pi/T$  is the mean motion of the particle and  $f$  is the true anomaly of the particle's orbit. At a given radius  $r$  we will be observing particles at different mean anomalies given by the standard expression:

$$r = \frac{a(1-e^2)}{1+e \cos f} \quad (21)$$

so we can re-express  $|v_r|$  and  $\delta v_\lambda$  in terms of  $r$

$$|v_r| = \frac{na^2}{r} \sqrt{e^2 - (r/a - 1)^2}, \quad (22)$$

$$\delta v_\lambda = \frac{na^2}{r} \left[ \sqrt{1 - e^2} - \sqrt{r/a} \right]. \quad (23)$$

Inserting these expressions into the above integrals, we find the density, flux and flux asymmetries can all be expressed as the following integrals over the eccentricity distribution (remember that  $a$  is implicitly a function of  $e$ ):

$$d(r) = \int_{e_{min}}^1 \frac{r\mathcal{F}(e)}{\pi a^2 \sqrt{e^2 - (r/a - 1)^2}} de, \quad (24)$$

$$F(r) = \int_{e_{min}}^1 \frac{n\mathcal{F}(e)}{4\pi} \sqrt{1 + \frac{(\sqrt{1 - e^2} - \sqrt{r/a})^2}{e^2 - (r/a - 1)^2}} de, \quad (25)$$

$$F_\lambda(r) = \int_{e_{min}}^1 \frac{n\mathcal{F}(e)(\sqrt{1 - e^2} - \sqrt{r/a})}{4\pi \sqrt{e^2 - (r/a - 1)^2}} de. \quad (26)$$

It turns out that the observed density distribution shown in Figure 16 can be matched reasonably well by assuming the eccentricity is a Lorentzian times a regularization term to avoid singularities at  $e = 0$ :

$$\mathcal{F}(e) = \frac{\mathcal{F}_0}{1 + e^2/e_0^2} [1 - \exp(-e/e_c)] \quad (27)$$

with constants  $\mathcal{F}_0$ ,  $e_0$  and  $e_c$ . The specific model density distribution shown in Figure 16 has  $e_0 = 0.17$  and  $e_c = 0.01$ . Note that  $e_c$  basically only affects the density levels close to Enceladus' orbit, while  $e_0$  determines how quickly the signal falls off away from the E-ring core.

Using this same ansatz for  $\mathcal{F}(e)$ , we obtain estimates for how both the flux and flux asymmetry vary with radius, which are shown in the third panel of Figure 16. First note that the flux is much less sharply peaked than the density. This occurs because the particles are moving faster relative to the local circular velocity at larger distances from Enceladus' orbit thanks to their higher eccentricities. Also note that azimuthal component of the flux is larger exterior to Enceladus' orbit than it is interior to that moon. This asymmetry arises because exterior to Enceladus the particles are all moving slower than the local circular velocity, while interior to Enceladus, the particles are all moving faster than the local circular speed, but the azimuthal components of their velocity can still fall below the local circular velocity depending on their true anomaly.

Finally, we can translate these trends in the relative flux into rough estimates of the absolute flux of E-ring particles using recent in-situ measurements of the particle number density in the E-ring core. In principle, the brightness density seen in images can be translated

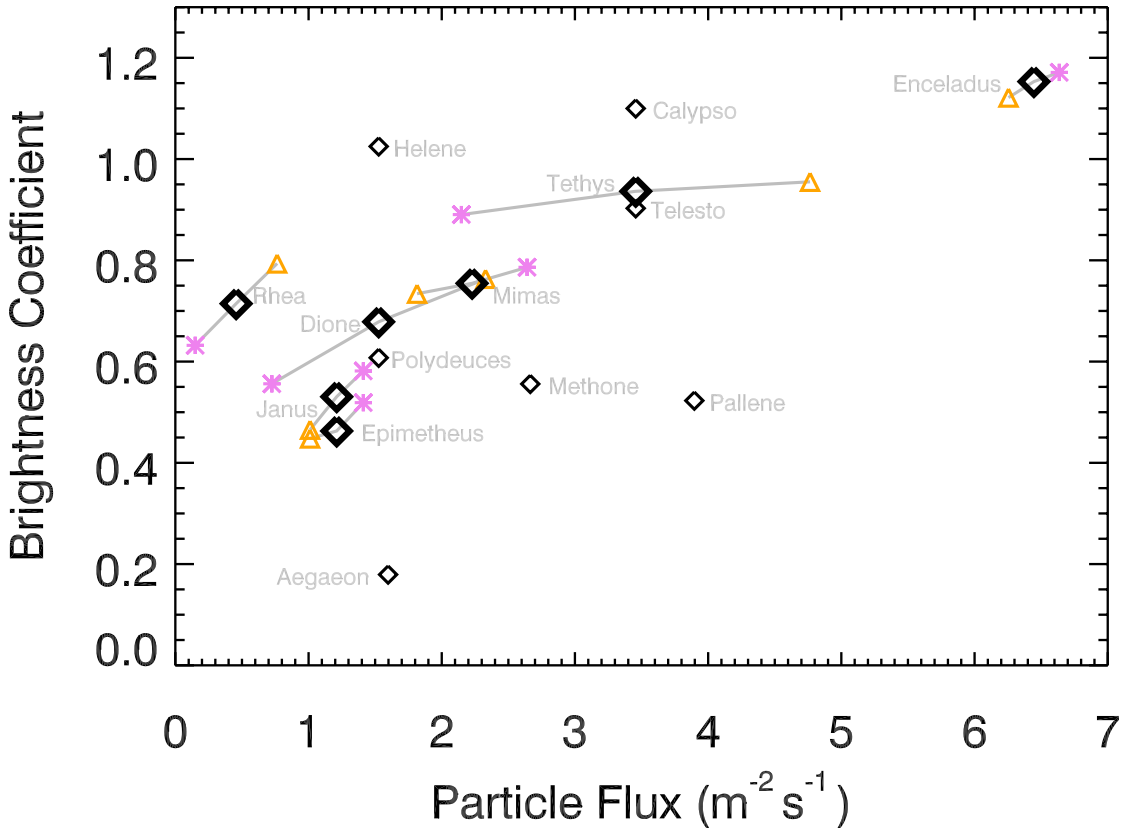


**Figure 17.** Moon brightness coefficients versus computed E-ring particle flux, assuming peak number density of  $0.03/\text{m}^3$ ,  $e_0 = 0.17$  and  $e_{\min} = 0.01$ . The diamonds are the average values for each moon, while the orange triangles and magenta stars indicate the values for the leading and trailing sides of the mid-sized moons.

into estimates of the particle number density, but in practice the relevant conversion factor depends on the size-dependent light scattering efficiency of the particles. By contrast, the peak E-ring particle density has been directly measured to be between  $0.02$  and  $0.2 \text{ /m}^3$  with various in-situ measurements (Kempf et al. 2008; Ye et al. 2016). Now, as mentioned above, these densities are for the particles larger than the detection thresholds of these instruments, which is slightly larger than the sizes of the particles seen in remote-sensing images. Hence the number density of visible particles could be somewhat larger than these measurements. Nevertheless, these are still the best estimates of the absolute particle density near the core of the E ring, and they should still provide a useful order-of-magnitude estimate of the visible particles. For the sake of concreteness, we will here assume a peak number density of  $0.03$  particles/ $\text{m}^3$ , which is the value measured by Ye et al. (2016) for particles larger than  $1 \mu\text{m}$  in radius.

Figure 17 and Table 6 give the brightness coefficients and estimated E-ring particle fluxes for all the moons known to be embedded in the E ring. For the mid-sized moons and the co-orbitals, there is a very good correlation between the moon's brightness coefficients and the estimated fluxes. This correlation not only applies to the average values for each moon,

but also to their leading and trailing sides, where the estimated flux values are taken to be  $F \pm \delta F_\lambda / \sqrt{2}$  (the factor of  $\sqrt{2}$  accounts for the fact that the observations span a full quadrant of each body). The one mid-sized moon that falls noticeably off the main trend is Rhea. This could be related to other unusual aspects of Rhea's surface. Rhea's visible spectrum is redder than any of the other mid-sized moons (Thomas et al. 2018), and its near-infrared spectrum exhibits stronger ice bands than Dione (Filacchione et al. 2012; Scipioni et al. 2014). Furthermore, radio-wave data indicate that Rhea has a higher albedo at centimeter wavelengths than Dione (Black et al. 2007; Le Gall et al. 2019). Various explanations have been put forward to these anomalies, including differences in the moons' regolith structure (Ostro et al. 2010), and variations in the energetic particle and/or ring particle flux (Scipioni et al. 2014; Thomas et al. 2018). The latter option is probably the more likely explanation for Rhea's excess brightness at visible wavelengths, since the moon is in a region where both the predicted fluxes of E-ring grains and energetic particles are expected to be very low (see also below). Indeed, our simple E-ring model is probably not completely accurate near Rhea's orbit. Detailed numerical simulations of the E-ring particles reveal that there could be a population of sub-micron particles orbiting in the outskirts of the E ring close to Rhea's orbit (Horányi et al. 2008). This population could potentially increase the particle flux into Rhea, moving that data point closer to the trend defined by Mimas and Dione, but it is not clear whether it could also explain that moon's spectral properties. In any case, overall these data confirm that the E-ring particle flux is an important factor for determining the surface brightness of the mid-sized and co-orbital satellites.

Turning to the smaller moons, however, the situation is more complicated. Two of the co-orbital moons –Telesto and Polydeuces– fall close to the same trend as their larger companions. However, the other two co-orbitals –Calypso and Helene– fall noticeably above this trend. Meanwhile, Aegaeon, Methone and Pallene all fall well below the trend for the mid-sized moons. This implies that something besides the E-ring flux is affecting the brightnesses of these small moons.

#### 4.3. Darkening Aegaeon, Methone and Pallene with radiation

Aegaeon, Methone and Pallene are all considerably darker than one would have predicted given their locations and the observed trend between Janus, Epimetheus, Mimas and Enceladus. Aegaeon in particular is exceptionally dark, with a surface brightness coefficient around 0.2. This conclusion is consistent with the few resolved images of these bodies, which show that only the dark side of Iapetus has a comparably low surface brightness as Aegaeon (see Figure 18). In principle, the darkness of these moons could be due to a number of different factors, including their small size and their associations with other dusty rings, but the most likely explanation involves their locations within Saturn's radiation belts.

Aegaeon, Methone and Pallene are much smaller than the mid-sized moons, and so their small sizes could somehow be responsible for their low surface brightness. Indeed, based on preliminary investigations of Aegaeon's low surface brightness, Hedman et al. (2010) suggested that a recent collision catastrophically disrupted the body, stripping off its bright outer layers to produce the debris that is now the G ring, and leaving behind a dark remnant. Deeper examination, however, does not support this model. For example, if a collision was

**Table 6.** Particle and radiation fluxes

Moon	$B_0^a$			E-ring flux <sup>b</sup> (part. m <sup>-2</sup> sec <sup>-1</sup> )			Radiation flux <sup>c</sup> (protons cm <sup>-2</sup> sec <sup>-1</sup> ) in range 25-59 MeV
	Ave.	Lead	Trail	Ave.	Lead	Trail	
Janus	0.53	0.47	0.58	1.21	1.01	1.41	5.4
Epimetheus	0.46	0.45	0.52	1.21	1.01	1.41	7.4
Aegaeon	0.18	0.16	0.24	1.60	1.32	1.88	920.4
Mimas	0.75	0.73	0.79	2.23	1.81	2.64	5.6
Methone	0.56	0.55	0.55	2.66	2.15	3.17	140.2
Pallene	0.53	0.47	0.53	3.89	3.19	4.60	162.0
Enceladus	1.15	1.12	1.17	6.44	6.25	6.63	4.4
Tethys	0.94	0.96	0.89	3.46	4.77	2.15	3.2
Telesto	0.90	0.84	0.84	3.46	4.77	2.15	3.2
Calypso	1.10	1.13	1.21	3.46	4.77	2.15	3.2
Dione	0.68	0.76	0.56	1.53	2.33	0.72	3.1
Helene	1.02	0.84	0.95	1.53	2.33	0.72	3.1
Polydeuces	0.61	0.65	0.63	1.53	2.33	0.72	3.1
Rhea <sup>d</sup>	0.71	0.79	0.63	0.46	0.76	0.15	3.1

<sup>a</sup> Brightness coefficient at 30° computed assuming surface follows Lambertian scattering law, see Table 3.

<sup>b</sup> E-ring flux computed assuming  $e_0 = 0.17$ ,  $e_c = 0.01$  and a peak number density of 0.03 particles per cubic meter. Leading and trailing side values given by  $F \pm \delta F_\lambda / \sqrt{2}$

<sup>c</sup> Radiation fluxes computed assuming  $\pi$  steradian viewing angle.

<sup>d</sup> Radiation fluxes at Rhea assumed to be the same as those for Dione

sufficient to expose the dark core of a kilometer-scale body, then small impacts should expose dark materials on the other moons, but no such dark patches have been seen in any of the high-resolution images obtained by Cassini. More fundamentally, attributing Aegaeon's extreme darkness to some discrete event in the past is difficult because the E-ring should be able to brighten this moon relatively quickly. Assuming typical particle sizes of around 1 μm, the above estimates of the E-ring flux implies that Aegaeon would acquire a layer of E-ring particles 10 μm thick in only 100,000 years. This calculation neglects mixing within Aegaeon's regolith and any material ejected from Aegaeon, but even this basic calculation shows that E-ring particles would cause Aegaeon to brighten on very short timescales, which strongly suggests that whatever process is making Aegaeon dark is actively ongoing.

Another possibility is that Aegaeon, Methone and Pallene are dark because they are embedded not only in the E ring, but also in narrower rings like the G ring. However, since these rings likely consist of debris knocked off the moons' surfaces, this does not necessarily explain why this material would be so dark. Another problem is that Prometheus and Pandora are rather bright, even though these moons are close to the F ring and therefore likely coated in F-ring material (see below). Furthermore, since the rings/arcs associated with Methone and Pallene are over an order of magnitude fainter than the G ring (Hedman et al. 2018), it seems unlikely that these tenuous rings could significantly affect the surface

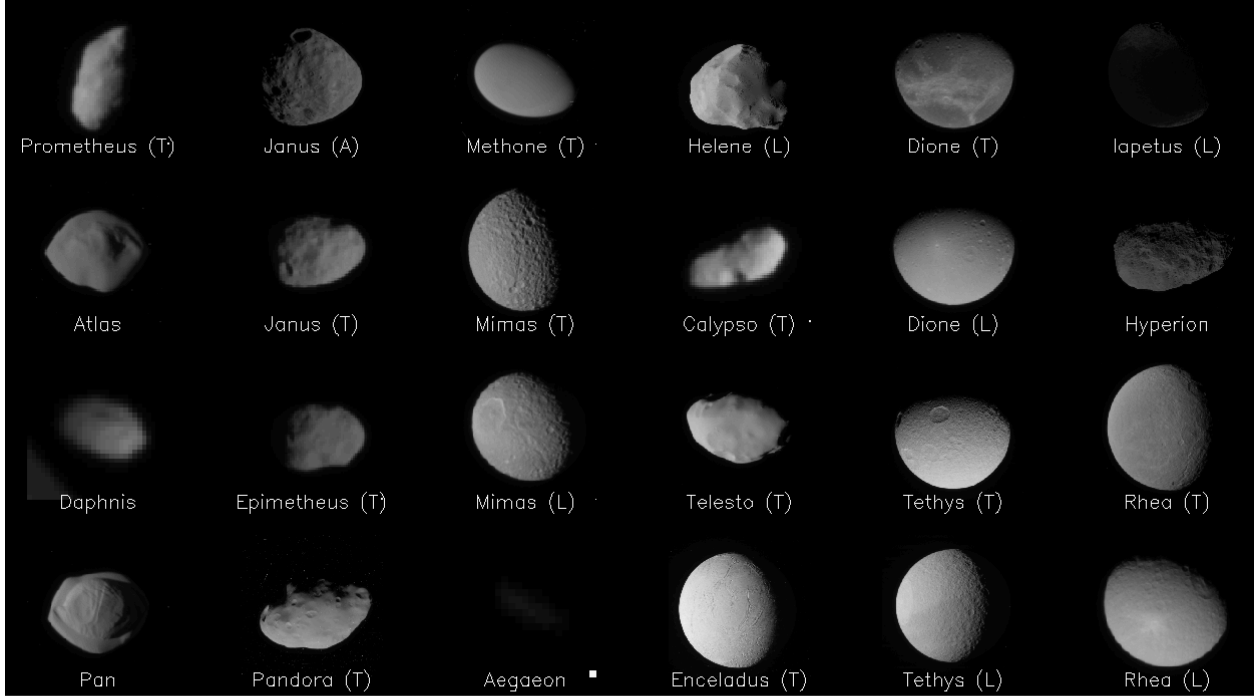


**Figure 18.** Resolved images of Saturn's moons at phase angles between  $50^\circ$  and  $60^\circ$ , shown with a common stretch with a gamma of 0.75. Letters following the names indicate the hemisphere observed (T=trailing, L=leading, A=anti-Saturn). This gallery clearly demonstrates that Aegaeon is anomalously dark and has a comparable surface brightness to Iapetus' dark side. Image files used for this mosaic are: N1643265020 = Aegaeon, N1870695654 = Atlas, N1506184171 = Calypso (T), N1656997840 = Daphnis, N1597675353 = Dione (T), N1606072353 = Dione (L), N1824725635 = Enceladus (T), N1521539514 = Epimetheus (T), N1687121104 = Helene (L), N1669612923 = Hyperion, N1510339442 = Iapetus (L), N1521539514 = Janus (T), N1627323065 = Janus (A), N1716192290 = Methone (T), N1484509816 = Mimas (L), N1855894795 = Mimas (T), N1867602424 = Pan, N1504612286 = Pandora (T), N1853392689 = Prometheus (T), N1505772509 = Rhea (L), N1591815592 = Rhea (T), N1514163567 = Telesto (T), N1855868106 = Tethys (L), N1563723519 = Tethys (T).

properties of those two moons. Thus the G ring and other dusty rings do not appear to provide a natural explanation for the darkness of these small moons.

A more plausible explanation for the low surface brightnesses of Aegaeon, Methone and Pallene is that these moons orbit Saturn within regions that have unique radiation environments. The bottom panel of Figure 16 shows profiles of energetic proton and electron fluxes from two of the highest energy channels of Cassini's Low-Energy Magnetospheric Measurement System (LEMMS) instrument (Krimigis et al. 2004). Note that while the electron flux has a broad peak centered around the orbit of Aegaeon, the high-energy proton flux is confined to three belts between the main rings and the orbits of Janus, Mimas and Enceladus (Roussos et al. 2008). This disjoint distribution of high-energy protons arises because energetic protons circle the planet under the influence of the corotation electric field, but their longitudinal motion is enhanced by gradient-curvature drifts, which act in the same direction as corotation. These particles therefore orbit the planet with a period of one to

a few hours. Combined with the alignment of the spin and dipole axes, this drift allows these protons to re-encounter the inner moons frequently, causing a permanent flux decrease (macrosignature) along their orbits for sufficiently energetic protons. It is important to realize that these macrosignatures are not just depressions in the energetic proton density, but are also regions where the *flux* of protons is greatly decreased. Proton macrosignatures along the moon orbits are visible in the data at energies of  $> 300$  keV or so, but are only expected to exist at much higher energies for electrons. Since Janus and Mimas are exposed to comparable amounts of energetic electrons as Aegaeon, Methone and Pallene, the electron flux is not a natural explanation for the smaller moons' low surface brightness. However, Aegaeon, Methone and Pallene are exposed to much higher fluxes of high-energy protons than any of Saturn's other moons, so this is a plausible potential explanation for the darkness of these three moons.

Table 6 provides more quantitative estimates of the proton fluxes into the different moons. Here we use the protons observed with the P8 channel on the LEMMS instrument as a proxy for the total flux of high-energy protons (Krimigis et al. 2004). In the radiation belts, this channel's sensitivity is mainly to protons of 25.2 to 59 MeV, and the numbers reported in Table 6 are for an acceptance solid angle of 1 steradian to facilitate comparisons with the E-ring particle flux. Since Mimas, Janus and Epimetheus occupy narrow gaps in the radiation belts, the fluxes provided in this table are averaged over the moons' true anomalies. Furthermore, for Janus and Epimetheus we also average over the semi-major axis variations associated with these moons' co-orbital interactions. Also note that while estimates of the Galactic Cosmic Ray background have been removed from these data, the fluxes for the moons beyond Enceladus are probably upper limits. Nevertheless, these numbers clearly show that Methone, Pallene and Aegaeon experience exceptionally high proton fluxes.

If radiation damage from high-energy protons is the dominant darkening process and the E-ring particles are the dominant brightening process, then we would expect the moons' equilibrium surface brightness to depend the ratio of the radiation flux to the E-ring particle flux. To make this ratio properly unitless, we consider the mass flux ratio for high-energy protons and E-ring particles. This quantity is computed by taking the number flux of protons given in Table 6 multiplied by the proton mass and dividing that number by the average flux of E-ring particles given in Table 6 multiplied by  $m_{\text{eff}}$ , the effective average mass of particles with radii larger than  $1 \mu\text{m}$ . Specifically, we assume  $m_{\text{eff}} = 4\pi \ln(100) \times 10^{-15} \text{ kg}$ , which is consistent with a power-law size distribution with a differential index of -4 (Ye et al. 2014) extending between 1 and 100 microns, and a particle mass density of  $1 \text{ g/cm}^3$ . Figure 19 shows that the moons' brightnesses do indeed systematically decrease as this ratio increases. Furthermore, Methone, Pallene and Aegaeon fall along the same basic trend in this plot as the mid-sized and co-orbital moons. This match provides strong evidence that radiation damage is the dominant process responsible for making Methone, Pallene and Aegaeon dark.

At the moment, we do not know precisely which components of the radiation flux are responsible for the darkening. The macrosignatures are most prominent in the highest-energy proton channels, which suggests energetic protons are the dominant agent, but other agents (e.g., electrons with even higher energies) may also contribute at some level. If the darkening agent is protons with energies greater than 1 MeV, there are several ways that

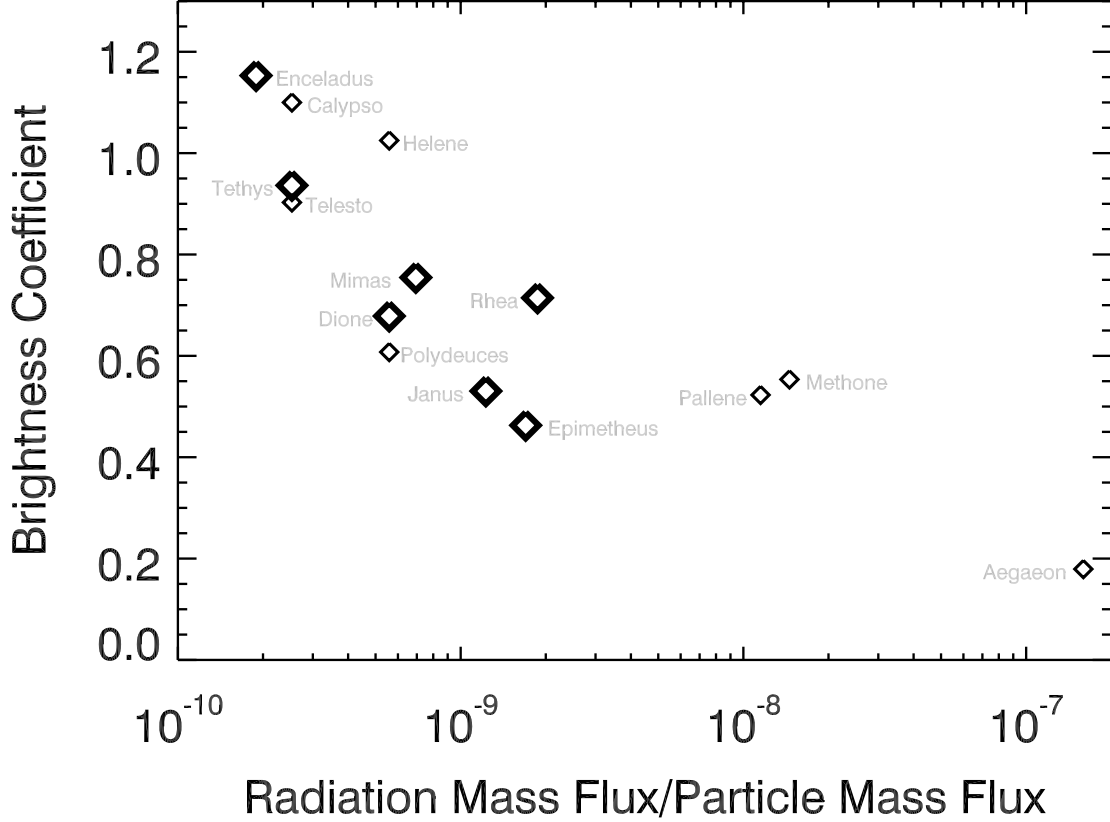


**Figure 19.** Moon brightness versus the ratio of the radiation mass flux to the E-ring particle flux. The radiation mass flux here is flux of protons with energies between 25 and 50 MeV, while the E-ring mass flux is the mass of particles larger than 1 micron. Note that the radiation fluxes for Methone, Pallene and Aegaeon are measured, while for the other moons they may represent upper limits. Still, the overall trend of decreasing brightness with increasing flux ratio is clear.

they could be altering the surface. Howett et al. (2011) suggested that energetic electrons “sinter” or fuse grains in the uppermost layer, which can affect the reflectance properties at a range of wavelengths (Schenk et al. 2011; Howett et al. 2018). Electrons are mainly slowed down by interactions with electrons in materials. Protons are initially slowed down mainly by interactions with electrons in materials, although as they slow down, they interact more with nuclei. So it is possible very energetic protons (in the first fraction of their mean range) are causing the same kinds of changes to the ice as energetic electrons. Furthermore, they have large gyroradii and so they can often affect the whole body, i.e. they don’t weather the surface differentially in many cases. Radiation damage can also change the chemical properties of surface materials, such as generating complex organics (Hapke 1986; Poston et al. 2018) or producing color centers in salts (Hand and Carlson 2015; Hibbitts et al. 2019; Trumbo et al. 2019), which could darken the surface and produce distinctive spectral signatures.

During its closest flybys of Aegaeon and Methone, Cassini’s NAC obtained images of both moons through multiple filters. We processed these high-resolution color images with the

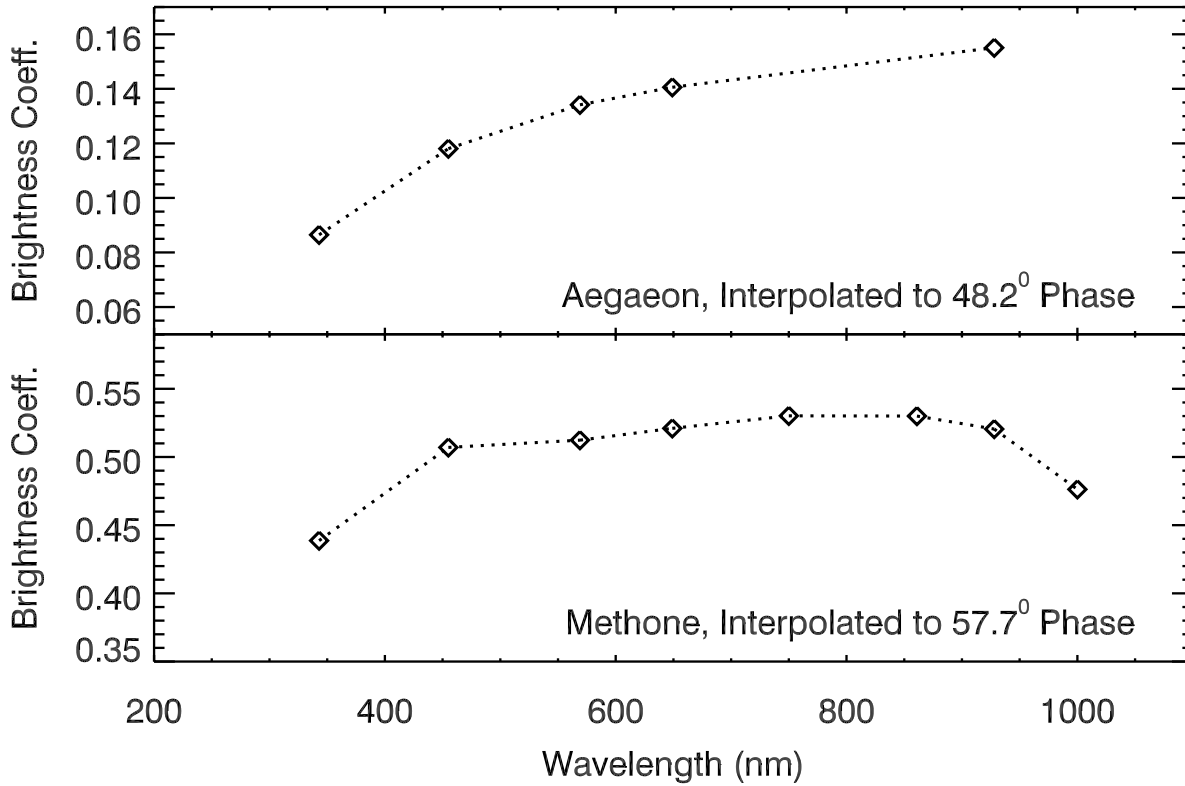


**Figure 20.** Visible spectra of Aegaeon and Methone obtained from resolved images during Cassini’s closest encounters with these moons. The only clear spectral feature is the break in slope around 500 nm, which is commonly found in spectra of the icy moons.

same methods as described above for the mid-sized moons, yielding the brightness coefficients given in Tables 27 and 28. We then interpolated these measurements to a single phase angle to obtain the visible spectra shown in Figure 20. Furthermore, during the close encounter with Methone, the Visual and Infrared Mapping Spectrometer (VIMS) (Brown et al. 2004) was able to obtain near-infrared spectra of the moon. While VIMS was unable to spatially resolve Methone, VIMS acquired five “cubes” with good signal-to-noise (V1716191964, V1716192051, V1716192374, V1716192461 and V1716192872) that could yield decent disk-integrated spectra. We calibrated these cubes with the standard pipelines (Brown et al. 2004; Clark et al. 2012, flux calibration RC19), co-added the signals in the pixels containing the moon signal, removed backgrounds based on adjacent pixels, normalized the resulting spectra and averaged them together to produce a single mean spectrum shown in Figure 21 (Note that this spectrum is arbitrarily normalized). The near-infrared spectrum of Methone is dominated by water-ice, while the visible spectra of the two moons are generally flat with a spectral break around 0.5 microns. These moon’s spectral properties are therefore very similar to those of the rest of Saturn’s moons (Filacchione et al. 2012; Buratti et al. 2010; Buratti et al. 2019). Furthermore, the depths of the water-ice bands at 1.5 and 2.0 microns (computed following the procedures laid out in Filacchione et al. (2012)) are  $0.45 \pm 0.04$  and  $0.60 \pm 0.06$ , respectively. These values are very similar to those previously found for Janus,

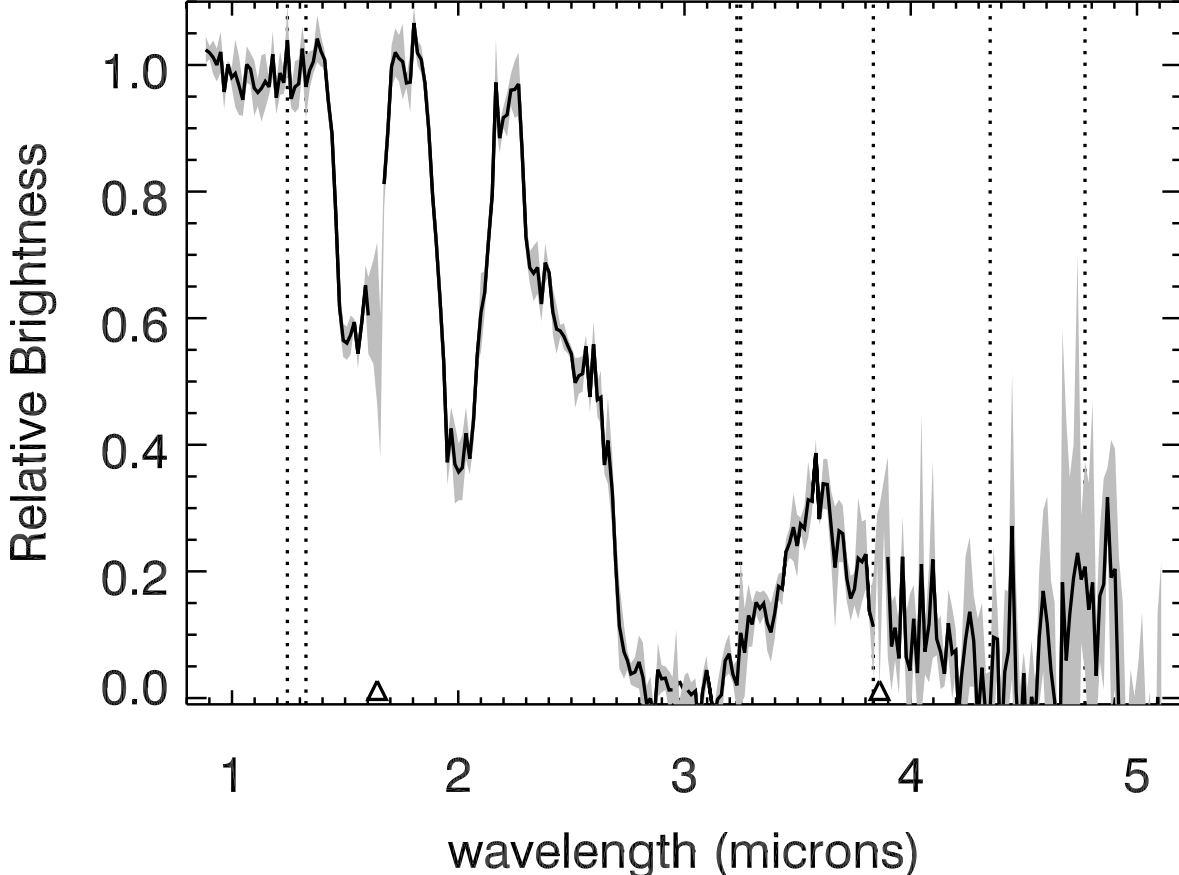


**Figure 21.** Near infrared spectrum of Methone derived from observations from the VIMS instrument. The brightness is shown at an arbitrarily normalized scale. Note the bands at 1.5, 2 and 3.1 microns are typical of water ice, and the overall shape of the spectrum is comparable to that of other small moons.

Epimetheus, Telesto, Dione and Rhea (Filacchione et al. 2012). Hence there is no evidence that these bodies have surfaces with distinctive spectrally active components, like irradiated salts (Hibbitts et al. 2019). Instead, the radiation appears to change the surface brightness relatively uniformly at all wavelengths.

An interesting point of comparison for these spectra is Jupiter's moon Callisto. Callisto and Aegaeon are probably exposed to similar fluxes of high-energy protons (roughly  $10/(\text{cm}^2 \text{ s sr keV})$  around energies of 1 MeV, Paranicas et al. 2018), and both objects are comparably dark (Callisto has a geometric albedo around 0.2 between 0.5 and 2.5 microns (Calvin et al. 1995), and extrapolating the available data suggests that Aegaeon's equivalent spherical albedo is around 0.15). Like Aegaeon, Callisto has a visible spectrum that is flat longwards of 0.6 microns and has a downturn at shorter wavelengths (Calvin et al. 1995; Moore et al. 2007). The structure in Callisto's spectrum in the near-infrared primarily consists of comparatively weak water-ice features, along with a weak carbon-dioxide band at  $4.2 \mu\text{m}$  (Moore et al. 2007), which is consistent with the compositional features seen in Methone and Saturn's other moons (Clark et al. 2008; Hendrix et al. 2018; Buratti et al. 2019). It may therefore

be that both Callisto and Aegaeon represent end-members of what ice-rich surfaces look like when exposed to large doses of high-energy radiation. If correct, it could mean that even if we had near-IR spectra of Aegaeon, they would not contain diagnostic spectral features of the chemicals responsible for making its surface dark. Whether the observed amount of darkening is consistent with structural changes in the regolith (Howett et al. 2011; Schenk et al. 2011) or chemical changes in a more spectrally neutral component (such as the non sulfur-bearing ices in Poston et al. 2018), will require detailed spectral models that are beyond the scope of this work.

#### 4.4. *The excess brightness of Prometheus, Pandora, Calypso and Helene*

After Aegaeon, Methone and Pallene, the next most obvious anomalies in Figure 17 are Helene and Calypso. Calypso is brighter than both Tethys and Telesto, while Helene is brighter than both Dione and Polydeuces. These findings are actually consistent with prior estimates of these moons' geometric albedos summarized in Verbiscer et al. (2007, 2018). At the same time, it is worth noting that despite being in a region where the E-ring flux should be extremely low, Pan, Atlas, Prometheus and Pandora are all reasonably bright, and in particular Prometheus and Pandora are brighter than any of the other moons in their vicinity. The excess brightness of these moons is probably related to distinctive aspects of their near-infrared spectra. For the mid-sized moons, the depths of the moon's water-ice bands are reasonably well correlated with their visible brightness (Filacchione et al. 2012). However, Calypso, Prometheus and Pandora all have deeper water-ice bands than Enceladus, while Atlas, Telesto and Helene have water-ice bands intermediate in strength between Tethys and Dione (Buratti et al. 2010; Filacchione et al. 2012, 2013). Note that even though Helene does not appear to have as exceptionally deep water-ice bands as Calypso, both Calypso and Helene have deeper bands than their respective large companions Tethys and Dione. The anomalous spectral and photometric properties of Prometheus, Pandora, Calypso and Helene could be attributed to a number of different factors, including the moons' size and differences in the local radiation environment. In practice, localized enhancements in the particle flux appears to be the most likely explanation, but the excess particle flux responsible for the high observed brightnesses of Helene and Calypso is far from clear.

In principle, the surface brightness of small moons could be different from the brightness of large moons in the same environment because their reduced surface gravity affects the porosity and structure of their regolith. In fact, one aspect of these moons' surface properties probably can be attributed to their small size: their general lack of a leading-trailing brightness asymmetries. In particular, all four of the trojan moons appear to lack the strong leading-trailing brightness asymmetries seen on Tethys and Dione.<sup>3</sup> For Tethys and Dione, this asymmetry is thought to arise because of asymmetries in the E-ring flux, so it is perhaps surprising that similar asymmetries are not seen in the smaller moons. However, the smaller size and much lower surface gravity of these moons means that secondary ejecta from the

<sup>3</sup> Hirata et al. (2014) also found that there was not a strong leading-trailing asymmetry in the morphology of deposits on Telesto and Calypso. However, they also found that Helene appears to have a higher crater density on its trailing side, perhaps implying a thicker mantling deposit on its leading side.

E-ring impacts can be more easily globally dispersed over their surfaces, providing a natural explanation for why these moons have more uniform surface properties.

While detailed modeling of impact debris transport around these small moons is beyond the scope of this paper, we can provide rough order-of-magnitude calculations that are sufficient to demonstrate the feasibility of this idea. Assuming that most of the E-ring particles striking these moons are near the apocenters of their eccentric orbits, we can assume  $r \simeq (1 + e)a$  in Equation 23 and estimate the E-ring particle's impact velocities at the orbits of Tethys and Dione to be 1.4 km/s and 3.6 km/s, respectively. Experimental studies of impacts into ice-rich targets by 20-100  $\mu\text{m}$  glass beads found impact yields at these velocities of order 100 (Koschny and Grün 2001), and assuming roughly comparable values for micron-sized E-ring grains would imply an effective average ejection velocity of at most 14 m/s and 36 m/s, respectively. These speeds are much less than the escape speeds from Tethys and Dione (which are 390 and 510 m/s respectively), but are comparable to the escape speeds of Telesto, Calypso, and Helene (which are 7, 19 and 9 m/s, respectively). Hence it is reasonable to think that the debris from E-ring particle impacts is more uniformly distributed on the smaller trojans than they are on Tethys and Dione, making their surfaces more uniform in brightness.

However, while their size is likely responsible for their lack of leading-trailing brightness asymmetries, it is unlikely that size-related phenomena can explain the overall high brightness of Prometheus, Pandora, Calypso and Helene. The problem with such ideas is that there are no clear trends between size and brightness excess. Telesto is intermediate in size between Helene and Calypso, but is roughly the same brightness as Tethys. Also, Prometheus and Pandora are themselves intermediate in size between Epimetheus and Atlas. This lack of obvious trends with mass or size suggests that the brightness excess of these moons most likely reflects something different about their environments.

Given the previous analyses of the trends among the other moons, the easiest way to increase the brightness of these moons would be either by decreasing the radiation flux or increasing the particle flux. Decreasing the radiation flux is an unlikely explanation because the high-energy proton flux onto many of the moons is already very low (see Table 6). Furthermore, for the radiation flux to be lower at Calypso than at Telesto, or lower at Helene than at Polydeuces, there would need to a strong asymmetry in the radiation flux on either side of Tethys and Dione. While both Tethys and Dione have been observed to produce localized reductions in plasma known as microsignatures, these do not extend all the way to the trojan moons. Also, given that the plasma is bound to the planet's magnetic field, which rotates faster than the moons orbit around the planet, it is hard to imagine any interaction with charged particles that would similarly affect Calypso (which trails Tethys) and Helene (which leads Dione).

The above considerations leave variations in the particle flux as the best remaining option. For Prometheus and Pandora, this is a perfectly reasonable explanation, since these moons fall within the outskirts of the F ring, which is a natural source of dust flux into these moons. If an excess flux of F-ring particles is indeed responsible for the high brightness of Prometheus and Pandora, this is interesting because it means that the dust impacting the moons does not have to be the relatively fresh ice found in the E ring to produce increases in

brightness. In this case, the lower-opacity dusty rings surrounding Pan and Atlas could be keeping those moons somewhat brighter than they would otherwise be given their locations well interior to the E ring.

Excess dust fluxes are also an attractive explanation for the excess brightness of Calypso and Helene because these moons are nearly as bright as Enceladus, an object whose brightness is certainly due to a high particle flux. However, there is no obvious source for the particles that would strike Calypso and Helene more than their co-orbital companions. The brightness differences cannot be easily attributed to differences in the E-ring flux, since Telesto, Calypso and Tethys are at basically the same orbital distance from Saturn, as are Helene, Polydeuces and Dione. Hence the E-ring flux into Telesto, Tethys and Calypso (or Helene, Dione and Polydeuces) should be nearly the same.

In principle, asymmetries in the particle flux could arise from either subtle interactions between the larger moons and the E-ring grains, or more local particle populations sourced from the larger moons. For example, particles on nearly circular orbits launched from Tethys that are carried outward by plasma drag would preferentially fall behind Tethys, and thus potentially be more likely to strike Calypso than Telesto. The problem with such explanations is that for Calypso and Helene to fall along the same trend as the other moons in Figure 17, the excess particle flux into these moons needs to be a substantial fraction of the E ring flux, which would imply a large excess density of particles around these moons compared to Tethys, Dione, Telesto or Polydeuces. These particles should produce localized brightness enhancements and/or longitudinal brightness asymmetries in the regions around Tethys' and Dione's orbits, and no such features have yet been seen in the Cassini images of the E ring. In principle, there could be some subtle interactions between E ring particles and the relevant moons that would cause the requisite variations in the particle flux without producing detectable asymmetries in the density of the rings. Fully exploring such possibilities would likely require numerical simulations that are beyond the scope of this work.

Given the above challenges with identifying a suitable dust population around these moons during the Cassini mission, it is worth considering whether Calypso's and Helene's current brightness are not their steady-state values, but are instead transient phenomena caused by some event in the relatively recent past. Specifically, we can consider the possibility that a recent impact into Calypso and/or Helene released enough material to affect the global surface properties of both these moons. A thorough quantitative evaluation of such scenarios is beyond the scope of this paper. Instead we will just provide some order-of-magnitude calculations which demonstrate that this is a viable possibility.

The total amount of material needed to affect the overall surface brightness of Calypso and Helene is simply the amount of material needed to coat these moons with a layer thick enough to determine its optical properties at optical wavelengths. Since light can only penetrate a few wavelengths through the surface regolith, we may conservatively estimate that a  $10\text{-}\mu\text{m}$  thick layer of material will be sufficient for these purposes. Given that Calypso and Helene have surface areas of around  $400 \text{ km}^2$  and  $1400 \text{ km}^2$  respectively, the total volume of material needed to coat these moons is  $4000 \text{ m}^3$  and  $14,000 \text{ m}^3$ . Conservatively assuming this is ice-rich material of negligible porosity, these volumes correspond to total debris masses of  $4 \times 10^6$  and  $14 \times 10^6 \text{ kg}$ , respectively.

The flux of objects large enough to produce these sorts of debris clouds is fairly well constrained thanks to observations of comparably-massive impact-generated debris clouds above Saturn's rings described by [Tiscareno et al. \(2013\)](#). The masses of those clouds are uncertain and depend on the assumed size distribution of the debris, but the feature designated Bx probably had a mass between  $2 \times 10^5$  kg and  $2 \times 10^7$  kg, which is comparable to that required to brighten Calypso or Helene. The estimated flux of impactors able of producing this amount of debris is  $3 \times 10^{-20} / \text{m}^2/\text{s}$  ([Tiscareno et al. 2013](#)). Assuming cross-sections consistent with the observed sizes of Calypso and Helene, this means the mean time between impacts should be between 1000 and 10,000 years.

The other relevant timescale in this problem is how long it would take E-ring material to coat these moons and erase any transient signals from an impact. Using the fluxes provided in Table 6, and assuming a typical E-ring particle radius of around 1  $\mu\text{m}$ , we estimate that E-ring material would accumulate on the surfaces at rates of between 0.2 nm/year for Helene and 0.5 nm/year for Calypso. It would therefore take 20,000 years for Calypso and 50,000 years for Helene to accumulate a 10-micron-thick layer of E-ring particles. These numbers could potentially be reduced by a factor of  $\sim 100$  if we account for the yield of secondary debris from each E-ring particle impact (see above). The resurfacing time due to E-ring particles is therefore likely comparable to the mean time between impacts capable of covering these entire moons in fresh impact debris. It is therefore not unreasonable that Calypso and Helene both experienced a recent impact that brightened their surfaces, while Telesto and Polydeuces managed to avoid such a recent collision. In principle, some of the material from a collision into Helene or Calypso could have been transported to the other moon, allowing a single impact to brighten both moons, but to properly explore the relative likelihood of such an event will require numerical simulations of both dynamics of the impact debris similar to those done by [Dobrovolskis et al. \(2010\)](#), perhaps including non-gravitational forces.

Note that this explanation for Calypso's and Helene's brightness means that impacts tend to increase the moons' brightness, rather than darken them. This might at first be counter-intuitive because cometary debris in the outer solar system is generally assumed to be much darker than Saturn's moons. However, it is important to realize that most of the debris produced by the impacts would come from Helene and Calypso, not the impactor. Indeed, the expected impact yields for such bodies is of order 10,000 ([Cuzzi and Estrada 1998](#); [Tiscareno et al. 2013](#)), and so the impactor required to produce  $4 - 14 \times 10^6$  kg of debris would be only  $4 - 14 \times 10^2$  kg, which corresponds to an ice-rich object with a radius between 0.5 and 0.7 meters. Thus most of the debris falling on the moons would be pure ice, and should be able to brighten moon surfaces like the E and F rings are apparently able to do. This bright deposit would also be much thinner than the deposits previously identified in high-resolution images, which affect both the morphology and the color of the surface ([Thomas et al. 2013](#); [Hirata et al. 2014](#)). While such a thin deposit would probably not produce obvious morphological structures (even the original crater would be near the resolution limit of the best images), it is not clear whether a fresh global covering of fine debris is consistent with the color variations currently observed on these moons ([Thomas et al. 2013](#)). Also, it is not obvious whether recent impacts are consistent with near-infrared spectra of these moons, which show that Prometheus, Pandora and Calypso have deeper ice bands than Telesto and

Helene (Filacchione et al. 2012). Even so, the above considerations indicate that a recent impact is a possible explanation for Calypso’s and Helene’s high surface brightness and so merits further investigation.

## 5. SUMMARY

In conclusion, we have used a new photometric model for non-spherical objects to obtain surface brightness estimates that are comparable to those for the mid-sized satellites. Applying this model to Saturn’s moons has revealed a number of interesting features and trends, which are summarized below in order of the moon’s increasing distance from Saturn.

- Prometheus and Pandora are brighter than moons orbiting exterior and interior to them, suggesting that dust from the F ring is brightening these moons.
- Janus and Epimetheus have brighter trailing hemispheres than leading hemispheres, which is consistent with the expected pattern for impacting E-ring particles.
- Aegaeon, Methone and Pallene are all darker than expected given their location within the E ring. This is most likely due to the high flux of high-energy radiation into these moons.
- The spectral data for Aegaeon and Methone indicate that whatever material is responsible for making these moons dark reduces their brightness over a broad range of wavelengths and does not have obvious spectral signatures.
- The photometric data indicate that Anthe probably has a shape similar to Methone.
- Pallene’s leading side is slightly darker than its trailing side.
- Telesto and Polydeuces have surface brightnesses similar to their larger orbital companions (Tethys and Dione, respectively).
- Calypso is substantially brighter than Tethys and Telesto, while Helene is substantially brighter than Dione and Polydeuces. These phenomena could either be due to an asymmetric flux of E-ring particles, or recent collisions with larger impactors.

## 6. ACKNOWLEDGEMENTS

Authors MMH and PH offer thanks to NASA’s Cassini Mission Project during various stages of this study. MMH acknowledges support from the Cassini Data Analysis Program Grant NNX15AQ67G. PH gratefully acknowledges that photometric modeling enhancements, as well as refinements and testing of computer software that are used and first-reported in this paper were developed under the auspices of NASA Planetary Geology and Geophysics Program grant NNX14AN04G. MH also wishes to acknowledge that the initial analyses of the small moons’ brightnesses were done by M. Rehnberg as part of the REU program, and the calculations regarding the deposition rates on the various small moons were inspired by conservations with S. Morrison, S.G. Zaidi and H. Sharma. We thank the anonymous reviewer for their helpful comments on an earlier draft of this manuscript.

## REFERENCES

- Acton, C. H., 1996. Ancillary data services of NASA's Navigation and Ancillary Information Facility. *Planet. Space Sci.* 44, 65–70.
- Black, G. J., Campbell, D. B., Carter, L. M., 2007. Arecibo radar observations of Rhea, Dione, Tethys, and Enceladus. *Icarus* 191 (2), 702–711.
- Brown, R. H., Baines, K. H., Bellucci, G., Bibring, J.-P., Buratti, B. J., Capaccioni, F., Cerroni, P., Clark, R. N., Coradini, A., Cruikshank, D. P., Drossart, P., Formisano, V., Jaumann, R., Langevin, Y., Matson, D. L., McCord, T. B., Mennella, V., Miller, E., Nelson, R. M., Nicholson, P. D., Sicardy, B., Sotin, C., 2004. The Cassini Visual And Infrared Mapping Spectrometer (Vims) Investigation. *SSR* 115, 111–168.
- Buratti, B., Veverka, J., 1984. Voyager photometry of Rhea, Dione, Tethys, Enceladus and Mimas. *Icarus* 58 (2), 254–264.
- Buratti, B. J., 1984. Voyager disk resolved photometry of the Saturnian satellites. *Icarus* 59 (3), 392–405.
- Buratti, B. J., Bauer, J. M., Hicks, M. D., Mosher, J. A., Filacchione, G., Momary, T., Baines, K. H., Brown, R. H., Clark, R. N., Nicholson, P. D., 2010. Cassini spectra and photometry 0.25–5.1  $\mu\text{m}$  of the small inner satellites of Saturn. *Icarus* 206 (2), 524–536.
- Buratti, B. J., Mosher, J. A., Johnson, T. V., 1990. Albedo and color maps of the Saturnian satellites. *Icarus* 87 (2), 339–357.
- Buratti, B. J., Mosher, J. A., Nicholson, P. D., McGhee, C. A., French, R. G., 1998. Near-Infrared Photometry of the Saturnian Satellites during Ring Plane Crossing. *Icarus* 136 (2), 223–231.
- Buratti, B. J., Thomas, P. C., Roussos, E., Howett, C., Seiß, M., Hendrix, A. R., Helfenstein, P., Brown, R. H., Clark, R. N., Denk, T., Filacchione, G., Hoffmann, H., Jones, G. H., Khawaja, N., Kollmann, P., Krupp, N., Lunine, J., Momary, T. W., Paranicas, C., Postberg, F., Sachse, M., Spahn, F., Spencer, J., Srama, R., Albin, T., Baines, K. H., Ciarniello, M., Economou, T., Hsu, H.-W., Kempf, S., Krimigis, S. M., Mitchell, D., Moragas-Klostermeyer, G., Nicholson, P. D., Porco, C. C., Rosenberg, H., Simolka, J., Soderblom, L. A., 2019. Close cassini flybys of saturn's ring moons pan, daphnis, atlas, pandora, and epimetheus. *Science* 364 (6445).
- Calvin, W. M., Clark, R. N., Brown, R. H., Spencer, J. R., 1995. Spectra of the icy Galilean satellites from 0.2 to 5  $\mu\text{m}$ : A compilation, new observations, and a recent summary. *J. Geophys. Res.* 100 (E9), 19041–19048.
- Clark, R. N., Cruikshank, D. P., Jaumann, R., Brown, R. H., Stephan, K., Dalle Ore, C. M., Eric Livo, K., Pearson, N., Curchin, J. M., Hoefen, T. M., Buratti, B. J., Filacchione, G., Baines, K. H., Nicholson, P. D., 2012. The surface composition of Iapetus: Mapping results from Cassini VIMS. *Icarus* 218 (2), 831–860.
- Clark, R. N., Curchin, J. M., Jaumann, R., Cruikshank, D. P., Brown, R. H., Hoefen, T. M., Stephan, K., Moore, J. M., Buratti, B. J., Baines, K. H., Nicholson, P. D., Nelson, R. M., 2008. Compositional mapping of Saturn's satellite Dione with Cassini VIMS and implications of dark material in the Saturn system. *Icarus* 193 (2), 372–386.
- Cuzzi, J. N., Estrada, P. R., 1998. Compositional Evolution of Saturn's Rings Due to Meteoroid Bombardment. *Icarus* 132 (1), 1–35.

- Dobrovolskis, A. R., Alvarellos, J. L., Zahnle, K. J., Lissauer, J. J., 2010. Exchange of ejecta between Telesto and Calypso: Tadpoles, horseshoes, and passing orbits. *Icarus* 210 (1), 436–445.
- Filacchione, G., Capaccioni, F., Ciarniello, M., Clark, R. N., Cuzzi, J. N., Nicholson, P. D., Cruikshank, D. P., Hedman, M. M., Buratti, B. J., Lunine, J. I., 2012. Saturn's icy satellites and rings investigated by Cassini-VIMS: III - Radial compositional variability. *Icarus* 220 (2), 1064–1096.
- Filacchione, G., Capaccioni, F., Clark, R. N., Nicholson, P. D., Cruikshank, D. P., Cuzzi, J. N., Lunine, J. I., Brown, R. H., Cerroni, P., Tosi, F., Ciarniello, M., Buratti, B. J., Hedman, M. M., Flaminii, E., 2013. The Radial Distribution of Water Ice and Chromophores across Saturn's System. *ApJ* 766 (2), 76.
- Franz, O. G., Millis, R. L., 1975. Photometry of Dione, Tethys, and Enceladus on the UVB System. *Icarus* 24 (4), 433–442.
- Hamilton, D. P., Burns, J. A., 1994. Origin of Saturn's E Ring: Self-Sustained, Naturally. *Science* 264 (5158), 550–553.
- Hand, K. P., Carlson, R. W., 2015. Europa's surface color suggests an ocean rich with sodium chloride. *Geophys. Res. Lett.* 42 (9), 3174–3178.
- Hapke, B., 1986. On the sputter alteration of regoliths of outer solar system bodies. *Icarus* 66 (2), 270–279.
- Hedman, M. M., Burns, J. A., Hamilton, D. P., Showalter, M. R., 2012. The three-dimensional structure of Saturn's E ring. *Icarus* 217 (1), 322–338.
- Hedman, M. M., Cooper, N. J., Murray, C. D., Beurle, K., Evans, M. W., Tiscareno, M. S., Burns, J. A., 2010. Aegaeon (Saturn LIII), a G-ring object. *Icarus* 207, 433–447.
- Hedman, M. M., Postberg, F., Hamilton, D. P., Renner, S., Hsu, H. W., 2018. *Dusty Rings*, pp. 308–337.
- Helfenstein, P., Veverka, J., 1989. Physical characterization of asteroid surfaces from photometric analysis. In: Binzel, R. P., Gehrels, T., Matthews, M. S. (Eds.), *Asteroids II*, pp. 557–593.
- Hendrix, A. R., Buratti, B. J., Cruikshank, D. P., Clark, R. N., Scipioni, F., Howett, C. J. A., 2018. *Surface Composition of Saturn's Icy Moons*, pp. 307.
- Hibbitts, C. A., Stockstill-Cahill, K., Wing, B., Paranicas, C., 2019. Color centers in salts - Evidence for the presence of sulfates on Europa. *Icarus* 326, 37–47.
- Hirata, N., Miyamoto, H., Showman, A. P., 2014. Particle deposition on the saturnian satellites from ephemeral cryovolcanism on Enceladus. *Geophys. Res. Lett.* 41 (12), 4135–4141.
- Horanyi, M., Burns, J. A., Hamilton, D. P., 1992. The dynamics of Saturn's E ring particles. *Icarus* 97 (2), 248–259.
- Horányi, M., Juhász, A., Morfill, G. E., 2008. Large-scale structure of Saturn's E-ring. *Geophys. Res. Lett.* 35 (4), L04203.
- Howett, C. J. A., Hendrix, A. R., Nordheim, T. A., Paranicas, C., Spencer, J. R., Verbiscer, A. J., 2018. *Ring and Magnetosphere Interactions with Satellite Surfaces*, pp. 343.
- Howett, C. J. A., Spencer, J. R., Schenk, P., Johnson, R. E., Paranicas, C., Hurford, T. A., Verbiscer, A., Segura, M., 2011. A high-amplitude thermal inertia anomaly of probable magnetospheric origin on Saturn's moon Mimas. *Icarus* 216 (1), 221–226.
- Kempf, S., Beckmann, U., Moragas-Klostermeyer, G., Postberg, F., Srama, R., Economou, T., Schmidt, J., Spahn, F., Grün, E., 2008. The E ring in the vicinity of Enceladus. I. Spatial distribution and properties of the ring particles. *Icarus* 193 (2), 420–437.
- Koschny, D., Grün, E., 2001. Impacts into Ice-Silicate Mixtures: Crater Morphologies, Volumes, Depth-to-Diameter Ratios, and Yield. *Icarus* 154 (2), 391–401.

- Krimigis, S. M., Mitchell, D. G., Hamilton, D. C., Livi, S., Dandouras, J., Jaskulek, S., Armstrong, T. P., Boldt, J. D., Cheng, A. F., Gloeckler, G., Hayes, J. R., Hsieh, K. C., Ip, W. H., Keath, E. P., Kirsch, E., Krupp, N., Lanzerotti, L. J., Lundgren, R., Mauk, B. H., McEntire, R. W., Roelof, E. C., Schlemm, C. E., Tossman, B. E., Wilken, B., Williams, D. J., 2004. Magnetosphere Imaging Instrument (MIMI) on the Cassini Mission to Saturn/Titan. *SSRv* 114 (1-4), 233–329.
- Le Gall, A., West, R. D., Bonnefoy, L. E., 2019. Dust and snow cover on saturn's icy moons. *Geophysical Research Letters* n/a (n/a).
- McEwen, A. S., 1991. Photometric functions for photoclinometry and other applications. *Icarus* 92 (2), 298–311.
- Minnaert, M., 1941. The reciprocity principle in lunar photometry. *ApJ* 93, 403–410.
- Moore, J. M., Chapman, C. R., Bierhaus, E. B., Greeley, R., Chuang, F. C., Klemaszewski, J., Clark, R. N., Dalton, J. B., Hibbitts, C. A., Schenk, P. M., 2007. *Callisto*, pp. 397.
- Muinonen, K., Lumme, K., 2015. Disk-integrated brightness of a Lommel-Seeliger scattering ellipsoidal asteroid. *A&A* 584, A23.
- Murray, C. D., Dermott, S. F., 1999. *Solar system dynamics*.
- Noland, M., Veverka, J., Morrison, D., Cruikshank, D. P., Lazarewicz, A. R., Morrison, N. D., Elliot, J. L., Goguen, J., Burns, J. A., 1974. Six-Color Photometry of Iapetus, Titan, Rhea, Dione, and Tethys. *Icarus* 23 (3), 334–354.
- Ostro, S. J., West, R. D., Wye, L. C., Zebker, H. A., Janssen, M. A., Stiles, B., Kelleher, K., Anderson, Y. Z., Boehmer, R. A., Callahan, P., Gim, Y., Hamilton, G. A., Johnson, W. T. K., Veeramachaneni, C., Lorenz, R. D., The Cassini Radar Team, 2010. New Cassini RADAR results for Saturn's icy satellites. *Icarus* 206 (2), 498–506.
- Paranicas, C., Hibbitts, C. A., Kollmann, P., Ligier, N., Hendrix, A. R., Nordheim, T. A., Roussos, E., Krupp, N., Blaney, D., Cassidy, T. A., 2018. Magnetospheric considerations for solar system ice state. *Icarus* 302, 560–564.
- Pitman, K. M., Buratti, B. J., Mosher, J. A., 2010. Disk-integrated bolometric Bond albedos and rotational light curves of saturnian satellites from Cassini Visual and Infrared Mapping Spectrometer. *Icarus* 206 (2), 537–560.
- Porco, C. C., West, R. A., Squyres, S., McEwen, A., Thomas, P., Murray, C. D., Del Genio, A., Ingersoll, A. P., Johnson, T. V., Neukum, G., Veverka, J., Dones, L., Brahic, A., Burns, J. A., Haemmerle, V., Knowles, B., Dawson, D., Roatsch, T., Beurle, K., Owen, W., 2004. Cassini Imaging Science: Instrument Characteristics And Anticipated Scientific Investigations At Saturn. *SSRv* 115, 363–497.
- Poston, M. J., Mahjoub, A., Ehlmann, B. L., Blacksberg, J., Brown, M. E., Carlson, R. W., Eiler, J. M., Hand, K. P., Hodyss, R., Wong, I., 2018. Visible Near-infrared Spectral Evolution of Irradiated Mixed Ices and Application to Kuiper Belt Objects and Jupiter Trojans. *ApJ* 856 (2), 124.
- Roussos, E., Krupp, N., Armstrong, T. P., Paranicas, C., Mitchell, D. G., Krimigis, S. M., Jones, G. H., Dialynas, K., Sergis, N., Hamilton, D. C., 2008. Discovery of a transient radiation belt at Saturn. *Geophys. Res. Lett.* 35 (22), L22106.
- Schenk, P., Hamilton, D. P., Johnson, R. E., McKinnon, W. B., Paranicas, C., Schmidt, J., Showalter, M. R., 2011. Plasma, plumes and rings: Saturn system dynamics as recorded in global color patterns on its midsize icy satellites. *Icarus* 211 (1), 740–757.
- Schröder, S. E., Mottola, S., Keller, H. U., Raymond, C. A., Russell, C. T., 2014. Reprint of: Resolved photometry of Vesta reveals physical properties of crater regolith. *Planet. Space Sci.* 103, 66–81.

- Scipioni, F., Tosi, F., Stephan, K., Filacchione, G., Ciarniello, M., Capaccioni, F., Cerroni, P., 2013. Spectroscopic classification of icy satellites of Saturn I: Identification of terrain units on Dione. *Icarus* 226 (2), 1331–1349.
- Scipioni, F., Tosi, F., Stephan, K., Filacchione, G., Ciarniello, M., Capaccioni, F., Cerroni, P., 2014. Spectroscopic classification of icy satellites of Saturn II: Identification of terrain units on Rhea. *Icarus* 234, 1–16.
- Shkuratov, Y., Kaydash, V., Korokhin, V., Velikodsky, Y., Opanasenko, N., Videen, G., 2011. Optical measurements of the Moon as a tool to study its surface. *Planet. Space Sci.* 59 (13), 1326–1371.
- Thomas, P., Helfenstein, P., 2019. The small inner satellites of saturn: Shapes, structures and some implications. *Icarus*.
- Thomas, P., Tiscareno, M. S., Helfenstein, P., 2018. The inner small satellites of saturn, and hyperion. In: Schenk, P., Clark, R., Howett, C. J. A., Verbiscer, A., Waite, J. H., Dotson, R. (Eds.), *Enceladus and the Icy Moons of Saturn*, pp. 387–408. University of Arizona Press.
- Thomas, P. C., 2010. Sizes, shapes, and derived properties of the saturnian satellites after the Cassini nominal mission. *Icarus* 208, 395–401.
- Thomas, P. C., Burns, J. A., Hedman, M., Helfenstein, P., Morrison, S., Tiscareno, M. S., Veverka, J., 2013. The inner small satellites of Saturn: A variety of worlds. *Icarus* 226, 999–1019.
- Tiscareno, M. S., Mitchell, C. J., Murray, C. D., Di Nino, D., Hedman, M. M., Schmidt, J., Burns, J. A., Cuzzi, J. N., Porco, C. C., Beurle, K., Evans, M. W., 2013. Observations of Ejecta Clouds Produced by Impacts onto Saturn’s Rings. *Science* 340 (6131), 460–464.
- Trumbo, S. K., Brown, M. E., Hand, K. P., 2019. Sodium chloride on the surface of Europa. *Science* 5 (6), aaw7123.
- Verbiscer, A., French, R., Showalter, M., Helfenstein, P., 2007. Enceladus: Cosmic Graffiti Artist Caught in the Act. *Science* 315, 815.
- Verbiscer, A., P. Helfenstein, Buratti, B., Royer, E., 2018. Surface properties of saturn’s moons from optical remote sensing. In: Schenk, P., Clark, R., Howett, C. J. A., Verbiscer, A., Waite, J. H., Dotson, R. (Eds.), *Enceladus and the Icy Moons of Saturn*, pp. 323–341. University of Arizona Press.
- Verbiscer, A. J., Veverka, J., 1989. Albedo dichotomy of Rhea: Hapke analysis of Voyager photometry. *Icarus* 82 (2), 336–353.
- Verbiscer, A. J., Veverka, J., 1992. Mimas: Photometric roughness and albedo map. *Icarus* 99 (1), 63–69.
- Verbiscer, A. J., Veverka, J., 1994. A Photometric Study of Enceladus. *Icarus* 110 (1), 155–164.
- Vickers, G., 1996. The projected areas of ellipsoids and cylinders. *Powder Technology* 86, 195–200.
- West, R., Knowles, B., Birath, E., Charnoz, S., Di Nino, D., Hedman, M., Helfenstein, P., McEwen, A., Perry, J., Porco, C., Salmon, J., Throop, H., Wilson, D., 2010. In-flight calibration of the Cassini imaging science sub-system cameras. *Planet. Space Sci.* 58, 1475–1488.
- Ye, S. Y., Gurnett, D. A., Kurth, W. S., 2016. In-situ measurements of Saturn’s dusty rings based on dust impact signals detected by Cassini RPWS. *Icarus* 279, 51–61.
- Ye, S. Y., Gurnett, D. A., Kurth, W. S., Averkamp, T. F., Kempf, S., Hsu, H. W., Srama, R., Grün, E., 2014. Properties of dust particles near Saturn inferred from voltage pulses induced by dust impacts on Cassini spacecraft. *Journal of Geophysical Research (Space Physics)* 119 (8), 6294–6312.

## APPENDIX A: PYTHON CODE TO EVALUATE PREDICTED AREAS

Note, the inputs to this program are the sub-solar longitude `slon`, the sub-solar latitude `slat`, the sub-observer longitude `clon`, the sub-observer latitude `clat`, the object's shape parameters `a, b, c` and the Minnaert parameter `k`

```
def objmod (slon,slat,clon,clat,a,b,c,k):
    import numpy as np
    theta=np.pi/180*np.array(range(181))
    phi=np.pi/180*np.array(range(361))
    mat=np.array(np.ones((361,181),float))
    thx=mat*1.0
    phix=mat*1.0
    for i in range(361):
        for j in range(181):
            thx[i,j]=np.pi*j/180
            phix[i,j]=np.pi*i/180
    areaf=np.sqrt(a**2*b**2*np.cos(thx)**2+c**2*(b**2*np.cos(phi)*phi**2 +a**2*np.sin(phi)*phi**2)*np.sin(thx)**2)
    rf=np.sqrt(areaf)
    xf=np.sin(thx)*np.cos(phi)/a
    yf=np.sin(thx)*np.sin(phi)/b
    zf=np.cos(thx)/c
    nx=xf/np.sqrt(xf**2+yf**2+zf**2)
    ny=yf/np.sqrt(xf**2+yf**2+zf**2)
    nz=zf/np.sqrt(xf**2+yf**2+zf**2)
    sln=slon*np.pi/180
    slt=(90-slat)*np.pi/180
    cln=clon*np.pi/180
    clt=(90-clat)*np.pi/180
    cosi=nx*np.sin(slt)*np.cos(sln)+ny*np.sin(slt)*np.sin(sln)+nz*np.cos(slt)
    cose=nx*np.sin(clt)*np.cos(cln)+ny*np.sin(clt)*np.sin(cln)+nz*np.cos(clt)
    cosi=.5*(cosi+abs(cosi))
    cose=.5*(cose+abs(cose))
    bright=cosi**k*cose**((1-k))
    brfact=bright*np.sin(thx)*areaf*cose*np.pi/180*np.pi/180
    pred=np.sum(brfact)

    return pred
```

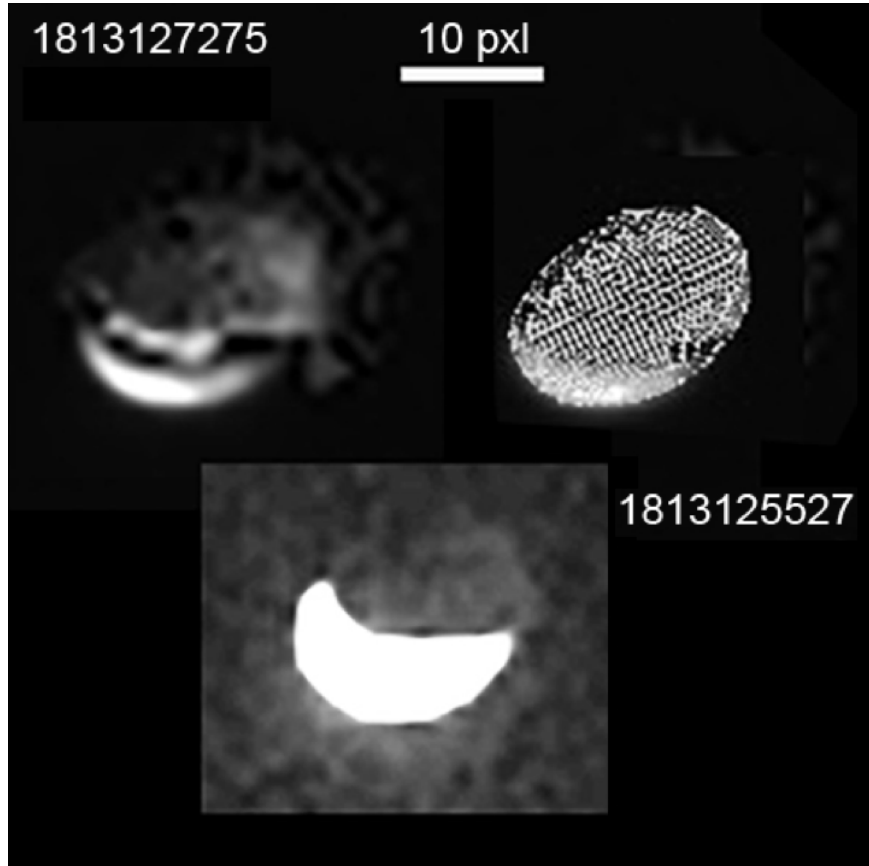
## APPENDIX B: A REVISED SHAPE FOR POLYDEUCES

The shape model of Polydeuces reported by Thomas et al. (2013) has relatively large uncertainties because it was based on a very limited number of resolved images. Fortunately, late in the Cassini mission there were two additional flybys of Polydeuces where the moon was over 10 pixels wide in the Narrow Angle Camera. Furthermore, in several of these images a large fraction of the limb is visible thanks to the combination of direct illumination and Saturn shine (see Figures 22- 23). The full set of resolved images listed in Table 7 were then manually fit to a ( $5^\circ \times 5^\circ$ ) shape model. Saturn shine was crucial in getting centers. Shape control is good for the  $a$  and  $c$  axes;  $a$  is the best constrained because of the Saturn shine images taken from near the intermediate axis showing the full projection of  $a$ . The  $b$  axis is poorly constrained, with the terminator in some images being the primary source of information about this dimension. Note the limb positions shown in Figure 23 are relatively smooth, but they do not approximate simple ellipsoids.

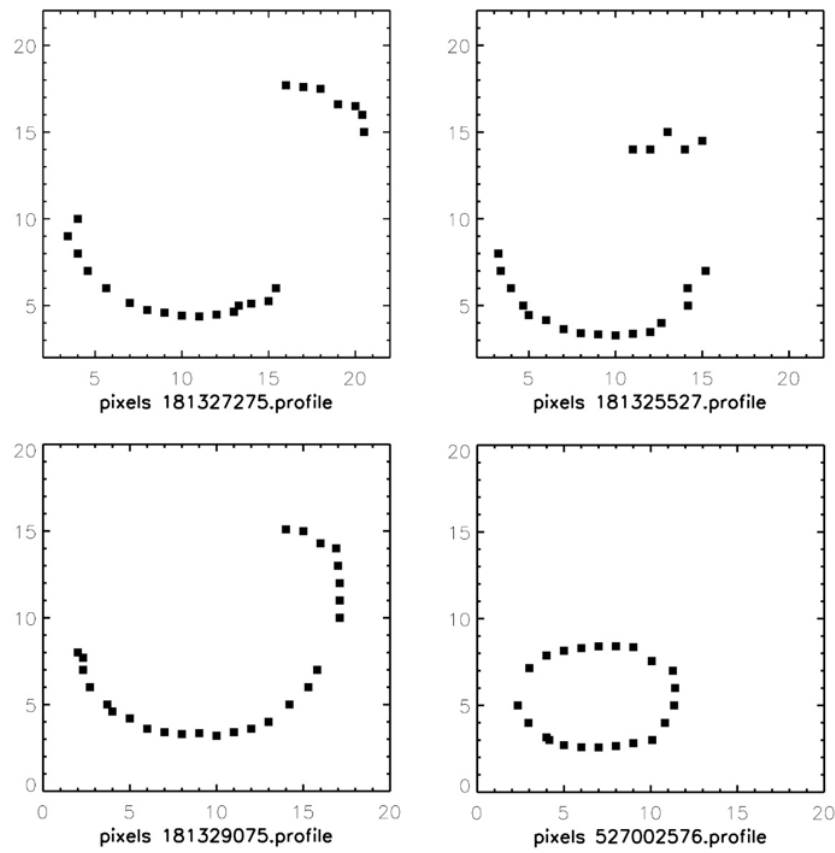
**Table 7.** Resolved images of Polydeuces used to derive its shape

Image	Sub-spacecraft Lat. (deg)	Sub-spacecraft Long. (deg)	Sub-solar Lat. (deg)	Sub-solar Long. (deg)	Range (km)	Pole <sup>a</sup> (deg)	x <sub>c</sub> (pixels)	y <sub>c</sub> (pixels)
N1526998156	-0.69	300.81	-17.38	265.61	70745.54	359.92	504.9	512.4
N1527002576	-0.51	282.09	-17.38	272.34	64087.42	359.92	524.1	511.2
N1527002708	-0.50	281.47	-17.38	272.54	64101.53	359.92	527.4	511.9
N1527006179	-0.28	265.98	-17.38	277.82	68549.73	359.92	552.1	511.8
N1809910321	-0.02	30.47	24.54	300.35	47250.34	99.94	511.1	575.9
N1809910848	-0.05	34.59	24.54	301.16	44829.21	99.92	520.7	580.0
N1813120961	0.76	221.86	24.76	146.90	54004.30	179.92	495.6	519.7
N1813121872	0.87	227.85	24.76	148.29	49544.58	179.92	511.8	418.4
N1813121938	0.88	228.31	24.76	148.39	49237.54	179.92	511.3	407.1
N1813123674	1.13	242.24	24.76	151.03	41948.07	179.92	539.3	571.7
N1813125527	1.41	261.21	24.76	153.85	36595.63	151.89	533.3	414.4
N1813125560	1.42	261.59	24.76	153.90	36528.47	151.89	533.8	413.8
N1813127275	1.60	282.26	24.76	156.51	34808.05	153.29	546.6	574.0
N1813129075	1.61	303.92	24.76	159.25	36813.49	157.30	543.7	424.7
N1813129108	1.61	304.29	24.76	159.30	36884.91	157.39	541.3	410.2

<sup>a</sup> Predicted positive pole azimuth in images, clockwise from up.



**Figure 22.** Shape analysis of Polydeuces from image N1813125527. Top left: Image with regions under direct illumination and Saturn-shine illumination stretched separately. Top right: Final shape model overlaid on image. Bottom: Image with a single stretch.



**Figure 23.** Estimated limb locations from representative images of Polydeuces.

## APPENDIX C: DATA TABLES FOR INDIVIDUAL OBSERVATIONS

In these tables, “Range” indicates the distance between the spacecraft and the body center. “Phase” is the solar phase angle at body center, “Sub S/C Latitude/Longitude” are the sub-spacecraft planetocentric latitude and (west) longitude, while “Sub-Solar Latitude/Longitude” are the sub-solar planetocentric latitude and (west) longitude. The value of  $A_{\text{eff}}$  is computed as described in the text, and the statistical error estimate is based on scatter of brightness values in regions near the planet (note this uncertainty is very small and so is not included for the larger moons).  $A_{\text{phys}}$  is the geometrical cross section of the moon from the perspective of the spacecraft, and the three values of  $a_{\text{pred}}$  are computed assuming Minnaert scattering laws with  $k = 1.0, 0.75$  and  $0.50$  assuming the shape parameters provided in Table 1. Note that since the shape of Anthe is not well determined and so these parameters could not be computed for that moon. All images were obtained using the Cassini ISS NAC clear filters except for those given in the last two tables. All these data tables are provided in machine-readable format in supplementary information associated with this article.

**Table 8.** Brightness estimates from clear-filter images of Aegaeon.

Filename	Range (km)	Phase (deg)	Sub-S/C Latitude (deg)	Sub-S/C Longitude (deg)	Sub-Solar Latitude (deg)	Sub-Solar Longitude (deg)	$A_{\text{eff}}$ Value ( $\text{km}^2$ )	$A_{\text{eff}}$ Error ( $\text{km}^2$ )	$A_{\text{phys}}$ ( $\text{km}^2$ )	$a_{\text{pred}}$	$a_{\text{pred}}$	$a_{\text{pred}}$
										$k=1$	$k=0.75$	$k=0.50$
N1560588018	1708521.8	42.9	0.5	94.9	-12.0	136.3	0.05365	0.00490	0.4384	0.2172	0.2323	0.2511
N1597476237	1188834.9	28.2	5.0	264.3	-5.6	238.1	0.07027	0.00199	0.4390	0.2630	0.2720	0.2826
N1597477967	1215347.6	28.2	5.2	273.2	-5.6	247.1	0.06765	0.00234	0.4404	0.2819	0.2871	0.2938
N1598073885	1170967.9	12.9	-0.8	91.4	-5.5	79.3	0.08536	0.00193	0.4397	0.3073	0.3084	0.3098
N1598104211	1179616.4	28.4	3.9	262.5	-5.5	235.7	0.05817	0.00382	0.4371	0.2573	0.2672	0.2787
N1598106121	1209151.0	28.4	4.0	272.3	-5.5	245.5	0.06960	0.00162	0.4403	0.2803	0.2861	0.2933
N1600657200	1205263.9	15.2	4.4	89.6	-5.0	77.6	0.07635	0.00125	0.4407	0.3020	0.3038	0.3063
N1600659110	1177824.9	15.5	4.8	99.5	-5.0	87.5	0.07693	0.00195	0.4355	0.3038	0.3034	0.3038
N1603168767	1203629.1	14.9	0.1	80.3	-4.6	66.1	0.07670	0.00263	0.4346	0.2859	0.2903	0.2951
N1603169886	1188076.4	14.9	0.3	86.0	-4.6	71.9	0.11391	0.00194	0.4390	0.2978	0.3008	0.3042
N1603171005	1172385.6	14.9	0.4	91.7	-4.6	77.6	0.09027	0.00139	0.4397	0.3050	0.3065	0.3084
N1603172124	1156722.9	15.0	0.6	97.5	-4.6	83.4	0.07553	0.00219	0.4366	0.3071	0.3071	0.3074
N1603831280	1199435.6	30.6	4.9	270.8	-4.4	241.6	0.09259	0.00632	0.4408	0.2719	0.2796	0.2888
N1603831616	1204569.2	30.6	4.9	272.5	-4.4	243.3	0.09025	0.00783	0.4405	0.2753	0.2821	0.2904
N1611860574	1180139.4	35.0	-1.5	271.8	-3.0	236.8	0.06200	0.00169	0.4398	0.2623	0.2723	0.2837
N1611861868	1199189.9	34.8	-1.2	278.3	-3.0	243.4	0.05355	0.00205	0.4361	0.2750	0.2811	0.2884
N1613784711	1186793.5	20.5	13.7	89.1	-2.7	76.6	0.06397	0.00299	0.4470	0.2931	0.2964	0.3015
N1613784773	1185609.4	20.5	13.7	89.5	-2.7	77.0	0.05710	0.00767	0.4471	0.2935	0.2967	0.3017
N1620768513	1048344.1	19.4	8.6	98.5	-1.4	81.9	0.05273	0.00550	0.4387	0.3015	0.3022	0.3039
N1693145818	2016283.8	20.7	0.1	259.2	10.9	277.0	0.06774	0.00886	0.4331	0.3001	0.2994	0.2997
N1697790446	672411.4	13.8	0.1	95.3	11.6	103.0	0.06472	0.00136	0.4382	0.3001	0.3011	0.3032
N1700932530	1086844.4	22.0	0.1	83.6	12.1	102.3	0.05768	0.00338	0.4376	0.2977	0.2986	0.3007
N1700935874	1056287.4	22.3	0.2	100.5	12.1	119.5	0.04449	0.00358	0.4334	0.2686	0.2747	0.2824
N1735282418	1616099.9	45.8	-13.5	40.5	17.0	75.1	0.02977	0.01038	0.3285	0.1757	0.1660	0.1605
N1735287671	1565889.8	48.0	-14.5	65.5	17.0	102.2	0.02999	0.00734	0.4167	0.2330	0.2319	0.2353
N1735287895	1563870.0	48.1	-14.6	66.3	17.0	103.1	0.03348	0.00395	0.4189	0.2336	0.2329	0.2367
N1735292924	1502396.9	49.6	-15.8	91.5	17.0	129.3	0.02843	0.00649	0.4492	0.2033	0.2144	0.2314
N1735293148	1500167.9	49.6	-15.8	92.4	17.0	130.2	0.03138	0.00277	0.4490	0.2008	0.2122	0.2295
N1735298177	1440448.0	50.2	-17.2	119.0	17.0	156.3	0.01708	0.00879	0.4085	0.1076	0.1202	0.1390
N1735298401	1438562.6	50.2	-17.2	120.0	17.0	157.3	0.01751	0.00440	0.4058	0.1042	0.1166	0.1351
N1735303430	1396492.8	49.7	-18.4	147.9	17.0	183.4	0.00603	0.02264	0.3087	0.0350	0.0384	0.0445

*Table 8 continued on next page*

**Table 8** (*continued*)

Filename	Range	Phase	Sub-S/C	Sub-S/C	Sub-Solar	Sub-Solar	$A_{\text{eff}}$	$A_{\text{eff}}$	$A_{\text{phys}}$	$a_{\text{pred}}$	$a_{\text{pred}}$	$a_{\text{pred}}$
	(km)	(deg)	Latitude	Longitude	Latitude	Longitude	Value	Error		k=1	k=0.75	k=0.50
			(deg)	(deg)	(deg)	(deg)	(km <sup>2</sup> )					
N1735303654	1395493.1	49.7	-18.4	148.9	17.0	184.3	0.00605	0.00932	0.3050	0.0338	0.0370	0.0428
N1738781138	1622316.6	53.3	-19.2	73.7	17.5	113.1	0.02857	0.00833	0.4405	0.2179	0.2223	0.2323
N1738785881	1563504.8	54.5	-20.5	97.6	17.5	137.6	0.01986	0.00835	0.4523	0.1675	0.1808	0.2009
N1738786055	1561911.8	54.6	-20.5	98.3	17.5	138.2	0.02414	0.00385	0.4518	0.1654	0.1788	0.1990
N1738790624	1509041.0	55.0	-21.8	122.7	17.5	162.0	0.01446	0.01037	0.4078	0.0814	0.0925	0.1096
N1738790798	1507733.5	55.0	-21.8	123.4	17.5	162.7	0.01268	0.00735	0.4059	0.0793	0.0901	0.1069
N1738804853	1474420.8	52.3	-24.0	202.7	17.5	235.3	0.01651	0.01175	0.3030	0.0940	0.0901	0.0901
N1738809596	1518111.4	51.0	-23.8	229.1	17.5	259.8	0.02672	0.00748	0.3885	0.1808	0.1772	0.1790
N1738809770	1519607.6	50.9	-23.8	229.9	17.5	260.4	0.02598	0.00641	0.3907	0.1828	0.1794	0.1813
N1738814339	1580446.6	50.0	-23.3	254.5	17.5	284.2	0.02897	0.00715	0.4481	0.2222	0.2256	0.2350
N1738814513	1582298.4	50.0	-23.3	255.2	17.5	284.9	0.03275	0.00298	0.4490	0.2222	0.2259	0.2355
N1746467285	1268854.0	43.0	-14.3	111.6	18.4	140.0	0.02565	0.00561	0.4228	0.1673	0.1784	0.1951
N1746472918	1209465.2	43.1	-15.9	142.6	18.4	169.1	0.01083	0.01027	0.3211	0.0612	0.0665	0.0755
N1746473092	1208454.9	43.0	-15.9	143.3	18.4	169.7	0.01113	0.00458	0.3182	0.0594	0.0646	0.0733
N1746484184	1204581.6	40.8	-17.7	207.8	18.4	227.2	0.01803	0.00840	0.2892	0.1052	0.1014	0.1009
N1746489747	1261513.1	39.7	-17.7	239.0	18.4	255.9	0.04403	0.02556	0.4036	0.2144	0.2122	0.2147
N1746489817	1262345.0	39.7	-17.7	239.3	18.4	256.2	0.03442	0.00456	0.4047	0.2154	0.2132	0.2158
N1746489991	1263991.6	39.7	-17.7	240.0	18.4	256.9	0.03450	0.00247	0.4067	0.2173	0.2152	0.2180
N1746495450	1341062.6	39.2	-17.4	269.0	18.4	285.2	0.04001	0.00461	0.4511	0.2459	0.2497	0.2589
N1746501083	1420238.2	39.4	-17.1	296.8	18.4	314.3	0.03096	0.00604	0.4149	0.1727	0.1806	0.1937
N1751405983	1516030.2	69.6	-37.4	358.7	19.0	42.1	0.00440	0.00554	0.3578	0.0368	0.0379	0.0415
N1751408802	1511466.5	71.2	-37.7	10.8	19.0	56.6	0.00805	0.00423	0.3654	0.0597	0.0597	0.0633
N1751411447	1500805.8	72.9	-38.3	22.4	19.0	70.5	0.00989	0.01400	0.3843	0.0871	0.0862	0.0899
N1751411621	1500161.6	73.0	-38.3	23.0	19.0	71.1	0.01096	0.00509	0.3854	0.0884	0.0875	0.0912
N1751414266	1483576.9	74.7	-39.1	34.7	19.0	85.0	0.01416	0.01190	0.4114	0.1150	0.1144	0.1193
N1751414440	1482671.8	74.8	-39.1	35.3	19.0	85.6	0.01312	0.00334	0.4127	0.1161	0.1155	0.1206
N1751417085	1460977.5	76.6	-40.1	47.2	19.0	99.5	0.01548	0.01164	0.4406	0.1342	0.1358	0.1437
N1751417259	1459856.1	76.7	-40.1	47.7	19.0	100.2	0.01518	0.00241	0.4419	0.1347	0.1365	0.1446
N1751419904	1434137.6	78.4	-41.3	59.9	19.0	114.1	0.00992	0.01450	0.4670	0.1382	0.1436	0.1561
N1751420078	1432857.0	78.5	-41.3	60.5	19.0	114.7	0.01418	0.00227	0.4680	0.1379	0.1436	0.1563
N1769540993	2234396.2	66.0	46.9	18.5	21.1	301.6	0.01409	0.02236	0.4268	0.1303	0.1334	0.1424
N1769549999	2255261.0	62.6	48.4	60.0	21.1	348.0	0.01367	0.01754	0.4867	0.1233	0.1443	0.1747
N1769550173	2253963.8	62.6	48.4	60.6	21.1	348.7	0.01338	0.00769	0.4875	0.1241	0.1455	0.1763
N1769559005	2158067.5	61.3	50.8	104.5	21.1	34.4	0.02032	0.03080	0.5056	0.2235	0.2480	0.2788
N1769559179	2156701.5	61.3	50.8	105.1	21.1	35.1	0.02237	0.00893	0.5053	0.2247	0.2488	0.2793
N1769563508	2113995.2	61.7	52.0	128.3	21.1	57.6	0.02118	0.01418	0.4871	0.2454	0.2568	0.2738
N1769568011	2081154.2	62.7	52.8	153.1	21.1	80.8	0.02418	0.01593	0.4629	0.2241	0.2266	0.2352
N1769572514	2063931.8	64.1	53.1	178.6	21.1	104.1	0.01483	0.04522	0.4506	0.1781	0.1802	0.1888
N1769572688	2063693.4	64.1	53.1	179.3	21.1	104.7	0.01569	0.00782	0.4506	0.1767	0.1789	0.1876
N1769581520	2080338.1	66.6	51.9	229.0	21.1	150.5	0.01535	0.01734	0.4837	0.1170	0.1317	0.1545
N1769586023	2108626.8	67.2	50.6	253.0	21.1	173.7	0.01446	0.01729	0.5036	0.1309	0.1558	0.1910
N1769586197	2109558.8	67.2	50.5	253.7	21.1	174.4	0.01373	0.00822	0.5039	0.1319	0.1571	0.1926
N1783325708	2736579.5	46.3	41.4	142.9	22.4	92.1	0.03034	0.01212	0.4257	0.2519	0.2482	0.2485
N1783332836	2706855.5	48.1	41.7	182.3	22.4	129.1	0.02242	0.04731	0.3847	0.1512	0.1520	0.1575
N1783333010	2706810.0	48.2	41.7	183.0	22.4	129.8	0.01871	0.02018	0.3848	0.1498	0.1508	0.1565
N1783343963	2761306.5	50.3	40.2	242.5	22.4	186.3	0.01940	0.01419	0.4675	0.1552	0.1793	0.2112
N1783347440	2796329.5	50.5	39.5	260.9	22.4	204.4	0.02220	0.04389	0.4856	0.2073	0.2329	0.2644
N1783347614	2797654.5	50.5	39.5	261.5	22.4	205.1	0.02294	0.01322	0.4859	0.2092	0.2347	0.2660
N1783351091	2835175.2	50.3	38.7	279.5	22.4	223.2	0.03761	0.03266	0.4840	0.2559	0.2740	0.2958
N1783351265	2836512.8	50.3	38.7	280.1	22.4	223.9	0.03240	0.01875	0.4835	0.2572	0.2749	0.2963
N1783358393	2903565.2	48.9	37.4	315.4	22.4	260.9	0.02451	0.04682	0.4250	0.2628	0.2592	0.2588
N1783358567	2904500.2	48.9	37.4	316.0	22.4	261.5	0.03220	0.01364	0.4235	0.2617	0.2578	0.2573
N1792001280	2408488.0	59.0	36.6	248.8	23.2	181.1	0.01603	0.02219	0.4676	0.1366	0.1584	0.1886
N1796027549	2961557.5	55.7	29.9	122.0	23.5	59.4	0.02975	0.01198	0.4305	0.2607	0.2633	0.2681
N1796033113	2900047.8	56.5	30.4	151.8	23.5	88.0	0.03016	0.01275	0.3523	0.2123	0.2003	0.1921

Table 8 continued on next page

**Table 8** (*continued*)

Filename	Range	Phase	Sub-S/C	Sub-S/C	Sub-Solar	Sub-Solar	$A_{\text{eff}}$	$A_{\text{eff}}$	$A_{\text{phys}}$	$a_{\text{pred}}$	$a_{\text{pred}}$	$a_{\text{pred}}$
	(km)	(deg)	Latitude	Longitude	Latitude	Longitude	Value	Error		k=1	k=0.75	k=0.50
			(deg)	(deg)	(deg)	(deg)	(km <sup>2</sup> )					
N1796035895	2880943.5	57.1	30.5	166.9	23.5	102.4	0.01793	0.01960	0.3209	0.1674	0.1556	0.1482
N1796041459	2870410.8	58.6	30.4	197.2	23.5	131.0	0.01133	0.02649	0.3274	0.0983	0.0962	0.0981
N1796052587	2945140.0	60.5	29.2	256.6	23.5	188.4	0.01582	0.01334	0.4614	0.1443	0.1658	0.1953
N1796055369	2974587.0	60.6	28.8	270.9	23.5	202.8	0.02235	0.01441	0.4683	0.1879	0.2102	0.2390
N1796058151	3004039.5	60.4	28.3	285.0	23.5	217.1	0.02656	0.01089	0.4583	0.2257	0.2422	0.2627
N1796060933	3031322.2	60.1	28.0	298.9	23.5	231.5	0.02693	0.01210	0.4331	0.2463	0.2526	0.2615
N1796085971	2972528.2	53.5	27.6	60.4	23.5	0.6	0.01429	0.01435	0.4304	0.1226	0.1392	0.1629
N1796088753	2931888.8	53.1	27.9	74.2	23.5	15.0	0.01875	0.01339	0.4564	0.1654	0.1870	0.2154
N1796091535	2888910.0	52.8	28.3	88.3	23.5	29.3	0.02567	0.01695	0.4673	0.2126	0.2335	0.2594
N1843274411	2476786.2	31.8	31.8	320.2	26.2	284.1	0.03697	0.03320	0.3910	0.2615	0.2525	0.2455
N1843274619	2477964.8	31.8	31.8	321.2	26.2	285.2	0.03477	0.03172	0.3882	0.2585	0.2493	0.2422
N1843274723	2478541.0	31.7	31.8	321.7	26.2	285.8	0.04172	0.03403	0.3868	0.2569	0.2477	0.2405
N1843274810	2479211.2	31.7	31.8	322.2	26.2	286.4	0.03202	0.02596	0.3852	0.2551	0.2458	0.2386
N1843275331	2481731.2	31.5	31.7	324.5	26.2	288.9	0.04013	0.03539	0.3787	0.2476	0.2382	0.2309
N1843275435	2482246.0	31.5	31.7	325.0	26.2	289.4	0.04567	0.03210	0.3774	0.2460	0.2365	0.2292
N1843276143	2485501.2	31.3	31.6	328.4	26.2	293.1	0.04055	0.03460	0.3682	0.2348	0.2253	0.2180
N1843276747	2487928.0	31.0	31.5	331.3	26.2	296.2	0.04212	0.03268	0.3605	0.2250	0.2157	0.2087
N1843276851	2488312.2	31.0	31.5	331.8	26.2	296.7	0.03818	0.03392	0.3593	0.2233	0.2141	0.2071
N1843282326	2493604.5	28.9	31.2	357.7	26.2	325.1	0.01795	0.04350	0.3166	0.1474	0.1446	0.1442
N1843285685	2481743.0	27.5	31.2	13.2	26.2	342.3	0.01391	0.04970	0.3264	0.1297	0.1328	0.1383
N1843286261	2478585.2	27.3	31.2	15.9	26.2	345.2	0.01712	0.01676	0.3307	0.1296	0.1337	0.1402
N1843286614	2476400.0	27.1	31.2	17.6	26.2	347.1	0.03177	0.03029	0.3338	0.1300	0.1347	0.1420
N1843287322	2471750.2	26.9	31.2	20.9	26.2	350.7	0.01900	0.04209	0.3406	0.1317	0.1377	0.1463
N1843288134	2465816.0	26.6	31.3	24.7	26.2	354.9	0.03163	0.03360	0.3494	0.1355	0.1429	0.1530
N1843289446	2454913.5	26.1	31.4	30.9	26.2	1.7	0.03742	0.04371	0.3652	0.1452	0.1549	0.1673
N1843289848	2450925.0	25.9	31.4	33.0	26.2	3.9	0.01680	0.03470	0.3708	0.1495	0.1599	0.1730
N1843290479	2445238.2	25.7	31.4	35.8	26.2	7.0	0.02622	0.03745	0.3786	0.1560	0.1673	0.1812
N1843291083	2439158.0	25.5	31.5	38.7	26.2	10.1	0.02569	0.05325	0.3866	0.1635	0.1755	0.1902
N1843291187	2438080.5	25.5	31.5	39.2	26.2	10.6	0.02753	0.04326	0.3880	0.1649	0.1770	0.1918
N1843291791	2431652.0	25.3	31.6	42.1	26.2	13.7	0.02979	0.03708	0.3960	0.1732	0.1860	0.2014
N1843291895	2430516.0	25.3	31.6	42.6	26.2	14.3	0.04201	0.03010	0.3974	0.1747	0.1876	0.2031
N1843292499	2423756.0	25.1	31.7	45.5	26.2	17.4	0.03229	0.03519	0.4053	0.1838	0.1972	0.2132
N1843292603	2422564.8	25.0	31.7	46.0	26.2	17.9	0.03199	0.03413	0.4067	0.1854	0.1989	0.2149
N1843293609	2410204.8	24.7	31.8	51.0	26.2	23.3	0.03338	0.02290	0.4199	0.2023	0.2165	0.2328
N1843294136	2404127.8	24.6	31.9	53.3	26.2	25.8	0.03289	0.03341	0.4259	0.2107	0.2250	0.2413
N1843294240	2402820.8	24.6	31.9	53.8	26.2	26.4	0.03729	0.03051	0.4271	0.2125	0.2268	0.2431
N1843294844	2395101.5	24.4	31.9	56.8	26.2	29.5	0.04880	0.03238	0.4341	0.2230	0.2373	0.2535
N1843294948	2393750.8	24.4	32.0	57.3	26.2	30.0	0.04290	0.02521	0.4352	0.2248	0.2391	0.2553
N1843295552	2385787.8	24.3	32.0	60.2	26.2	33.1	0.04703	0.02514	0.4417	0.2354	0.2495	0.2654
N1843295656	2384397.0	24.2	32.1	60.7	26.2	33.7	0.04585	0.02882	0.4428	0.2372	0.2513	0.2671
N1843296260	2376213.8	24.1	32.2	63.7	26.2	36.8	0.04793	0.02582	0.4488	0.2478	0.2615	0.2769
N1843296364	2374787.0	24.1	32.2	64.2	26.2	37.3	0.03207	0.06414	0.4498	0.2495	0.2633	0.2785
N1843296968	2366407.8	24.0	32.3	67.1	26.2	40.4	0.04852	0.02449	0.4552	0.2598	0.2731	0.2878
N1843297072	2364949.5	24.0	32.3	67.6	26.2	41.0	0.03309	0.02143	0.4560	0.2616	0.2747	0.2893
N1843297370	2360238.0	23.9	32.3	69.3	26.2	42.7	0.04673	0.01502	0.4587	0.2671	0.2799	0.2941
N1843297544	2358407.2	23.9	32.4	69.9	26.2	43.4	0.04415	0.00777	0.4597	0.2692	0.2819	0.2959
N1843297897	2353239.0	23.8	32.4	71.7	26.2	45.2	0.05251	0.01692	0.4624	0.2749	0.2873	0.3009
N1843298001	2351746.0	23.8	32.4	72.2	26.2	45.8	0.04723	0.01801	0.4631	0.2765	0.2888	0.3022
N1843298605	2343011.8	23.7	32.5	75.2	26.2	48.9	0.05501	0.01592	0.4669	0.2857	0.2972	0.3097
N1843298709	2341497.8	23.7	32.6	75.7	26.2	49.4	0.04934	0.01990	0.4675	0.2872	0.2985	0.3110
N1843299313	2332654.5	23.6	32.7	78.7	26.2	52.5	0.06102	0.01425	0.4706	0.2955	0.3060	0.3175
N1843300021	2322200.0	23.6	32.8	82.3	26.2	56.2	0.05444	0.01498	0.4733	0.3043	0.3138	0.3241
N1843300125	2320658.0	23.6	32.8	82.8	26.2	56.7	0.05971	0.01464	0.4737	0.3055	0.3148	0.3250
N1843300729	2311681.0	23.5	32.9	85.8	26.2	59.8	0.05778	0.01442	0.4751	0.3120	0.3203	0.3294
N1843301131	2305156.2	23.5	33.0	88.1	26.2	62.1	0.05222	0.01391	0.4758	0.3161	0.3236	0.3320

Table 8 continued on next page

**Table 8** (*continued*)

Filename	Range	Phase	Sub-S/C	Sub-S/C	Sub-Solar	Sub-Solar	$A_{\text{eff}}$	$A_{\text{eff}}$	$A_{\text{phys}}$	$a_{\text{pred}}$	$a_{\text{pred}}$	$a_{\text{pred}}$
	(km)	(deg)	Latitude	Longitude	Latitude	Longitude	Value	Error		k=1	k=0.75	k=0.50
			(deg)	(deg)	(deg)	(deg)	(km <sup>2</sup> )					
N1843303074	2276817.2	23.5	33.3	97.8	26.2	71.9	0.05189	0.01546	0.4742	0.3277	0.3317	0.3366
N1843303886	2264898.8	23.5	33.5	102.0	26.2	76.1	0.05259	0.01856	0.4714	0.3292	0.3318	0.3352
N1843304490	2256137.8	23.5	33.6	105.1	26.2	79.2	0.06772	0.01400	0.4685	0.3290	0.3306	0.3329
N1843304594	2254640.0	23.5	33.6	105.6	26.2	79.8	0.06453	0.01359	0.4679	0.3289	0.3302	0.3324
N1843304892	2249854.0	23.6	33.7	107.4	26.2	81.5	0.05648	0.01250	0.4660	0.3282	0.3289	0.3306
N1843305419	2242891.5	23.6	33.8	109.9	26.2	84.0	0.05743	0.01608	0.4627	0.3265	0.3264	0.3273
N1843305523	2241428.8	23.6	33.8	110.5	26.2	84.6	0.05838	0.01526	0.4620	0.3260	0.3258	0.3265
N1843306231	2231595.2	23.7	33.9	114.2	26.2	88.2	0.05790	0.01631	0.4565	0.3221	0.3207	0.3204
N1843306835	2223395.2	23.8	34.0	117.4	26.2	91.3	0.05931	0.01469	0.4511	0.3175	0.3153	0.3142
N1843306939	2222002.5	23.8	34.0	117.9	26.2	91.9	0.05318	0.01915	0.4502	0.3166	0.3143	0.3130
N1843307543	2214034.8	23.9	34.1	121.1	26.2	95.0	0.05229	0.01559	0.4442	0.3109	0.3078	0.3058
N1843308251	2204977.0	24.0	34.3	124.9	26.2	98.6	0.05414	0.01792	0.4366	0.3029	0.2991	0.2964
N1843309180	2193604.2	24.2	34.4	129.9	26.2	103.4	0.05301	0.02014	0.4259	0.2908	0.2861	0.2828
N1843310596	2177532.2	24.5	34.6	137.5	26.2	110.7	0.04706	0.01828	0.4083	0.2692	0.2638	0.2600
N1843310700	2176417.2	24.5	34.6	138.1	26.2	111.3	0.05056	0.02039	0.4070	0.2675	0.2620	0.2582
N1843312012	2163183.8	24.9	34.8	145.3	26.2	118.0	0.04840	0.02405	0.3903	0.2452	0.2397	0.2361
N1843312116	2162203.2	24.9	34.8	145.8	26.2	118.6	0.04842	0.01979	0.3890	0.2434	0.2379	0.2344
N1843312414	2159126.0	25.0	34.8	147.7	26.2	120.3	0.03289	0.02771	0.3849	0.2375	0.2322	0.2288
N1843316175	2132533.2	26.1	35.1	168.4	26.2	139.7	0.03017	0.02334	0.3482	0.1761	0.1742	0.1746
N1848936800	1645356.4	44.6	44.5	8.4	26.4	317.3	0.01755	0.01384	0.4055	0.1625	0.1666	0.1755
N1848940466	1627431.8	42.3	44.8	24.0	26.4	336.2	0.02107	0.01062	0.4220	0.1499	0.1613	0.1779
N1848944132	1600212.8	40.3	45.5	39.9	26.4	355.1	0.01971	0.00987	0.4485	0.1632	0.1824	0.2076
N1848947798	1565324.1	38.7	46.4	56.1	26.4	14.0	0.02722	0.00825	0.4763	0.2026	0.2268	0.2562
N1848951464	1525110.0	37.8	47.6	72.9	26.4	32.9	0.03266	0.01107	0.4974	0.2536	0.2762	0.3027
N1848955130	1482520.0	37.5	49.0	90.6	26.4	51.8	0.03959	0.00642	0.5065	0.2954	0.3116	0.3309
N1848962462	1403810.4	38.9	51.8	128.9	26.4	89.6	0.03821	0.00591	0.4860	0.2967	0.3003	0.3082
N1848969794	1355281.1	42.0	53.4	171.2	26.4	127.4	0.02102	0.00995	0.4534	0.2108	0.2173	0.2292

**Table 9.** Brightness estimates from clear-filter images of Anthe.

Filename	Range	Phase	Sub-S/C	Sub-S/C	Sub-Solar	Sub-Solar	$A_{\text{eff}}$	$A_{\text{eff}}$
	(km)	(deg)	Latitude	Longitude	Latitude	Longitude	Value	Error
			(deg)	(deg)	(deg)	(deg)	(km <sup>2</sup> )	(km <sup>2</sup> )
N1575629162	1802888.5	14.3	4.6	314.9	-9.4	312.0	0.87980	0.00018
N1579321873	1440656.1	11.3	2.1	36.8	-8.8	34.0	0.94105	0.00006
N1579364158	1258508.1	17.9	6.6	213.0	-8.8	203.9	0.76642	0.00094
N1580356175	1214750.8	20.0	3.0	247.6	-8.6	231.3	0.88177	0.00086
N1581514393	1472790.1	21.2	12.5	210.3	-8.4	206.6	0.74765	0.00064
N1591878477	1067058.5	9.7	-2.1	117.6	-6.6	109.0	1.11239	0.00026
N1595481922	869685.1	30.3	-13.2	225.5	-5.9	195.6	0.56951	0.00006
N1596338308	1242696.0	28.9	22.9	42.6	-5.8	38.7	0.57676	0.00029
N1596721036	861845.3	21.8	-17.3	156.5	-5.7	137.6	0.67246	0.00010
N1599961164	1029589.9	30.0	-5.2	234.4	-5.1	204.3	0.68365	0.00041
N1600583458	965677.7	28.8	-8.2	215.1	-5.0	186.3	0.62410	0.00036
N1601479534	854860.4	48.2	40.9	205.6	-4.9	189.0	0.35513	0.00018
N1601778096	1097635.0	34.8	-19.0	341.5	-4.8	308.9	0.62173	0.00122
N1603880961	1059766.6	22.0	13.8	136.4	-4.4	123.9	0.74229	0.00024
N1610855232	960895.8	49.9	-44.4	115.4	-3.2	83.5	0.54718	0.00055
N1610855412	959598.4	49.9	-44.4	116.2	-3.2	84.2	0.53848	0.00049

Table 9 continued on next page

**Table 9** (*continued*)

Filename	Range	Phase	Sub-S/C	Sub-S/C	Sub-Solar	Sub-Solar	$A_{\text{eff}}$	$A_{\text{eff}}$
	(km)	(deg)	Latitude	Longitude	Latitude	Longitude	Value	Error
			(deg)	(deg)	(deg)	(deg)	(km <sup>2</sup> )	(km <sup>2</sup> )
N1610855592	958311.1	50.0	-44.5	117.0	-3.2	84.9	0.54300	0.00010
N1610855772	957034.2	50.1	-44.5	117.8	-3.2	85.7	0.54123	0.00041
N1610855952	955768.0	50.1	-44.5	118.6	-3.2	86.4	0.54628	0.00006
N1610856132	954512.9	50.2	-44.6	119.4	-3.2	87.1	0.54934	0.00014
N1610856312	953269.1	50.3	-44.6	120.2	-3.2	87.8	0.53285	0.00038
N1610856492	952036.9	50.3	-44.6	121.0	-3.2	88.6	0.54727	0.00030
N1610856672	950816.8	50.4	-44.7	121.8	-3.2	89.3	0.53833	0.00028
N1610856852	949608.9	50.5	-44.7	122.7	-3.2	90.0	0.54268	0.00097
N1610857032	948413.6	50.5	-44.7	123.5	-3.2	90.7	0.53503	0.00052
N1610857212	947231.2	50.6	-44.8	124.3	-3.2	91.5	0.53591	0.00058
N1610857392	946062.1	50.7	-44.8	125.1	-3.2	92.2	0.53497	0.00016
N1610857572	944906.6	50.8	-44.9	125.9	-3.2	92.9	0.52675	0.00026
N1610857752	943764.9	50.8	-44.9	126.8	-3.2	93.6	0.53394	0.00030
N1610857932	942637.4	50.9	-44.9	127.6	-3.2	94.4	0.52640	0.00011
N1610858112	941524.4	51.0	-44.9	128.4	-3.2	95.1	0.52267	0.00024
N1610858292	940426.2	51.1	-45.0	129.3	-3.2	95.8	0.51957	0.00019
N1610858472	939343.1	51.1	-45.0	130.1	-3.2	96.5	0.51918	0.00032
N1610858652	938275.4	51.2	-45.0	131.0	-3.2	97.3	0.50773	0.00009
N1610858832	937223.4	51.3	-45.1	131.8	-3.2	98.0	0.50947	0.00034
N1610859012	936187.5	51.4	-45.1	132.6	-3.2	98.7	0.51529	0.00023
N1610859192	935167.9	51.5	-45.1	133.5	-3.2	99.4	0.51627	0.00065
N1610859372	934164.9	51.5	-45.1	134.3	-3.2	100.2	0.49846	0.00025
N1610859552	933178.8	51.6	-45.2	135.2	-3.2	100.9	0.50344	0.00001
N1610859732	932209.9	51.7	-45.2	136.1	-3.2	101.6	0.48854	0.00008
N1610859912	931258.6	51.8	-45.2	136.9	-3.2	102.3	0.49146	0.00003
N1610860092	930325.0	51.9	-45.2	137.8	-3.2	103.1	0.48421	0.00019
N1610860272	929409.6	51.9	-45.2	138.6	-3.2	103.8	0.48255	0.00001
N1610860452	928512.5	52.0	-45.3	139.5	-3.2	104.5	0.48190	0.00030
N1610860632	927634.1	52.1	-45.3	140.4	-3.2	105.2	0.47563	0.00012
N1610860812	926774.7	52.2	-45.3	141.2	-3.2	106.0	0.47711	0.00039
N1610860992	925934.4	52.3	-45.3	142.1	-3.2	106.7	0.45831	0.00002
N1610861172	925113.8	52.4	-45.3	143.0	-3.2	107.4	0.46662	0.00041
N1610861352	924312.8	52.4	-45.3	143.9	-3.2	108.1	0.45948	0.00025
N1610861532	923531.9	52.5	-45.3	144.7	-3.2	108.9	0.47336	0.00019
N1610861712	922771.3	52.6	-45.3	145.6	-3.2	109.6	0.45676	0.00064
N1610861892	922031.3	52.7	-45.3	146.5	-3.2	110.3	0.46357	0.00039
N1610862072	921312.2	52.8	-45.3	147.4	-3.2	111.1	0.45168	0.00053
N1610862252	920614.1	52.9	-45.4	148.3	-3.2	111.8	0.44673	0.00021
N1610900922	1220808.4	50.5	-26.5	314.5	-3.2	267.6	0.56035	0.00015
N1611719913	1268561.8	44.8	-26.6	359.9	-3.0	320.2	0.30967	0.00142
N1612882076	1271672.4	41.2	37.2	323.0	-2.8	312.5	0.46697	0.00375
N1619668364	1246895.4	55.2	53.6	235.3	-1.6	234.0	0.39506	0.00006
N1623651133	1732446.6	73.3	50.5	341.9	-0.9	43.9	0.14602	0.00012
N1649429446	928449.7	37.4	0.2	298.3	3.7	335.6	0.54989	0.00004
N1649462986	1184913.1	65.0	0.2	45.4	3.7	110.3	0.41295	0.00025
N1649609387	1704980.8	67.9	0.3	271.0	3.7	338.9	0.47019	0.00179
N1649697048	1937056.1	74.6	0.3	256.7	3.7	331.3	0.38334	0.00140
N1658886983	1149689.9	69.4	0.1	124.8	5.3	194.2	0.24427	0.00306
N1684433502	3004417.2	37.8	0.2	263.6	9.5	300.5	0.91734	0.00498
N1685875491	3910912.8	66.0	0.3	271.4	9.8	337.1	0.85410	0.02495
N1688602748	2174916.2	69.4	0.3	70.9	10.2	140.1	0.33232	0.00136
N1693342778	2518139.8	37.1	0.2	76.9	10.9	112.6	0.66934	0.00341
N1693975122	2650397.2	56.6	0.3	78.3	11.0	134.2	0.51854	0.00509
N1694061583	2584867.0	59.4	0.3	62.9	11.1	121.7	0.50842	0.00940
N1694254124	2033752.0	68.8	0.3	107.3	11.1	175.7	0.20736	0.00080

Table 9 continued on next page

**Table 9** (*continued*)

Filename	Range	Phase	Sub-S/C	Sub-S/C	Sub-Solar	Sub-Solar	$A_{\text{eff}}$	$A_{\text{eff}}$
	(km)	(deg)	Latitude	Longitude	Latitude	Longitude	Value	Error
			(deg)	(deg)	(deg)	(deg)	(km <sup>2</sup> )	(km <sup>2</sup> )
N1694911248	1669813.0	22.5	0.1	277.3	11.2	297.0	1.03249	0.00585
N1695096650	2198955.2	33.9	0.2	289.9	11.2	322.1	0.61286	0.00146
N1696388358	1449181.0	30.8	0.2	84.8	11.4	113.7	0.82853	0.00073
N1696835941	2480039.5	50.2	0.2	63.4	11.5	112.7	0.52591	0.00088
N1696923121	2551409.2	52.7	0.2	51.2	11.5	103.1	0.56464	0.00133
N1712158718	2363073.8	60.1	0.3	79.9	13.8	139.1	0.61620	0.00502
N1718468718	2764670.8	69.5	-14.7	239.5	14.7	303.3	0.35076	0.00014
N1727788818	2414334.5	64.5	-24.4	280.1	16.0	331.7	0.28420	0.00513
N1733156512	1701262.4	58.0	-29.0	275.7	16.7	312.7	0.35325	0.00150
N1733324513	1552533.4	79.4	-44.8	213.0	16.7	268.3	0.18347	0.00113
N1735266905	1354943.0	46.9	-14.0	122.0	17.0	157.7	0.35434	0.00004
N1737789081	1552145.0	69.8	-36.0	170.7	17.3	218.3	0.17100	0.00065
N1738779808	1425111.0	48.5	-21.8	212.5	17.5	241.6	0.41682	0.00056
N1741128483	1544441.5	66.9	-38.3	285.4	17.8	324.4	0.26809	0.00065
N1741891187	1240196.6	41.1	-10.7	120.4	17.9	150.3	0.47779	0.00398
N1741938588	1564829.5	38.7	-14.5	319.8	17.9	341.3	0.42804	0.00151
N1741941656	1591693.8	39.6	-14.6	330.6	17.9	353.6	0.41039	0.00072
N1741944724	1611902.5	40.8	-14.8	341.2	17.9	5.9	0.38595	0.00193
N1741947792	1624972.6	42.0	-15.1	351.8	17.9	18.2	0.35194	0.00008
N1741953928	1628900.4	44.8	-15.8	12.8	17.9	42.8	0.37065	0.00063
N1741956996	1619922.9	46.2	-16.2	23.4	17.9	55.1	0.42687	0.00103
N1741963132	1582190.2	49.1	-17.4	44.9	17.9	79.6	0.53164	0.00014
N1741966200	1554958.0	50.5	-18.0	55.9	17.9	92.0	0.57036	0.00029
N1741969268	1523541.6	51.7	-18.8	67.2	17.9	104.3	0.53154	0.00046
N1741972336	1489261.2	52.8	-19.7	78.8	17.9	116.6	0.52990	0.00140
N1741975404	1453639.6	53.7	-20.6	90.7	17.9	128.9	0.48314	0.00028
N1741978472	1418368.8	54.4	-21.5	102.9	17.9	141.3	0.43273	0.00066
N1744739586	1342930.0	31.8	-2.9	57.8	18.2	82.0	0.88665	0.00159
N1745006947	1396910.8	68.2	-34.1	31.1	18.2	76.9	0.28020	0.00076
N1745473570	885166.3	13.9	16.1	138.3	18.3	152.7	0.92863	0.00161
N1746655338	1123073.9	70.9	-43.7	186.5	18.5	223.7	0.14883	0.00031
N1747372882	1196892.6	51.0	-27.0	204.9	18.5	228.4	0.37191	0.00015
N1747380322	1255851.4	49.3	-26.7	238.3	18.5	258.4	0.51543	0.00057
N1747387762	1340452.5	48.1	-25.8	269.1	18.5	288.4	0.54037	0.00049
N1747395202	1425531.1	48.0	-25.0	297.5	18.5	318.4	0.45307	0.00002
N1747402642	1490160.6	49.2	-24.6	324.1	18.5	348.4	0.32049	0.00117
N1747410083	1520797.5	51.6	-24.8	349.5	18.5	18.3	0.28569	0.00055
N1747417523	1511671.0	55.0	-25.6	14.5	18.5	48.1	0.31930	0.00019
N1747424963	1464470.6	58.9	-27.3	39.7	18.5	77.9	0.39640	0.00010
N1747436063	1344008.1	64.5	-31.1	79.5	18.5	122.4	0.33953	0.00175
N1750033279	1023947.0	15.5	13.3	108.4	18.9	123.5	1.03273	0.00001
N1750357371	1489901.9	64.2	-36.7	312.5	18.9	346.5	0.17311	0.00290
N1751379648	1393194.9	74.1	-38.3	85.6	19.0	135.8	0.26613	0.00001
N1751382351	1364627.9	75.2	-39.6	96.1	19.0	146.6	0.26006	0.00068
N1751385054	1337225.2	76.1	-40.9	106.9	19.0	157.4	0.20350	0.00167
N1751387757	1311955.1	76.8	-42.2	118.1	19.0	168.3	0.16289	0.00061
N1751390460	1289749.0	77.2	-43.5	129.7	19.0	179.1	0.14474	0.00123
N1751393163	1271452.9	77.4	-44.7	141.7	19.0	190.0	0.15133	0.00125
N1751395866	1257775.2	77.3	-45.6	154.1	19.0	200.8	0.14081	0.00204
N1751398569	1249236.8	77.0	-46.4	166.7	19.0	211.7	0.13449	0.00141
N1757884909	1607022.5	71.5	-37.6	319.5	19.8	4.9	0.13732	0.00005
N1760112793	1567569.5	62.8	47.1	30.8	20.0	319.6	0.33984	0.00116
N1760179784	1395592.5	59.0	46.5	294.6	20.0	229.0	0.55231	0.00053
N1764310790	1680190.5	49.8	40.2	326.8	20.5	272.7	0.65858	0.00039
N1766819846	2155617.5	74.7	47.1	6.9	20.8	277.3	0.22800	0.00178

Table 9 continued on next page

**Table 9** (*continued*)

Filename	Range	Phase	Sub-S/C	Sub-S/C	Sub-Solar	Sub-Solar	$A_{\text{eff}}$	$A_{\text{eff}}$
	(km)	(deg)	Latitude	Longitude	Latitude	Longitude	Value	Error
			(deg)	(deg)	(deg)	(deg)	(km <sup>2</sup> )	(km <sup>2</sup> )
N1767477400	1257364.9	73.1	-35.2	350.5	20.8	40.0	0.13848	0.00058
N1772108799	2745604.0	69.7	45.2	17.0	21.3	294.9	0.20006	0.00922
N1772255590	2349339.8	64.8	48.7	240.4	21.3	164.8	0.39814	0.00454
N1783366114	2720605.0	49.7	40.1	238.6	22.4	183.2	0.47521	0.00468
N1783369677	2751414.0	49.9	39.4	253.3	22.4	197.5	0.49537	0.00062
N1783373240	2785330.2	49.9	38.7	267.6	22.4	211.9	0.49412	0.00239
N1783376803	2820033.2	49.6	38.0	281.7	22.4	226.2	0.62437	0.00365
N1783383929	2882811.2	48.4	36.7	308.9	22.4	254.9	0.59227	0.00326
N1783955265	1955743.5	14.9	9.6	39.6	22.5	31.7	0.76782	0.00246
N1786521631	2274599.2	23.5	16.6	292.3	22.7	268.1	1.18754	0.00239
N1786610252	2069137.5	21.5	10.9	283.2	22.7	264.4	1.06902	0.00118
N1786782693	1532191.6	28.6	-5.5	242.3	22.7	237.5	0.84695	0.00298
N1791961506	2476469.5	61.7	37.6	248.5	23.2	177.3	0.29148	0.00241
N1791968455	2537352.5	61.8	36.2	276.3	23.2	205.2	0.46371	0.00021
N1791975404	2595731.8	60.9	34.9	302.9	23.2	233.1	0.55470	0.00077
N1792420449	1184056.2	28.4	11.7	249.6	23.2	222.3	0.82803	0.00008
N1833918994	1649241.1	73.7	14.8	84.3	25.9	5.5	0.22512	0.00261
N1835820917	1972754.5	58.9	23.2	155.0	25.9	89.7	0.29235	0.00745
N1840467286	2582647.8	41.6	28.9	91.7	26.1	44.5	0.62184	0.00785
N1840470496	2537728.2	41.5	29.4	104.6	26.1	57.4	0.68228	0.00180
N1840477239	2453130.0	42.1	30.3	132.4	26.1	84.6	0.66211	0.00060
N1840483982	2394976.2	43.5	30.9	161.2	26.1	111.7	0.53994	0.00459
N1840490725	2374012.2	45.3	31.0	190.5	26.1	138.8	0.46504	0.00109
N1840497468	2391706.5	47.0	30.5	219.5	26.1	165.8	0.45506	0.00011
N1840504211	2439687.8	48.1	29.6	247.6	26.1	192.9	0.50879	0.00217
N1840510954	2502760.2	48.3	28.6	274.7	26.1	219.9	0.60094	0.00109
N1840517697	2563548.8	47.5	27.6	300.7	26.1	247.0	0.74689	0.00092
N1840524440	2606537.5	45.9	26.9	325.8	26.1	274.1	0.68571	0.00302
N1840531183	2620614.8	43.8	26.5	350.4	26.1	301.2	0.57756	0.00132
N1840537926	2600335.8	41.5	26.6	14.9	26.1	328.3	0.41272	0.00199
N1840898139	1396296.1	12.9	17.3	346.2	26.1	336.1	0.88599	0.00283
N1842534559	3135807.8	57.7	37.0	141.6	26.2	73.7	0.41641	0.00094
N1843368285	1990834.1	26.1	34.1	213.6	26.2	184.8	0.57734	0.00374
N1844971025	2408598.8	59.8	45.1	219.6	26.3	147.0	0.32117	0.00406
N1845142566	2250048.2	46.7	46.3	170.4	26.3	116.5	0.55028	0.00349
N1845329417	1972732.1	35.8	44.7	185.9	26.3	147.6	0.43958	0.00066
N1847240079	2476519.2	48.7	40.3	324.6	26.3	267.6	0.46665	0.00309
N1847383720	2005952.5	35.3	44.7	162.8	26.3	125.1	0.63602	0.00317
N1849021281	1325512.4	40.7	46.1	272.9	26.4	227.7	0.79609	0.00055
N1849967637	1295529.0	75.2	52.3	171.9	26.4	71.8	0.34280	0.00058
N1853087187	1357371.5	68.6	49.2	99.6	26.5	12.3	0.43148	0.00140

**Table 10.** Brightness estimates from clear-filter images of Methone.

Filename	Range	Phase	Sub-S/C	Sub-S/C	Sub-Solar	Sub-Solar	$A_{\text{eff}}$	$A_{\text{eff}}$	$A_{\text{phys}}$	$a_{\text{pred}}$	$a_{\text{pred}}$	$a_{\text{pred}}$
	(km)	(deg)	Latitude	Longitude	Latitude	Longitude	Value	Error		k=1	k=0.75	k=0.50
			(deg)	(deg)	(deg)	(deg)	(km <sup>2</sup> )					
N1502651083	2157110.5	61.1	-16.3	195.6	-20.7	131.0	0.85344	0.00034	5.3901	1.7843	1.7464	1.7810
N1502796764	2182712.0	49.2	-16.1	63.9	-20.7	12.0	1.23989	0.00288	7.0567	2.7398	2.9195	3.1932

*Table 10 continued on next page*

**Table 10** (*continued*)

Filename	Range (km)	Phase (deg)	Sub-S/C (deg)	Sub-S/C (deg)	Sub-Solar (deg)	Sub-Solar (deg)	$A_{\text{eff}}$ ( $\text{km}^2$ )	$A_{\text{eff}}$ ( $\text{km}^2$ )	$A_{\text{phys}}$ ( $\text{km}^2$ )	$a_{\text{pred}}$ ( $\text{km}^2$ )	$a_{\text{pred}}$ ( $\text{km}^2$ )	$a_{\text{pred}}$ ( $\text{km}^2$ )
			Latitude (deg)	Longitude (deg)	Latitude (deg)	Longitude (deg)	Value	Error ( $\text{km}^2$ )	k=1	k=0.75	k=0.50	
N1505466661	2597383.5	75.2	-0.3	304.2	-20.4	229.8	1.08037	0.00377	6.7187	2.6551	2.7021	2.8410
N1506716564	2357443.8	78.3	-0.3	65.0	-20.2	347.3	0.59662	0.00542	7.0143	1.2778	1.3753	1.5609
N1513354056	2991500.0	75.9	-0.2	90.1	-19.3	14.9	0.92142	0.00364	7.3746	1.9798	2.1500	2.4335
N1513572473	2639783.5	77.0	-0.3	272.5	-19.3	196.2	0.92816	0.00253	7.3726	1.9867	2.1553	2.4368
N1513697664	2444116.8	64.6	-0.3	55.8	-19.3	352.7	0.46728	0.00244	6.7177	1.6638	1.7749	1.9790
N1513745334	2160722.2	70.8	-0.3	259.1	-19.3	189.4	0.74070	0.00250	7.3012	1.9526	2.1226	2.4042
N1513875625	1857151.5	53.5	-0.3	58.0	-19.3	6.9	0.95244	0.00261	6.7962	2.2552	2.4016	2.6437
N1549374867	1488836.9	53.5	24.1	307.3	-13.9	345.9	0.95830	0.00073	6.8320	2.1726	2.3225	2.5697
N1550921692	1263299.0	51.2	23.1	212.6	-13.6	249.0	1.36761	0.00068	6.1086	2.8708	2.8150	2.8398
N1552348681	1744683.8	52.9	21.0	336.5	-13.4	17.4	0.69036	0.00413	5.7918	1.6529	1.7078	1.8359
N1552477337	1665437.8	76.6	37.4	126.9	-13.4	188.1	0.33085	0.00518	7.0929	1.1680	1.2762	1.4717
N1553981291	1846244.4	73.5	38.7	218.1	-13.1	274.1	0.77444	0.00144	6.7758	2.3565	2.3575	2.4577
N1555091749	1551002.1	53.1	15.9	130.9	-12.9	176.0	0.82913	0.00269	6.5525	1.9826	2.1190	2.3466
N1555144069	1980605.1	50.9	16.2	349.8	-12.9	32.0	0.69191	0.00046	5.3206	1.7679	1.7666	1.8321
N1555229284	2110571.5	56.4	20.6	337.5	-12.9	23.6	0.68280	0.00489	5.7481	1.5533	1.5951	1.7087
N1555449471	1956717.2	76.9	34.1	147.9	-12.9	212.0	0.36695	0.00397	6.4686	1.0418	1.0920	1.2108
N1555555222	1949552.6	77.3	37.7	226.0	-12.9	288.5	0.65621	0.00122	6.9344	2.3479	2.3740	2.5015
N1556567938	1911929.1	57.2	15.4	96.6	-12.7	147.0	1.13862	0.00344	7.3882	2.8855	3.0701	3.3593
N1556952120	2040361.9	69.2	27.9	234.4	-12.6	292.3	1.09950	0.00496	6.9305	2.8228	2.8522	2.9808
N1557987247	1878589.1	49.2	11.8	200.0	-12.5	243.2	1.16365	0.00019	5.3884	2.6219	2.5184	2.4853
N1558331184	2040010.9	67.3	18.5	161.7	-12.4	222.3	0.56417	0.00201	5.5292	1.2949	1.2951	1.3611
N1558376799	2363321.5	66.0	16.4	350.6	-12.4	50.7	0.54316	0.00005	5.3119	1.4682	1.4402	1.4801
N1558548655	2074314.1	72.7	19.2	333.3	-12.4	39.8	0.44191	0.00679	5.8334	1.1293	1.1468	1.2281
N1559173514	1701136.0	42.3	3.1	58.2	-12.3	97.9	2.00250	0.00239	6.8061	4.1068	4.0630	4.0763
N1559286225	1741789.0	45.9	5.9	160.4	-12.2	202.9	0.73349	0.00058	5.2748	1.8294	1.8454	1.9250
N1559451496	2115250.0	55.8	7.9	112.4	-12.2	164.8	0.94293	0.00547	7.0863	2.3768	2.5649	2.8566
N1559627912	2193923.8	62.4	9.8	113.9	-12.2	172.7	0.85035	0.00342	7.0546	1.9639	2.1353	2.4127
N1559709797	2246929.5	65.8	10.3	88.3	-12.2	150.6	1.16382	0.00444	7.3932	2.5992	2.7863	3.0839
N1559927929	1941583.5	65.1	12.7	270.0	-12.1	330.7	1.17934	0.00260	7.4035	2.5936	2.7812	3.0799
N1560620783	1841235.8	33.9	0.5	277.7	-12.0	309.4	2.12819	0.00193	7.3431	4.1569	4.2799	4.4546
N1560830019	2350589.5	51.7	0.8	42.3	-12.0	92.8	1.61959	0.00064	6.1803	3.4798	3.3789	3.3469
N1561309317	1797861.6	63.5	1.6	207.7	-11.9	270.3	1.23418	0.00166	5.5359	2.6750	2.5537	2.5112
N1563933254	1870782.6	12.2	0.0	292.9	-11.4	296.9	2.93053	0.00044	7.0738	4.6458	4.6631	4.6933
N1571562423	2145634.2	61.1	4.0	38.4	-10.1	98.1	1.26005	0.00069	6.0235	3.0582	2.9649	2.9494
N1572465220	2367464.8	20.8	2.1	206.9	-10.0	223.9	2.02699	0.00262	5.5026	3.2749	3.2017	3.1541
N1574755016	2345316.8	24.2	6.0	295.1	-9.6	313.7	2.33193	0.00299	7.0238	4.0386	4.1363	4.2705
N1575055798	1837730.6	45.6	8.3	72.9	-9.5	115.0	1.98799	0.00180	7.2221	4.0488	4.1033	4.2244
N1575629432	1824263.9	14.1	4.5	324.4	-9.4	322.5	2.27128	0.00150	5.9062	3.4566	3.4495	3.4587
N1575757158	1900792.2	22.8	8.6	115.6	-9.4	129.6	2.43865	0.00203	7.0011	4.1209	4.1990	4.3119
N1575913219	2360204.8	27.0	10.5	35.1	-9.4	53.6	1.77757	0.00018	5.9506	3.4878	3.4252	3.4027
N1575960919	2131982.0	25.5	12.6	237.6	-9.4	250.7	2.66410	0.00331	6.8151	4.2774	4.2508	4.2642
N1576171491	2393457.0	35.2	14.0	12.9	-9.3	39.5	1.39510	0.00499	5.3038	2.5739	2.5283	2.5360
N1577214553	2262254.8	27.7	14.8	10.5	-9.2	24.5	1.34446	0.00538	5.2813	2.5349	2.5334	2.5739
N1579322353	1297401.9	11.2	2.4	83.4	-8.8	83.9	3.27737	0.00075	7.3532	5.0568	5.0603	5.0751
N1579399258	1667702.6	16.5	7.6	39.1	-8.8	41.4	2.26201	0.00040	6.0811	3.5602	3.5583	3.5779
N1579447529	1546038.0	21.4	11.8	246.8	-8.8	240.8	2.52779	0.00105	7.0846	4.3727	4.4145	4.4903
N1580484276	1466640.4	21.8	13.1	202.0	-8.6	199.8	1.78870	0.00010	5.4814	2.7260	2.7572	2.8208
N1580614807	1983817.9	26.2	16.4	10.3	-8.6	18.4	1.48372	0.00030	5.3258	2.5069	2.5267	2.5868
N1580653327	1639264.6	32.2	22.0	167.1	-8.6	177.4	1.13591	0.00055	5.5366	2.2511	2.3189	2.4407
N1581772425	1774869.1	37.2	23.7	96.9	-8.4	116.3	2.17841	0.00427	7.4375	4.1107	4.1984	4.3577
N1582719892	1717954.0	35.3	24.5	53.2	-8.2	66.8	1.90156	0.00043	6.8547	3.8120	3.8155	3.8852
N1583323256	1377267.9	10.5	1.1	42.3	-8.1	37.2	2.63506	0.00021	6.1786	3.6513	3.6771	3.7127
N1583324096	1372028.6	10.4	1.2	45.3	-8.1	40.7	2.66673	0.00072	6.3073	3.7906	3.8150	3.8491
N1583344421	1179916.6	12.4	4.1	127.2	-8.1	124.5	2.79961	0.00209	6.5885	4.2142	4.2048	4.2086
N1583757119	1646713.1	41.8	30.6	11.1	-8.0	28.0	1.07735	0.00165	5.9237	2.2746	2.3286	2.4532

Table 10 continued on next page

**Table 10** (*continued*)

Filename	Range	Phase	Sub-S/C	Sub-S/C	Sub-Solar	Sub-Solar	$A_{\text{eff}}$	$A_{\text{eff}}$	$A_{\text{phys}}$	$a_{\text{pred}}$	$a_{\text{pred}}$	$a_{\text{pred}}$
	(km)	(deg)	Latitude	Longitude	Latitude	Longitude	Value	Error		k=1	k=0.75	k=0.50
			(deg)	(deg)	(deg)	(deg)	(km <sup>2</sup> )					
N1583788019	1315605.2	53.5	40.2	130.1	-8.0	155.4	1.06861	0.00068	7.0865	2.3506	2.5165	2.7852
N1584374043	1651236.5	20.6	12.6	51.6	-7.9	54.2	2.41936	0.00066	6.6279	3.9940	4.0021	4.0420
N1584714966	1559630.6	44.5	33.0	2.8	-7.8	21.4	1.01339	0.00100	5.9788	2.0787	2.1525	2.3006
N1584746136	1238327.6	58.3	43.1	118.6	-7.8	149.9	1.05444	0.00033	7.3670	2.4198	2.5952	2.8815
N1585394126	1578001.0	32.3	24.1	309.9	-7.7	304.6	2.01372	0.00011	6.7527	3.6544	3.6854	3.7771
N1585438211	1363918.8	41.4	32.1	114.2	-7.7	126.3	1.88744	0.00126	7.2736	3.5510	3.6565	3.8466
N1585593672	1254011.6	54.6	41.5	22.2	-7.7	48.1	0.97819	0.00047	6.5965	2.3631	2.4147	2.5573
N1586002605	1389411.9	21.0	3.0	314.1	-7.6	296.0	2.44959	0.00010	6.3353	4.1058	4.0305	3.9792
N1587226314	1254156.2	49.5	41.9	301.7	-7.4	306.6	1.41741	0.00135	7.3084	3.1259	3.2320	3.4381
N1587747477	1539042.2	24.0	12.8	310.7	-7.3	297.5	2.27158	0.00123	6.5454	4.0368	4.0019	4.0032
N1588781885	1329890.8	43.1	35.9	250.5	-7.1	246.7	1.69377	0.00079	7.4046	3.7309	3.8080	3.9749
N1590864949	992020.2	38.6	28.8	219.3	-6.7	203.6	1.36908	0.00003	6.4944	2.6581	2.7864	2.9891
N1591525464	1113836.8	35.2	28.5	46.9	-6.6	49.7	1.74592	0.00052	6.7465	3.4025	3.4592	3.5839
N1591762166	945241.9	31.6	-19.4	336.3	-6.6	306.5	1.82229	0.00007	5.7473	3.2516	3.1775	3.1502
N1591878207	2111504.1	9.3	-1.9	73.5	-6.6	65.4	3.25077	0.00014	7.2199	4.8287	4.8583	4.8935
N1595481232	832258.1	26.4	-13.9	199.7	-5.9	174.2	1.43111	0.00002	5.4308	2.4522	2.5113	2.6105
N1595510182	1239201.0	26.8	-5.9	320.6	-5.9	293.6	2.32179	0.00017	6.0792	3.9035	3.7963	3.7211
N1597581487	1026620.9	35.1	23.3	221.4	-5.6	200.8	1.43911	0.00056	6.4149	2.7438	2.8762	3.0749
N1598065750	1286290.8	13.5	-1.8	52.2	-5.5	39.1	2.56346	0.00150	6.5823	3.8711	3.9431	4.0276
N1599961704	1318808.6	26.9	-3.9	329.3	-5.1	302.3	2.14558	0.00039	5.7032	3.5293	3.4194	3.3433
N1600651648	1289874.6	29.5	3.3	297.5	-5.0	269.1	2.49523	0.00031	6.9468	4.5603	4.5150	4.5031
N1603214386	1309244.9	16.7	6.3	56.0	-4.5	43.4	2.52582	0.00022	6.7403	3.9728	4.0469	4.1409
N1604534936	1226394.4	21.5	15.4	100.8	-4.3	92.1	2.78799	0.00008	7.3461	4.8244	4.8353	4.8791
N1604570261	1228796.8	34.7	20.2	262.9	-4.3	237.9	2.18718	0.00060	7.4120	4.1813	4.2885	4.4558
N1605988176	1281627.0	33.8	25.9	344.4	-4.0	328.3	1.32750	0.00006	5.7871	2.6181	2.6480	2.7348
N1606638671	1030992.6	32.2	26.8	142.0	-3.9	132.3	1.76265	0.00031	6.3966	3.3053	3.3324	3.4176
N1613054783	973837.9	79.9	66.3	270.1	-2.8	326.8	0.67922	0.00027	7.8050	1.8783	2.0439	2.3287
N1616993335	1334927.9	37.1	34.9	17.7	-2.1	19.8	1.29183	0.00039	6.2270	2.4907	2.6005	2.7798
N1618011993	1255908.9	58.8	-27.7	318.9	-1.9	263.6	1.43103	0.00025	6.5483	3.2149	3.1722	3.2147
N1619668079	1294438.2	52.4	50.7	261.7	-1.6	258.3	1.56801	0.00005	7.6687	3.5316	3.6153	3.8075
N1619787750	1494740.0	67.1	54.5	347.4	-1.6	32.2	0.60549	0.00126	7.0738	1.7188	1.8319	2.0436
N1622273223	1331850.1	66.0	61.5	182.8	-1.1	210.1	0.68932	0.00011	7.3065	1.8715	2.0136	2.2630
N1649428786	867025.0	36.1	0.2	282.0	3.7	317.9	2.09290	0.00035	7.2946	3.8749	4.0384	4.2585
N1662535579	2161484.5	74.4	-1.2	327.4	5.9	41.6	0.46042	0.00238	5.7696	1.0774	1.0920	1.1679
N1671766642	1423115.5	53.0	-0.0	287.9	7.5	340.5	1.16969	0.00007	7.1909	2.6778	2.8856	3.1944
N1675508506	1914195.0	69.4	0.3	235.7	8.1	304.9	1.13053	0.00203	6.6890	2.9724	3.0120	3.1374
N1682451270	2753647.2	72.0	0.3	86.5	9.2	158.4	0.94757	0.00358	7.3697	2.2605	2.4557	2.7652
N1689640275	2563583.0	31.5	0.2	274.1	10.4	304.1	2.22585	0.00060	7.3672	4.3676	4.4708	4.6175
N1693344098	2538475.8	36.9	0.2	71.3	10.9	106.8	2.13630	0.00094	7.1727	4.4359	4.4498	4.5106
N1694061943	2369926.0	58.8	0.3	130.5	11.1	188.7	0.90263	0.01177	6.4487	1.6970	1.8122	2.0160
N1695406582	2493573.0	46.0	0.2	291.7	11.3	336.7	1.35036	0.00056	7.1047	2.9625	3.1550	3.4355
N1696836421	2466988.0	50.3	0.2	67.2	11.5	116.5	1.52760	0.00229	7.0744	3.8852	3.9258	4.0348
N1696921561	2535867.8	52.8	0.2	55.9	11.5	107.8	1.51239	0.00197	6.7195	3.7261	3.7007	3.7443
N1697961188	1699283.9	31.1	0.2	48.3	11.7	77.4	2.27974	0.00197	6.4278	4.1318	4.0370	3.9819
N1701295529	2139450.0	43.7	0.2	113.5	12.2	155.8	1.56905	0.00217	7.0408	3.0241	3.2111	3.4808
N1707672909	2704191.5	63.0	-0.5	130.9	13.1	193.0	0.61680	0.00162	6.4314	1.5297	1.6278	1.8114
N1710535827	2276659.8	57.1	0.3	72.3	13.6	128.4	1.85788	0.00278	7.1944	3.4977	3.5981	3.7818
N1710890850	2427006.0	69.7	0.4	84.5	13.6	153.7	0.98371	0.00094	7.3597	2.4773	2.6632	2.9602
N1711206872	2081134.8	73.7	0.4	304.9	13.7	18.2	0.35033	0.00221	6.6927	1.2476	1.3322	1.4984
N1712589220	2224602.2	66.2	0.4	258.0	13.9	323.6	1.18665	0.00140	7.2858	2.8612	3.0217	3.2844
N1725789245	2243164.8	56.4	-12.7	35.1	15.7	84.3	1.28471	0.00108	5.9863	2.9697	2.8752	2.8610
N1727787618	2565619.2	67.3	-22.8	355.1	16.0	51.3	0.46687	0.00086	5.5094	1.4789	1.4578	1.5070
N1733157952	1550904.9	62.6	-32.2	211.6	16.7	252.4	0.89825	0.00005	6.3879	2.4331	2.4114	2.4814
N1733981997	1245003.2	22.0	6.2	32.9	16.8	52.5	2.30742	0.00143	5.8084	3.6412	3.5460	3.4769
N1733983737	1237356.5	23.0	6.0	38.9	16.8	59.7	2.38283	0.00030	6.0594	3.8844	3.7874	3.7175

Table 10 continued on next page

**Table 10** (*continued*)

Filename	Range	Phase	Sub-S/C	Sub-S/C	Sub-Solar	Sub-Solar	$A_{\text{eff}}$	$A_{\text{eff}}$	$A_{\text{phys}}$	$a_{\text{pred}}$	$a_{\text{pred}}$	$a_{\text{pred}}$
	(km)	(deg)	Latitude	Longitude	Latitude	Longitude	Value	Error		k=1	k=0.75	k=0.50
			(deg)	(deg)	(deg)	(deg)	(km <sup>2</sup> )					
N1733984825	1231548.0	23.7	5.9	42.8	16.8	64.2	2.45545	0.00049	6.2192	4.0337	3.9384	3.8709
N1733985913	1224992.0	24.3	5.7	46.7	16.8	68.7	2.47384	0.00051	6.3779	4.1768	4.0856	4.0227
N1733987001	1217728.8	24.9	5.6	50.6	16.8	73.2	2.57059	0.00044	6.5328	4.3104	4.2256	4.1697
N1733988089	1209802.8	25.4	5.4	54.5	16.8	77.7	2.61348	0.00024	6.6813	4.4311	4.3553	4.3089
N1733989177	1201262.9	25.9	5.3	58.5	16.8	82.2	2.64621	0.00022	6.8211	4.5360	4.4716	4.4369
N1733991353	1182557.4	26.9	5.0	66.6	16.8	91.2	2.63522	0.00008	7.0653	4.6878	4.6523	4.6477
N1733992441	1172511.1	27.3	4.9	70.7	16.8	95.7	2.72223	0.00022	7.1654	4.7302	4.7116	4.7248
N1733995705	1140404.9	28.2	4.5	83.3	16.8	109.2	2.62876	0.00039	7.3552	4.7058	4.7427	4.8149
N1733996793	1129296.2	28.4	4.3	87.6	16.8	113.7	2.61082	0.00009	7.3767	4.6455	4.7006	4.7925
N1733997881	1118119.1	28.6	4.2	92.0	16.8	118.2	2.52023	0.00033	7.3757	4.5599	4.6321	4.7426
N1733998969	1106960.2	28.7	4.1	96.4	16.8	122.7	2.48487	0.00024	7.3516	4.4505	4.5379	4.6655
N1734001145	1085060.2	28.8	3.7	105.5	16.8	131.7	2.32927	0.00022	7.2289	4.1694	4.2800	4.4340
N1735137785	1019027.2	25.9	5.8	117.9	17.0	141.7	2.30910	0.00072	6.9212	3.8386	3.9517	4.1042
N1738703487	1531994.1	43.8	-11.2	60.6	17.4	94.2	1.83183	0.00007	6.9240	3.9562	3.9305	3.9755
N1744739106	1102725.5	31.2	-3.4	135.4	18.2	158.1	1.62057	0.00037	6.2533	2.9521	3.0419	3.1863
N1745005487	1164660.5	75.1	-42.2	128.8	18.2	177.3	0.47262	0.00176	7.1613	1.2671	1.3809	1.5861
N1745860953	1294780.5	76.0	-39.0	53.8	18.4	107.2	0.91035	0.00066	7.1640	2.3807	2.4191	2.5633
N1746652598	1275970.8	72.4	-37.2	84.7	18.4	133.8	0.68855	0.00563	7.5601	2.3828	2.5090	2.7502
N1747226121	1421647.1	24.7	-3.5	329.2	18.5	340.6	1.71456	0.00166	5.7020	2.8532	2.8826	2.9508
N1747376602	1219949.0	50.3	-27.0	219.5	18.5	241.4	1.38261	0.00050	6.4510	2.8511	2.8430	2.9211
N1747384042	1293824.0	48.7	-26.3	252.6	18.5	272.2	1.68094	0.00037	7.3307	3.6938	3.7275	3.8567
N1747391482	1382301.9	48.0	-25.4	283.0	18.5	303.0	1.53811	0.00075	7.3965	3.4494	3.5471	3.7417
N1747398922	1460113.1	48.5	-24.7	311.1	18.5	333.7	1.12364	0.00023	6.7252	2.4715	2.5858	2.7903
N1747406362	1508684.6	50.4	-24.6	337.7	18.5	4.4	0.71220	0.00129	5.8852	1.7476	1.8134	1.9542
N1747413803	1517850.8	53.4	-25.2	3.6	18.5	35.1	0.80073	0.00096	5.6058	1.8267	1.8304	1.9064
N1747421243	1485795.9	57.1	-26.5	29.4	18.5	65.7	1.10889	0.00001	6.1530	2.5002	2.4644	2.5151
N1747435523	1337786.0	64.5	-31.2	81.8	18.5	124.5	1.23034	0.00103	7.4924	2.8878	2.9950	3.2137
N1750034029	1249779.8	13.6	10.8	36.4	18.9	47.6	2.69135	0.00236	6.0050	3.8268	3.7618	3.7087
N1755868536	1708706.6	74.9	-40.3	318.1	19.5	6.4	0.42251	0.00099	6.9384	1.1557	1.2466	1.4196
N1757884589	1647062.6	74.1	-36.5	356.1	19.8	47.3	0.39762	0.00105	6.1600	1.2915	1.3076	1.3958
N1760114493	1568512.9	70.6	46.9	333.4	20.0	250.8	1.04247	0.00002	6.8912	2.8755	2.8873	2.9975
N1760179184	1254689.1	57.7	53.9	220.3	20.0	158.0	1.05150	0.00063	7.2974	2.4191	2.5886	2.8665
N1764310070	1696985.5	48.3	39.8	339.8	20.5	287.7	1.71283	0.00354	6.4911	3.3316	3.2870	3.3215
N1767477520	1254935.2	73.3	-35.3	351.0	20.8	40.7	0.46329	0.00035	6.1325	1.2179	1.2406	1.3331
N1769462443	2435173.8	71.3	47.4	38.0	21.0	313.0	0.78092	0.00180	7.0837	1.9543	2.0272	2.1996
N1769728984	2015874.2	45.0	40.9	21.0	21.1	333.0	1.20589	0.00491	6.5514	2.6354	2.7270	2.8996
N1772107869	2504764.0	68.1	51.0	151.8	21.3	70.6	1.35090	0.00003	7.0483	3.0268	3.0523	3.1778
N1772256750	2533690.8	58.4	44.1	31.2	21.3	325.2	1.21698	0.00051	6.8541	2.2853	2.3766	2.5642
N1777325813	3441096.5	72.8	40.8	88.8	21.8	3.2	1.05953	0.00730	7.6002	2.2358	2.4402	2.7657
N1777843866	3241642.8	56.2	37.0	44.3	21.9	340.9	0.88513	0.00420	6.8959	2.2615	2.3901	2.6163
N1782845588	2827763.8	69.3	49.1	182.8	22.4	99.0	1.19146	0.00827	6.7616	2.5054	2.5011	2.5961
N1783384451	2662930.0	47.8	40.3	215.2	22.4	162.4	1.18827	0.00267	6.7672	2.5538	2.6855	2.9061
N1783387824	2683617.2	48.3	39.8	229.9	22.4	176.3	1.15998	0.00133	7.0771	2.6996	2.8845	3.1643
N1783391197	2710353.8	48.6	39.2	244.3	22.4	190.2	1.39159	0.00019	7.3511	2.9985	3.2183	3.5341
N1783394570	2741276.0	48.8	38.5	258.4	22.4	204.1	1.54215	0.00142	7.5281	3.3809	3.6023	3.9136
N1791369517	3181335.8	78.5	40.2	84.7	23.1	350.3	0.52476	0.01100	7.5864	1.8782	2.0464	2.3307
N1791951006	2636590.8	62.1	35.5	301.1	23.2	229.7	1.54303	0.00548	7.2008	3.4315	3.5218	3.6986
N1791953106	2651926.0	61.7	35.1	309.2	23.2	238.4	1.45998	0.00025	7.0082	3.4638	3.5041	3.6277
N1791961015	2688858.0	59.6	34.2	339.0	23.2	271.0	1.29001	0.00183	6.2525	3.0670	2.9916	3.0006
N1799229302	1686130.5	57.2	26.0	89.0	23.8	25.4	1.50404	0.00067	7.4800	3.1394	3.3378	3.6365
N1834003495	1507586.9	75.8	14.3	332.6	25.9	251.6	0.92779	0.00065	5.7285	2.4371	2.3514	2.3480
N1835727146	2260504.0	70.2	21.7	241.6	25.9	163.8	0.78231	0.00986	7.0352	1.7545	1.8691	2.0831
N1835819767	2101099.8	66.3	21.8	259.3	25.9	186.0	0.98056	0.00389	7.3876	2.3281	2.5094	2.8038
N1839950543	3454463.8	63.7	26.3	23.8	26.1	311.8	0.83633	0.01026	5.9897	1.9283	1.9215	1.9957
N1840145994	3084911.2	55.0	28.8	101.0	26.1	38.3	2.19187	0.00047	7.4413	3.5809	3.7350	3.9749

Table 10 continued on next page

**Table 10** (*continued*)

Filename	Range	Phase	Sub-S/C	Sub-S/C	Sub-Solar	Sub-Solar	$A_{\text{eff}}$	$A_{\text{eff}}$	$A_{\text{phys}}$	$a_{\text{pred}}$	$a_{\text{pred}}$	$a_{\text{pred}}$
	(km)	(deg)	Latitude	Longitude	Latitude	Longitude	Value	Error		k=1	k=0.75	k=0.50
			(deg)	(deg)	(deg)	(deg)	(km <sup>2</sup> )					
N1840468986	2756520.5	47.4	26.9	344.6	26.1	291.3	1.57798	0.00319	5.8241	3.1374	3.0271	2.9866
N1840897599	1226364.1	17.3	19.9	277.5	26.1	260.0	3.13758	0.00111	7.4117	5.0888	5.0935	5.1125
N1843103363	2833679.2	35.7	33.6	43.6	26.2	3.0	1.91452	0.00987	6.7850	3.1254	3.2715	3.4839
N1843367625	2267024.8	19.6	29.5	35.5	26.2	13.6	2.04995	0.00508	6.4344	3.4951	3.5857	3.7027
N1843453605	2038689.5	13.1	26.5	23.1	26.2	8.5	2.33235	0.00137	5.9783	3.3566	3.3960	3.4487
N1844971205	2417794.2	60.0	44.8	224.5	26.3	151.7	1.23247	0.00736	7.1011	2.3433	2.4629	2.6855
N1845142986	2255703.8	48.8	46.1	197.5	26.3	140.6	1.15150	0.00054	6.7129	2.7953	2.8588	3.0094
N1845330957	2035109.6	38.9	42.9	239.9	26.3	196.4	1.78973	0.00414	7.3374	3.5046	3.7105	3.9888
N1845353747	2198210.2	34.4	37.7	329.2	26.3	290.5	2.10915	0.00003	6.6005	3.9878	3.9282	3.9216
N1845368630	2180285.2	28.1	37.1	22.7	26.3	352.0	1.80662	0.00120	6.4113	3.1717	3.2696	3.4151
N1845383513	2032627.0	24.4	39.2	78.3	26.3	53.4	2.65155	0.00002	7.5402	4.6925	4.7966	4.9301
N1845398396	1862374.0	26.3	42.3	140.4	26.3	114.8	2.32516	0.00100	6.9252	4.3197	4.3033	4.3277
N1845413279	1814782.8	30.6	42.2	208.2	26.3	176.2	1.78888	0.00013	6.6998	3.2317	3.3716	3.5666
N1846755606	2629193.0	71.3	37.0	42.0	26.3	316.4	0.72392	0.00398	6.8407	1.8547	1.9104	2.0596
N1846927922	2691616.8	62.9	39.0	22.8	26.3	307.5	1.00435	0.00464	6.4974	2.2505	2.2669	2.3743
N1847239229	2235686.2	48.3	45.8	208.7	26.3	152.4	1.22980	0.00119	6.8504	2.7328	2.8405	3.0379
N1847382690	2217485.5	31.2	39.6	58.5	26.3	24.6	2.28940	0.00239	7.2701	3.8349	4.0109	4.2381
N1848935350	1668244.6	45.1	43.9	4.8	26.4	312.8	1.34389	0.00166	6.5406	3.0319	3.0522	3.1514
N1849019981	1467473.6	34.0	40.8	339.6	26.4	302.1	1.97697	0.00017	6.5362	3.7314	3.7011	3.7270
N1853153967	1149432.1	62.1	59.3	164.2	26.5	84.9	1.41556	0.00061	7.2603	3.2422	3.2679	3.3978

**Table 11.** Brightness estimates from clear-filter images of Pallene.

Filename	Range	Phase	Sub-S/C	Sub-S/C	Sub-Solar	Sub-Solar	$A_{\text{eff}}$	$A_{\text{eff}}$	$A_{\text{phys}}$	$a_{\text{pred}}$	$a_{\text{pred}}$	$a_{\text{pred}}$
	(km)	(deg)	Latitude	Longitude	Latitude	Longitude	Value	Error		k=1	k=0.75	k=0.50
			(deg)	(deg)	(deg)	(deg)	(km <sup>2</sup> )					
N1502276381	2437835.2	78.9	-10.4	287.9	-20.8	205.9	2.01443	0.00006	16.3913	5.0531	5.3314	5.8471
N1502795579	2300004.0	56.1	-15.3	339.6	-20.7	280.6	2.70475	0.00006	13.2926	6.5691	6.3338	6.2744
N1505466121	2520183.0	76.3	-0.3	279.6	-20.4	204.1	1.68066	0.00263	16.5546	4.9522	5.2495	5.7894
N1506716999	2173371.8	78.1	-0.3	118.7	-20.2	41.4	1.67143	0.00796	15.7004	5.3684	5.5332	5.9192
N1506907435	2497063.0	71.6	-0.3	79.2	-20.2	8.8	1.63914	0.00849	16.5278	4.4971	4.8088	5.3639
N1508412740	2300827.8	74.2	-0.4	117.9	-20.0	44.6	1.74305	0.00371	15.7529	5.8123	5.9700	6.3476
N1511332959	2177036.2	70.4	-0.3	218.9	-19.6	149.7	1.25172	0.00081	14.0280	3.1824	3.2588	3.5060
N1511457594	2063485.1	65.9	-0.3	303.6	-19.6	239.2	2.54285	0.00214	15.4411	6.7978	6.8418	7.0881
N1513573553	2819354.8	70.9	-0.2	29.3	-19.3	319.5	1.22749	0.01477	13.3699	3.1804	3.1936	3.3680
N1513745544	2272592.5	71.0	-0.3	291.1	-19.3	221.2	2.37342	0.00109	16.1621	6.0496	6.2639	6.7042
N1515599256	2346652.5	79.4	-0.2	153.6	-19.0	74.7	1.29584	0.00946	13.0692	4.7170	4.5739	4.6172
N1551095123	1789854.9	78.7	37.1	26.2	-13.6	90.4	1.17227	0.00032	15.4873	4.4198	4.4345	4.6616
N1552347901	1526118.6	51.2	24.1	257.9	-13.4	293.7	3.43603	0.00021	16.9000	7.9927	8.1648	8.5534
N1552386211	1821652.0	61.9	24.3	22.3	-13.4	72.6	1.81939	0.00237	14.0863	5.3697	5.2881	5.4052
N1552476182	1935793.1	67.6	31.4	344.7	-13.4	37.5	1.42801	0.00400	14.5211	3.4194	3.5093	3.7797
N1552559912	1862984.2	73.4	40.1	285.3	-13.4	339.6	1.93685	0.00164	17.4716	4.1806	4.5287	5.1349
N1553899121	1954346.6	73.6	30.6	73.8	-13.1	135.5	1.83648	0.00218	17.0562	5.4011	5.6719	6.1952
N1553980301	2145123.8	74.1	32.5	7.7	-13.1	68.9	1.30821	0.00523	14.4718	3.9132	3.9037	4.0859
N1555052913	1703912.0	39.0	10.9	310.6	-12.9	341.7	3.16841	0.00124	15.0937	6.4476	6.7113	7.1410
N1556544748	1963600.0	45.3	13.7	291.5	-12.7	328.6	3.42907	0.00086	16.3109	7.0540	7.3839	7.9113
N1556568688	2146357.8	52.3	13.7	10.0	-12.7	55.6	2.24587	0.00251	12.7510	5.3120	5.1843	5.2257
N1556714579	1939059.2	62.3	22.1	168.9	-12.7	221.6	1.58742	0.00067	13.3571	3.7634	3.7802	3.9681
N1557986827	2063796.2	55.7	10.7	85.3	-12.5	136.4	2.75759	0.00385	16.7161	7.2662	7.5646	8.0781

Table 11 continued on next page

**Table 11** (*continued*)

Filename	Range	Phase	Sub-S/C	Sub-S/C	Sub-Solar	Sub-Solar	$A_{\text{eff}}$	$A_{\text{eff}}$	$A_{\text{phys}}$	$a_{\text{pred}}$	$a_{\text{pred}}$	$a_{\text{pred}}$
	(km)	(deg)	Latitude	Longitude	Latitude	Longitude	Value	Error		k=1	k=0.75	k=0.50
			(deg)	(deg)	(deg)	(deg)	(km <sup>2</sup> )					
N1558292948	2195802.8	68.8	16.7	98.6	-12.4	161.7	1.59402	0.00427	16.7657	4.8284	5.1928	5.8082
N1558375539	2342136.2	69.8	16.5	35.9	-12.4	100.2	1.64986	0.00352	14.3416	5.7109	5.6228	5.7361
N1558434309	2049777.2	65.1	19.4	253.9	-12.4	311.6	2.51514	0.00106	16.6399	6.4985	6.7443	7.2246
N1559285895	1873818.4	49.7	5.5	100.6	-12.2	147.3	2.81385	0.00097	16.5361	7.1501	7.5094	8.0725
N1559364585	2267913.8	49.8	5.9	25.0	-12.2	71.6	2.69325	0.00418	13.1398	6.6018	6.3828	6.3285
N1559467411	2387654.2	54.5	7.2	31.7	-12.2	82.9	2.14177	0.00033	13.6482	6.7572	6.5561	6.5309
N1559626997	2195680.5	53.6	9.8	249.2	-12.2	298.3	3.41465	0.00404	16.2209	8.0038	8.1288	8.4430
N1559670812	2429143.5	62.6	9.2	38.2	-12.2	97.4	2.00621	0.00425	14.2024	6.5106	6.3763	6.4321
N1559730468	2187425.2	57.1	10.7	259.4	-12.2	312.0	2.94879	0.00357	16.6002	7.3511	7.6086	8.0783
N1559972029	2017582.5	76.0	12.0	32.5	-12.1	105.1	1.37582	0.00516	13.8833	5.1244	5.0283	5.1272
N1561136051	2314424.8	54.3	1.2	294.7	-11.9	347.7	2.18978	0.00126	15.9850	5.6303	5.9860	6.5636
N1561178606	2227845.0	65.9	1.2	77.0	-11.9	142.0	1.93848	0.00219	16.4700	6.3728	6.6714	7.1970
N1561201182	1959031.5	63.4	1.4	160.6	-11.9	223.0	1.70241	0.00277	12.6193	3.6315	3.6065	3.7431
N1561262382	2263260.8	65.8	1.2	19.6	-11.9	84.6	2.23469	0.00316	12.7298	5.3561	5.1454	5.1189
N1561364698	2030236.8	71.3	1.4	23.5	-11.9	94.1	1.86039	0.00030	12.9680	5.1906	5.0049	5.0057
N1564454117	3440900.5	36.1	0.1	55.4	-11.4	89.9	3.66395	0.00949	15.3687	9.3793	9.2579	9.2473
N1567945989	3339838.2	34.9	-3.9	64.4	-10.8	99.0	4.23591	0.00197	15.9495	9.8327	9.7884	9.8443
N1571517663	2335113.5	53.9	3.8	343.5	-10.1	35.8	1.83850	0.00686	12.5938	4.2983	4.2856	4.4327
N1571563203	1826274.0	61.8	4.7	140.9	-10.1	201.1	1.58767	0.00150	14.0860	3.6671	3.8080	4.1303
N1572464980	2341122.5	21.1	2.1	200.0	-10.0	217.4	4.45198	0.00098	12.6646	7.2524	7.1313	7.0719
N1573672698	1677865.0	57.1	4.9	202.9	-9.8	258.3	2.60958	0.00010	12.8856	6.0761	5.8515	5.8014
N1575630032	1564079.9	16.9	5.3	117.7	-9.4	126.1	5.52287	0.00111	15.7946	9.6606	9.7492	9.8900
N1575675932	1878167.4	15.5	6.0	293.4	-9.4	291.9	6.10954	0.00031	16.0848	10.3209	10.3284	10.3840
N1575718188	1966862.4	21.1	7.1	71.0	-9.4	84.1	5.62590	0.00167	16.2973	10.5096	10.4876	10.5326
N1576021265	2309103.0	33.1	12.7	73.6	-9.4	98.6	4.40749	0.00187	16.4892	9.8484	9.8852	10.0444
N1577009966	1748123.9	19.0	7.9	60.3	-9.2	68.6	5.87645	0.00066	15.7560	9.9784	9.9461	9.9757
N1577097747	2077027.4	22.1	11.0	16.5	-9.2	25.5	4.05249	0.00070	12.8462	6.7398	6.7325	6.8010
N1577765477	1699021.1	52.3	32.4	244.1	-9.1	277.5	3.20803	0.00032	16.7817	7.8503	7.9600	8.2926
N1579654710	1756221.2	30.8	21.8	255.7	-8.7	259.7	4.69897	0.00004	16.7691	9.7220	9.8080	10.0350
N1580356385	1362338.2	20.4	2.7	290.5	-8.6	273.4	6.38313	0.00087	16.1972	10.6257	10.5800	10.5874
N1580527536	1515542.8	24.8	15.9	166.9	-8.6	171.2	3.60799	0.00120	12.9047	6.1263	6.2210	6.4086
N1581771720	1982200.5	30.8	21.0	334.3	-8.4	343.8	3.22868	0.00096	13.9924	6.2628	6.4372	6.7407
N1583629498	1466758.4	36.8	28.7	210.1	-8.0	212.6	3.29237	0.00069	14.7842	6.4697	6.6417	6.9755
N1583839319	1188437.5	54.4	45.1	237.5	-8.0	250.4	2.81944	0.00085	17.2472	7.0359	7.2253	7.6635
N1584374373	1732124.6	19.9	12.0	22.1	-7.9	21.9	4.20549	0.00024	13.1920	6.9005	6.9519	7.0717
N1585394936	1436024.2	35.9	26.8	96.5	-7.7	106.9	3.77075	0.00051	17.0898	9.3129	9.4724	9.8025
N1585439051	1435319.1	38.5	30.4	272.9	-7.7	267.1	4.45004	0.00061	17.2496	9.2350	9.3793	9.7120
N1586003505	1074484.4	13.7	4.1	151.7	-7.6	144.6	4.95981	0.00009	13.2374	7.7584	7.7048	7.6856
N1586193031	1428734.8	32.7	24.2	100.9	-7.6	108.8	4.21562	0.00064	16.9301	9.4895	9.6346	9.9320
N1587716367	1227015.9	24.4	11.9	225.3	-7.3	210.2	4.36941	0.00025	14.7548	7.6721	7.8583	8.1369
N1587848623	1649831.5	28.8	21.0	333.6	-7.3	328.1	4.09376	0.00009	14.0341	6.8758	6.9648	7.1715
N1589547370	1391854.5	33.3	25.9	347.4	-7.0	342.3	3.33406	0.00098	13.8672	5.9476	6.1062	6.4043
N1591878927	1024670.9	10.2	-2.1	130.0	-6.6	120.8	5.94140	0.00027	14.9160	9.7147	9.6297	9.5603
N1595480632	806982.6	25.2	-14.5	190.7	-5.9	166.7	3.81182	0.00018	12.7297	6.2030	6.2723	6.4254
N1595509222	1186348.5	29.9	-6.3	300.6	-5.9	270.5	5.37631	0.00005	15.6787	9.9842	9.8861	9.8675
N1597416216	1355543.8	24.2	-3.5	341.1	-5.6	316.9	4.81017	0.00043	12.7157	7.3397	7.1847	7.0998
N1597581787	999603.2	35.4	23.9	214.1	-5.6	194.0	3.44382	0.00013	14.6258	6.1405	6.4040	6.8212
N1598065360	978283.2	16.7	-2.5	156.8	-5.5	140.3	4.54015	0.00091	12.8656	7.6690	7.5438	7.4578
N1599452540	1100518.9	22.2	15.8	117.0	-5.2	109.8	5.00482	0.00003	16.0536	9.9107	9.9279	10.0283
N1599960489	950462.7	18.9	-5.7	162.7	-5.1	143.8	4.57237	0.00069	12.5783	7.2799	7.1638	7.0965
N1602671923	1049455.4	37.1	22.4	240.6	-4.6	214.7	4.31812	0.00007	16.1629	7.6006	7.9263	8.4166
N1605247441	1081021.0	29.6	21.5	170.3	-4.2	155.3	3.49507	0.00036	13.2662	6.2102	6.2854	6.4742
N1605987636	1271215.6	35.7	26.1	327.9	-4.0	308.1	3.52184	0.00005	14.7622	7.4009	7.4284	7.6043
N1606638391	1006296.6	32.9	27.5	148.5	-3.9	138.3	3.47326	0.00011	14.7573	7.1853	7.2926	7.5407
N1614669638	1338211.6	36.8	-16.9	13.5	-2.5	339.0	2.70513	0.00011	13.0953	5.5702	5.6532	5.8698

Table 11 continued on next page

**Table 11** (*continued*)

Filename	Range	Phase	Sub-S/C	Sub-S/C	Sub-Solar	Sub-Solar	$A_{\text{eff}}$	$A_{\text{eff}}$	$A_{\text{phys}}$	$a_{\text{pred}}$	$a_{\text{pred}}$	$a_{\text{pred}}$
	(km)	(deg)	Latitude	Longitude	Latitude	Longitude	Value	Error		k=1	k=0.75	k=0.50
			(deg)	(deg)	(deg)	(deg)	(km <sup>2</sup> )					
N1618011333	997161.4	62.3	-36.0	223.4	-1.9	166.8	1.66760	0.00022	16.0736	4.2019	4.5160	5.0592
N1618270264	1390177.6	30.0	27.8	25.6	-1.8	21.1	3.74743	0.00000	14.5642	6.6652	6.8879	7.2406
N1619786865	1473278.5	74.6	55.6	38.9	-1.6	98.1	1.44249	0.00061	17.5070	5.5148	5.6800	6.1049
N1619851576	1406067.1	75.9	61.2	274.9	-1.6	331.1	1.35669	0.00041	18.3789	4.6402	5.0626	5.7719
N1621003314	1299829.1	64.9	59.8	143.3	-1.4	171.0	1.46714	0.00011	17.7224	4.5442	4.9939	5.7200
N1622137757	1284512.6	35.5	32.2	319.7	-1.2	306.7	3.86424	0.00016	15.6931	7.8629	7.9808	8.2585
N1647980256	1434496.0	68.3	0.3	317.6	3.4	25.9	1.30723	0.00181	14.3896	3.2502	3.3826	3.6924
N1649509127	1345249.8	73.7	0.2	72.3	3.7	146.0	1.64058	0.00022	16.3083	5.5462	5.8505	6.3879
N1649553527	1393347.2	62.4	0.3	244.6	3.7	307.0	2.88167	0.00011	15.8990	7.1649	7.3281	7.6880
N1658886683	1225769.6	71.6	0.1	97.5	5.3	169.1	1.50619	0.00032	16.5794	4.4824	4.8597	5.4856
N1660687866	1513947.5	76.6	-0.6	116.7	5.6	193.2	0.96645	0.00092	15.8257	3.0340	3.2661	3.6996
N1662535309	2135755.0	72.9	-1.2	312.1	5.9	24.8	0.86379	0.00064	14.8202	2.9905	3.1354	3.4579
N1684434342	2882811.2	38.6	0.2	225.9	9.5	263.6	3.73472	0.00063	14.5925	8.7609	8.5760	8.5102
N1688399527	2403494.2	59.9	0.3	122.3	10.2	181.7	1.73222	0.00006	15.4681	4.4974	4.7968	5.3140
N1688602148	1992662.8	69.1	0.3	124.7	10.2	193.5	1.14479	0.00071	15.3035	3.4908	3.7135	4.1388
N1689640995	2701255.0	32.4	0.2	313.9	10.4	344.8	3.82606	0.00440	14.6792	6.8182	7.0666	7.4418
N1693974522	2585436.0	56.9	0.3	96.6	11.0	152.9	1.95900	0.00173	16.5957	6.4745	6.8641	7.4791
N1694061223	2640209.0	59.0	0.3	47.6	11.1	105.9	2.61215	0.00557	14.7936	7.3549	7.2705	7.3641
N1694911668	1676019.6	22.1	0.2	278.5	11.2	297.8	6.16960	0.00011	16.5753	10.3138	10.4354	10.6200
N1695302331	2242959.8	43.0	0.3	226.5	11.2	268.4	3.86649	0.00129	14.6426	8.5345	8.3621	8.3245
N1695406252	2311850.5	46.0	0.3	238.7	11.3	283.7	3.60619	0.00192	15.5375	8.7985	8.7546	8.8551
N1697959688	1477436.8	32.8	0.2	112.6	11.7	143.5	3.80137	0.00009	16.0510	8.3492	8.6350	9.0440
N1698202029	2179226.2	34.2	0.2	267.0	11.7	299.4	4.85401	0.00065	16.6368	9.7078	9.8684	10.1403
N1703195141	2887286.5	49.1	-0.5	282.0	12.5	329.8	2.90467	0.00058	16.4972	7.1513	7.5162	8.0824
N1712870742	1588008.0	78.6	0.4	270.2	13.9	348.5	1.53086	0.00081	16.6486	4.1186	4.4494	5.0236
N1713624647	2086002.4	56.1	0.4	135.7	14.0	190.7	1.68931	0.00003	14.4673	4.3629	4.5611	4.9518
N1718469678	3060490.8	70.9	-13.3	340.9	14.7	46.7	0.81983	0.00635	13.1020	3.1237	3.1165	3.2672
N1718765120	2991309.5	78.9	-15.7	319.8	14.7	33.4	0.62565	0.01359	14.6072	2.4816	2.5670	2.8068
N1725788225	1916523.8	57.7	-14.9	145.1	15.7	194.5	1.70148	0.00207	14.1074	3.9249	4.0720	4.4025
N1733323073	1838043.2	75.9	-36.4	344.9	16.7	42.4	0.98692	0.00250	15.0669	2.9084	2.9939	3.2522
N1735137305	1108126.4	27.9	5.4	88.0	17.0	113.9	4.88981	0.00014	16.6707	10.3061	10.4055	10.5890
N1738778008	1589768.9	44.1	-19.3	276.4	17.5	301.2	3.80374	0.00075	16.8783	8.2793	8.4773	8.8759
N1741126463	1523289.4	78.5	-38.8	82.7	17.8	140.9	1.32750	0.00111	17.5312	4.5146	4.7951	5.3312
N1745005197	1346896.1	71.6	-35.5	57.1	18.2	107.0	1.73042	0.00171	16.7058	5.6675	5.7806	6.1390
N1746448826	1305194.4	31.4	-11.2	270.2	18.4	280.9	4.87169	0.00065	16.7446	9.8274	9.8939	10.1001
N1747228401	1066214.9	26.6	-5.2	203.2	18.5	215.5	4.14692	0.00004	12.9099	6.9835	6.8854	6.8820
N1750357531	1516038.9	63.9	-35.9	320.8	18.9	355.4	1.69742	0.00004	15.9341	3.8058	4.0471	4.5044
N1760113013	1592865.9	64.6	46.1	16.2	20.0	302.3	2.30553	0.00002	16.1591	5.5943	5.7097	6.0555
N1760179444	1289739.5	60.2	51.8	248.9	20.0	181.9	2.46349	0.00137	17.8666	6.2567	6.7766	7.5685
N1764309060	1711258.5	43.1	39.6	19.8	20.5	334.4	3.41634	0.00257	15.5337	6.6225	6.8453	7.2502
N1766817806	1963881.0	69.0	53.6	116.4	20.8	33.9	1.90176	0.00053	17.8559	6.7758	7.1880	7.8627
N1767476400	964437.9	80.0	-48.4	206.6	20.8	251.4	1.34364	0.00007	16.5585	3.8299	3.9185	4.2216
N1772108029	2513639.0	67.0	50.8	136.4	21.3	57.0	2.71851	0.00182	17.2147	7.2541	7.4726	7.9309
N1772255800	2501332.5	65.1	44.9	305.9	21.3	230.3	2.78405	0.00052	17.1679	7.4240	7.6771	8.1601
N1777328113	3469264.5	79.2	40.4	281.5	21.8	187.1	1.81029	0.01680	17.5466	4.9871	5.3903	6.0628
N1782844733	3089644.8	68.3	43.7	28.0	22.4	307.2	1.67685	0.00585	16.2043	5.1309	5.2603	5.6198
N1786522171	2275443.5	23.9	16.6	291.6	22.7	267.0	6.08660	0.00061	16.3799	10.8345	10.7758	10.7738
N1786609772	1929250.6	20.9	11.7	242.2	22.7	223.5	5.24642	0.00279	15.8970	9.4696	9.6013	9.7976
N1786723352	1820064.6	24.0	1.3	284.5	22.7	273.5	5.63374	0.00025	16.4252	10.4867	10.4565	10.5148
N1786725901	1845363.9	24.0	1.0	293.1	22.7	282.6	5.53996	0.00004	16.0671	10.1832	10.1244	10.1538
N1786728450	1868707.8	23.9	0.7	301.5	22.7	291.7	5.18386	0.00190	15.5766	9.7233	9.6419	9.6478
N1791975906	2398846.0	60.3	38.2	229.8	23.2	160.2	2.31006	0.00045	16.5232	5.4413	5.7454	6.2880
N1791981955	2441792.5	61.1	37.1	252.6	23.2	182.2	2.46198	0.00011	17.2720	6.0541	6.4885	7.1784
N1791988004	2493045.2	61.1	35.9	274.5	23.2	204.2	2.70517	0.00021	17.4431	7.0516	7.4794	8.1472
N1792418829	1468830.6	25.1	9.6	342.0	23.2	319.9	4.66584	0.00008	12.8581	7.5588	7.3643	7.2473

Table 11 continued on next page

**Table 11** (*continued*)

Filename	Range	Phase	Sub-S/C	Sub-S/C	Sub-Solar	Sub-Solar	$A_{\text{eff}}$	$A_{\text{eff}}$	$A_{\text{phys}}$	$a_{\text{pred}}$	$a_{\text{pred}}$	$a_{\text{pred}}$
	(km)	(deg)	Latitude	Longitude	Latitude	Longitude	Value	Error		k=1	k=0.75	k=0.50
			(deg)	(deg)	(deg)	(deg)	(km <sup>2</sup> )					
N1796431694	1876837.1	30.6	19.0	82.6	23.5	50.0	4.83795	0.00315	16.8564	9.9154	10.1209	10.4233
N1799229002	1551076.2	58.3	28.5	136.6	23.8	71.1	2.94393	0.00100	15.5151	7.9327	7.8944	8.0383
N1816569833	807950.9	57.8	-0.3	103.7	25.0	49.9	2.71797	0.00097	16.4218	7.4694	7.6451	8.0321
N1833919214	1481788.8	74.9	16.5	139.0	25.9	58.1	1.98652	0.00253	14.6277	6.0081	5.9766	6.1451
N1834006225	1354210.2	63.0	15.9	79.4	25.9	12.1	2.21407	0.00205	16.7231	5.8585	6.1977	6.7809
N1835729636	2154115.8	66.7	22.8	190.1	25.9	115.9	1.82981	0.00258	13.3963	4.7909	4.6790	4.7556
N1839518861	3167064.2	77.9	26.6	207.8	26.1	118.7	1.21968	0.00464	14.4842	3.8208	3.8128	3.9945
N1840148314	3215971.2	61.8	27.5	302.5	26.1	232.2	2.92310	0.00673	16.2888	7.7454	7.8740	8.1994
N1840468786	2780888.8	46.2	26.6	1.0	26.1	309.1	3.36505	0.00874	13.7624	6.6348	6.5218	6.5716
N1840898509	1303760.0	7.7	18.5	58.8	26.1	60.3	7.35613	0.00098	15.9583	10.6547	10.6079	10.5739
N1842362148	3428986.2	64.9	32.5	21.9	26.2	306.2	2.48640	0.02032	14.8592	5.1222	5.1385	5.3609
N1842537249	3325472.0	63.5	34.5	293.3	26.2	218.7	2.82769	0.00504	17.0149	7.4752	7.7616	8.2673
N1843102443	2589353.5	35.9	37.3	139.3	26.2	98.8	4.42416	0.00151	16.0525	9.7097	9.6396	9.6925
N1843368575	2315113.5	22.1	28.8	5.0	26.2	340.2	4.14713	0.00047	14.0245	7.7862	7.8044	7.8926
N1843454975	2004608.6	20.0	26.9	314.9	26.2	292.5	5.77241	0.00165	15.5777	10.2598	10.1324	10.0518
N1844969275	2587143.2	53.2	41.2	63.2	26.3	0.2	2.71661	0.00935	17.2408	6.8571	7.2829	7.9446
N1845144316	2524581.2	49.7	40.1	331.0	26.3	272.8	3.68193	0.00072	15.8825	8.4653	8.4088	8.5333
N1845331147	2110245.0	39.7	41.0	272.4	26.3	227.4	4.48797	0.00261	17.6471	9.7722	10.0875	10.5456
N1846755446	2609516.8	70.2	37.3	54.8	26.3	330.5	1.94374	0.00658	16.7238	4.8117	5.0470	5.5229
N1846930593	2684001.8	67.2	39.2	324.1	26.3	243.1	2.80346	0.00652	16.0640	7.2124	7.2652	7.5310
N1847382110	2095952.6	31.1	42.4	105.3	26.3	72.7	5.28133	0.00073	17.5527	10.8740	11.0116	11.2522
N1848935560	1670787.8	48.6	43.8	340.0	26.4	283.1	4.02385	0.00079	15.9946	8.2480	8.2256	8.3921
N1849021451	1339481.2	41.0	45.4	278.9	26.4	233.0	4.47295	0.00093	17.7816	9.8848	10.1766	10.6199
N1849967077	1308601.4	72.0	51.5	141.3	26.4	47.2	2.30032	0.00092	17.1384	6.8700	7.1060	7.5842
N1853153657	1212789.2	55.9	54.6	102.0	26.5	34.3	3.38679	0.00083	18.1013	8.2715	8.7103	9.3784
N1855715334	1170809.1	78.0	42.8	23.3	26.5	284.8	1.51894	0.00032	15.9761	4.8080	4.8510	5.1197

**Table 12.** Brightness estimates from clear-filter images of Telesto.

Filename	Range	Phase	Sub-S/C	Sub-S/C	Sub-Solar	Sub-Solar	$A_{\text{eff}}$	$A_{\text{eff}}$	$A_{\text{phys}}$	$a_{\text{pred}}$	$a_{\text{pred}}$	$a_{\text{pred}}$
	(km)	(deg)	Latitude	Longitude	Latitude	Longitude	Value	Error		k=1	k=0.75	k=0.50
			(deg)	(deg)	(deg)	(deg)	(km <sup>2</sup> )					
N1495206641	1158822.1	41.0	-20.6	283.1	-21.7	239.0	209.49303	0.00203	510.9615	291.6927	296.2795	304.6195
N1495310692	533103.5	48.7	-16.1	57.3	-21.6	108.6	186.92639	0.00024	477.0852	267.6940	266.3135	269.2979
N1513353874	3223840.5	76.1	-0.2	38.3	-19.3	323.0	55.22128	0.02512	418.3909	80.5283	81.8249	87.6863
N1513525391	2910381.2	70.1	-0.2	50.4	-19.3	341.4	60.29562	0.02358	448.4575	98.7257	103.0927	113.0088
N1515851740	1677181.9	64.8	-0.1	138.3	-19.0	75.1	125.14794	0.00486	424.5765	195.9870	191.5797	192.7610
N1550920790	1675677.8	54.1	17.0	20.2	-13.6	65.3	118.35385	0.00402	402.1162	166.1985	162.1580	163.5099
N1551094911	1848412.8	78.9	35.6	24.2	-13.6	89.6	67.92459	0.01501	474.1757	127.2060	127.8723	134.8444
N1552385974	1908353.1	60.3	23.1	9.4	-13.4	58.5	91.43609	0.00739	409.6214	135.3984	133.7996	137.6850
N1552559265	2051421.1	79.1	35.6	15.1	-13.4	80.9	63.43113	0.01314	465.5626	115.4674	115.9241	122.3549
N1553937429	1710299.9	73.7	39.0	186.0	-13.1	242.1	59.57480	0.00959	472.9421	110.4580	112.4599	120.3907
N1555230242	1686252.1	63.3	26.2	163.6	-12.9	214.8	70.75269	0.01395	425.2228	100.3798	102.8213	110.4162
N1555402564	1841843.0	73.0	34.4	176.3	-12.9	235.1	59.51403	0.01079	451.8094	99.5404	101.1081	108.0919
N1555449934	2158281.5	66.2	30.8	287.8	-12.9	339.6	85.16799	0.01633	524.5949	138.3026	149.8189	169.1897
N1555487104	2344866.5	73.6	29.0	358.8	-12.9	61.5	64.92888	0.02412	430.3364	101.9326	101.9700	107.2863
N1556521996	1630357.8	55.3	15.0	136.9	-12.7	185.2	98.90849	0.00312	442.8657	122.5332	129.3526	142.0109
N1556544211	1620021.0	50.2	16.7	193.2	-12.7	234.3	117.79137	0.00657	388.6341	157.4426	154.1312	155.8152
N1558030490	1937903.6	47.5	12.9	233.5	-12.4	273.9	159.97809	0.00569	462.9385	242.9264	240.7927	243.7864

*Table 12 continued on next page*

**Table 12** (*continued*)

Filename	Range	Phase	Sub-S/C	Sub-S/C	Sub-Solar	Sub-Solar	$A_{\text{eff}}$	$A_{\text{eff}}$	$A_{\text{phys}}$	$a_{\text{pred}}$	$a_{\text{pred}}$	$a_{\text{pred}}$
	(km)	(deg)	Latitude	Longitude	Latitude	Longitude	Value	Error		k=1	k=0.75	k=0.50
			(deg)	(deg)	(deg)	(deg)	(km <sup>2</sup> )					
N1558205931	2154753.2	54.0	15.7	254.5	-12.4	301.0	147.17648	0.00987	501.4184	230.7871	236.3979	248.2033
N1558416937	2408235.8	66.5	16.3	345.9	-12.4	46.6	69.01051	0.02443	391.3528	98.6231	98.2407	102.6095
N1558476623	1961755.8	79.7	20.3	104.4	-12.4	178.3	51.85561	0.01283	508.7431	93.1729	101.9688	117.4549
N1559365948	2228171.0	41.5	6.2	303.4	-12.2	340.7	165.25931	0.01079	464.6898	190.3606	199.6945	214.3080
N1559409149	2403058.8	52.6	6.2	26.5	-12.2	76.0	129.29919	0.01237	392.8512	191.0666	184.0101	181.9988
N1559773141	2168064.8	70.9	10.9	91.7	-12.2	159.3	77.13753	0.01650	505.1436	144.1852	155.2659	173.8198
N1559886872	2314825.5	66.3	10.6	347.4	-12.1	50.2	69.11478	0.02118	375.3102	101.1352	99.5741	102.6834
N1559972402	1566011.1	75.5	15.7	168.0	-12.1	239.0	50.36079	0.00788	384.2037	85.9451	84.4698	87.4581
N1560553056	1832322.5	41.7	0.2	40.0	-12.0	80.2	175.41454	0.00645	422.5960	241.7769	234.8206	231.8358
N1560793117	1902283.0	43.7	1.0	208.0	-12.0	250.0	161.91130	0.00834	390.3971	211.2555	203.3552	199.6722
N1560831187	2314850.0	41.9	0.9	293.9	-12.0	334.0	177.20706	0.00680	480.8654	210.4633	220.8157	236.3631
N1561089534	2102052.2	63.6	1.2	121.4	-11.9	184.1	88.33342	0.01312	465.3134	119.3996	127.7693	142.5404
N1561136349	2054613.4	53.1	1.5	235.6	-11.9	287.4	147.49379	0.00908	458.7888	239.8140	238.3510	241.7947
N1561179565	2430652.8	56.6	1.2	327.2	-11.9	22.7	98.29389	0.01671	404.5493	115.2873	118.1714	126.0831
N1561261870	1845021.8	69.6	1.5	135.6	-11.9	204.4	70.00312	0.00829	431.6801	89.9035	93.7985	102.8369
N1562557608	2709559.5	66.1	0.1	118.0	-11.7	183.6	79.63545	0.02158	472.0964	116.7877	125.4787	140.7095
N1562860550	2954937.0	74.0	0.0	58.4	-11.6	132.0	98.74263	0.02522	466.3000	175.5937	179.7803	190.1768
N1564498831	3298726.8	38.7	0.1	109.9	-11.4	147.1	185.63046	0.02960	485.8323	230.2819	240.3596	255.0147
N1567917097	3177356.2	36.0	-4.1	94.3	-10.8	130.1	214.79488	0.01330	500.6017	272.6781	280.3248	291.5386
N1571518216	2086276.0	63.2	4.2	94.9	-10.1	156.7	105.08574	0.01033	500.4346	168.2747	180.2294	199.3778
N1574754129	2365399.2	33.6	5.8	67.6	-9.6	97.6	222.87148	0.00899	484.6575	291.3797	290.6327	293.1114
N1574856430	2328364.5	25.9	6.5	303.1	-9.6	323.4	230.63721	0.00987	465.5342	243.1202	249.6417	259.1083
N1575012031	1943647.5	30.4	8.1	281.8	-9.5	306.8	232.20114	0.00546	498.5188	275.6513	282.1013	292.0008
N1575628905	1481550.2	16.4	5.7	234.5	-9.4	228.1	252.84238	0.00944	457.9160	267.4259	269.7123	273.6444
N1575717976	2079613.5	21.2	6.6	50.6	-9.4	64.6	245.85684	0.00617	451.5925	276.3047	273.4821	272.7399
N1577010264	1902639.4	17.7	7.1	29.4	-9.2	36.4	225.53220	0.00666	400.5535	221.8065	220.5901	221.1160
N1577142175	2189670.2	22.0	12.4	323.4	-9.2	327.6	218.14926	0.00855	425.2936	218.1100	220.9176	226.3626
N1577763840	1614241.2	53.3	34.6	227.1	-9.1	259.5	129.23853	0.00507	500.7132	209.5028	212.3064	222.0069
N1578547010	1524998.6	31.0	21.1	180.2	-8.9	187.8	143.99078	0.00659	395.9479	159.2747	163.4208	171.4278
N1579446912	1912424.9	18.3	9.4	11.3	-8.8	13.7	201.04716	0.00399	371.5325	185.4010	186.1274	188.7381
N1580481319	1443861.0	23.1	13.0	128.1	-8.6	136.5	227.45395	0.00482	459.6920	246.9959	251.2273	258.3226
N1580482879	1434070.8	23.2	13.2	131.9	-8.6	139.9	220.69582	0.00373	451.4015	237.8867	242.0748	249.1355
N1580765781	2020616.1	35.3	21.4	25.2	-8.5	44.3	163.30405	0.00687	423.6796	195.5479	196.1073	201.0398
N1582720315	1856001.5	33.0	22.4	25.2	-8.2	37.7	168.66747	0.00612	426.9428	193.3983	195.6853	202.2206
N1586193359	1279023.6	35.7	27.3	134.3	-7.6	142.3	160.89963	0.00462	477.3673	208.8741	216.6075	229.6020
N1587746950	1692960.0	21.7	11.5	341.9	-7.3	331.0	206.26352	0.00568	385.1717	197.0645	196.6934	198.6219
N1588710877	1611800.5	33.1	24.5	308.2	-7.1	298.3	199.91443	0.00262	483.3095	249.0759	251.8690	259.3772
N1589547683	1464674.0	31.8	24.4	350.3	-7.0	345.0	152.46004	0.00046	414.9273	167.5692	172.7775	182.1605
N1592073391	922180.9	35.3	28.1	165.9	-6.5	159.0	141.17822	0.00173	430.7503	167.3411	173.3710	184.1453
N1595508425	824454.5	27.6	-8.8	207.5	-5.9	179.7	182.98239	0.00518	395.6596	177.6395	182.5472	190.3410
N1596878535	1499139.5	24.8	8.5	343.8	-5.7	323.4	202.71219	0.00135	376.5753	198.7633	195.9993	195.6493
N1597461859	920070.7	23.9	4.0	192.7	-5.6	170.7	181.34186	0.00120	362.9894	170.9711	172.2782	175.8780
N1598768518	941128.4	26.9	10.2	196.4	-5.3	174.3	170.26416	0.00145	376.8849	167.1003	170.0828	175.9429
N1600167428	1329276.8	27.1	21.5	26.7	-5.1	21.5	176.75436	0.00084	426.6898	191.9160	197.6301	206.9197
N16011778459	1203647.2	29.3	-17.5	3.7	-4.8	336.8	178.53476	0.00108	386.9159	178.0458	179.5795	184.1895
N1601856880	840756.4	21.5	-9.1	171.0	-4.8	149.8	211.48958	0.00124	365.6704	194.5565	192.2200	191.7049
N1602502465	883423.9	16.1	-6.5	150.5	-4.7	134.4	251.63901	0.00124	397.2510	237.6207	233.6276	230.6913
N1603175429	925423.8	29.3	1.8	208.2	-4.6	179.6	170.61258	0.00128	390.9523	170.9356	175.5654	183.3015
N1603721673	1318401.5	32.7	-10.5	337.5	-4.5	305.1	203.15038	0.00195	390.9171	216.2917	210.6147	208.0453
N1606531823	1430647.6	15.9	5.0	39.5	-3.9	26.4	235.79596	0.00109	423.0655	225.6273	229.8677	235.4291
N1607327459	1328935.8	29.3	21.0	358.1	-3.8	342.1	163.20976	0.00224	398.3627	171.4987	175.0697	182.1732
N1610901285	1368868.6	44.9	-23.6	349.9	-3.2	308.5	158.11038	0.00069	412.0261	179.6289	178.3682	181.9213
N1611720211	1357725.6	45.0	-24.9	356.4	-3.0	315.6	145.30849	0.00121	413.9643	168.9751	169.4192	174.7376
N1611808772	888516.9	33.6	-15.6	182.7	-3.0	151.0	166.71329	0.00164	377.8222	168.7008	168.8803	172.5389
N1620680764	1225512.1	49.8	-15.2	337.1	-1.4	288.5	153.85884	0.00068	402.1224	195.2347	189.6256	188.9157

Table 12 continued on next page

**Table 12** (*continued*)

Filename	Range	Phase	Sub-S/C	Sub-S/C	Sub-Solar	Sub-Solar	$A_{\text{eff}}$	$A_{\text{eff}}$	$A_{\text{phys}}$	$a_{\text{pred}}$	$a_{\text{pred}}$	$a_{\text{pred}}$
	(km)	(deg)	Latitude	Longitude	Latitude	Longitude	Value	Error		k=1	k=0.75	k=0.50
			(deg)	(deg)	(deg)	(deg)	(km <sup>2</sup> )					
N1622381527	1750357.0	75.0	51.1	17.3	-1.1	81.5	78.25792	0.00187	530.5090	149.3507	154.1364	166.5599
N1632444528	1793774.8	67.0	11.7	260.9	0.7	327.6	100.88271	0.00567	502.7958	178.6458	190.1372	208.7101
N1632483483	2257921.0	75.3	9.9	338.4	0.7	53.6	38.11750	0.01712	388.2464	83.8061	83.3152	87.2156
N1649509760	1162517.8	77.0	0.1	111.5	3.7	188.4	52.78316	0.00178	483.4889	91.0364	99.1012	113.4353
N1671765835	1469025.0	49.4	0.2	294.7	7.5	343.7	143.18315	0.00307	479.3947	179.3624	191.0298	208.8515
N1675509139	1951904.2	65.8	0.4	258.4	8.1	324.0	111.18420	0.00127	495.5160	187.4149	197.4261	214.1506
N1682450823	2742420.8	74.1	0.2	88.1	9.2	162.0	68.59486	0.01418	500.6082	139.3062	150.6040	169.3065
N1693343471	2688942.8	37.3	0.1	43.1	10.9	79.0	192.06427	0.00504	430.3936	254.8099	248.2731	245.2039
N1694912121	1706054.1	19.8	0.3	284.0	11.2	300.7	273.27173	0.00357	493.9292	301.9405	305.4961	310.7300
N1695097523	2350703.5	33.6	0.3	317.8	11.2	349.8	171.37567	0.00666	428.1188	185.7540	192.5500	203.2645
N1695406945	2412453.5	43.4	0.4	270.3	11.3	312.7	183.56741	0.00765	500.6685	253.5242	261.8937	274.9337
N1698202602	2446790.0	35.6	0.2	328.3	11.7	2.2	150.46939	0.00815	401.8066	164.8828	169.3469	177.7620
N1701924426	1941813.0	55.6	0.4	241.0	12.3	295.9	139.44794	0.00271	470.1577	235.9730	237.1366	243.4511
N1703587576	2976971.8	59.6	-0.6	307.7	12.5	6.3	97.28157	0.00444	453.0673	124.5182	131.8575	145.2976
N1707326920	2967569.0	45.5	-0.6	294.9	13.1	338.7	153.84373	0.01037	479.0653	195.4986	205.9750	222.1530
N1707881144	2772241.5	71.6	-0.4	50.9	13.2	121.8	106.06903	0.01968	449.7052	183.7927	184.4953	191.0743
N1710210418	1003599.8	28.6	0.5	196.6	13.5	222.4	191.50732	0.00082	367.2131	200.1999	194.5721	191.6917
N1710348479	1653217.9	51.3	0.3	117.0	13.5	167.1	118.36427	0.00182	474.0378	169.4228	179.9413	196.7215
N1711210625	1679568.6	76.4	0.7	193.6	13.7	269.8	70.44753	0.00265	362.6772	126.7922	120.7310	119.8745
N1712159351	2089950.4	59.5	0.5	144.9	13.8	203.5	79.38415	0.00506	407.7859	109.5623	112.5083	120.5548
N1712870055	1508629.4	75.9	0.5	256.4	13.9	331.9	79.45444	0.00111	493.6378	152.6365	162.0366	178.5384
N1713625100	2003207.0	56.9	0.4	142.5	14.0	198.3	86.11520	0.00400	413.9291	116.9269	120.8189	129.9577
N1714312164	1625309.2	76.3	0.7	198.6	14.1	274.6	74.33327	0.00200	370.5564	135.2521	129.2204	128.5118
N1716810880	2512068.2	55.6	-6.8	337.2	14.5	28.9	81.52333	0.01127	385.8169	114.8018	115.6173	121.1977
N1716980921	2504446.2	63.2	-8.2	344.7	14.5	44.2	62.21692	0.01243	374.5862	104.2273	102.9773	106.3937
N1718765513	3016234.0	77.2	-15.6	310.7	14.7	22.6	52.17443	0.02846	459.8988	75.1800	79.3173	88.4252
N1733979900	1053784.9	30.3	7.8	87.3	16.8	117.0	248.34412	0.00108	502.9047	302.4851	305.9884	312.1620
N1735136858	935672.7	29.1	6.7	122.2	17.0	150.0	209.80750	0.00086	465.8559	239.1864	246.2674	256.5351
N1735266398	1676284.9	45.8	-11.3	39.4	17.0	75.9	149.04788	0.00346	430.1395	219.0667	214.1076	214.2087
N1738702980	1559648.5	46.5	-11.0	62.0	17.4	99.2	177.77927	0.00119	479.1848	251.1204	250.3826	254.9598
N1738777561	1425047.4	45.0	-21.5	240.9	17.5	263.8	157.14168	0.00139	491.1741	240.0076	240.8259	247.7421
N1741127406	1757118.2	68.6	-33.1	0.7	17.8	49.1	56.40424	0.00584	448.1396	103.9302	105.5777	112.7165
N1744740099	1311059.2	35.9	-3.0	71.6	18.2	101.0	224.12495	0.00179	489.2337	286.9331	286.5162	290.0034
N1745863126	1439959.5	69.7	-34.7	11.6	18.3	59.2	64.85744	0.00023	459.0892	115.4593	116.6798	123.7830
N1750356354	1223413.8	71.1	-46.5	223.7	18.9	254.5	84.20554	0.00135	533.1237	145.5554	150.1521	162.2932
N1760177657	1548612.4	46.5	40.8	17.3	20.0	328.1	154.10590	0.00202	489.0661	197.9290	205.3612	218.8479
N1764308223	1449919.9	40.5	49.2	119.7	20.5	83.7	217.17583	0.00224	555.1010	305.3929	312.2136	324.5432
N1769462056	2513156.2	71.9	45.3	23.0	21.0	297.8	91.25581	0.00753	511.5319	158.6058	162.7730	174.2236
N1769728157	1735003.0	54.9	49.8	225.1	21.1	165.0	144.96034	0.00274	544.1949	194.0115	209.0695	232.1159
N1772108292	2593256.8	64.0	48.7	92.2	21.3	17.7	133.42886	0.00635	566.1969	210.4758	228.1431	254.3412
N1772257903	2539449.2	55.2	43.8	49.6	21.3	347.9	123.77380	0.00378	532.5200	189.3327	203.1328	224.6111
N1777325486	3412929.8	71.1	41.2	94.9	21.8	11.5	104.07353	0.01492	551.3716	182.9346	198.2793	222.1631
N1777845459	2955172.8	55.1	41.4	141.1	21.9	79.0	160.26814	0.01006	511.1036	257.2190	259.2126	267.2324
N1782844576	3133038.8	67.4	42.9	30.6	22.4	311.2	93.56756	0.00594	509.2371	160.7974	166.2984	179.0277
N1783953628	1739760.9	23.6	10.8	260.0	22.5	238.6	262.45270	0.00335	501.4108	308.5045	311.4398	316.5202
N1791369005	3011943.2	77.3	43.1	136.4	23.1	42.2	99.62952	0.00645	522.2576	195.4733	203.7562	219.3909
N1791951519	2732697.0	62.9	33.9	319.7	23.2	247.6	136.19589	0.00993	489.9996	234.3922	235.3256	242.2479
N1792421022	1066982.9	30.0	12.5	233.2	23.2	203.6	212.44080	0.00233	461.17977	235.6160	241.5771	250.9181
N1795592562	3874942.0	66.6	31.8	78.3	23.5	2.2	95.11597	0.01252	530.9053	172.7713	185.7700	206.7733
N1796026425	3200873.0	63.0	27.4	310.1	23.5	239.5	135.24649	0.01249	486.9284	234.0736	235.9039	243.4709
N1796431497	1874921.2	28.1	19.2	83.3	23.5	53.4	252.12662	0.00576	512.8786	308.0044	313.2608	320.9467
N1796516828	1568499.6	39.5	13.2	282.1	23.6	241.7	209.77679	0.00125	502.5739	290.8144	293.5372	300.0113
N1799227535	1443808.2	61.4	31.1	173.0	23.8	103.2	123.88239	0.00103	438.1882	191.5201	187.5969	189.6116
N1823332869	1310528.5	76.6	-0.2	92.2	25.3	17.2	79.06044	0.00492	500.4580	138.0555	146.2844	161.7108
N1833918777	1784477.5	72.6	13.8	56.1	25.9	339.0	61.45686	0.00442	471.3583	114.7354	119.5277	130.5006

Table 12 continued on next page

**Table 12** (*continued*)

Filename	Range	Phase	Sub-S/C	Sub-S/C	Sub-Solar	Sub-Solar	$A_{\text{eff}}$	$A_{\text{eff}}$	$A_{\text{phys}}$	$a_{\text{pred}}$	$a_{\text{pred}}$	$a_{\text{pred}}$
	(km)	(deg)	Latitude	Longitude	Latitude	Longitude	Value	Error		k=1	k=0.75	k=0.50
			(deg)	(deg)	(deg)	(deg)	(km <sup>2</sup> )					
N1835728159	2391251.0	60.1	20.4	77.9	25.9	12.1	119.18430	0.05255	511.4440	189.6820	200.6236	218.7485
N1835820000	2221651.8	68.8	20.6	290.5	25.9	214.8	118.84238	0.01269	503.3264	203.1614	210.8329	225.2190
N1839312143	3179810.8	78.3	23.5	89.5	26.1	1.4	82.48747	0.02696	520.3099	143.1562	153.1970	170.9523
N1839519134	3071503.0	76.6	27.4	186.0	26.1	98.2	86.30243	0.02398	422.0842	142.6924	139.0724	141.3879
N1839950196	3496919.2	61.9	26.0	39.4	26.1	329.5	94.19481	0.02718	464.0839	149.3624	153.2610	163.4279
N1840145807	3055901.8	53.2	29.0	101.7	26.1	41.1	164.81406	0.00232	525.2321	258.9710	268.1838	283.0370
N1840467099	2645384.0	39.8	28.1	75.1	26.1	30.2	205.29742	0.00934	521.9205	266.7880	277.7308	293.2663
N1842364471	3493286.5	68.4	31.9	337.0	26.2	257.2	114.74281	0.01426	458.4042	205.5327	202.6559	205.9363
N1842536142	3504514.8	61.7	32.7	347.9	26.2	276.1	120.17165	0.01354	450.6790	206.2648	202.3371	204.4666
N1843369038	2373853.8	25.1	28.1	342.3	26.2	314.1	245.29195	0.01058	437.0358	258.7452	255.0612	253.6749
N1843453308	1651845.0	13.0	33.3	152.6	26.2	140.1	301.06851	0.00436	466.9107	284.4768	285.1140	286.6764
N1845330130	2348358.8	33.4	36.3	359.3	26.3	321.7	212.42972	0.01224	462.4044	240.1777	241.7120	247.1292
N1846758069	2714067.0	78.0	35.8	326.8	26.3	232.8	101.21885	0.01672	486.3921	191.8174	194.4236	203.6272
N1846930816	2761986.8	67.5	38.0	335.0	26.3	254.0	117.92370	0.00665	484.6873	218.0057	217.5734	223.5897
N1848934583	1684486.6	38.3	43.4	38.3	26.4	355.7	194.80782	0.00652	518.9847	238.6373	251.3600	269.4138

**Table 13.** Brightness estimates from clear-filter images of Calypso.

Filename	Range	Phase	Sub-S/C	Sub-S/C	Sub-Solar	Sub-Solar	$A_{\text{eff}}$	$A_{\text{eff}}$	$A_{\text{phys}}$	$a_{\text{pred}}$	$a_{\text{pred}}$	$a_{\text{pred}}$
	(km)	(deg)	Latitude	Longitude	Latitude	Longitude	Value	Error		k=1	k=0.75	k=0.50
			(deg)	(deg)	(deg)	(deg)	(km <sup>2</sup> )					
N1495209871	890860.8	16.6	-26.6	140.6	-21.7	123.2	215.58528	0.00317	286.1855	174.0992	172.8976	172.3568
N1495306082	744442.8	8.1	-13.8	337.8	-21.6	335.5	175.25667	0.00123	226.2691	127.2145	124.7317	122.5648
N1511290086	2690833.8	65.2	-0.4	36.6	-19.6	332.9	17.58906	0.08132	232.8271	49.1007	49.7600	52.9677
N1513526081	2894673.2	79.3	-0.2	306.3	-19.3	227.6	74.90391	0.00928	263.6748	94.7175	95.4810	99.6274
N1513746037	2373977.8	60.5	-0.4	51.7	-19.3	353.0	46.70824	0.01034	260.2657	63.1165	66.3753	72.8773
N1515907721	1464391.1	60.9	-0.2	142.6	-19.0	83.5	83.69676	0.00505	233.0732	113.9775	108.6222	106.2716
N1552346494	1321233.1	61.8	27.5	159.6	-13.4	207.5	37.35155	0.00874	268.3173	44.9510	47.2656	52.3660
N1553898744	2159565.5	64.2	27.7	341.8	-13.1	33.1	26.20873	0.02650	268.3491	44.8040	46.7589	51.4545
N1555145582	1602579.5	48.5	20.1	228.9	-12.9	265.0	128.16917	0.00516	281.0121	125.2374	124.5597	127.3711
N1555190012	2097829.5	50.7	18.5	322.5	-12.9	2.9	39.47476	0.01584	260.9357	60.1786	64.1787	71.3580
N1555274343	1812271.9	69.0	27.1	131.1	-12.9	189.1	31.87351	0.01509	299.3892	42.9117	47.2454	54.9205
N1555664915	1918925.6	79.3	40.0	267.1	-12.8	331.1	51.07096	0.01515	357.6467	65.9734	73.7674	86.7310
N1556521366	2124381.2	50.5	11.7	16.7	-12.7	61.2	87.37073	0.01306	214.2203	85.7543	82.0514	81.1018
N1556568311	1816584.5	59.6	16.0	112.1	-12.7	164.9	62.80946	0.00839	296.6408	75.6986	82.6768	93.8821
N1556714997	2215423.5	66.7	19.2	69.2	-12.7	128.7	81.70742	0.02135	304.0080	106.9473	111.4394	120.0853
N1557011323	2360458.2	73.8	24.8	357.4	-12.6	62.6	37.76826	0.02989	249.1161	49.0864	48.7027	50.9821
N1558292301	2439352.2	58.5	15.1	317.7	-12.4	9.8	29.54416	0.03834	260.6194	52.2587	55.7865	62.3853
N1558330642	2453930.0	68.4	15.4	31.4	-12.4	94.5	84.06678	0.02181	243.6646	91.1192	88.2564	88.6631
N1558376152	1995388.1	73.5	19.3	127.7	-12.4	195.0	28.37722	0.01927	283.8266	38.2415	41.6240	47.9221
N1558417507	1944583.8	64.3	20.3	229.9	-12.4	286.3	99.63658	0.01160	282.8874	109.8669	110.2467	114.3704
N1558475948	2330584.0	69.9	17.3	351.1	-12.4	55.1	28.24998	0.02038	223.6661	46.0808	45.2069	46.7252
N1559410109	2172015.2	42.6	7.1	278.8	-12.2	317.0	142.45853	0.00861	296.3020	133.2359	139.0636	147.9507
N1559467709	2455537.0	55.5	7.1	31.7	-12.2	84.1	111.10362	0.01622	228.2931	107.7024	102.6843	100.5764
N1559514269	2044787.6	59.3	8.9	131.1	-12.2	186.9	47.28204	0.01470	259.9281	55.3777	59.3984	66.6149
N1559627445	2550783.5	60.1	8.5	19.9	-12.2	76.6	83.04800	0.01898	211.6786	86.4458	81.6622	79.8166
N1559710245	1983506.0	58.6	11.5	205.5	-12.2	259.5	78.59654	0.01269	224.0959	93.8710	89.5297	88.1963
N1559841331	1953362.6	73.4	12.4	119.1	-12.1	188.8	33.53320	0.01340	282.8366	43.7245	47.8704	55.2652
N1559928227	2162493.0	64.9	11.6	319.7	-12.1	20.5	21.61255	0.02107	250.3355	43.8564	46.1218	51.0418

Table 13 continued on next page

**Table 13** (*continued*)

Filename	Range	Phase	Sub-S/C	Sub-S/C	Sub-Solar	Sub-Solar	$A_{\text{eff}}$	$A_{\text{eff}}$	$A_{\text{phys}}$	$a_{\text{pred}}$	$a_{\text{pred}}$	$a_{\text{pred}}$
	(km)	(deg)	Latitude	Longitude	Latitude	Longitude	Value	Error		k=1	k=0.75	k=0.50
			(deg)	(deg)	(deg)	(deg)	(km <sup>2</sup> )					
N1560792667	2222075.8	54.3	0.7	75.3	-12.0	128.5	118.75926	0.01453	290.2368	135.0753	138.8638	145.6301
N1561200490	2070487.9	54.2	1.4	255.7	-11.9	308.6	133.42230	0.01501	290.2240	134.7319	138.5987	145.4686
N1561223620	2283223.2	56.1	1.4	304.7	-11.9	359.6	45.43766	0.02388	266.3030	68.8923	74.1325	82.8675
N1561348151	1624854.8	63.3	1.7	212.3	-11.9	274.6	86.30444	0.00852	223.6208	104.3188	99.1893	96.9795
N1562041275	2274783.8	39.2	0.2	326.6	-11.8	4.3	54.05247	0.01957	226.8024	75.3125	77.9847	83.0341
N1563933057	1555692.1	12.0	-0.2	215.6	-11.4	219.8	193.53433	0.00412	229.5669	126.2845	124.7330	123.8108
N1564455060	3290650.0	28.7	0.2	265.4	-11.4	291.9	214.40285	0.01994	295.00005	173.4810	175.0044	177.9725
N1567918252	3498571.8	29.9	-3.5	346.2	-10.8	15.5	72.21117	0.06698	197.7470	79.8365	79.7157	81.1813
N1567945807	3467532.8	35.1	-3.7	41.7	-10.8	76.3	168.41463	0.02815	243.4125	144.2670	138.9589	135.3353
N1571562766	2053392.9	65.8	4.0	74.7	-10.1	139.2	84.32400	0.01663	290.5911	109.9527	115.4586	124.6244
N1573672081	2054265.9	65.9	3.9	49.5	-9.8	114.3	100.23022	0.01399	257.6729	115.2269	114.0575	115.8784
N1574755269	2507745.0	24.3	5.8	325.9	-9.6	344.8	106.29633	0.01654	231.0265	96.2268	99.0816	103.5777
N1575013831	1626026.8	41.5	9.3	158.4	-9.5	195.5	67.85991	0.00766	213.9213	63.6261	65.1083	68.8926
N1575675720	1561748.8	16.5	7.1	217.2	-9.4	216.2	172.01657	0.00781	236.7784	118.5833	119.0319	120.6330
N1575756916	2257082.8	20.8	7.4	23.0	-9.4	35.3	143.20299	0.00918	214.3405	104.4876	102.9543	102.7325
N1575800176	1939662.1	26.5	9.6	112.2	-9.4	130.8	174.94144	0.00739	287.7252	146.6231	150.6472	156.6880
N1575961877	2157357.8	32.9	12.3	102.7	-9.4	127.6	165.52187	0.01168	299.0423	147.7167	152.5755	160.0216
N1577214236	2364121.2	26.6	14.3	358.6	-9.1	11.3	74.99866	0.01705	211.7020	76.8524	78.1901	81.3845
N1577456923	1938431.9	43.1	25.7	160.7	-9.1	187.0	60.53453	0.01854	260.2091	63.3658	67.7465	75.2573
N1578546350	1946025.8	29.6	16.3	55.2	-8.9	70.9	178.95003	0.00759	282.5652	148.1217	148.1072	150.5487
N1579305656	1453987.1	20.1	0.9	324.3	-8.8	306.6	178.86302	0.00447	231.2740	132.9125	129.3184	126.6930
N1579399811	1261748.0	18.7	9.7	151.4	-8.8	154.3	141.90799	0.00386	225.6590	101.6938	102.9144	105.4921
N1579490607	1991357.0	20.6	11.8	353.2	-8.8	354.7	87.38792	0.01164	206.2777	81.7506	82.9517	85.6128
N1579654213	2088430.8	28.4	18.4	347.1	-8.7	355.7	71.85966	0.00857	230.1162	76.9045	79.9138	85.1638
N1580479759	1914862.0	18.7	9.9	14.7	-8.6	17.4	109.98628	0.00694	208.0965	89.6664	90.2054	92.0252
N1580566805	1511818.4	27.0	18.4	209.9	-8.6	209.6	122.57142	0.00672	248.3243	98.1550	100.9036	105.9550
N1580652185	2066545.5	28.9	17.3	24.9	-8.5	37.9	119.77299	0.01115	239.6160	99.8625	100.5340	103.4265
N1581600807	2015579.8	22.3	13.9	331.6	-8.4	331.2	123.06594	0.01194	235.4691	101.4656	103.0852	106.4719
N1582769275	1832420.1	36.0	25.2	15.6	-8.2	29.4	82.06274	0.00948	256.7000	83.3340	86.3721	92.3071
N1584357436	1672003.0	23.3	11.3	307.1	-7.9	293.9	200.36845	0.00645	270.6229	151.3246	150.3446	151.0569
N1584374886	1809900.9	20.9	11.8	339.5	-7.9	332.3	114.24538	0.00401	219.1190	96.9571	97.2781	99.0759
N1586106989	1177283.2	28.0	18.3	205.0	-7.6	194.2	97.29561	0.00294	241.2699	85.2603	89.0941	95.2527
N1586192729	1735432.9	27.6	19.8	20.0	-7.6	23.4	97.18635	0.00571	241.4554	89.0358	91.8384	96.9362
N1586251605	1241250.5	42.8	34.0	142.5	-7.6	153.3	86.32487	0.00408	308.4870	88.4394	95.9272	107.6777
N1586903704	1134827.2	22.0	14.5	154.5	-7.4	152.1	132.86641	0.00405	231.1806	98.6937	100.2313	103.4781
N1587820481	1742903.6	25.1	17.8	14.8	-7.3	14.9	87.61818	0.00367	229.6145	84.3905	87.0642	91.7539
N1588451505	1464852.5	19.7	-0.3	345.8	-7.2	327.3	122.05051	0.00483	196.8704	100.4171	97.8136	96.1176
N1588711657	1207959.5	40.5	33.3	181.1	-7.1	181.2	66.93749	0.00562	283.3141	68.9886	75.2202	85.1115
N1591877410	1454391.4	21.1	-1.4	346.8	-6.6	326.2	118.36034	0.00445	196.0068	99.7327	96.9828	95.2024
N1596293621	1471073.6	24.4	15.0	3.1	-5.8	350.1	73.84960	0.00982	213.9322	79.7885	81.6885	85.3045
N1597416574	1417368.2	27.0	-3.1	334.9	-5.6	307.9	138.42833	0.00265	213.1046	117.8256	113.3444	110.1459
N1597580945	1409743.1	30.7	17.0	331.7	-5.5	310.6	127.76479	0.00108	243.1682	111.6233	110.9400	112.4370
N1601199015	1330577.2	16.7	-8.8	30.2	-4.9	13.8	147.07910	0.00225	228.0644	103.1925	106.2978	110.1929
N1602576855	935124.3	27.7	7.9	198.8	-4.7	174.1	97.47256	0.00124	207.6467	77.5014	79.4615	83.0771
N1602670786	1395905.2	22.7	16.5	29.9	-4.6	21.4	121.13968	0.00211	244.1276	99.1327	102.8873	108.5084
N1603215014	937380.2	19.9	8.7	157.0	-4.5	142.2	145.28311	0.00116	214.8727	107.3859	105.8515	105.4352
N1603880509	926099.6	29.9	15.6	193.1	-4.4	170.7	93.87047	0.00129	219.9086	75.2951	77.9073	82.5502
N1604535429	1003881.0	31.6	19.0	197.6	-4.3	175.9	89.62401	0.00188	234.8824	75.6794	79.5716	85.8416
N1604965932	807536.4	29.0	-30.8	58.2	-4.2	45.9	173.61394	0.00146	320.5685	146.7854	155.1022	166.4238
N1605195123	1043318.4	33.0	13.8	219.5	-4.2	191.7	88.57489	0.00195	251.9867	89.3379	94.9402	103.0797
N1607850782	1414892.0	33.8	-2.8	325.9	-3.7	292.1	152.48941	0.00113	228.7918	131.2987	126.0431	122.4082
N1609330528	1464121.0	32.6	-9.0	350.0	-3.4	317.7	89.50838	0.00141	202.0770	94.8542	91.9838	90.8082
N1610316936	1402164.5	27.7	17.2	353.4	-3.3	334.5	88.40804	0.00196	222.0422	86.3975	87.6274	90.7394
N1611120432	1399566.1	30.9	13.5	334.0	-3.1	307.8	129.74280	0.00012	230.8181	113.1981	110.9280	110.5582
N1630270023	1723062.2	71.6	10.1	21.3	0.3	92.7	76.89257	0.00576	216.5256	83.8882	79.6209	78.2999

Table 13 continued on next page

**Table 13** (*continued*)

Filename	Range	Phase	Sub-S/C	Sub-S/C	Sub-Solar	Sub-Solar	$A_{\text{eff}}$	$A_{\text{eff}}$	$A_{\text{phys}}$	$a_{\text{pred}}$	$a_{\text{pred}}$	$a_{\text{pred}}$
	(km)	(deg)	Latitude	Longitude	Latitude	Longitude	Value	Error		k=1	k=0.75	k=0.50
			(deg)	(deg)	(deg)	(deg)	(km <sup>2</sup> )					
N1632482868	1771666.6	72.6	12.5	224.3	0.7	296.6	83.94632	0.01150	257.5734	104.5753	104.2272	106.9986
N1647979569	1067318.6	64.8	0.0	228.3	3.4	293.1	104.45621	0.00143	253.4014	118.1615	116.7473	118.1136
N1649610140	1488499.6	67.9	0.1	223.0	3.7	290.9	90.52240	0.00022	243.5828	110.2340	107.8992	108.4032
N1666418840	2114878.2	77.4	-1.6	222.3	6.6	299.5	68.40034	0.00576	242.4543	94.5422	93.3803	95.2189
N1684260314	2809382.5	39.2	0.3	37.7	9.5	76.0	145.15578	0.01633	234.9170	133.7102	128.1673	124.6262
N1689830629	2744047.5	47.6	0.2	83.7	10.4	130.5	128.62248	0.00301	294.6870	142.1605	147.0683	154.6660
N1690349333	2189119.2	63.5	0.2	132.2	10.5	195.3	45.64143	0.01405	252.3329	50.4124	53.6863	59.9262
N1690636494	1852636.5	79.8	0.4	29.4	10.5	109.2	65.18357	0.00370	219.6082	82.6150	79.0285	78.3779
N1694062336	2679050.5	60.5	0.3	50.0	11.1	110.0	106.12705	0.01017	257.4239	125.6748	123.6141	124.3226
N1694253557	2026909.4	71.5	0.2	100.9	11.1	172.0	47.35077	0.01896	292.3951	67.3809	74.3253	85.4716
N1695099983	1877283.4	35.5	0.0	206.0	11.2	240.0	118.54104	0.00686	212.2605	115.1282	109.5458	105.8848
N1697960201	1782619.6	32.7	0.3	41.2	11.7	72.1	168.23708	0.00350	241.4933	141.7162	136.5779	133.1342
N1701608764	2179294.2	53.8	0.0	150.6	12.2	203.4	49.97982	0.00696	218.1942	55.3874	56.3980	59.8745
N1703079193	2476583.5	52.0	-0.6	157.3	12.4	208.1	54.78057	0.01648	206.7803	56.6186	56.6296	58.9774
N1710536340	2423008.2	57.8	0.2	45.4	13.6	102.2	111.84757	0.00481	249.1733	126.0379	122.2859	121.2905
N1710889383	2400657.2	72.0	0.2	89.6	13.6	161.2	51.79247	0.01752	295.5714	81.2533	88.3453	99.6970
N1712589853	2152300.2	64.1	0.6	249.6	13.9	313.0	106.43626	0.00980	284.5899	119.2261	122.8637	129.8476
N1713881422	2224220.5	56.8	0.5	226.9	14.0	282.8	112.81591	0.00287	250.8626	128.6518	125.0629	124.2021
N1716436358	1440598.6	48.1	-2.9	114.9	14.4	160.1	88.14597	0.00107	279.9382	98.2535	104.6812	114.5962
N1716809440	1992483.0	55.1	-8.3	212.7	14.5	263.2	88.26826	0.00986	230.3112	107.3262	102.4854	100.6213
N1716982721	2023016.5	60.4	-9.9	229.9	14.5	285.6	108.23836	0.00703	262.8272	119.0178	117.2363	118.6905
N1717966847	2030071.5	45.8	-8.2	257.0	14.6	297.0	152.60495	0.00230	294.5377	146.4212	148.6198	153.8322
N1718126628	2322127.0	55.3	-11.2	240.2	14.7	289.5	124.02041	0.00669	280.2693	130.1247	130.1307	133.4493
N1718469231	2821395.5	67.1	-14.3	264.3	14.7	325.5	84.63593	0.00679	304.7908	94.8876	101.2325	111.9092
N1727789451	2589291.2	63.7	-22.6	319.9	16.0	11.6	15.00955	0.02907	276.2160	44.8385	48.0126	54.1721
N1733156185	1805955.5	55.2	-26.9	300.6	16.7	335.3	74.67876	0.00301	311.6341	79.0239	85.2789	95.9059
N173322026	1745741.2	71.0	-38.5	293.7	16.7	341.3	46.79972	0.00754	347.1267	57.8566	64.5004	75.7645
N1735139378	1411209.6	22.6	3.9	13.4	17.0	32.2	123.69183	0.00634	197.6900	102.8981	99.0187	96.3939
N1737787314	1823197.5	72.0	-30.2	60.2	17.3	116.5	66.21950	0.00143	320.7208	93.7942	97.1985	105.1094
N1741129101	1436896.9	67.1	-41.4	258.1	17.8	292.3	85.91299	0.00067	359.2470	97.9683	103.6217	114.6169
N1741891700	1101362.4	42.0	-12.1	145.7	17.9	175.4	83.43786	0.00187	239.8496	70.7975	73.3003	78.5773
N1745006580	1049408.5	76.8	-47.9	166.7	18.2	210.5	29.98110	0.00127	344.5522	36.2588	39.6591	46.1399
N1745472883	793326.6	16.2	18.1	142.6	18.3	159.7	167.30605	0.00086	258.7120	131.3118	134.3433	138.0744
N1747435036	1164998.2	69.5	-36.4	125.3	18.5	170.5	39.03998	0.00065	332.2612	49.1028	54.4096	63.6645
N1750033022	903289.5	17.3	15.1	126.8	18.9	144.4	199.35818	0.00130	276.6178	151.6248	154.4991	158.1070
N1750354874	1412976.4	78.5	-38.9	77.8	18.9	134.8	45.06311	0.00428	353.2713	73.8887	79.7655	90.5257
N1751140569	1425618.6	31.6	-2.6	45.4	19.0	68.8	169.26070	0.00069	249.7005	141.5450	136.9758	134.5372
N1755867479	1833638.1	77.3	-37.3	5.1	19.5	60.9	32.88967	0.00171	301.6254	47.3399	48.5368	52.7243
N1760112116	1329938.5	59.6	59.2	131.7	20.0	67.9	121.87257	0.00137	391.8657	170.6210	181.5091	198.0723
N1764308883	1777440.9	42.7	37.7	14.0	20.5	328.6	83.19444	0.00059	306.1795	121.7262	127.2218	136.1775
N1769730667	1854403.0	39.3	44.9	89.6	21.1	51.5	184.12152	0.00383	369.2750	191.4184	202.7398	217.3591
N1772109072	2815264.8	72.9	43.8	345.8	21.3	259.4	70.82700	0.00497	330.5321	130.3083	132.9295	140.0960
N1772256053	2520101.0	67.0	44.6	301.9	21.3	223.6	90.38284	0.00533	358.7227	151.3893	161.4975	176.2943
N1777327826	3664160.5	77.9	37.8	345.4	21.8	254.0	65.82609	0.00996	306.9759	118.4645	119.2051	124.0575
N1777843629	3355839.5	57.3	35.4	16.7	21.9	312.1	49.79362	0.00894	298.1214	107.8916	110.2312	116.3925
N1782847471	3001098.2	75.2	45.6	284.5	22.4	193.1	54.21432	0.00670	368.7462	123.0847	136.6117	156.0842
N1783954578	1651646.4	11.4	11.7	119.7	22.5	115.9	258.60895	0.00314	281.1577	180.9764	178.4352	176.4726
N1786609325	1854478.9	21.9	12.3	234.3	22.7	214.1	171.68404	0.00515	273.5347	148.0670	149.9153	153.0174
N1786783386	1490993.1	29.5	-5.7	246.3	22.7	238.2	175.16220	0.00504	282.7109	148.2388	148.2035	150.8454
N1791952359	2339016.0	59.2	41.0	193.7	23.2	125.1	82.19664	0.01060	318.1353	119.1538	122.2638	129.6144
N1795595382	4039557.5	73.4	30.1	329.0	23.5	245.2	85.62851	0.01581	289.6335	128.9757	128.3810	131.2812
N1796025415	2797284.8	58.0	32.2	180.0	23.5	114.2	86.23233	0.01013	278.2598	118.0333	116.4613	118.3678
N1796434437	2110568.0	40.5	16.4	339.6	23.5	297.0	126.38712	0.00139	231.1839	130.0094	123.2915	118.8104
N1796513108	1348395.0	21.3	16.5	132.0	23.5	110.5	218.92651	0.00202	271.4470	176.1468	171.3437	167.3768
N1798932903	2356928.5	78.1	31.5	141.6	23.7	51.2	72.10830	0.00050	300.9473	125.8651	127.9507	133.6940

Table 13 continued on next page

**Table 13** (*continued*)

Filename	Range	Phase	Sub-S/C	Sub-S/C	Sub-Solar	Sub-Solar	$A_{\text{eff}}$	$A_{\text{eff}}$	$A_{\text{phys}}$	$a_{\text{pred}}$	$a_{\text{pred}}$	$a_{\text{pred}}$
	(km)	(deg)	Latitude	Longitude	Latitude	Longitude	Value	Error		k=1	k=0.75	k=0.50
			(deg)	(deg)	(deg)	(deg)	(km <sup>2</sup> )					
N1799229635	1852877.1	56.8	23.3	48.8	23.8	346.2	59.18151	0.00361	289.9250	93.5452	98.2854	106.8077
N1816568996	612503.9	62.4	0.3	154.5	25.0	95.1	75.00108	0.00059	211.3343	97.3088	90.5299	86.9250
N1824545837	1085132.5	78.6	0.0	134.8	25.4	57.5	66.63097	0.00190	247.6681	95.0705	92.8115	93.8922
N1832537008	1480733.0	79.8	3.9	129.9	25.8	49.4	70.76275	0.00547	257.5965	97.8830	96.9491	99.4044
N1835727429	2575205.5	71.1	18.8	326.2	25.9	248.6	88.30817	0.02199	256.3730	122.6206	118.4664	117.4695
N1835820550	1885840.5	58.0	24.4	158.8	25.9	94.1	93.73144	0.00324	257.4987	133.5177	127.9551	125.4256
N1839519974	3468544.5	73.2	24.3	59.0	26.1	336.6	38.44019	0.04124	304.6511	79.1399	83.3084	91.6059
N1840147077	3377924.5	60.1	26.1	348.1	26.1	280.2	84.19775	0.01728	257.8621	123.8456	118.9510	117.3135
N1842362961	3051376.2	67.5	37.0	210.1	26.2	129.6	65.76057	0.02123	312.6518	103.0653	105.6899	112.6023
N1843103726	2966931.2	37.8	32.1	7.2	26.2	324.1	97.77728	0.02733	280.3792	132.2723	133.0215	136.3068
N1843452758	2116282.5	11.4	25.7	27.0	26.2	14.3	184.51326	0.01021	269.6994	147.7486	149.2011	151.0388
N1844970788	2315158.0	58.5	47.2	195.0	26.3	124.0	89.61644	0.00757	342.7249	136.3929	141.2199	150.7364
N1845143259	2190019.0	50.1	47.7	203.2	26.3	144.5	90.12336	0.00871	347.3875	140.1627	148.1839	160.7592
N1846757039	2303697.2	73.7	43.2	197.6	26.3	105.6	67.04183	0.00675	328.5642	115.4755	117.5044	124.1893
N1846929666	2360000.2	65.9	45.7	208.1	26.3	126.6	71.43553	0.01573	342.8134	120.7272	125.6640	135.5284
N1847237932	2207370.0	41.5	46.5	133.0	26.3	86.8	168.07338	0.00622	356.8108	200.8280	205.2153	212.6835
N1847381933	2191578.0	28.4	40.4	74.4	26.3	44.6	213.31459	0.00868	355.7267	201.4902	210.6357	221.5562
N1849018624	1373661.4	22.3	44.6	72.5	26.4	56.4	244.80183	0.00234	365.3816	216.2545	224.7267	234.8414
N1849966230	1463313.4	68.7	44.9	73.0	26.4	347.5	62.75907	0.00208	366.2650	120.6390	132.1339	149.4668

**Table 14.** Brightness estimates from clear-filter images of Helene.

Filename	Range	Phase	Sub-S/C	Sub-S/C	Sub-Solar	Sub-Solar	$A_{\text{eff}}$	$A_{\text{eff}}$	$A_{\text{phys}}$	$a_{\text{pred}}$	$a_{\text{pred}}$	$a_{\text{pred}}$
	(km)	(deg)	Latitude	Longitude	Latitude	Longitude	Value	Error		k=1	k=0.75	k=0.50
			(deg)	(deg)	(deg)	(deg)	(km <sup>2</sup> )					
N1495206161	1294705.5	42.7	-18.2	304.9	-21.7	259.4	396.51160	0.00187	967.6930	517.9379	516.7247	523.9229
N1495311312	759950.5	37.1	-11.6	23.3	-21.6	60.7	441.52603	0.00102	875.4782	473.1956	464.6283	463.5204
N1518953101	2748696.2	79.6	-0.2	105.4	-18.5	26.3	112.52875	0.00832	936.0639	252.2294	259.4079	278.8613
N1551142776	1958827.1	79.7	37.5	358.6	-13.6	64.0	131.82022	0.00863	1073.9272	202.1025	211.6382	233.8763
N1552435415	1408418.5	71.1	39.7	182.1	-13.4	233.0	156.52940	0.00212	1089.9978	236.4063	248.8237	275.2325
N1552559550	2128087.8	76.1	34.2	359.5	-13.4	62.1	153.74387	0.00710	1041.6052	216.2016	225.0033	246.5506
N1553980614	2283324.2	73.3	30.3	5.3	-13.1	66.7	174.85187	0.01106	1003.6191	232.7841	239.9312	259.7333
N1555144412	2156979.0	50.5	14.9	356.3	-12.9	38.9	316.47403	0.01079	875.6731	318.9241	321.5581	335.0835
N1555273968	1665478.9	64.1	29.9	187.0	-12.9	236.5	193.77692	0.00647	994.6682	268.8191	276.9818	298.2223
N1555401574	2415179.8	70.1	25.4	10.8	-12.9	71.1	192.75861	0.00907	960.7724	252.7399	257.6930	275.0952
N1556545051	2219317.0	45.2	12.1	333.7	-12.7	11.8	340.58374	0.00476	882.4210	337.5416	343.4905	359.8299
N1556569001	2307571.0	51.5	12.7	3.5	-12.7	48.7	316.04825	0.00779	862.8815	325.3941	325.8289	337.0183
N1556952478	1866877.1	69.0	30.8	216.6	-12.6	272.4	150.78854	0.00571	1030.1263	288.1357	296.9921	319.8018
N1557011713	2268143.0	66.8	25.6	306.1	-12.6	2.4	162.30626	0.01023	1016.3857	247.6260	261.1973	288.2414
N1557986015	2425273.5	49.8	9.0	1.4	-12.4	46.7	324.66608	0.01284	844.9227	333.6497	332.8806	342.3620
N1558206261	2562325.5	55.2	13.0	332.3	-12.4	21.7	269.83435	0.01769	889.4637	290.5526	296.4654	313.6449
N1558476233	2405448.5	72.0	16.5	6.8	-12.4	73.6	191.58578	0.01046	887.8761	242.2543	243.3533	255.8533
N1559173272	1960418.1	40.3	2.6	17.0	-12.2	54.7	395.02835	0.00430	838.8480	403.6191	399.0562	402.8810
N1559365678	2305052.2	40.3	5.8	310.7	-12.2	347.0	369.34073	0.00773	904.3394	391.6766	399.6628	417.0681
N1559514584	1889372.9	57.3	9.9	161.7	-12.2	214.9	252.79872	0.01056	853.8653	281.0759	283.6821	297.1134
N1559671140	2572193.2	64.1	8.7	32.4	-12.2	93.4	227.86804	0.01322	878.6083	319.5333	318.2630	328.4988
N1559886572	2401420.0	67.4	10.2	357.0	-12.1	60.9	222.57225	0.01090	850.3652	253.6271	253.5106	264.3657
N1561089249	2581302.8	62.1	1.0	31.4	-11.9	92.6	238.32806	0.01118	861.0454	337.2661	334.2683	342.3338
N1561117509	2353191.5	67.2	1.2	69.6	-11.9	136.0	222.93089	0.01282	932.7590	325.7448	333.1288	352.7357

*Table 14 continued on next page*

**Table 14 (continued)**

Filename	Range	Phase	Sub-S/C	Sub-S/C	Sub-Solar	Sub-Solar	$A_{\text{eff}}$	$A_{\text{eff}}$	$A_{\text{phys}}$	$a_{\text{pred}}$	$a_{\text{pred}}$	$a_{\text{pred}}$
	(km)	(deg)	Latitude	Longitude	Latitude	Longitude	Value	Error		k=1	k=0.75	k=0.50
			(deg)	(deg)	(deg)	(deg)	(km <sup>2</sup> )					
N1561200190	1811109.2	57.5	1.6	204.5	-11.9	260.8	248.09805	0.00453	842.3796	347.0933	342.7486	348.9815
N1561285390	2342509.0	60.0	1.2	331.4	-11.9	30.3	250.19084	0.08687	855.8781	278.9850	282.1362	296.0902
N1561347671	2098805.5	76.5	1.4	50.5	-11.9	126.4	150.99098	0.01828	900.5274	275.5203	279.1347	294.5289
N1561414016	1356047.9	78.2	2.1	149.4	-11.9	226.8	152.62238	0.00270	854.1989	190.8567	192.9834	205.1608
N1564497886	3080985.5	31.2	0.2	212.3	-11.3	241.4	465.98166	0.01521	856.5229	464.3621	458.7878	459.3194
N1571562946	1736556.0	66.3	5.0	129.0	-10.1	193.8	203.92458	0.00601	901.6169	249.6471	257.9624	277.9005
N1575914177	2488505.5	21.4	9.9	322.1	-9.4	331.5	525.98230	0.00668	893.8436	461.8132	466.4456	476.4771
N1575961562	2574319.0	28.9	10.4	22.8	-9.4	44.0	496.04745	0.00842	869.1016	437.9756	437.7117	444.2743
N1577009574	1300982.4	20.1	10.6	202.3	-9.2	199.1	529.40784	0.00222	862.8268	440.9673	444.4305	452.9818
N1577141005	2293137.0	25.1	11.7	23.9	-9.2	37.9	528.58759	0.00641	877.0230	445.3959	446.8535	454.6005
N1578545975	2160501.8	25.1	14.6	5.6	-8.9	14.4	516.29395	0.00551	874.7224	417.9103	422.9840	434.8341
N1579363901	1052422.2	18.0	8.0	186.4	-8.8	179.9	581.84210	0.00115	835.4179	434.3670	436.2368	442.2091
N1580567090	1444176.2	28.2	19.6	211.5	-8.6	209.4	444.43683	0.00143	930.8489	427.6823	437.1272	455.0531
N1581514076	1333423.6	23.8	13.9	218.0	-8.4	209.5	496.60602	0.00173	906.8398	450.6001	457.5530	470.9750
N1583400909	1121263.4	24.4	11.9	212.9	-8.1	198.8	497.03778	0.00153	887.0904	436.7301	443.4785	456.3821
N1583757662	1806759.0	38.9	27.6	3.6	-8.0	19.9	376.34769	0.00219	977.5132	371.2711	385.4135	411.2812
N1586080184	1705619.2	23.6	10.1	327.2	-7.6	311.5	514.71783	0.00176	884.8733	471.2603	471.3751	476.9484
N1587747235	1761800.1	22.3	11.1	339.1	-7.3	326.4	519.98242	0.00553	869.5925	450.6735	452.3500	459.3382
N1591997910	1579766.4	26.9	9.8	332.3	-6.5	310.8	486.62674	0.00134	874.2587	457.7090	457.1375	462.5024
N1597487899	1525445.8	13.8	5.2	31.1	-5.6	22.5	635.38409	0.00193	866.2375	476.3902	479.1696	484.4000
N1598768218	859075.4	28.0	10.8	195.4	-5.3	172.5	470.97433	0.00070	854.6850	407.4724	412.8254	424.5183
N1600750652	1498650.0	31.1	14.1	333.2	-5.0	308.5	446.05090	0.00172	893.7626	444.9729	446.7085	455.7498
N1602671176	1519618.0	24.2	15.2	6.1	-4.6	352.0	510.86896	0.00171	878.5617	424.3953	431.2123	444.1418
N1603720473	693668.0	28.8	-20.2	176.1	-4.5	151.3	538.52130	0.00052	907.0762	439.4939	447.0701	461.3525
N1604536389	1605851.5	29.2	11.8	336.8	-4.3	312.4	468.62271	0.00260	876.3060	446.2913	446.8938	453.9558
N1604967432	897195.8	64.9	-27.0	313.6	-4.2	249.7	242.62457	0.00118	1016.2253	362.4859	373.5974	398.2668
N1605246614	1607870.9	29.7	14.1	337.5	-4.2	313.9	462.21298	0.00230	887.7900	442.4802	444.6826	453.8120
N1607850437	1552298.6	29.3	-2.9	349.0	-3.7	319.7	484.26187	0.00283	832.8319	435.2847	432.9487	435.9515
N1618012426	1472040.4	49.0	-23.4	5.8	-1.9	320.3	341.66315	0.00144	940.3441	357.1938	366.4480	387.0603
N1632483168	2275855.0	72.0	9.8	323.7	0.7	35.5	176.14481	0.00344	890.3460	222.8717	228.7668	245.6552
N1636035774	1766098.5	73.5	0.4	328.6	1.3	42.1	173.52956	0.00270	860.9166	212.9737	216.7365	230.9419
N1649696361	1722643.0	71.7	0.3	229.7	3.7	301.4	173.33395	0.00179	893.9953	302.0786	306.0701	321.7315
N1660688499	1961869.8	75.1	-0.5	22.9	5.6	97.9	141.54219	0.02287	845.8147	261.8375	260.5449	270.1954
N1662535072	2258732.5	70.0	-1.1	317.0	5.9	26.7	179.99170	0.00566	885.0303	230.5957	236.8423	254.1596
N1671767515	1739798.2	56.6	0.0	344.6	7.5	40.8	274.86978	0.00215	835.3491	298.5072	299.7029	311.2268
N1675509739	2051975.4	63.4	0.3	278.1	8.1	341.3	212.41296	0.00580	942.9828	313.4964	325.6915	350.3798
N1682451063	3011469.2	73.3	0.3	42.8	9.2	115.9	157.82495	0.00391	884.3154	291.9289	293.6045	306.8139
N1684433115	2734119.8	36.9	0.2	220.5	9.5	256.4	410.49365	0.00295	874.1315	463.0967	458.4818	461.0135
N1685875044	3647537.2	64.8	0.4	228.1	9.8	292.5	204.10558	0.01876	890.5197	341.9791	343.3954	356.2104
N168860100	2336572.0	63.5	0.3	115.7	10.2	178.8	223.84819	0.00206	922.0167	285.6974	296.5164	319.4350
N1688601581	2327195.0	72.3	0.3	52.8	10.2	124.9	180.52028	0.00422	904.7711	300.9055	304.9022	320.7396
N1689641748	2365699.5	28.5	0.2	243.2	10.4	270.0	487.06366	0.01453	920.2180	523.9509	521.9274	525.1798
N1689831229	2383959.0	45.0	0.2	154.6	10.4	198.6	326.50797	0.00093	843.4966	346.4109	349.9259	362.7167
N1694062696	2417706.8	63.8	0.3	98.3	11.1	161.6	231.75577	0.00196	941.8748	311.6583	323.3450	347.4618
N1694254757	2432183.8	68.1	0.3	25.4	11.1	93.1	176.31598	0.00317	849.9486	301.6216	298.9103	307.3667
N1695098363	2118780.2	29.1	0.2	271.5	11.2	298.6	487.07919	0.00260	944.4158	520.4816	524.0893	533.4182
N1695301464	2049549.4	42.6	0.3	206.8	11.2	248.2	359.75320	0.00512	846.0081	416.5070	410.9694	413.8700
N1696388971	1549410.9	36.5	0.2	67.4	11.4	102.4	433.34335	0.00122	929.6314	496.1530	496.2551	503.6116
N1696921114	2133174.8	54.7	0.2	139.8	11.5	193.7	268.75980	0.00288	873.2916	307.1957	313.6575	330.9644
N1698201582	2432919.8	32.4	0.2	311.4	11.7	341.9	443.65018	0.00507	896.3166	437.4453	443.7981	457.1444
N1701609484	2538635.0	58.6	0.2	70.6	12.2	128.4	267.49387	0.00687	933.7238	379.1159	385.2230	402.7987
N1703079673	2406319.2	52.9	-0.5	154.9	12.4	206.6	259.07013	0.00160	842.9556	309.4790	312.0155	324.8663
N1703195774	3184902.5	49.8	-0.4	333.3	12.5	21.8	307.05615	0.00531	852.1712	328.6469	331.6847	344.7783
N1710208858	1035889.2	19.9	0.3	237.0	13.5	252.0	588.04303	0.00092	909.0258	537.2376	533.0588	532.6994
N1710347999	2017003.5	52.2	0.2	51.1	13.5	102.1	294.29483	0.00246	901.3614	411.9529	410.5717	419.4525

Table 14 continued on next page

**Table 14** (*continued*)

Filename	Range	Phase	Sub-S/C	Sub-S/C	Sub-Solar	Sub-Solar	$A_{\text{eff}}$	$A_{\text{eff}}$	$A_{\text{phys}}$	$a_{\text{pred}}$	$a_{\text{pred}}$	$a_{\text{pred}}$
	(km)	(deg)	Latitude	Longitude	Latitude	Longitude	Value	Error		k=1	k=0.75	k=0.50
			(deg)	(deg)	(deg)	(deg)	(km <sup>2</sup> )					
N1710890103	2126567.8	71.1	0.4	137.3	13.6	208.0	159.06314	0.00316	878.8105	227.4836	232.3284	248.2181
N1711207985	1896058.2	67.5	0.5	263.8	13.7	330.8	209.99460	0.00856	942.9764	311.9363	321.7185	344.0449
N1712587993	1922622.5	67.1	0.5	203.8	13.9	270.3	169.32951	0.00441	840.6546	304.9792	301.2415	308.6054
N1712869335	1528851.5	72.5	0.5	265.2	13.9	337.3	182.40956	0.00261	943.5058	279.1182	289.0846	311.6564
N1714311264	2075010.8	69.5	0.4	300.7	14.1	9.6	162.14114	0.00563	917.0049	251.3150	259.1657	278.9300
N1718123808	2844669.5	58.7	-9.2	352.7	14.7	46.8	246.91296	0.01412	847.4247	285.8237	285.7181	296.4889
N1718765873	2610437.8	76.4	-18.0	234.4	14.7	304.4	135.64430	0.00671	961.4229	261.4116	267.9160	287.0902
N1725788618	1836708.9	62.0	-15.6	130.2	15.7	184.3	246.00084	0.00413	939.3950	264.7848	274.1548	295.8246
N1727790051	2545278.2	61.2	-23.1	300.4	16.0	348.5	219.12448	0.00460	1006.0016	281.8504	294.8056	321.3884
N1733157625	1389524.5	65.5	-36.5	197.1	16.7	237.5	205.70659	0.00086	1064.0367	263.2197	274.0001	298.8550
N1733980170	1408948.0	24.7	5.8	25.5	16.8	48.1	525.58649	0.00143	857.3345	487.1190	480.0129	477.5479
N1735265498	1101272.4	45.0	-17.1	176.4	17.0	206.2	319.41815	0.00073	883.7277	328.4194	331.8739	346.1672
N1737787914	1980909.1	68.9	-27.4	31.7	17.3	85.8	175.49725	0.00313	999.1306	273.8503	279.4186	298.2211
N1738705500	1812969.2	40.4	-9.7	13.1	17.4	43.4	378.09326	0.00192	853.8370	378.9753	376.3766	383.3395
N1750034352	1465515.1	13.3	9.1	12.0	18.9	21.4	645.70758	0.00321	850.5880	499.3119	493.3980	489.5821
N1757882832	1729962.4	79.9	-34.3	33.0	19.8	94.9	118.44857	0.00438	1062.4910	219.8805	227.2520	247.4980
N1760114826	1693788.9	73.0	42.6	340.3	20.0	255.3	231.29866	0.00165	1130.2377	397.1366	412.9457	444.9672
N1760176977	1572322.0	41.3	40.4	31.5	20.0	349.3	412.05539	0.00185	1118.2714	506.4561	531.6719	568.8798
N1764312623	1362348.4	57.0	52.3	226.8	20.5	164.6	290.66397	0.00190	1229.7863	466.0094	501.1394	554.3657
N1766817359	1992176.9	63.8	52.5	90.7	20.8	17.0	234.79649	0.00209	1247.7673	463.0150	499.2106	554.3561
N1769463736	2113472.0	70.7	57.8	170.2	21.0	83.3	193.62801	0.00370	1258.4637	447.4030	474.6621	521.3593
N1769730267	1633003.1	50.2	53.6	179.6	21.1	128.9	333.19339	0.00164	1222.8599	521.7776	551.8433	598.2960
N1772110332	2491194.5	76.7	51.3	245.4	21.3	150.2	168.05469	0.00921	1232.4080	365.6164	393.5731	440.7462
N1783955598	1442318.1	14.2	13.1	176.5	22.5	165.3	689.67316	0.00275	857.9477	507.5548	500.8781	496.4251
N1795595562	4047452.0	75.0	30.2	315.2	23.5	229.4	201.92909	0.00479	1040.5631	375.7236	385.4683	409.3777
N1796026685	2851267.0	63.8	31.3	237.0	23.5	164.4	251.75717	0.00568	1061.5244	381.7466	397.5765	427.9364
N1796516408	1281433.1	38.5	16.6	230.4	23.6	189.9	433.31195	0.00194	946.1154	467.0157	472.5834	486.5791
N1799229935	1837922.2	53.2	23.6	58.9	23.8	0.3	311.50436	0.00354	1008.8786	423.7661	435.4211	459.2378
N1823333229	1469824.9	74.7	-0.4	64.9	25.3	352.0	166.46611	0.00225	925.9879	241.2473	245.5345	261.7837
N1832536798	1940767.5	79.3	2.7	43.0	25.8	323.6	119.10365	0.00263	886.1736	211.9690	212.6424	224.1174
N1835726939	2058892.6	70.5	24.0	215.4	25.9	136.4	198.76543	0.00174	970.5026	321.5685	325.7298	343.0531
N1835818870	2489487.2	64.7	18.3	347.9	25.9	277.8	242.48827	0.00478	903.1990	370.8875	365.5130	372.1534
N1839949316	3003841.5	60.7	30.7	150.4	26.1	80.5	292.95038	0.00682	1020.0542	460.3075	463.3163	478.8967
N1840145597	3165755.0	51.9	28.0	78.8	26.1	19.9	302.68246	0.00407	1058.3743	482.0661	496.2725	522.5649
N1840469439	2298233.2	49.0	32.9	207.7	26.1	151.2	351.46826	0.00625	1038.3135	467.5544	478.3155	500.9127
N1842534322	3110570.0	53.9	37.3	116.0	26.2	52.8	329.01239	0.00446	1118.7013	534.8895	550.7411	579.1905
N1843452568	2192910.5	11.3	24.6	22.3	26.2	9.9	708.43866	0.00628	963.1409	581.7944	582.0585	583.5315
N1845141379	2311559.2	38.8	44.7	100.4	26.3	57.6	468.59232	0.00988	1187.8579	635.9054	659.1654	692.5485
N1845328210	2401465.0	30.3	35.3	16.5	26.3	342.6	530.00415	0.00469	1057.6222	566.3369	578.7728	598.1917
N1846755259	2585467.5	66.0	37.6	71.6	26.3	352.7	241.93739	0.00993	1129.2595	418.5833	438.9892	475.3304
N1846931004	2826905.0	67.8	36.8	340.6	26.3	259.5	261.05359	0.01266	1074.4624	437.2476	445.3151	467.8445
N1847237652	2526746.2	38.6	39.4	49.9	26.3	6.1	436.74103	0.00176	1125.8260	564.4305	586.4680	618.5906
N1848933153	1471724.1	34.8	52.1	94.9	26.4	63.6	507.64670	0.00137	1244.1029	673.6230	703.2541	743.4528

**Table 15.** Brightness estimates from clear-filter images of Polydeuces.

Filename	Range	Phase	Sub-S/C	Sub-S/C	Sub-Solar	Sub-Solar	$A_{\text{eff}}$	$A_{\text{eff}}$	$A_{\text{phys}}$	$a_{\text{pred}}$	$a_{\text{pred}}$	$a_{\text{pred}}$
	(km)	(deg)	Latitude	Longitude	Latitude	Longitude	Value	Error		k=1	k=0.75	k=0.50
			(deg)	(deg)	(deg)	(deg)	(km <sup>2</sup> )					
N1495210661	786145.6	20.5	-30.4	160.4	-21.7	139.7	2.90468	0.00001	7.0605	4.2419	4.2603	4.3066
N1495210808	785039.1	20.5	-30.5	160.6	-21.7	139.9	2.91503	0.00050	7.0595	4.2381	4.2567	4.3035
N1495306772	654423.7	23.8	-15.1	314.0	-21.6	289.8	3.43378	0.00023	6.9841	4.3321	4.3030	4.3052
N1502650213	2702061.5	61.8	-13.0	352.9	-20.7	288.4	0.97387	0.00811	6.5699	2.6354	2.6208	2.6964
N1502795114	1786225.5	57.4	-19.8	206.2	-20.7	144.6	0.98527	0.00242	6.8046	2.6539	2.6866	2.8104
N1506004925	1776319.6	42.5	-0.3	24.1	-20.3	345.8	1.53273	0.00150	6.5743	3.0580	3.0755	3.1661
N1506764534	2079087.6	74.1	-0.3	130.9	-20.2	57.7	1.00535	0.00187	6.8619	2.3180	2.3419	2.4618
N1552385671	1995458.6	58.7	22.0	2.3	-13.4	50.1	1.07005	0.00245	6.7750	2.4551	2.4817	2.6011
N1552606368	2087051.8	75.1	37.9	328.4	-13.3	27.1	0.67719	0.00367	7.4350	1.7321	1.8083	1.9824
N1555091419	1332245.4	52.9	18.5	165.6	-12.9	208.8	0.99503	0.00121	6.6734	2.5446	2.5833	2.7098
N1555091462	1332261.4	52.9	18.5	165.7	-12.9	208.8	0.94004	0.01212	6.6730	2.5452	2.5838	2.7102
N1555190239	2157844.2	49.0	17.8	322.9	-12.9	1.6	1.33106	0.00567	6.9248	2.7767	2.8460	3.0035
N1558030777	2407675.0	46.3	10.3	322.7	-12.4	3.3	1.18414	0.00451	6.8025	2.8972	2.9558	3.0961
N1558417869	1797863.5	72.8	22.1	164.8	-12.4	230.3	0.54380	0.00386	6.7731	1.8176	1.8478	1.9676
N1559365245	1715561.5	47.0	7.9	188.3	-12.2	231.0	1.37511	0.00158	6.4435	2.9600	2.9504	3.0176
N1559513956	2528715.5	59.3	7.4	39.3	-12.2	95.6	1.36331	0.00166	6.7973	2.8733	2.8741	2.9650
N1559840928	1754254.5	68.9	14.0	170.1	-12.1	234.4	0.71377	0.00420	6.5474	2.0002	2.0138	2.1162
N1560621083	2066508.8	31.4	0.5	313.5	-12.0	342.5	2.08340	0.00199	6.8635	3.6089	3.6605	3.7648
N1561136876	2609882.8	57.2	1.1	348.8	-11.9	44.9	1.11829	0.00427	6.4677	2.4963	2.5045	2.5982
N1561178366	2469734.8	66.8	1.2	39.8	-11.9	105.8	1.12059	0.00516	6.7725	2.5903	2.5980	2.6984
N1561261497	1701628.9	65.9	1.6	169.1	-11.9	234.1	0.70072	0.00249	6.4122	2.1431	2.1467	2.2377
N1561261540	1701470.2	65.9	1.6	169.2	-11.9	234.1	0.61190	0.00611	6.4117	2.1441	2.1476	2.2385
N1561285092	1699752.4	59.5	1.6	212.9	-11.9	271.2	1.33068	0.00360	6.6346	2.8366	2.8266	2.9045
N1561364263	2158679.5	62.8	1.3	329.2	-11.9	31.0	0.86685	0.00205	6.6532	2.2224	2.2577	2.3825
N1561413718	2026736.1	77.3	1.4	26.9	-11.9	103.7	0.79491	0.00539	6.6073	2.0544	2.0569	2.1494
N1562860807	2936958.8	76.0	0.2	67.1	-11.6	142.7	1.29436	0.00908	7.1051	2.1852	2.2497	2.4131
N1563933494	2135249.2	12.2	0.0	333.1	-11.4	337.4	3.56572	0.00077	6.6057	3.9867	3.9886	4.0041
N1563933537	2135624.5	12.2	0.0	333.1	-11.4	337.4	2.89955	0.02893	6.6051	3.9860	3.9879	4.0035
N1567946919	3372250.5	25.7	-3.9	291.2	-10.8	316.2	3.20892	0.00263	7.1275	4.1172	4.1640	4.2483
N1573720878	2047785.4	67.2	3.8	21.4	-9.8	87.5	1.03067	0.00571	6.5563	2.4027	2.3950	2.4786
N1574856027	2556926.2	29.4	5.9	350.3	-9.6	15.5	2.14297	0.00339	6.4843	3.4323	3.4477	3.5111
N1576021955	2584612.2	25.6	11.3	333.1	-9.4	348.3	2.18132	0.00536	6.6913	3.6068	3.6442	3.7253
N1577098962	1519768.4	25.8	15.2	172.8	-9.2	181.5	2.39052	0.00254	6.5612	3.4713	3.5049	3.5841
N1577099005	1519819.9	25.8	15.2	172.9	-9.2	181.5	2.07378	0.01746	6.5610	3.4713	3.5048	3.5840
N1577213773	2437797.2	25.3	13.7	349.1	-9.1	359.9	2.06309	0.00275	6.6002	3.5349	3.5663	3.6417
N1578631223	2166443.0	28.1	17.8	346.3	-8.9	355.0	2.13633	0.00026	6.7041	3.4668	3.5117	3.6088
N1579323043	1641023.2	17.3	1.9	340.6	-8.8	327.0	3.09868	0.00051	6.5300	3.9026	3.8902	3.8993
N1579323086	1641321.2	17.2	1.9	340.7	-8.8	327.1	3.13915	0.00127	6.5296	3.9022	3.8898	3.8989
N1579490159	1427019.5	25.7	16.2	224.3	-8.8	218.0	2.66359	0.00257	6.9423	3.8192	3.8623	3.9522
N1579490202	1427374.9	25.7	16.2	224.4	-8.8	218.1	2.43917	0.00643	6.9433	3.8201	3.8632	3.9532
N1580528466	2087463.9	20.2	11.5	357.7	-8.6	359.8	2.37828	0.00056	6.5334	3.6585	3.6787	3.7310
N1580766128	2125791.2	31.3	20.4	349.1	-8.5	1.2	1.78432	0.00187	6.7550	3.3594	3.4129	3.5263
N1581600104	1411274.0	28.3	19.7	181.8	-8.4	185.7	1.99782	0.00116	6.6574	3.4075	3.4536	3.5526
N1581600147	1411342.2	28.3	19.7	181.9	-8.4	185.8	2.08472	0.00922	6.6576	3.4077	3.4538	3.5528
N1583629108	1952681.8	31.6	21.1	22.6	-8.0	34.9	2.02815	0.00175	6.8509	3.5199	3.5584	3.6573
N1586902986	1760128.0	20.2	9.5	347.9	-7.4	336.8	2.68607	0.00011	6.5371	3.7385	3.7458	3.7833
N1587848338	1805815.4	27.2	19.1	341.8	-7.3	335.4	2.20404	0.00001	6.7653	3.5833	3.6221	3.7113
N1591997007	898291.4	27.1	17.3	178.8	-6.5	165.8	2.15088	0.00114	6.5966	3.4662	3.5019	3.5855
N1591997040	898287.2	27.1	17.3	178.9	-6.5	165.9	2.02151	0.00141	6.5967	3.4656	3.5014	3.5850
N1596371038	1379430.4	30.4	23.3	0.1	-5.8	350.9	1.88417	0.00058	6.8113	3.4118	3.4714	3.5896
N1596371081	1379301.9	30.4	23.3	0.2	-5.8	350.9	1.59699	0.00014	6.8114	3.4118	3.4714	3.5896
N1600750094	850989.2	37.4	25.3	200.4	-5.0	177.7	1.74939	0.00029	6.9015	3.1762	3.2552	3.4068
N1600750127	851073.7	37.4	25.3	200.5	-5.0	177.8	1.74432	0.00289	6.9022	3.1759	3.2550	3.4067
N1602626622	844936.0	28.6	19.2	173.3	-4.7	157.2	2.08666	0.00011	6.6542	3.4763	3.5127	3.6001
N1602626665	844884.6	28.6	19.2	173.3	-4.7	157.3	1.99521	0.00079	6.6542	3.4752	3.5116	3.5991

Table 15 continued on next page

**Table 15 (continued)**

Filename	Range	Phase	Sub-S/C	Sub-S/C	Sub-Solar	Sub-Solar	$A_{\text{eff}}$	$A_{\text{eff}}$	$A_{\text{phys}}$	$a_{\text{pred}}$	$a_{\text{pred}}$	$a_{\text{pred}}$
	(km)	(deg)	Latitude	Longitude	Latitude	Longitude	Value	Error		k=1	k=0.75	k=0.50
			(deg)	(deg)	(deg)	(deg)	(km <sup>2</sup> )					
N1607831119	821236.7	35.0	-10.4	204.5	-3.7	169.9	1.86522	0.00027	6.6024	3.2726	3.3182	3.4224
N1607831162	821439.6	35.0	-10.4	204.6	-3.7	170.0	1.60051	0.00109	6.6031	3.2721	3.3179	3.4222
N1609330140	1503733.5	37.5	-9.0	335.9	-3.4	298.5	2.22455	0.00065	6.6298	3.5493	3.5338	3.5780
N1609330183	1503933.1	37.5	-9.0	335.9	-3.4	298.6	2.04597	0.00413	6.6292	3.5492	3.5337	3.5778
N1623517047	1429461.4	49.0	47.4	306.4	-0.9	315.8	1.59027	0.00095	7.8596	3.2466	3.3841	3.6282
N1623517090	1429768.9	49.0	47.3	306.5	-0.9	315.8	1.56149	0.00267	7.8592	3.2461	3.3836	3.6278
N1649508527	951116.8	72.4	0.4	152.0	3.7	224.5	0.61628	0.00072	6.5688	1.8136	1.8408	1.9548
N1649508560	951137.0	72.4	0.4	152.1	3.7	224.5	0.56507	0.00029	6.5680	1.8143	1.8414	1.9553
N1649609027	1962121.8	65.7	0.3	315.8	3.7	21.4	0.80913	0.00277	6.8318	2.1201	2.1779	2.3283
N1658887283	1604479.6	70.0	0.1	27.1	5.3	97.0	0.85431	0.00011	6.6072	2.3580	2.3561	2.4451
N1658887316	1604506.5	70.0	0.1	27.1	5.3	97.0	0.71942	0.00052	6.6076	2.3577	2.3559	2.4449
N1671766222	1077715.0	50.2	0.0	222.6	7.5	272.4	1.90624	0.00086	6.7677	3.3069	3.3003	3.3722
N1671766255	1078080.0	50.2	0.0	222.6	7.5	272.4	1.83231	0.00410	6.7686	3.3077	3.3012	3.3731
N1682164588	1998692.4	49.9	0.4	234.1	9.2	283.5	1.92876	0.00077	6.9306	3.4053	3.4165	3.5068
N1682164621	1999044.4	49.9	0.4	234.2	9.2	283.5	1.55592	0.00114	6.9313	3.4057	3.4170	3.5074
N1689830896	3003373.5	46.8	0.2	41.3	10.4	87.2	1.80468	0.00006	6.7914	3.4264	3.4138	3.4760
N1690349900	2378662.5	67.4	0.3	88.0	10.5	155.1	0.97524	0.00051	7.2031	2.4503	2.5386	2.7280
N1693543720	2910682.5	33.4	0.2	305.8	11.0	337.6	1.90535	0.00180	6.9641	3.6250	3.6861	3.8037
N1694912568	1452919.4	18.6	0.2	242.1	11.2	257.3	3.71339	0.00025	7.0305	4.4184	4.4060	4.4165
N1694912601	1453316.9	18.6	0.2	242.2	11.2	257.3	3.67594	0.00000	7.0311	4.4190	4.4065	4.4171
N1695407242	2273088.2	42.3	0.3	249.4	11.3	290.5	2.48256	0.00125	7.1055	3.7586	3.7850	3.8799
N1695407275	2273401.2	42.3	0.3	249.5	11.3	290.5	2.18934	0.00104	7.1060	3.7587	3.7852	3.8802
N1696922581	2770542.0	52.9	0.2	25.6	11.5	77.7	1.29484	0.00367	6.5906	3.0252	3.0068	3.0712
N1703077540	3099035.2	52.4	-0.4	21.5	12.4	72.8	1.36003	0.00081	6.5479	2.9924	2.9729	3.0356
N1703197541	2500398.5	50.5	-0.5	201.8	12.5	251.1	1.65727	0.00114	6.4993	3.0508	3.0268	3.0819
N1703197574	2500547.2	50.5	-0.5	201.9	12.5	251.1	1.81111	0.01852	6.4999	3.0517	3.0277	3.0828
N1707246186	2612761.5	41.8	-0.8	244.2	13.1	284.0	2.05696	0.00027	7.0537	3.7617	3.7753	3.8572
N1707246219	2613092.0	41.8	-0.8	244.2	13.1	284.1	3.20217	0.00540	7.0543	3.7619	3.7757	3.8576
N1707673569	2499211.5	63.9	-0.5	149.8	13.1	212.9	0.78547	0.00379	6.5967	2.1519	2.1841	2.3057
N1707882851	2515143.8	74.9	-0.3	97.6	13.2	172.0	0.62169	0.00171	7.1887	1.9952	2.0787	2.2620
N1712159738	2072965.4	62.5	0.4	130.0	13.8	191.7	0.89810	0.00315	6.8743	2.2840	2.3488	2.5079
N1713881929	2208542.2	54.8	0.4	236.2	14.0	289.9	1.62335	0.00048	6.9585	3.2077	3.2262	3.3311
N1716983288	2221235.5	56.6	-9.1	274.7	14.5	326.6	1.29114	0.00063	7.2396	2.9088	2.9913	3.1707
N1716983321	2221539.0	56.6	-9.1	274.7	14.5	326.6	1.16241	0.00021	7.2395	2.9083	2.9907	3.1702
N1717967354	2462931.5	49.1	-6.9	340.5	14.6	25.0	1.19682	0.00454	6.5624	2.7428	2.7679	2.8744
N1718126175	2159999.2	56.9	-12.2	212.1	14.7	262.8	1.51539	0.00131	6.7177	2.8578	2.8534	2.9384
N1718126208	2160236.8	56.9	-12.2	212.2	14.7	262.9	1.52732	0.00252	6.7184	2.8586	2.8543	2.9394
N1733321653	1824032.0	69.1	-36.8	306.3	16.7	352.6	0.54182	0.00400	7.5674	2.0368	2.1349	2.3395
N1735267445	1731925.0	47.4	-11.0	39.6	17.0	78.3	1.62108	0.00010	6.8420	3.2844	3.2779	3.3535
N1735267478	1731796.4	47.4	-11.0	39.7	17.0	78.4	1.33382	0.00402	6.8426	3.2844	3.2780	3.3536
N1738780228	1939329.0	46.2	-15.9	357.5	17.5	29.9	1.11458	0.00012	6.6199	2.8455	2.8662	2.9683
N1741128763	1761666.6	62.9	-32.9	329.4	17.8	8.4	0.68126	0.00095	7.2660	2.1644	2.2446	2.4261
N1741892147	1517998.5	44.8	-8.8	56.8	17.9	93.2	1.76834	0.00032	7.0367	3.5431	3.5482	3.6317
N1741892180	1517800.5	44.8	-8.9	56.9	17.9	93.3	1.63449	0.00386	7.0373	3.5430	3.5480	3.6317
N1744740426	1255014.2	39.8	-3.2	80.5	18.2	114.6	2.37967	0.00053	7.1950	3.8180	3.8482	3.9481
N1744740459	1254760.4	39.8	-3.2	80.6	18.2	114.7	2.12503	0.00046	7.1951	3.8175	3.8478	3.9478
N1745472130	777396.1	24.0	18.8	123.7	18.3	149.0	3.07430	0.00003	7.1386	4.1414	4.1960	4.2841
N1745472163	777240.8	24.0	18.8	123.8	18.3	149.1	2.78999	0.00031	7.1379	4.1409	4.1955	4.2836
N1750355731	1695508.8	63.2	-31.5	354.8	18.9	34.5	0.71208	0.00576	7.0844	2.1686	2.2227	2.3747
N1751140956	991139.9	36.2	-3.4	121.9	19.0	150.8	2.28940	0.00003	6.9880	3.5642	3.6144	3.7304
N1751140989	990933.3	36.2	-3.4	121.9	19.0	150.9	2.04994	0.00054	6.9873	3.5634	3.6136	3.7296
N1764307910	1610313.2	34.2	42.8	71.7	20.5	40.8	2.28128	0.00217	7.8235	4.2320	4.3537	4.5392
N1764307943	1610043.2	34.1	42.8	71.8	20.5	40.8	2.29037	0.00500	7.8237	4.2326	4.3543	4.5397
N1772108489	2597342.5	62.4	48.5	88.2	21.3	16.3	0.97562	0.00362	7.9876	3.0684	3.2188	3.4842
N1772256200	2605254.5	67.6	42.6	317.3	21.3	238.7	1.07361	0.00054	7.6595	2.9516	3.0330	3.2231

Table 15 continued on next page

**Table 15** (*continued*)

Filename	Range	Phase	Sub-S/C	Sub-S/C	Sub-Solar	Sub-Solar	$A_{\text{eff}}$	$A_{\text{eff}}$	$A_{\text{phys}}$	$a_{\text{pred}}$	$a_{\text{pred}}$	$a_{\text{pred}}$
	(km)	(deg)	Latitude	Longitude	Latitude	Longitude	Value	Error		k=1	k=0.75	k=0.50
			(deg)	(deg)	(deg)	(deg)	(km <sup>2</sup> )					
N1777325263	3348015.0	69.9	42.1	106.0	21.8	24.0	0.69034	0.00009	7.8042	2.7613	2.8836	3.1197
N1777845756	2860879.5	56.1	42.9	160.1	21.9	96.6	1.43998	0.00013	7.5000	3.3390	3.3913	3.5426
N1783954845	2126404.0	15.0	8.9	27.7	22.5	21.2	3.36674	0.00187	6.6669	4.0684	4.0538	4.0580
N1783954878	2126176.8	15.0	8.9	27.7	22.5	21.2	3.51804	0.01008	6.6674	4.0689	4.0543	4.0584
N1786518811	2550880.5	22.8	14.9	340.7	22.7	318.0	2.81226	0.00272	6.6806	4.0395	4.0071	4.0055
N1786518844	2550920.0	22.8	14.9	340.7	22.7	318.0	2.32321	0.00306	6.6802	4.0391	4.0068	4.0051
N1792421529	1549076.9	30.8	8.7	325.6	23.2	297.2	2.31163	0.00180	6.7464	3.9507	3.9100	3.9172
N1792421562	1549118.2	30.8	8.7	325.7	23.2	297.3	1.89255	0.00076	6.7459	3.9504	3.9097	3.9169
N1816569466	1058655.2	52.7	-0.2	52.7	25.0	4.8	1.38246	0.00070	6.9454	2.8297	2.8784	3.0179
N1835727946	2389879.0	58.3	20.4	78.9	25.9	15.1	1.33076	0.00095	7.3654	3.0051	3.0882	3.2707
N1835820227	1919473.0	68.6	24.0	235.3	25.9	158.5	0.74357	0.00185	7.2318	2.3568	2.4236	2.5927
N1839519641	3271904.8	70.8	25.7	97.8	26.1	17.6	1.20180	0.00670	7.4645	2.5819	2.6695	2.8643
N1840466876	2735832.2	39.1	27.2	60.8	26.1	16.9	2.44058	0.01658	7.3823	3.8081	3.8871	4.0353
N1840897819	1507244.5	19.4	16.0	328.5	26.1	310.7	2.98409	0.00152	6.8240	4.2783	4.2385	4.2228
N1840897852	1507238.2	19.4	16.0	328.5	26.1	310.7	2.93648	0.00204	6.8235	4.2779	4.2382	4.2225
N1841897315	2719247.0	76.0	31.5	120.1	26.2	31.0	1.02455	0.00204	7.4544	2.4952	2.5728	2.7575
N1843366805	1948036.0	16.0	35.1	122.0	26.2	106.4	4.11041	0.00009	7.5307	4.8356	4.8556	4.8937
N1843366838	1947720.8	16.0	35.1	122.0	26.2	106.5	4.52515	0.00363	7.5303	4.8352	4.8551	4.8933
N1844969055	2564126.8	49.3	41.7	75.9	26.3	18.3	1.68873	0.00067	7.8110	3.6470	3.7748	3.9957
N1844969088	2563878.0	49.3	41.7	76.0	26.3	18.3	1.59917	0.00081	7.8113	3.6476	3.7754	3.9963
N1846929427	2304880.2	65.6	47.4	202.5	26.3	120.7	1.45812	0.00210	7.6685	2.8429	2.9176	3.1032
N1847240469	2457654.8	54.5	40.6	296.1	26.3	231.4	1.89825	0.00675	7.7347	3.6198	3.7091	3.8939
N1847381610	2008120.5	29.1	44.9	115.1	26.3	87.2	3.16207	0.00368	7.8317	4.6649	4.7287	4.8421
N1849967367	1219807.8	67.9	57.3	146.1	26.4	56.4	1.22365	0.00116	8.0284	3.1093	3.2193	3.4465
N1849967400	1219680.4	67.9	57.3	146.2	26.4	56.5	1.07899	0.00129	8.0285	3.1091	3.2190	3.4462
N1853388939	126176.9	69.3	-41.1	202.4	26.5	219.0	0.69534	0.00011	7.4470	1.9653	2.0275	2.1915

**Table 16.** Brightness estimates from clear-filter images of Pan.

Filename	Range	Phase	Sub-S/C	Sub-S/C	Sub-Solar	Sub-Solar	$A_{\text{eff}}$	$A_{\text{eff}}$	$A_{\text{phys}}$	$a_{\text{pred}}$	$a_{\text{pred}}$	$a_{\text{pred}}$
	(km)	(deg)	Latitude	Longitude	Latitude	Longitude	Value	Error		k=1	k=0.75	k=0.50
			(deg)	(deg)	(deg)	(deg)	(km <sup>2</sup> )					
N1577141695	1928322.1	23.9	14.1	255.1	-9.2	260.7	222.3964	0.0696	578.4056	329.4306	331.6341	337.6532
N1578630786	1758181.6	32.0	22.1	241.8	-8.9	249.6	184.8326	0.0461	584.9566	296.6020	301.0208	311.0923
N1579656793	1773520.2	33.9	21.7	108.1	-8.7	123.4	178.0623	0.0538	593.9390	290.1136	297.4645	310.7608
N1579750304	1820849.6	38.5	24.4	60.8	-8.7	80.9	166.6279	0.0497	592.5009	285.7020	290.0645	300.9773
N1580566295	1680456.4	25.2	16.6	232.0	-8.6	233.0	195.7154	0.0450	555.9801	293.7928	297.1923	304.7319
N1580653070	1733973.4	31.7	20.7	129.4	-8.6	141.7	163.4020	0.0510	565.7847	265.4792	272.7606	285.4930
N1580766531	1705000.6	35.9	25.8	232.9	-8.5	243.8	166.9957	0.0418	585.8973	276.7147	282.0406	293.7582
N1581513746	1618819.1	20.3	11.3	262.5	-8.4	257.6	239.9507	0.0549	578.0841	339.4847	341.6902	346.8926
N1582637274	1579629.0	30.4	21.2	110.2	-8.2	117.9	186.9957	0.0390	590.8297	301.4664	307.5970	319.1276
N1583401389	1432863.0	20.6	9.3	265.2	-8.1	254.1	244.7941	0.0396	576.1828	340.2280	342.5082	347.5359
N1586106329	1511835.6	21.9	14.3	53.5	-7.6	52.3	210.6914	0.0376	554.9140	303.3425	306.4228	312.9069
N1586166659	1398029.8	29.7	22.1	127.3	-7.6	129.4	172.7843	0.0337	572.9932	282.6779	288.6509	299.8736
N1587821651	1424136.5	30.3	21.9	248.5	-7.3	240.3	192.3089	0.0311	591.4235	300.6793	307.2238	319.1403
N1588711307	1360694.5	36.6	29.4	208.6	-7.1	206.2	131.8954	0.0287	570.1411	230.8775	240.0550	255.8435
N1591525867	1025931.0	37.9	31.2	76.5	-6.6	78.5	164.6477	0.0154	627.2568	293.8886	302.3364	318.1253
N1591997460	1267001.9	27.0	12.2	274.9	-6.5	255.4	228.3243	0.0254	580.8421	329.8860	333.0538	339.9074
N1592072551	1191633.0	27.9	21.1	83.2	-6.5	79.4	207.0485	0.0198	599.6579	322.8549	328.0792	338.2477

Table 16 continued on next page

**Table 16** (*continued*)

Filename	Range	Phase	Sub-S/C	Sub-S/C	Sub-Solar	Sub-Solar	$A_{\text{eff}}$	$A_{\text{eff}}$	$A_{\text{phys}}$	$a_{\text{pred}}$	$a_{\text{pred}}$	$a_{\text{pred}}$
	(km)	(deg)	Latitude	Longitude	Latitude	Longitude	Value	Error		k=1	k=0.75	k=0.50
			(deg)	(deg)	(deg)	(deg)	(km <sup>2</sup> )					
N1596292976	1235300.4	24.6	17.6	65.4	-5.8	57.8	208.9829	0.0216	578.4270	312.3223	317.5454	326.7676
N1596338651	1213565.4	30.1	23.5	35.7	-5.8	28.7	154.7138	0.0213	556.9010	254.7925	262.5057	275.4599
N1596720449	1105775.5	30.3	-13.5	304.7	-5.7	275.0	229.2640	0.0279	555.8362	322.3647	321.6082	324.1404
N1597462699	1220196.6	26.5	2.9	278.0	-5.6	252.8	238.7705	0.0156	569.9943	335.4424	337.3920	342.0592
N1600167203	1164411.4	30.8	25.0	54.4	-5.1	47.8	173.8201	0.0177	587.2896	283.3856	291.4429	305.0741
N1602109109	1024253.1	37.3	32.5	80.1	-4.7	77.5	168.0533	0.0137	632.9182	299.1546	308.4430	325.0340
N1603175729	1194785.5	28.9	1.1	273.9	-4.6	245.6	228.9991	0.0096	570.6019	328.2749	331.5308	337.7646
N1603315800	1020402.0	34.3	24.9	198.5	-4.5	180.4	137.2631	0.0139	539.6896	221.9088	230.3357	244.4412
N1603721403	1054447.9	34.3	-13.1	272.7	-4.5	239.1	216.0386	0.0256	582.6179	316.1304	322.0682	332.0253
N1604570544	1309380.9	31.5	18.9	293.1	-4.3	271.4	211.2726	0.0217	583.1643	315.9542	318.9507	326.6708
N1604687380	1168687.0	38.5	34.2	39.8	-4.3	37.9	134.0222	0.0166	606.3586	249.7376	260.9557	279.5397
N1605247724	1166849.9	27.6	19.9	151.5	-4.2	137.8	173.0014	0.0182	530.5668	264.9402	267.9360	275.1566
N1606638984	1067777.6	32.2	25.9	150.5	-3.9	138.0	154.1523	0.0146	555.6049	257.1036	262.8557	274.0487
N1607328329	1031726.7	32.6	28.0	99.8	-3.8	92.5	188.1515	0.0124	617.7155	315.5556	322.8064	336.1137
N1607730646	904715.6	39.8	-31.2	158.1	-3.7	127.4	151.4390	0.0150	572.2009	257.4519	263.0847	274.9801
N1610355462	1107042.0	33.0	29.4	70.0	-3.3	65.0	180.6792	0.0140	617.4885	303.2404	312.1667	327.3705
N1610899555	1122210.8	39.2	-29.3	78.0	-3.2	47.2	173.3374	0.0203	621.5580	291.9020	304.2845	323.1557
N1611119577	1057592.5	31.9	17.6	226.0	-3.1	201.3	152.6058	0.0126	549.1956	253.1143	261.8125	275.3593
N1786520584	2193207.0	22.1	17.3	263.1	22.7	240.2	277.7693	0.1401	589.8528	362.1715	364.0525	367.9735
N1796432087	1862630.8	32.9	19.1	87.3	23.5	52.2	223.4152	0.1062	595.3240	340.1232	344.2018	352.0305
N1843369458	2209490.0	25.1	30.3	316.1	26.2	287.9	266.3685	0.1296	594.1578	367.1298	366.1883	367.8058
N1845329010	2066491.1	31.6	42.2	118.9	26.3	85.4	251.3473	0.1026	656.3629	386.3264	393.0872	404.0984
N1847384203	2123172.2	39.3	41.7	260.3	26.3	215.9	236.7225	0.0959	664.1030	347.4792	361.5294	381.3286
N1849020734	1275502.4	37.8	48.5	232.7	26.4	193.1	223.4009	0.0384	675.4461	335.2540	353.0933	377.3273

**Table 17.** Brightness estimates from clear-filter images of Atlas.

Filename	Range	Phase	Sub-S/C	Sub-S/C	Sub-Solar	Sub-Solar	$A_{\text{eff}}$	$A_{\text{eff}}$	$A_{\text{phys}}$	$a_{\text{pred}}$	$a_{\text{pred}}$	$a_{\text{pred}}$
	(km)	(deg)	Latitude	Longitude	Latitude	Longitude	Value	Error		k=1	k=0.75	k=0.50
			(deg)	(deg)	(deg)	(deg)	(km <sup>2</sup> )					
N1495208581	1200176.6	20.9	-19.6	50.0	-21.7	27.8	281.1014	0.0047	657.0602	362.1453	363.9504	367.7587
N1503007485	1538741.6	34.7	-19.2	68.2	-20.7	31.3	223.5278	0.0023	668.9564	338.6541	343.4461	352.5163
N1503007793	1533078.1	34.6	-19.2	70.2	-20.7	33.4	227.3121	0.0027	670.7019	341.2420	346.0067	355.0086
N1503008105	1527283.9	34.5	-19.3	72.3	-20.7	35.5	228.6507	0.0051	672.3640	343.8194	348.5363	357.4478
N1503008417	1521438.0	34.4	-19.4	74.3	-20.7	37.7	231.1872	0.0018	673.9126	346.3409	350.9915	359.7968
N1503008885	1512585.0	34.2	-19.5	77.4	-20.7	40.9	232.9991	0.0036	676.0113	349.9915	354.5059	363.1126
N1503009353	1503649.2	34.1	-19.6	80.6	-20.7	44.2	232.8272	0.0053	677.8268	353.4491	357.7854	366.1541
N1503009821	1494651.4	34.0	-19.7	83.7	-20.7	47.4	237.5102	0.0028	679.3419	356.6757	360.7953	368.8904
N1503010289	1485613.0	33.9	-19.8	86.9	-20.7	50.6	240.1510	0.0030	680.5445	359.6346	363.5007	371.2880
N1503069320	1141798.9	26.9	-22.4	128.2	-20.7	99.3	281.0052	0.0022	680.1461	383.0209	383.2054	386.1073
N1503069548	1138044.1	27.0	-22.5	129.9	-20.7	100.9	278.8551	0.0014	679.1027	381.7504	381.8692	384.7297
N1503088546	1123235.6	35.9	-21.3	271.0	-20.7	232.5	230.6600	0.0038	692.4507	361.1300	366.2135	375.5454
N1503088992	1127668.8	35.8	-21.2	274.0	-20.7	235.5	231.6408	0.0030	691.3143	362.6784	367.2585	376.0347
N1503089442	1132117.4	35.7	-21.0	277.0	-20.7	238.7	234.0510	0.0018	689.8846	363.9960	368.0461	376.2427
N1503089892	1136522.9	35.6	-20.9	280.0	-20.7	241.8	236.7225	0.0022	688.1845	365.0535	368.5562	376.1566
N1503090342	1140867.0	35.5	-20.8	283.0	-20.7	244.9	237.7026	0.0023	686.2238	365.8393	368.7841	375.7775
N1503090792	1145132.0	35.4	-20.7	285.9	-20.7	248.0	236.5353	0.0025	684.0197	366.3465	368.7301	375.1164
N1503091242	1149300.4	35.2	-20.5	288.9	-20.7	251.2	238.0905	0.0018	681.5891	366.5717	368.3963	374.1814
N1575055051	1844073.1	36.5	8.3	294.0	-9.5	326.0	128.4136	0.0111	602.0613	252.8918	258.4691	269.6866

*Table 17 continued on next page*

**Table 17** (*continued*)

Filename	Range	Phase	Sub-S/C	Sub-S/C	Sub-Solar	Sub-Solar	$A_{\text{eff}}$	$A_{\text{eff}}$	$A_{\text{phys}}$	$a_{\text{pred}}$	$a_{\text{pred}}$	$a_{\text{pred}}$
	(km)	(deg)	Latitude	Longitude	Latitude	Longitude	Value	Error		k=1	k=0.75	k=0.50
			(deg)	(deg)	(deg)	(deg)	(km <sup>2</sup> )					
N1575757516	1887835.5	21.5	8.7	138.7	-9.4	150.3	191.7764	0.0103	572.8109	265.0569	268.0252	274.8315
N1575799861	2112820.8	23.3	8.9	68.9	-9.4	83.4	185.9164	0.0112	607.1602	303.9649	304.8911	309.9042
N1576172089	2156696.0	38.0	15.6	112.1	-9.3	141.0	152.1582	0.0062	641.6019	246.3600	254.7862	270.1486
N1577098360	1935359.2	23.7	11.9	63.7	-9.2	74.8	186.2885	0.0115	616.9760	295.7788	298.1462	305.1944
N1577458138	2315257.5	39.2	21.5	21.1	-9.1	46.1	99.7812	0.0068	647.4346	222.9210	229.8096	244.1751
N1579656313	1726775.2	34.1	22.3	132.8	-8.7	147.2	137.9804	0.0042	674.5298	239.0070	250.1127	268.9570
N1579750094	1830687.5	38.3	24.2	56.7	-8.7	76.7	132.1571	0.0063	702.8215	257.0954	266.6726	284.6741
N1580480539	1631814.4	20.7	11.5	89.7	-8.6	94.7	214.0425	0.0025	626.9536	310.4175	313.5979	321.0620
N1580527879	1786693.2	22.9	13.4	56.0	-8.6	62.5	179.9720	0.0039	618.4705	287.7510	291.3048	299.6782
N1580614475	1861123.1	26.2	17.5	299.2	-8.6	302.1	137.6042	0.0063	650.5163	279.1954	286.2520	299.3879
N1582637664	1629831.2	28.9	20.6	273.6	-8.2	271.4	148.9960	0.0038	686.8517	289.7183	298.5442	314.4331
N1584357766	1598980.5	21.1	11.6	310.3	-7.9	302.2	162.8924	0.0051	600.7305	287.4982	289.8784	296.3688
N1584373656	1620256.2	20.7	12.8	51.4	-7.9	52.3	176.5108	0.0034	609.8085	285.0650	288.9704	297.2383
N1586192474	1569255.2	29.6	21.9	43.4	-7.6	46.5	142.3328	0.0036	670.1107	258.2845	267.9531	284.7338
N1586251260	1460347.8	37.2	28.7	84.8	-7.6	93.6	145.6554	0.0029	756.0443	271.5092	285.7771	309.6484
N1586278920	1457980.0	38.3	30.7	286.9	-7.6	285.2	117.3816	0.0031	772.3850	264.5622	280.1543	305.9281
N1586902549	1453993.4	22.8	11.4	296.4	-7.4	283.5	181.0038	0.0040	614.4594	300.9220	303.3055	309.8945
N1587820841	1351998.9	30.4	23.1	163.5	-7.3	162.1	137.2186	0.0052	655.7429	229.7043	240.3861	258.2387
N1589546543	1147782.0	39.9	31.9	240.8	-7.0	231.6	119.8960	0.0013	775.9841	248.6452	265.9461	293.7305
N1591998210	1337540.5	25.8	11.7	306.4	-6.5	287.9	164.7549	0.0023	605.7007	290.5469	292.5713	298.9698
N1592072731	1181500.2	28.1	21.4	87.5	-6.5	84.1	177.4802	0.0025	693.0607	295.0261	304.9084	321.7418
N1595483015	1125571.9	26.3	-10.0	324.4	-5.9	298.1	194.9982	0.0036	575.6722	295.4880	294.8534	296.9477
N1596292421	1071337.4	28.2	20.4	153.7	-5.8	143.0	156.6119	0.0016	637.4205	249.8666	258.1966	272.7347
N1596338111	1082648.0	32.5	26.5	103.1	-5.8	99.3	165.2272	0.0022	733.5688	285.6292	299.0405	320.9540
N1596370751	1152914.6	36.1	28.2	337.8	-5.8	325.1	117.0854	0.0031	714.4532	235.1089	248.9180	271.4896
N1596719969	992529.4	31.9	-15.1	254.5	-5.7	223.5	192.6202	0.0021	642.8896	299.0190	308.3432	321.9556
N15968777995	1193852.9	28.1	10.8	260.6	-5.7	237.7	180.5299	0.0040	621.4342	292.8031	298.4526	308.5900
N1597670700	1071528.8	39.6	32.5	338.2	-5.5	326.6	111.0055	0.0022	759.5994	229.5945	246.4972	273.5208
N1599451493	1253386.6	21.5	13.7	67.8	-5.2	57.4	201.3924	0.0019	630.8519	299.2293	305.4053	315.8389
N1600748642	1267621.5	24.0	16.5	50.3	-5.0	39.6	173.2922	0.0016	633.4282	275.5876	283.8763	297.2490
N1602109611	972137.7	39.3	34.5	105.8	-4.7	103.4	146.5496	0.0014	807.3161	273.8361	293.0294	323.2942
N1602626305	1192849.9	21.4	13.4	92.8	-4.6	81.3	216.9491	0.0007	637.3005	314.6500	319.7686	328.9360
N1603316010	1014325.2	34.2	25.1	194.6	-4.5	176.9	131.7211	0.0014	675.0623	225.4153	238.6441	259.6350
N1604570034	1199470.2	32.7	20.6	241.9	-4.3	220.3	145.2604	0.0035	674.2288	265.3786	277.5944	296.7433
N1605073633	1020464.0	20.1	-7.5	127.6	-4.2	107.7	239.4766	0.0024	582.1202	315.9179	315.2140	316.2223
N1605988474	1227964.9	34.9	27.2	338.2	-4.0	322.1	124.7473	0.0029	704.0568	244.1088	257.4861	279.1331
N1606638074	1062936.2	32.3	25.9	153.3	-3.9	140.5	146.7671	0.0029	690.2189	250.2845	262.8414	283.0983
N1610124739	1036106.3	38.4	-20.6	198.7	-3.3	163.4	148.3225	0.0014	633.5627	235.8659	246.1392	262.7712
N1610317386	1167498.6	26.0	20.8	67.4	-3.3	57.3	183.7278	0.0010	681.0826	294.7581	305.9185	323.1626
N1610356255	1187479.8	34.0	27.4	342.0	-3.3	326.7	132.7424	0.0056	704.0374	245.0878	259.0637	281.2255
N1611119817	1077528.6	32.6	17.3	239.6	-3.1	213.8	152.8713	0.0013	646.0879	263.0491	273.8803	290.7448
N1618071706	1039053.1	36.6	-17.5	145.4	-1.9	111.7	170.2198	0.0018	620.8710	272.7044	277.0379	286.7606
N1620768130	1097592.8	20.6	8.1	81.1	-1.4	62.8	235.3553	0.0014	610.5947	316.4950	320.5165	326.9741
N1746449509	1202180.9	35.1	-12.3	208.4	18.4	225.7	110.0710	0.0050	576.6354	228.2202	226.9265	232.0539
N1757516440	1017899.1	32.9	41.5	207.6	19.7	178.5	273.0833	0.0015	852.8023	384.8564	412.5593	448.1802
N1792419402	1376916.8	25.2	10.2	324.6	23.2	302.0	222.5188	0.0063	576.2045	329.2625	319.4176	312.9196
N1796432677	1944216.0	34.0	18.2	47.8	23.5	11.7	218.9823	0.0101	643.8836	326.9903	328.0055	333.3567
N1796515508	1513232.2	34.0	14.1	260.0	23.5	225.3	226.6783	0.0040	639.1445	341.3206	339.9079	342.7689
N1843369278	2231088.2	24.5	29.9	330.4	26.2	303.0	296.1875	0.0056	736.9771	421.8929	424.3390	429.4765
N1845329830	2062721.6	37.6	42.2	240.8	26.3	198.9	301.6717	0.0060	875.9155	435.5607	460.2308	492.1293
N1847383273	2204552.5	32.6	39.9	53.9	26.3	18.0	309.3090	0.0083	851.6417	438.8438	459.9862	486.8789
N1849020884	1279952.2	38.1	48.3	238.3	26.4	198.0	321.4743	0.0021	930.8977	455.5864	487.5333	528.2131

**Table 18.** Brightness estimates from clear-filter images of Prometheus

Filename	Range	Phase	Sub-S/C	Sub-S/C	Sub-Solar	Sub-Solar	$A_{\text{eff}}$	$A_{\text{phys}}$	$a_{\text{pred}}$	$a_{\text{pred}}$	$a_{\text{pred}}$
	(km)	(deg)	Latitude	Longitude	Latitude	Longitude	Value		k=1	k=0.75	k=0.50
			(deg)	(deg)	(deg)	(deg)	(km <sup>2</sup> )				
N1575914492	2251982.5	23.7	11.0	290.4	-9.4	302.5	3789.8745	5945.7690	3187.5754	3251.0505	3354.0364
N1577051965	1729552.4	21.7	10.5	105.2	-9.2	114.1	2767.1677	6027.8188	3416.9006	3461.8240	3542.7866
N1577098105	1950314.6	23.5	11.7	56.7	-9.2	67.5	3105.4451	5615.8433	3143.3091	3130.0500	3154.3108
N1577215016	1997065.0	30.5	16.9	126.3	-9.2	142.4	1868.2275	5680.9424	2381.0442	2488.8511	2652.8489
N1579655833	1695057.1	33.8	22.7	159.5	-8.7	172.1	1180.3311	4969.6963	1394.5358	1483.8430	1628.8689
N1579750574	1792714.6	39.1	24.8	75.0	-8.7	95.8	2139.3582	6508.8945	3160.9849	3228.7004	3371.5254
N1580566520	1695084.1	25.1	16.5	241.6	-8.6	242.1	2460.6575	5902.4258	3075.2437	3117.7126	3207.7449
N1580613950	1675761.0	28.5	19.4	198.9	-8.6	204.3	1072.9626	4690.8086	1637.4780	1684.0397	1775.9514
N1580652770	1801057.0	31.4	19.9	94.4	-8.5	107.9	2452.1985	6411.5083	3319.8735	3397.4214	3536.6499
N1581773008	1698358.5	36.4	24.8	146.6	-8.4	162.0	1182.3083	5469.3691	1606.8419	1726.7169	1913.2938
N1586079839	1442448.0	23.3	12.0	287.5	-7.6	274.8	2862.1841	6028.7764	3563.9360	3569.4072	3610.9387
N1586106584	1416035.8	22.9	15.3	97.1	-7.6	97.1	2748.2263	6247.6646	3591.8118	3629.8403	3711.1384
N1586166389	1371952.5	30.1	22.5	142.4	-7.6	143.5	1808.0951	5442.7378	2097.8689	2179.0181	2316.6392
N1586903434	1336024.4	20.1	12.5	115.6	-7.4	113.2	2706.5364	5847.9570	3315.0120	3334.9653	3389.2551
N1587821441	1406194.5	30.5	22.2	240.6	-7.3	232.6	2182.4778	6109.1963	2787.7090	2888.3137	3050.9341
N1588712027	1346888.9	37.0	29.8	163.8	-7.1	166.0	1134.1011	5461.6343	1424.0609	1538.7045	1720.5079
N1588750338	1493945.4	37.5	29.5	57.6	-7.1	66.0	1993.5881	6418.7622	2793.6892	2878.4128	3041.4404
N1596371471	1142672.0	34.6	28.5	30.8	-5.8	26.1	1489.6841	5684.5845	1803.7579	1929.3861	2123.7568
N1596720239	1022205.6	32.1	-14.6	267.6	-5.7	236.2	2637.0425	6253.5815	3424.3486	3539.9983	3688.3384
N1597580600	1293142.2	28.7	18.2	340.3	-5.5	324.0	1472.1934	4651.6562	1867.7140	1879.8541	1933.7797
N1599451973	1193172.8	21.9	14.5	93.4	-5.2	83.7	2891.4980	6245.8203	3683.6533	3721.5933	3795.7317
N1601855695	1078166.6	30.4	-7.5	252.1	-4.8	221.7	2370.9624	5920.1396	2967.6516	3109.1467	3283.5059
N1603316955	1146441.0	27.9	22.2	81.3	-4.5	73.2	2603.9099	6469.6626	3435.5002	3520.0684	3660.9407
N1603880074	1315240.8	27.7	11.0	324.2	-4.4	301.1	2301.0032	4810.0913	2590.0444	2525.2651	2493.8823
N1604687620	1181663.5	38.1	33.8	32.3	-4.3	29.7	1495.1580	6110.2178	1881.6860	2033.1892	2265.2725
N1605073273	983238.6	22.5	-7.8	153.0	-4.2	130.6	2140.7432	4331.9316	2396.5515	2316.1519	2255.9370
N1605195763	1268863.4	29.8	11.3	269.0	-4.2	243.4	2741.6208	6175.3862	3435.6851	3516.3647	3634.0420
N1606637704	1299221.0	30.6	20.9	342.6	-3.9	324.2	1427.8378	4790.1597	1836.4938	1862.2802	1933.5624
N1607327189	1184835.5	32.4	23.9	347.8	-3.8	330.5	1292.1589	4936.9248	1677.9589	1733.2003	1839.2050
N1610318121	1008273.4	30.6	24.4	153.2	-3.3	139.7	1638.4796	5254.9771	2071.8608	2124.1711	2228.4114
N1610355722	1160812.9	32.0	28.0	41.9	-3.3	34.9	1793.6746	5937.4790	2218.8184	2357.9014	2564.1885
N1611119307	1031424.0	31.1	18.0	208.4	-3.1	185.2	1213.1506	4865.0806	1547.9807	1653.6503	1809.1509
N1611809162	1084474.9	37.3	-13.0	230.4	-3.0	194.1	1382.4642	5421.7090	1901.5269	2064.2068	2285.4607
N1792422642	1156344.6	24.7	11.5	225.0	23.2	202.1	2194.2708	5170.2173	2530.6130	2569.3579	2639.4707
N1796432277	1772149.4	33.5	20.1	130.7	23.5	94.7	2739.4849	5686.1440	3657.5493	3557.2522	3484.5955
N1843367928	2016262.5	22.9	33.6	174.5	26.2	149.5	2428.7129	5688.7319	2956.5659	2984.6509	3040.5974
N1845329620	2020437.4	36.2	43.4	202.2	26.3	162.8	1983.8071	6668.6719	2902.5671	3083.3992	3330.9578
N1847382333	2107069.2	32.8	42.2	110.5	26.3	75.2	3063.2388	7273.1177	4432.3950	4535.7607	4679.2939
N1849019314	1370693.4	27.4	44.5	66.9	26.4	41.4	3042.2461	7372.1523	4080.3401	4304.1514	4568.3413
N1851194541	923521.4	31.7	52.2	90.5	26.4	65.9	3167.0044	7841.3213	4524.7026	4731.9082	4997.5713

**Table 19.** Brightness estimates from clear-filter images of Pandora

Filename	Range	Phase	Sub-S/C	Sub-S/C	Sub-Solar	Sub-Solar	$A_{\text{eff}}$	$A_{\text{phys}}$	$a_{\text{pred}}$	$a_{\text{pred}}$	$a_{\text{pred}}$
	(km)	(deg)	Latitude	Longitude	Latitude	Longitude	Value		k=1	k=0.75	k=0.50
			(deg)	(deg)	(deg)	(deg)	(km <sup>2</sup> )				
N1509277557	468022.3	22.9	-0.4	265.5	-19.9	253.3	2551.8445	5090.0981	3120.5850	3123.7810	3154.0962
N1509278230	472646.5	22.6	-0.4	269.5	-19.9	257.8	2570.1541	5096.4727	3147.9783	3147.3135	3173.4172

Table 19 continued on next page

**Table 19** (*continued*)

Filename	Range	Phase	Sub-S/C	Sub-S/C	Sub-Solar	Sub-Solar	$A_{\text{eff}}$	$A_{\text{phys}}$	$a_{\text{pred}}$	$a_{\text{pred}}$	$a_{\text{pred}}$
	(km)	(deg)	Latitude	Longitude	Latitude	Longitude	Value		k=1	k=0.75	k=0.50
			(deg)	(deg)	(deg)	(deg)	(km <sup>2</sup> )				
N1509279125	478756.8	22.3	-0.4	274.7	-19.9	263.7	2566.7014	5092.3550	3167.1782	3161.3831	3181.8542
N1580567525	1640145.8	26.5	17.1	154.1	-8.6	160.8	1430.8479	4400.8467	2070.5557	2112.7646	2190.2957
N1580765496	1904911.6	35.2	22.9	17.8	-8.5	34.0	1456.2356	4503.1094	1980.4275	2009.6714	2086.2158
N1586165759	1350404.0	30.7	22.8	196.6	-7.6	192.5	1438.1946	4457.3887	1918.5052	1974.0736	2072.5266
N1587847451	1348720.8	33.2	25.9	181.8	-7.3	180.1	1434.0127	4492.5977	1816.3823	1879.5070	1989.8180
N1588712327	1356261.8	36.9	29.6	149.3	-7.1	152.9	1364.9861	4862.9883	1992.1320	2069.7925	2203.2756
N1588750068	1531763.5	36.4	28.7	36.2	-7.1	43.1	1643.4033	4929.4019	2191.9797	2248.6235	2360.1055
N1589546843	1256224.4	37.1	28.9	295.2	-7.0	285.6	1808.1101	5304.1875	2643.2776	2693.0691	2801.2913
N1591526167	1010910.1	38.5	31.7	83.3	-6.6	86.1	1962.8497	5486.4746	2716.8032	2780.9421	2908.3020
N1592072971	1121265.0	29.4	22.6	114.7	-6.5	110.8	2147.5969	5156.9810	2797.9487	2835.7644	2917.5547
N1596878265	1302059.8	26.8	9.9	306.9	-5.7	285.0	2196.9902	4783.1089	2847.6919	2827.5632	2835.4563
N1597462189	1096356.0	24.8	3.1	219.8	-5.6	196.6	1713.3755	4441.5923	2221.1108	2274.6731	2354.3560
N1597581215	1198794.7	32.7	19.7	286.2	-5.6	265.2	2132.0186	5201.0415	2898.5701	2927.1389	2999.0171
N1598767858	1137598.9	27.2	8.1	235.7	-5.3	212.0	1803.2091	4789.8413	2463.8076	2532.6562	2632.4731
N1599451733	1238672.9	21.5	13.9	74.4	-5.2	64.5	2556.5435	5119.2578	3007.8596	3044.0444	3106.3528
N1600168223	996016.1	35.7	29.8	142.2	-5.1	134.4	1600.6156	4964.4370	2257.1306	2315.6045	2427.9509
N1602108859	1096514.6	35.1	30.1	44.1	-4.7	39.3	1651.9224	5081.7544	2280.2715	2362.0244	2498.9377
N1602515395	1096482.1	29.0	-3.3	243.1	-4.7	214.1	2046.6665	4882.6831	2552.2395	2629.0273	2735.8005
N1603316415	1040816.9	30.6	24.5	134.2	-4.5	124.0	1890.8737	4923.0596	2528.1089	2561.8376	2639.5671
N1603721913	1165292.8	31.3	-11.7	323.4	-4.5	292.6	1975.2272	4496.1567	2601.4390	2562.0261	2553.0195
N1604569449	1137551.8	29.4	21.7	164.6	-4.3	150.6	1563.3486	4409.4082	2060.9636	2092.1526	2161.7671
N1605039972	1094691.9	22.8	-12.4	52.0	-4.2	30.5	2026.7488	4794.7354	2556.2061	2624.1267	2714.6670
N1605072793	1123066.8	32.9	-6.9	280.1	-4.2	247.2	2186.5544	5091.9795	2964.2534	2995.8557	3057.1838
N1607328119	1060464.9	31.6	27.1	85.7	-3.8	78.9	2203.3826	5395.5054	2910.5017	2967.7634	3074.4683
N1607831552	1042813.4	30.1	-8.0	206.1	-3.7	176.1	1716.7115	4219.6147	1942.6383	1984.7761	2059.7554
N1610317821	1078006.5	27.6	22.7	107.2	-3.3	97.7	2358.4861	5236.2056	2978.7854	3012.6272	3085.7417
N1611809402	1246033.6	37.5	-11.2	303.0	-3.0	266.2	1985.8206	4864.1021	2796.7686	2783.6406	2806.6631
N1654245770	100283.7	28.8	-12.2	84.5	4.5	60.9	2289.6917	5157.7026	2923.0667	2974.4148	3058.2896
N1654245985	100761.6	27.9	-12.6	84.5	4.5	62.3	2338.8330	5161.6616	2948.7871	2997.5830	3077.9707
N1735114284	1036456.8	20.0	10.0	87.9	17.0	107.2	2768.2666	5142.8467	3268.7817	3277.7913	3301.6609
N1786781406	1597904.5	28.0	-5.1	256.6	22.7	253.1	2237.1089	5051.9429	2926.1587	2926.2256	2966.4312
N1792422102	1164316.1	25.1	11.5	229.6	23.2	206.2	2005.5613	4717.0322	2580.7053	2611.7505	2669.8767
N1796433277	1728485.9	37.6	20.5	196.0	23.5	155.4	1470.2101	4375.0098	2094.3120	2095.9780	2139.7974
N1843103936	2832849.8	39.3	33.6	345.0	26.2	300.1	1798.4371	4889.7490	2647.8115	2634.0527	2665.4753
N1843369838	2169518.0	26.2	30.8	292.2	26.2	262.7	2718.2549	5378.6226	3422.6873	3432.3577	3463.6953
N1845330380	2215698.5	35.1	38.7	338.4	26.3	299.1	1966.6671	5142.5542	2874.6060	2883.7512	2934.8882
N1847384513	2157195.2	39.4	40.8	279.8	26.3	235.2	2199.5051	5684.2764	3171.7117	3260.7358	3394.8762
N1849020234	1407241.4	35.7	42.9	317.6	26.4	278.5	2136.0720	5475.6226	3170.3301	3198.3408	3269.7178

**Table 20.** Brightness estimates from clear-filter images of Janus.

Filename	Range	Phase	Sub-S/C	Sub-S/C	Sub-Solar	Sub-Solar	$A_{\text{eff}}$	$A_{\text{phys}}$	$a_{\text{pred}}$	$a_{\text{pred}}$	$a_{\text{pred}}$
	(km)	(deg)	Latitude	Longitude	Latitude	Longitude	Value		k=1	k=0.75	k=0.50
			(deg)	(deg)	(deg)	(deg)	(km <sup>2</sup> )				
N1524964907	216295.5	32.9	-0.2	231.7	-17.7	260.0	7242.8188	23032.1738	13006.3779	12950.2812	13073.6650
N1524965120	218050.4	33.1	-0.2	232.7	-17.7	261.3	7309.7822	23068.7754	13013.6660	12960.8555	13088.8672
N1524965317	219704.9	33.2	-0.2	233.7	-17.7	262.4	7263.7207	23101.8184	13018.2275	12968.6035	13101.0693
N1559172642	1524436.8	32.8	3.4	240.2	-12.3	269.3	7429.6016	23336.8145	13109.0371	13110.5742	13289.6104
N1574754459	2196734.8	30.9	6.4	117.4	-9.6	143.9	5808.9624	23470.2305	12579.3428	12747.0762	13089.3350

*Table 20 continued on next page*

**Table 20** (*continued*)

Filename	Range	Phase	Sub-S/C	Sub-S/C	Sub-Solar	Sub-Solar	$A_{\text{eff}}$	$A_{\text{phys}}$	$a_{\text{pred}}$	$a_{\text{pred}}$	$a_{\text{pred}}$
	(km)	(deg)	Latitude	Longitude	Latitude	Longitude	Value		k=1	k=0.75	k=0.50
			(deg)	(deg)	(deg)	(deg)	(km <sup>2</sup> )				
N1575011551	1781307.5	35.9	8.7	214.5	-9.5	245.6	6037.6162	22617.5801	12008.4717	11995.7139	12184.7939
N1575756631	2123755.0	20.2	7.7	25.9	-9.4	36.7	7426.0449	22477.6230	13007.3262	13013.5850	13124.5449
N1577098705	1741632.5	24.1	13.2	158.3	-9.2	167.3	5780.8052	22500.2676	12159.1025	12271.3994	12527.1123
N1579447272	1512084.6	21.1	12.1	219.4	-8.8	216.3	7683.9600	22952.0625	13004.3496	13092.5225	13302.1230
N1579749394	1653319.0	37.8	27.0	216.0	-8.7	228.6	5322.4150	24143.4258	11435.9316	11649.8604	12127.4639
N1580766801	1651062.2	37.4	26.7	199.6	-8.5	212.4	5162.1396	23746.8281	11012.5127	11237.3252	11720.3486
N1581772738	1756360.9	36.6	24.0	108.8	-8.4	126.5	4950.7778	24718.5781	12182.1338	12443.0762	12958.5420
N1582637844	1643237.9	28.7	20.4	279.1	-8.2	276.5	8087.4097	24595.2891	13451.8340	13611.4590	13967.5234
N1582719655	1730270.9	34.2	24.3	35.1	-8.2	46.0	5776.4194	23971.8652	11870.9883	12061.6836	12489.2822
N1584357016	1384841.8	21.2	13.3	150.2	-7.9	148.9	6521.0107	22723.7754	12757.7979	12842.7500	13050.4404
N1586107289	1323425.2	25.8	16.5	218.4	-7.6	208.9	6903.3584	23215.2871	12458.3232	12620.9434	12944.6201
N1586163489	1346807.8	30.8	22.8	202.8	-7.6	197.9	5825.4756	23373.0332	11608.5654	11828.1445	12256.9541
N1586902774	1498527.8	22.2	11.1	314.1	-7.4	301.8	9216.6641	23249.3086	13499.9814	13530.9824	13683.6924
N1587746665	1553493.4	22.2	12.6	334.1	-7.3	324.3	8501.2480	22734.5469	12814.6807	12871.5029	13053.5303
N1587847751	1361509.4	33.3	25.7	214.5	-7.3	209.4	5665.6255	23962.5586	11655.0967	11912.6875	12404.5752
N1589547143	1323751.4	34.9	27.3	331.4	-7.0	324.9	6480.6851	24149.3770	11597.3320	11845.9404	12342.1006
N1591761909	885668.8	33.3	-20.8	321.3	-6.6	290.1	7537.8843	23731.7324	12936.2539	13018.6084	13287.9482
N1591997640	1290874.4	27.3	12.0	284.3	-6.5	264.2	8378.4365	24023.8848	13754.7295	13838.2979	14074.7412
N1595482715	1125337.9	27.5	-10.1	318.7	-5.9	291.3	8326.1855	23049.8105	13384.1377	13370.6602	13487.9971
N1596292736	1114166.6	26.3	19.6	118.4	-5.8	111.2	6177.2969	24156.4531	13463.4600	13599.7119	13906.0293
N1597462969	1312601.9	25.3	2.7	315.3	-5.6	291.3	8818.1182	22938.3555	13488.8154	13458.1143	13546.1221
N1598767678	1106403.5	26.6	8.2	221.6	-5.3	198.7	6850.5703	22838.9395	12374.2383	12529.4854	12827.0566
N1600583981	1248525.8	27.6	-6.3	322.5	-5.0	294.8	8176.1162	22775.8262	13194.6436	13163.0215	13261.5039
N1601290596	1130962.0	27.9	4.1	239.5	-4.9	213.0	7211.2280	23326.2812	12830.5742	13000.1299	13313.2539
N1602109316	1012092.6	37.7	32.9	85.2	-4.7	84.0	5186.4556	25720.8086	12563.5195	12871.8154	13462.6123
N1602627205	1336790.0	27.1	12.1	333.5	-4.6	312.0	7971.9609	22718.1914	12634.8301	12664.8164	12843.1621
N1603316640	1029680.4	30.9	24.8	136.6	-4.5	126.6	5425.7554	24107.1602	12550.6553	12742.8691	13144.5332
N1603719993	1147329.1	21.2	-12.2	47.5	-4.5	27.5	7342.9014	23357.8398	13376.2344	13530.0723	13780.3555
N1604535789	1253768.9	31.2	15.2	264.8	-4.3	240.2	7496.8311	24252.9648	13216.1963	13399.7334	13766.4971
N1604687050	1128043.1	39.9	35.5	67.0	-4.3	68.7	5021.1631	25840.4707	12117.2822	12460.7705	13105.8311
N1605040122	1108004.8	22.6	-12.2	48.5	-4.2	27.1	7233.7554	23387.6211	13262.2773	13425.5391	13695.4639
N1605072583	1054513.8	33.3	-7.4	253.5	-4.2	220.3	6946.8145	23757.1523	12729.1904	12932.8135	13312.1436
N1605195483	1253737.5	30.3	11.5	263.7	-4.2	237.6	7777.9951	24047.3047	13292.9600	13459.0820	13793.0752
N1607327939	1078520.6	31.0	26.6	78.0	-3.8	71.6	5950.4458	25082.2734	13262.3506	13510.1924	13977.3877
N1607830802	1088861.2	33.5	-7.8	240.7	-3.7	207.2	6446.8247	23457.7617	12252.6885	12470.8945	12870.5527
N1609329583	1087686.2	36.8	-12.6	235.0	-3.5	198.9	5905.6187	23497.5566	11684.8018	11935.2910	12396.1309
N1610124049	1269819.4	39.6	-16.8	322.0	-3.3	284.1	6473.9438	23371.8535	12091.0254	12149.9463	12432.2490
N1618071421	1089035.6	33.4	-16.8	111.0	-1.9	80.6	5598.1060	24124.4531	13307.8271	13431.4697	13739.4902
N1649342285	74818.2	38.5	-1.4	143.8	3.6	105.6	4601.8169	22488.5996	11982.3057	11952.2930	12122.9062
N1733981010	987284.7	21.7	8.1	127.3	16.8	147.6	6967.9243	23215.4980	13610.1191	13681.5693	13852.1230
N1741892720	1440877.5	38.7	-9.4	51.3	17.9	79.2	5170.1465	23340.1602	12043.8730	12045.9219	12285.5420
N1751140149	1248490.4	29.5	-2.6	81.8	19.0	102.3	6230.1357	23802.8770	13604.7764	13619.8672	13807.3184
N1757516140	1014110.2	34.0	41.8	213.6	19.7	183.1	6890.5415	25904.6289	13318.1895	13754.4170	14413.9521
N1786519444	2288907.8	22.2	16.7	302.7	22.7	279.9	9723.2627	23920.6895	14866.0049	14804.9346	14837.4277
N1796432857	1986931.5	35.1	17.8	26.0	23.5	348.8	5798.1333	23127.8574	12238.9023	12302.0547	12559.7744
N1845330570	2209407.2	36.1	38.8	325.4	26.3	284.8	7427.8682	25665.2812	14306.0234	14469.5938	14845.3350
N1847383453	2237179.8	33.0	39.1	36.2	26.3	359.7	6623.8315	25729.2852	13913.9170	14234.1924	14753.5254
N1849018874	1289233.6	29.3	48.2	114.8	26.4	89.8	7448.1792	27134.0273	15771.6973	16096.2617	16603.3164

**Table 21.** Brightness estimates from clear-filter images of Epimetheus

Filename	Range (km)	Phase (deg)	Sub-S/C	Sub-S/C	Sub-Solar	Sub-Solar	$A_{\text{eff}}$	$A_{\text{phys}}$	$a_{\text{pred}}$	$a_{\text{pred}}$	$a_{\text{pred}}$
			Latitude (deg)	Longitude (deg)	Latitude (deg)	Longitude (deg)	Value		k=1	k=0.75	k=0.50
								$(\text{km}^2)$	$(\text{km}^2)$	$(\text{km}^2)$	$(\text{km}^2)$
N1564454340	3290726.2	35.7	0.2	102.2	-11.4	136.2	2377.4211	10843.6914	5896.0864	5991.3555	6178.0361
N1575054751	1876191.9	36.5	8.1	305.2	-9.5	337.3	2441.1824	10606.0703	5452.1060	5553.2422	5752.8184
N1575800491	1999183.2	23.9	9.4	116.1	-9.4	130.8	3085.0137	10715.6104	6366.2119	6423.5264	6536.9209
N1577051695	1832468.5	21.1	9.9	62.7	-9.2	71.6	3373.8743	10739.0752	6656.8516	6666.2461	6722.8457
N1577141905	1907909.6	24.0	14.3	248.9	-9.2	254.0	3560.7798	10821.0596	6570.8481	6597.0679	6682.7441
N1578545720	1936707.5	26.9	16.3	20.4	-8.9	29.8	2513.5916	10150.9297	5696.2822	5726.6514	5825.5596
N1579749784	1883149.0	37.0	23.5	30.9	-8.7	49.6	2117.9294	10441.0947	5433.1025	5473.6685	5617.6523
N1580482099	1570688.6	21.3	12.1	115.5	-8.6	120.5	3110.6165	10744.9404	6555.0938	6591.6235	6677.4932
N1580528164	1840117.9	22.2	13.0	31.9	-8.6	37.4	2827.2590	10258.7510	6044.1182	6064.4678	6137.0151
N1580652470	1905801.2	30.1	18.8	49.7	-8.5	62.4	2659.8137	10640.1279	6071.2495	6099.3809	6208.2104
N1581772048	1847311.4	31.9	22.7	289.6	-8.4	297.4	3308.5974	10964.4697	6122.3062	6192.7378	6353.8491
N1582637064	1660073.0	29.6	20.2	74.2	-8.2	82.7	2957.2468	10963.3877	6369.7432	6413.1924	6537.6694
N1584373866	1618017.4	20.8	12.9	56.4	-7.9	58.0	3091.4875	10671.7412	6508.7788	6533.7217	6606.7080
N1586079059	1277391.0	23.5	13.4	211.3	-7.6	200.9	3053.2739	10184.1455	5809.9600	5863.1372	5972.2422
N1586193734	1343066.8	33.5	25.9	168.6	-7.6	169.0	2008.1456	10228.1924	5201.0713	5282.7725	5457.8574
N1586252190	1334590.5	39.6	31.7	154.0	-7.6	159.7	1738.4790	10533.5264	5007.2651	5116.3501	5340.6294
N1586279190	1528024.4	36.8	29.2	321.5	-7.6	321.6	2506.4094	10683.3789	5423.6050	5512.3003	5708.5171
N1587717250	1486752.0	21.6	10.0	316.8	-7.3	303.7	3426.7292	10418.9395	6356.9395	6399.4805	6499.4956
N1587821171	1354488.2	31.0	23.0	213.9	-7.3	207.3	2630.3787	10407.2227	5552.1045	5630.5801	5794.2134
N1592073781	1054741.1	31.5	24.2	155.0	-6.5	147.7	2261.2397	10310.5430	5502.7163	5562.6553	5709.0166
N1595508845	1040241.1	27.9	-7.2	252.9	-5.9	224.8	3128.6216	10815.5713	6279.2759	6364.6934	6513.4951
N1596337691	991765.9	35.9	29.1	161.9	-5.8	153.1	1985.2577	10375.3076	5214.2710	5295.9214	5479.4238
N1596720629	1146727.8	29.4	-13.0	320.1	-5.7	291.2	3341.9189	10393.0635	6160.6299	6145.5483	6198.0410
N1599452243	1130365.2	22.8	15.4	118.9	-5.2	108.9	3167.6387	10727.8018	6567.8511	6585.6938	6657.0059
N1600167698	1103464.1	32.0	26.6	83.7	-5.1	79.7	2757.3462	11094.9062	6275.7432	6342.9873	6501.9756
N1601110235	933053.8	36.6	-26.8	1.7	-4.9	330.9	2023.9740	10295.8770	5250.2964	5313.4609	5475.1079
N1601198115	946166.1	22.5	-12.5	159.1	-4.9	137.6	2752.8606	10014.5176	6006.1138	5994.2583	6029.1235
N1604569794	1145838.4	32.5	21.6	214.9	-4.3	194.9	2405.4292	10392.3525	5412.0522	5509.4702	5694.9854
N1605039582	878200.8	26.7	-15.6	157.1	-4.2	132.5	2831.6426	10092.5625	5902.6025	5896.0903	5950.6855
N1607830532	1307195.1	30.0	-6.5	335.9	-3.7	305.9	2819.0298	10065.4414	5830.9590	5807.9277	5854.1226
N1610317641	1074962.0	27.5	22.7	107.0	-3.3	98.0	3072.9380	10963.8975	6494.3345	6538.4536	6655.0811
N1610356115	1202382.0	33.5	26.9	345.2	-3.3	330.2	2435.6731	10356.1777	5403.8359	5470.5317	5630.0420
N1611120087	1111970.6	33.5	16.8	258.6	-3.1	231.3	2930.9856	10938.1641	6058.9541	6153.2847	6335.1152
N1684260734	2555409.5	38.6	0.2	99.3	9.5	136.9	2442.0220	10863.4131	5750.6260	5853.9922	6057.2246
N1698204102	2146301.2	35.9	0.2	249.6	11.7	284.0	3075.7854	10761.2158	6143.9072	6172.9155	6289.2017
N1735138298	1024435.8	23.6	5.6	128.5	17.0	149.7	2789.8442	10482.6523	6155.3511	6211.7568	6320.7715
N1746446639	1416607.1	32.1	-10.0	312.6	18.4	327.6	2756.1760	10494.4404	5681.6914	5738.3042	5882.8447
N1751141839	1344849.8	28.4	-2.6	43.5	19.0	62.1	2708.5510	10379.0566	6137.4810	6118.3975	6168.6777
N1757516800	997270.1	31.2	42.5	182.2	19.7	156.9	2555.5740	10761.4043	5848.3784	5951.1201	6137.8638
N1786521124	2188447.8	22.5	17.4	262.8	22.7	239.5	4181.2017	10968.0469	6818.9399	6861.5737	6948.7935
N1796434267	1965976.5	39.7	17.9	323.2	23.5	281.1	2769.3918	10414.9873	5792.6064	5769.9727	5845.1157
N1796514548	1601802.6	25.1	13.4	65.5	23.5	41.2	2998.3516	10804.7715	6447.3022	6501.0557	6611.5654
N1843102876	2760097.2	35.5	34.7	70.5	26.2	30.1	2572.2026	11157.4072	6109.0063	6228.6929	6441.0391
N1843368138	2018244.5	25.0	33.5	207.3	26.2	179.7	2897.5396	10602.7363	6135.6392	6210.0371	6342.1304
N1845328620	2115431.0	30.3	41.0	88.6	26.3	56.4	3008.9731	11325.6035	6677.6089	6770.0552	6935.9019
N1847383943	2032029.1	36.4	44.0	179.4	26.3	139.7	2416.3079	10815.6953	5797.5098	5868.4727	6039.3354
N1849021134	1339975.6	38.6	45.5	277.8	26.4	235.5	2876.2207	11394.7754	6259.7661	6371.7935	6586.4419

**Table 22.** Brightness estimates from clear-filter images of Mimas.

Filename	Range	Phase	Sub-S/C	Sub-S/C	Sub-Solar	Sub-Solar	$A_{\text{eff}}$	$A_{\text{phys}}$	$a_{\text{pred}}$	$a_{\text{pred}}$	$a_{\text{pred}}$
	(km)	(deg)	Latitude	Longitude	Latitude	Longitude	Value		k=1	k=0.75	k=0.50
			(deg)	(deg)	(deg)	(deg)	(km <sup>2</sup> )				
N1481705814	901668.0	26.0	1.2	328.3	-23.1	318.9	58778.3984	120528.9844	72071.1719	72161.4062	72962.6797
N1488814545	1607311.0	36.1	-0.0	92.4	-22.4	63.2	48915.5898	124417.2969	69472.8047	70052.2266	71725.5547
N1488829675	1389412.9	38.3	-0.3	160.1	-22.4	127.9	43297.4219	118568.5938	64146.7969	64234.5859	65466.9531
N148881205	1509689.5	33.6	0.1	25.5	-22.4	359.8	47407.6680	119972.6641	66077.2109	66508.0078	67946.8750
N1488897255	1261645.8	28.7	-0.1	87.2	-22.4	68.7	54479.7578	124463.9375	74076.8281	74477.5938	75695.7109
N1488913065	1011333.3	30.2	-0.4	157.8	-22.4	136.5	51089.8398	118754.7812	68925.3750	68958.1172	69846.3750
N1488923681	968930.9	34.8	-0.5	211.3	-22.4	183.4	47263.4258	119611.2031	64885.4414	65408.5273	66984.3828
N1490685953	1217789.1	27.1	-0.1	73.3	-22.2	57.0	55973.9688	124187.1406	74193.6562	74603.1797	75775.0391
N1493535431	1568050.6	31.5	-19.1	87.8	-21.9	54.3	51982.8047	124988.4766	72796.9688	73410.1172	74912.5781
N1496631451	1693633.4	36.9	-19.0	100.0	-21.5	60.7	46542.9180	124733.3438	69656.1016	70284.1953	72002.0703
N1501505763	1313331.6	25.1	-18.8	31.7	-20.9	5.1	57043.0195	121423.2344	72094.4922	72548.1250	73661.9297
N1501555686	839143.4	30.9	-22.8	259.5	-20.9	226.2	56292.1523	124922.0703	72522.4844	73248.6328	74844.0312
N1506062255	1335305.0	39.0	-0.5	21.0	-20.3	346.6	42642.9023	119614.9062	62306.2266	62789.1875	64467.1523
N1506062740	1330147.4	38.7	-0.5	22.8	-20.3	348.8	42950.7266	119749.9375	62533.7500	63033.3633	64719.6875
N1506082771	992983.8	31.3	-0.2	104.1	-20.3	79.5	52520.4297	124045.0703	72811.5078	73162.2344	74411.8672
N1542758143	147700.7	36.9	-49.0	228.3	-14.9	211.1	49039.9336	125608.4531	67210.2500	68334.0156	70623.4219
N1549237751	1345972.1	33.1	-1.3	21.2	-13.9	52.2	48286.9727	119637.4844	68026.1797	68122.2969	69173.3984
N1549237807	1345781.5	33.1	-1.3	21.4	-13.9	52.4	48435.7656	119652.2344	68022.7422	68118.6797	69171.0312
N1549237867	1345574.2	33.2	-1.3	21.7	-13.9	52.7	48363.1836	119668.1641	68019.1328	68114.8750	69168.5703
N1549237927	1345364.1	33.2	-1.2	21.9	-13.9	52.9	47987.6367	119684.2188	68015.5703	68111.1094	69166.0234
N1549237987	1345151.0	33.3	-1.2	22.1	-13.9	53.2	49182.5664	119700.4141	68012.0625	68107.4766	69163.8906
N1549238047	1344935.0	33.3	-1.2	22.3	-13.9	53.4	49173.6172	119716.7344	68008.6094	68103.8828	69161.7344
N1549238107	1344716.1	33.3	-1.2	22.5	-13.9	53.7	48783.4531	119733.1719	68005.2188	68100.3828	69159.6484
N1549238167	1344494.2	33.4	-1.2	22.7	-13.9	53.9	48180.5938	119749.7422	68001.8594	68096.8906	69157.3828
N1549238227	1344269.5	33.4	-1.2	22.9	-13.9	54.2	48391.2383	119766.4375	67998.5859	68093.5625	69155.6719
N1549238287	1344041.8	33.5	-1.2	23.2	-13.9	54.5	48266.2930	119783.2656	67995.3438	68090.2656	69153.8828
N1549284728	1138140.8	35.8	9.9	235.9	-13.9	262.9	50606.1016	122558.4688	68912.2109	69199.0547	70560.5391
N1558927289	192322.6	27.9	-33.9	69.0	-12.3	49.6	56036.1797	125506.1953	74008.9766	74742.5391	76262.5625
N1558927322	192498.5	27.9	-34.0	69.0	-12.3	49.8	56174.2891	125509.1172	74043.9688	74775.5078	76291.6953
N1558927355	192674.1	27.8	-34.0	69.0	-12.3	49.9	56233.2305	125512.0547	74078.6875	74808.1797	76320.3828
N1558927388	192849.3	27.8	-34.0	69.1	-12.3	50.1	56283.0859	125515.0078	74113.1406	74840.6172	76348.9375
N1558929451	203024.0	25.5	-35.0	71.8	-12.3	59.1	58344.5352	125698.1953	75778.6641	76395.3203	77707.1719
N1558929484	203173.5	25.4	-35.0	71.8	-12.3	59.2	58460.9688	125701.0625	75798.3438	76413.5078	77722.9531
N1558929517	203322.4	25.4	-35.0	71.9	-12.3	59.4	58482.6055	125703.9375	75817.8125	76431.4922	77738.6328
N1558929550	203470.9	25.4	-35.1	71.9	-12.3	59.5	58557.5352	125706.8047	75837.1016	76449.3672	77754.3438
N1558938273	227041.5	25.4	-37.6	95.6	-12.3	97.3	58678.1562	126065.0625	76572.3828	77083.3672	78302.2266
N1558940293	228980.5	25.8	-38.0	103.8	-12.3	105.9	58102.1406	125862.3438	76061.8359	76601.4062	77864.2969
N1558941873	230158.0	26.0	-38.2	110.9	-12.3	112.6	57680.3945	125570.9062	75577.5938	76141.0859	77434.2031
N1558945693	233833.0	25.8	-38.0	130.7	-12.3	128.9	57165.6289	124321.1406	74195.3203	74791.3125	76107.5938
N1558946626	235342.1	25.7	-37.8	136.0	-12.3	132.8	56945.2500	123911.5547	73829.7578	74425.3594	75734.4922
N1558947559	237253.1	25.5	-37.4	141.4	-12.3	136.8	56936.2617	123476.1797	73460.6875	74052.8516	75350.7812
N1558948492	239645.2	25.3	-37.0	147.0	-12.3	140.8	56894.1406	123026.3281	73092.8906	73679.3984	74963.2266
N1558949673	243480.9	25.1	-36.3	154.1	-12.3	145.8	56925.7031	122460.4766	72638.7188	73216.3594	74480.7500
N1561690178	197127.0	29.7	-3.2	51.5	-11.8	22.8	50982.9258	122552.2812	70161.3672	70827.7031	72339.4609
N1564277442	2937352.5	25.6	0.1	273.7	-11.4	296.8	63248.3281	124469.0156	75660.3359	76102.7734	77211.3906
N1571997272	808128.9	34.3	-1.9	261.2	-10.1	227.6	52973.5547	124281.0234	69788.5859	70563.1875	72344.9219
N1572295234	2142000.0	20.3	1.5	86.4	-10.0	103.2	64057.4609	124470.3516	78579.6172	78825.6250	79530.9531
N1574707192	2397624.2	23.2	5.6	307.3	-9.6	324.9	60376.0195	122710.7422	74074.7891	74553.1016	75625.3281
N1575426777	800983.9	38.6	-4.0	306.8	-9.5	268.3	49590.4570	122729.3516	67585.5156	67867.7031	69288.6250
N1577180769	2048444.1	29.3	15.0	81.8	-9.2	98.5	55008.5234	124759.3281	73794.0156	74219.4609	75489.0156
N1578718039	1910226.6	37.7	23.2	34.2	-8.9	54.2	44517.3828	122070.9688	65506.8359	65980.1875	67635.9297
N1579494985	1658729.5	23.1	14.2	256.2	-8.8	253.0	65813.8047	124346.0547	76598.6719	76934.7266	7780.2266
N1579752207	1841931.5	34.4	24.3	299.7	-8.7	309.9	51361.7539	124281.3281	68640.0625	69354.6484	71150.2969
N1581734261	1921437.4	32.7	20.4	52.8	-8.4	68.6	49617.8945	123423.5938	70260.9844	70658.5469	72053.2812
N1583579754	1753459.1	29.0	20.9	312.2	-8.0	310.9	56655.8164	123041.0703	71341.0000	71826.4766	73169.8359

Table 22 continued on next page

**Table 22** (*continued*)

Filename	Range	Phase	Sub-S/C	Sub-S/C	Sub-Solar	Sub-Solar	$A_{\text{eff}}$	$A_{\text{phys}}$	$a_{\text{pred}}$	$a_{\text{pred}}$	$a_{\text{pred}}$
	(km)	(deg)	Latitude	Longitude	Latitude	Longitude	Value		k=1	k=0.75	k=0.50
			(deg)	(deg)	(deg)	(deg)	(km <sup>2</sup> )				
N1586731996	815808.3	30.3	-15.4	231.8	-7.5	201.9	53688.0000	122401.8672	69431.7266	70244.7266	71925.2656
N1587766044	1418809.1	23.2	15.8	93.2	-7.3	95.0	60746.4414	124779.9609	77016.0469	77344.0391	78285.2500
N1591211808	925518.6	27.0	-10.1	232.6	-6.7	205.5	58181.0586	122221.7500	71412.3359	72120.1719	73557.1016
N1591469930	1193306.2	34.8	22.7	286.2	-6.6	267.0	53218.2891	124913.8516	70241.7188	70764.9766	72360.9141
N1595040885	1140843.6	28.9	12.2	236.0	-6.0	213.4	55600.4570	122663.2969	70737.9453	71447.9531	72980.5625
N1595691086	1103097.5	31.6	17.8	229.3	-5.9	208.1	52012.9648	122304.7109	68473.7188	69247.6172	70962.8984
N1596985109	938317.4	39.8	32.6	182.3	-5.7	170.6	42082.9453	120984.0312	61060.6719	61942.3516	64088.5391
N1598214937	1046732.2	35.0	22.5	228.1	-5.4	206.5	48618.7656	122559.2109	66215.8359	67087.5703	69042.2266
N1598254468	1245657.1	29.4	23.2	28.5	-5.4	21.4	51482.7852	121614.7031	69041.1719	69669.8750	71168.4766
N1598893062	1253109.4	32.5	22.9	338.2	-5.3	321.8	50098.8555	121131.4844	67677.8594	68142.9766	69589.3828
N1599459466	1349192.2	28.2	13.5	327.0	-5.2	305.7	56502.2734	121116.1641	71467.2891	71647.6484	72612.8047
N1599497506	1054981.8	29.6	23.7	124.7	-5.2	118.3	52865.3125	123343.0234	71848.3984	72301.2344	73630.3750
N1599545927	1218440.1	33.7	25.2	343.0	-5.2	328.0	48858.2539	121153.2812	66500.3438	67058.0000	68651.1953
N1602673569	1050695.5	28.7	22.9	126.4	-4.6	118.1	54172.0898	123122.2578	72293.6875	72702.0781	73947.8516
N1610948468	1332400.1	33.9	-16.2	10.2	-3.2	338.3	48277.6016	119812.1406	65663.3906	66159.6172	67663.2500
N1622060187	808080.5	26.0	19.9	154.3	-1.2	138.7	55983.3359	120185.1719	71242.6406	71517.2734	72499.7031
N1623375817	737713.9	38.7	34.1	211.2	-0.9	193.6	44176.4766	122471.2188	62875.0898	63892.1250	66140.5547
N1855871395	186252.2	20.6	20.6	175.7	26.6	197.3	63497.9102	119185.3125	73447.6016	73525.6797	74083.8438
N1855877635	181436.5	27.5	-0.0	216.3	26.6	223.9	58780.7969	120149.1094	71238.2812	71331.8359	72195.6172
N1855878190	183863.3	29.1	-1.8	219.6	26.6	226.2	57425.1992	120528.7344	70589.8359	70736.6875	71720.8281
N1855880814	200130.1	36.4	-9.7	234.0	26.6	237.4	50928.5117	122353.8281	67149.5703	67542.4922	69076.6875

**Table 23.** Brightness estimates from clear-filter images of Enceladus.

Filename	Range	Phase	Sub-S/C	Sub-S/C	Sub-Solar	Sub-Solar	$A_{\text{eff}}$	$A_{\text{phys}}$	$a_{\text{pred}}$	$a_{\text{pred}}$	$a_{\text{pred}}$
	(km)	(deg)	Latitude	Longitude	Latitude	Longitude	Value		k=1	k=0.75	k=0.50
			(deg)	(deg)	(deg)	(deg)	(km <sup>2</sup> )				
N1477565247	765619.5	33.6	4.8	269.2	-23.6	250.8	129597.7109	200214.7812	114034.1094	114808.4453	117213.5234
N1481509793	1980087.2	38.1	-3.6	37.2	-23.2	3.3	112414.9297	198977.5781	107244.1953	108142.8125	110943.3359
N1481706474	671641.8	31.8	1.9	262.1	-23.2	242.0	134909.2031	200088.9375	115689.9297	116444.5000	118710.9219
N1488878396	1267780.9	29.5	-0.2	107.2	-22.4	87.3	131631.8125	199811.5156	118290.2266	118853.9844	120768.7969
N1490643112	1433963.0	30.3	-0.2	73.8	-22.2	52.4	131019.1172	200326.0312	117010.0703	117714.7188	119840.6875
N1490687213	978323.2	38.4	-0.2	219.8	-22.2	187.5	113043.2344	197782.8125	105885.6484	106861.8672	109754.1641
N1495039341	1616055.4	38.8	-20.1	140.7	-21.7	99.0	109264.4844	198342.5156	108068.6719	108744.9062	111325.3438
N1499868413	1547410.6	29.0	-18.2	51.8	-21.1	21.1	133408.5625	200039.6406	117567.9141	118313.5156	120384.3125
N1501504263	1398906.6	32.4	-17.5	349.5	-20.9	315.4	127095.5000	198437.7969	113908.2109	114500.0703	116622.1797
N1502971691	1461577.5	36.7	-21.5	135.8	-20.7	96.4	114585.1250	198719.9844	110699.1016	111351.0156	113779.3359
N1507580980	1322266.9	39.6	-0.3	105.5	-20.1	70.5	110396.4297	199874.6719	107714.0391	108624.1719	111502.2266
N1516160530	149649.2	23.0	-0.4	223.0	-18.9	236.9	154650.1875	198001.8594	122308.2188	122591.4688	123804.0156
N1516160576	149625.8	23.0	-0.4	223.1	-18.9	237.0	154612.8906	198010.0469	122306.8438	122590.6562	123804.6797
N1516160622	149602.9	23.0	-0.4	223.2	-18.9	237.2	154736.3594	198018.0000	122305.3125	122589.6328	123805.1328
N1516160668	149580.5	23.0	-0.4	223.3	-18.9	237.3	154336.7656	198025.9844	122303.6797	122588.4375	123805.1953
N1516160714	149558.6	23.1	-0.4	223.4	-18.9	237.4	155010.6250	198034.3125	122301.9609	122587.1328	123805.2109
N1516168806	152570.7	28.8	-0.1	240.0	-18.9	262.2	142343.0469	199158.2188	118600.7656	119079.4766	120854.5391
N1516171418	156203.1	32.2	-0.0	243.5	-18.9	270.2	135236.2969	199359.5625	115447.5938	116050.2188	118169.9297
N1549135567	1176560.2	20.4	-25.4	37.8	-13.9	55.8	152122.7188	199817.1250	125137.1797	125491.2266	126614.1406
N1559168830	1677419.8	29.7	3.0	295.2	-12.2	320.9	133316.9062	200170.6250	117011.6875	117776.6875	119919.7812
N1563700852	489283.9	26.5	-0.3	85.3	-11.5	61.1	139339.8438	200277.8125	120824.3672	121447.9609	123224.7188
N1563702378	485300.2	25.6	-0.3	88.9	-11.5	65.7	142057.7188	200193.2031	121724.5000	122307.2422	123978.1641

*Table 23 continued on next page*

**Table 23** (*continued*)

Filename	Range	Phase	Sub-S/C	Sub-S/C	Sub-Solar	Sub-Solar	$A_{\text{eff}}$	$A_{\text{phys}}$	$a_{\text{pred}}$	$a_{\text{pred}}$	$a_{\text{pred}}$
	(km)	(deg)	Latitude	Longitude	Latitude	Longitude	Value		k=1	k=0.75	k=0.50
			(deg)	(deg)	(deg)	(deg)	(km <sup>2</sup> )				
N1564621004	3749622.8	34.0	0.2	305.9	-11.3	338.1	123905.3359	199783.3281	112144.2266	113050.7812	115609.0547
N1564967686	4019247.5	39.6	0.2	273.8	-11.3	311.9	112378.3594	200258.6094	107138.4062	108215.3359	111278.1094
N1567638903	2514086.5	27.1	-3.4	128.2	-10.8	154.6	133804.3125	198633.8281	118069.9844	118828.9531	120783.0625
N1567745224	2909583.8	31.1	-3.5	87.5	-10.8	118.0	127971.3125	200250.7188	116677.1953	117452.9766	119665.9219
N1572036346	912788.0	22.3	-0.8	225.1	-10.1	204.6	151860.7500	198151.5938	121733.8750	122303.5859	123759.8281
N1572040347	971851.9	23.1	-0.7	237.9	-10.1	216.7	151010.3281	199028.4062	122031.8281	122642.3047	124185.7812
N1579493845	1489229.0	24.5	15.8	199.2	-8.8	199.4	146234.9844	197007.8750	118966.9922	119505.0625	121085.2266
N1580702134	1797818.5	30.8	22.1	269.4	-8.5	272.6	136464.8906	200718.1406	116858.6562	117594.1172	119795.8047
N1581735341	1611871.5	35.5	24.6	161.4	-8.4	174.8	117347.3750	197615.9219	108357.0859	109332.3594	112063.2188
N1584378959	1660130.6	23.3	12.9	302.5	-7.9	291.9	152705.5469	200084.5000	123016.2578	123447.4766	124846.7734
N1585072145	862903.2	38.6	-13.8	278.9	-7.8	240.0	117185.0938	200520.8906	108840.6172	109847.5391	112755.8672
N1586300953	1602952.4	37.2	28.9	7.8	-7.6	15.5	115637.6328	199222.2031	107692.7578	108705.7812	111597.2109
N1586729956	926055.4	36.3	-14.0	277.0	-7.5	240.6	123887.1875	200517.3438	111409.5625	112356.2891	115065.2422
N1587764964	1242181.6	25.6	18.2	148.9	-7.3	147.8	138931.8594	197746.1250	118804.6641	119385.2578	121077.6172
N1588491089	1080486.1	22.2	5.6	213.9	-7.2	195.7	149748.5156	197425.3906	121142.4219	121680.4844	123099.3594
N1589201008	736862.4	35.9	-18.8	229.1	-7.0	194.2	120087.5547	198888.7031	109173.4766	110273.1016	113134.3672
N1589212774	908585.8	36.1	-13.1	266.0	-7.0	229.8	123555.3594	200351.1562	111114.7422	112140.4844	114926.8828
N1591135607	940857.3	31.8	-20.4	345.1	-6.7	315.5	128406.8750	198710.7031	114257.1719	114924.0781	117093.3594
N1591210668	836004.9	25.7	-11.8	210.2	-6.7	184.6	142386.6719	197372.5781	118102.1484	118770.5625	120545.4062
N1591250208	1342924.1	23.9	-2.9	327.7	-6.7	304.0	148469.3906	198730.9375	121875.8125	122214.2266	123530.5547
N1591471010	1163622.5	37.1	23.2	278.4	-6.6	255.8	122601.6250	200837.5000	110316.7891	111250.1641	114034.2734
N1591816252	938477.6	33.5	-12.3	259.3	-6.6	225.8	129601.8281	200175.9375	113572.5547	114547.4922	117123.0312
N1592112354	1237899.1	30.1	23.6	44.3	-6.5	45.1	132195.4062	199972.6562	116236.1719	116992.5078	119173.0625
N1592801699	1019036.1	39.3	32.2	348.9	-6.4	341.1	110745.3281	199549.5000	105519.6250	106615.5391	109714.7031
N1593021181	1072960.9	32.4	-14.0	320.9	-6.4	288.9	129830.5703	199313.5625	114713.5312	115322.4609	117465.8750
N1595041857	1457797.1	25.5	9.5	333.0	-6.0	312.6	144952.6875	198611.1875	120100.7344	120533.9453	122062.6406
N1595692058	1053161.6	25.2	18.6	136.1	-5.9	129.9	140982.8281	198548.3906	120162.3359	120684.8438	122296.8594
N1596059680	686372.9	32.3	-23.2	196.2	-5.8	167.9	124764.4609	197414.2500	111901.4766	112751.9297	115141.2734
N1596296064	963572.9	32.1	23.4	180.4	-5.8	166.6	126398.7188	197162.5312	111774.1562	112591.7734	114947.1953
N1596811827	1375734.8	27.1	0.9	320.8	-5.7	294.4	142593.0625	199064.7656	119491.6641	119922.4141	121541.8359
N1596986348	1027932.5	35.0	29.3	102.3	-5.7	104.9	120996.7344	200771.0625	112328.5312	113232.5703	115878.4375
N1597673913	1113221.8	37.0	31.4	32.8	-5.5	35.0	115062.0312	200037.2188	108724.2578	109747.1875	112637.5469
N1597676553	1087531.0	38.1	32.4	38.8	-5.5	43.0	112978.0391	200314.7188	107745.4219	108789.5000	111771.9531
N1598216617	1156673.9	36.8	20.4	272.8	-5.4	246.1	122909.6641	200696.3594	110534.9844	111501.9219	114295.4609
N1598681021	1047397.7	33.0	-6.1	251.5	-5.4	218.2	128614.4219	199790.5781	113545.6797	114529.0234	117083.9844
N1599494986	947823.4	35.0	25.8	189.6	-5.2	172.9	120745.6094	197471.3125	108838.6719	109789.2031	112460.7969
N1599803748	739329.2	35.2	-37.7	45.5	-5.2	30.8	120927.4219	200897.5469	111283.7969	112374.4219	115216.3750
N1599889729	1178204.8	34.6	-14.9	326.7	-5.1	292.9	125734.3359	199076.1719	112138.2656	112813.1016	115166.3516
N1600087730	987528.0	29.8	17.3	195.0	-5.1	175.2	131393.7969	196951.4844	113934.8125	114682.8984	116814.5938
N1600605774	1383018.2	26.7	-2.8	336.6	-5.0	309.9	140801.5156	198333.3594	119112.7891	119536.1406	121120.2344
N1601293799	1208415.9	32.8	4.3	273.9	-4.9	242.4	132034.0625	200284.7500	114943.9766	115776.8594	118156.8750
N1601984104	998819.4	30.0	14.8	204.1	-4.8	181.1	130939.2969	197175.7656	113923.8438	114705.6250	116879.8047
N1601986924	1014384.9	31.5	15.0	214.4	-4.8	189.7	128730.3047	197770.3906	112896.9844	113775.8281	116142.2656
N1602675009	1009053.4	29.1	23.9	127.2	-4.6	121.2	132272.7812	199375.8438	117317.8359	117991.6250	120015.2500
N1603338793	1312098.5	30.2	21.5	355.1	-4.5	339.5	131450.3125	198620.7812	114994.3672	115727.1328	117808.8672
N1603681816	1146257.1	36.4	-17.5	337.5	-4.5	302.8	117884.1797	198762.0156	109776.1875	110524.1484	113061.0234
N1605089006	1233133.4	35.3	-3.9	297.1	-4.2	261.7	124952.8516	200120.2188	112404.5234	113125.5703	115539.9062
N1610947328	1115921.6	26.6	-20.0	94.0	-3.2	72.9	139540.6406	200578.7969	121031.8203	121661.0156	123450.1562
N1611847879	1377466.5	34.2	-3.5	326.4	-3.0	292.1	125558.4297	198801.3125	112465.6094	113090.4453	115364.1875
N1611854902	1414371.0	30.5	-2.2	343.8	-3.0	313.3	129547.5781	198075.0000	115330.1797	115871.5156	117821.0312
N1613706388	986633.1	36.1	-4.6	218.5	-2.7	182.4	119676.2812	197721.8281	108093.8828	109105.5703	111887.9609
N1613828792	1014094.2	37.7	27.6	218.2	-2.6	194.7	117388.8438	198774.2812	106694.9375	107839.8828	110875.8281
N1613833911	1054902.1	39.1	27.7	236.0	-2.6	210.4	114633.1484	199770.2969	106188.4453	107388.3828	110559.6250
N1613840631	1120999.6	39.7	27.5	257.8	-2.6	231.0	114820.5859	200689.7656	106777.6406	107932.9297	111092.7344
N1614869680	1056841.9	31.2	28.4	123.5	-2.5	118.9	127586.5156	199841.8125	115547.7578	116322.4766	118587.6250

Table 23 continued on next page

**Table 23** (*continued*)

Filename	Range	Phase	Sub-S/C	Sub-S/C	Sub-Solar	Sub-Solar	$A_{\text{eff}}$	$A_{\text{phys}}$	$a_{\text{pred}}$	$a_{\text{pred}}$	$a_{\text{pred}}$
	(km)	(deg)	Latitude	Longitude	Latitude	Longitude	Value		k=1	k=0.75	k=0.50
			(deg)	(deg)	(deg)	(deg)	(km <sup>2</sup> )				
N1618208220	1013731.2	34.5	21.5	216.2	-1.9	190.2	123554.8984	198237.7656	109940.4844	110959.4141	113665.1562
N1660446193	93578.1	31.0	8.9	64.3	5.6	95.4	135453.8125	200219.9844	116853.2891	117458.0703	119487.3281
N1693385375	2384859.8	38.2	0.2	130.4	11.0	167.3	109497.1719	198468.7500	106366.4531	107470.8906	110477.0625
N1708809612	1655276.1	38.8	0.3	228.1	13.3	265.0	117182.6719	198366.4219	108013.7656	108711.0312	111312.4609
N1823501498	121421.5	27.3	0.7	155.3	25.4	143.1	141428.5000	196821.3281	117500.7109	117881.9531	119473.5078

**Table 24.** Brightness estimates from clear-filter images of Tethys

Filename	Range	Phase	Sub-S/C	Sub-S/C	Sub-Solar	Sub-Solar	$A_{\text{eff}}$	$A_{\text{phys}}$	$a_{\text{pred}}$	$a_{\text{pred}}$	$a_{\text{pred}}$
	(km)	(deg)	Latitude	Longitude	Latitude	Longitude	Value		k=1	k=0.75	k=0.50
			(deg)	(deg)	(deg)	(deg)	(km <sup>2</sup> )				
N1477564227	668321.5	34.3	5.5	108.6	-23.6	127.2	467384.2500	888561.6875	501631.5938	505492.8750	516790.9688
N1481443192	2092752.0	38.5	-5.2	82.3	-23.2	46.9	418260.5312	890977.5000	482936.9062	487384.6250	500435.1562
N1488790300	1703386.8	35.0	-0.2	87.5	-22.4	59.7	453760.6875	890506.1250	500846.7188	504735.3750	516249.4062
N1488792254	1675049.4	34.9	-0.2	91.7	-22.4	64.0	452431.1562	890194.3750	501912.9062	505747.7500	517133.7812
N1488822445	1311927.4	38.4	0.0	162.6	-22.4	130.6	428045.9062	875014.5000	474645.6562	477596.4375	488958.7188
N1488925841	1396850.2	28.3	-0.4	17.0	-22.4	358.8	497584.6562	882233.8125	521838.3750	524370.2500	532586.0625
N1490557912	1967571.0	39.0	-0.3	33.5	-22.2	0.3	409800.2500	884963.8750	473073.0312	477229.9375	490086.0312
N1493533631	1427707.1	28.7	-21.0	117.6	-21.9	86.8	514314.7812	887667.5625	530566.8750	532909.5000	540927.2500
N1495251742	1033161.4	31.4	-18.6	311.5	-21.7	278.1	456368.3750	888833.3125	517746.8125	520331.3438	529449.4375
N1496638951	1490964.0	35.4	-21.2	137.4	-21.5	99.3	453459.3438	882876.6250	497749.6562	500517.2500	510863.5625
N1499721172	1831862.2	39.4	-18.5	102.8	-21.1	60.9	414988.3750	890073.7500	480800.4688	485146.9062	498193.5938
N1499869493	1549904.4	26.5	-18.2	56.2	-21.1	28.2	519526.4688	890003.2500	534405.6250	537350.3125	545469.3125
N1506049675	1499477.4	39.2	-0.4	20.6	-20.3	346.0	403768.5000	882720.0000	471013.4062	474991.9688	487694.7500
N1506065851	1321774.1	32.4	-0.3	47.8	-20.3	21.7	467339.3125	887831.6250	506933.7188	510482.1250	520950.7500
N1563760839	1000148.8	36.0	0.0	293.7	-11.5	259.3	407339.3750	890593.1250	497138.9062	500583.2500	511809.5312
N1564276362	3043398.8	24.2	0.2	295.5	-11.4	317.0	487072.5000	890401.5000	543915.8750	546476.0625	553540.5000
N1564451143	3520473.8	30.0	0.2	314.8	-11.4	342.6	481607.0000	887319.6875	516961.7812	520324.8750	529876.6250
N1564622084	3861526.5	34.5	0.2	327.1	-11.3	359.9	444622.1250	884858.3750	494673.6562	498459.7812	509713.8750
N1564769865	3918099.8	35.7	0.3	292.0	-11.3	326.0	422411.9375	890739.5625	494278.5000	498560.7812	510688.6875
N1572062107	1049403.5	21.0	-0.3	237.0	-10.0	218.3	553479.0625	885288.0625	551194.3750	553532.4375	559438.2500
N1572471790	2828057.8	24.4	1.7	20.8	-10.0	42.3	539196.3125	882755.9375	538944.6250	540681.9375	546959.6250
N1572811538	3169973.5	34.9	2.5	39.2	-9.9	72.0	450751.6562	886144.3125	498790.5312	501752.4688	512288.6562
N1574708272	2339555.8	21.0	5.9	283.5	-9.6	297.7	535726.1875	891125.4375	557506.6875	559455.3750	564986.1250
N1574928113	2327952.8	37.3	6.5	29.1	-9.5	62.8	425920.0312	884297.8125	485541.5000	488812.8438	500299.5312
N1575051894	1965435.1	33.2	7.9	307.6	-9.5	336.0	451203.0312	888800.8750	503662.8438	507558.0000	518588.7188
N1575192415	11771715.6	40.0	11.4	251.8	-9.5	286.1	375726.9062	888835.8750	477377.2500	481535.0000	494557.0938
N1577178609	2295874.0	24.0	13.3	340.8	-9.2	349.2	528141.6250	883312.1875	538203.6250	540497.4375	547250.1250
N1579492705	1894393.1	23.2	12.1	45.7	-8.8	55.8	553837.1875	887814.0625	546736.6250	548589.7500	554678.0000
N1579754367	1728798.9	35.2	26.1	267.8	-8.7	273.3	413709.1562	891783.6875	500395.2500	504132.5938	515598.1250
N1580394511	1362788.2	22.8	6.5	263.1	-8.6	245.9	499634.3125	890060.2500	551733.1875	553991.3125	560303.1250
N1580701054	1553137.9	35.4	25.8	193.5	-8.5	202.4	436773.8125	878153.3125	485207.9688	489067.6250	500663.4688
N1583582754	1723146.5	32.4	21.1	67.2	-8.0	81.6	477289.5312	891419.5000	512812.4688	516001.1250	526118.0000
N1584662821	1625371.4	38.7	30.8	302.8	-7.8	305.1	395373.8125	891344.2500	479795.9375	484227.0625	497380.9062
N1586213473	1338132.1	37.2	27.8	115.2	-7.6	127.0	447423.1250	888906.3125	486566.9062	490938.5938	503572.0312
N1586298793	1582556.5	37.1	29.4	318.9	-7.6	315.3	409567.6250	889027.8125	485896.2188	490064.3750	502504.0312
N1586730976	702897.2	34.5	-18.2	222.7	-7.5	189.0	455797.4688	882477.3125	491972.8438	496416.6875	508311.5312
N1586898931	1148338.0	26.2	14.1	214.7	-7.4	199.7	516337.6562	879830.0625	526693.7500	529621.3750	537629.0000
N1586899290	1151134.2	26.3	14.1	215.6	-7.4	200.5	518410.5000	880075.4375	526524.0000	529476.2500	537536.3125

*Table 24 continued on next page*

**Table 24** (*continued*)

Filename	Range	Phase	Sub-S/C	Sub-S/C	Sub-Solar	Sub-Solar	$A_{\text{eff}}$	$A_{\text{phys}}$	$a_{\text{pred}}$	$a_{\text{pred}}$	$a_{\text{pred}}$
	(km)	(deg)	Latitude	Longitude	Latitude	Longitude	Value		k=1	k=0.75	k=0.50
			(deg)	(deg)	(deg)	(deg)	(km <sup>2</sup> )				
N1587593182	1279437.5	27.6	-5.0	319.4	-7.3	291.7	491210.0938	886467.1875	531071.5625	533131.8125	540640.8750
N1589213854	1090554.6	36.0	-10.4	304.5	-7.0	268.2	416135.0000	889418.9375	496498.2500	499677.2188	510653.6562
N1589413295	1630780.4	21.7	12.4	358.1	-7.0	348.3	553948.0625	881899.0625	545495.4375	547353.7500	553020.1875
N1590790905	988218.8	27.0	19.7	153.9	-6.8	148.4	534075.7500	878723.5000	523941.7812	526539.6250	534464.7500
N1592455257	970072.6	34.3	-8.2	255.8	-6.5	221.3	439097.6562	889323.2500	501259.3750	505689.5312	517472.7188
N1595558389	1117422.8	33.3	0.3	261.9	-5.9	229.2	439724.0625	889871.0000	507580.0938	511696.0000	522865.0625
N1596298109	1284544.6	23.1	17.3	61.7	-5.8	61.5	561091.6875	890632.8125	549073.8125	551203.0625	557549.8125
N1598019456	1197212.8	36.5	-8.6	296.9	-5.5	260.2	406192.4688	890377.8125	494865.2188	498300.8438	509623.5938
N1598253098	1236345.6	28.5	23.0	54.1	-5.4	55.8	508879.4375	890118.1875	527238.3125	530164.8750	538894.5625
N1598682461	1337754.0	32.0	-4.4	315.5	-5.4	283.3	453005.0312	887242.3750	513198.9062	515840.0000	525227.2500
N1598854842	1390686.5	31.8	17.0	326.6	-5.3	303.7	456067.5938	885988.0000	511150.0938	514027.1250	523627.3438
N1599456826	969621.1	34.7	19.0	217.3	-5.2	192.1	448229.4062	881193.0000	490088.1875	494400.9688	506231.2812
N1601295239	1421025.2	30.7	3.9	318.5	-4.9	289.1	464534.3438	886620.7500	518407.1562	520879.6875	529702.0000
N1603336033	970084.7	33.8	29.3	111.2	-4.5	112.7	475878.3438	889783.7500	504872.2812	508539.2812	519542.0938
N1604522002	1107237.4	35.7	15.4	239.9	-4.3	209.9	428239.0312	886624.1875	490409.3438	495075.9062	507540.6562
N1605865051	1443273.5	31.5	8.1	322.8	-4.1	293.7	459509.7188	885939.1250	514073.7500	516677.4375	525866.6875
N1610260144	1323622.2	35.7	8.3	306.6	-3.3	272.7	415483.7812	888996.3125	497140.5625	500286.3125	511226.6562
N1613705368	1466112.6	32.0	-3.4	347.7	-2.7	315.6	469954.5000	881772.8125	507423.7188	510138.6875	519568.7812
N1618206780	930931.6	33.2	23.4	191.3	-1.9	169.2	469363.0625	877286.3125	494543.7500	498266.0000	509079.3750
N1623377197	1013717.6	26.1	24.2	51.9	-0.9	59.2	532072.3750	889929.8750	537093.1250	539610.5625	547228.0000
N1784050563	1811672.9	22.3	0.3	28.3	22.5	31.1	575617.5625	883990.6875	546504.6875	548108.1875	553691.0000
N1784050696	1810629.4	22.3	0.3	28.5	22.5	31.4	570253.6875	884027.0000	546476.6875	548082.1875	553673.4375
N1784050829	1809580.6	22.4	0.3	28.7	22.5	31.7	563898.5000	884074.6875	546448.6250	548056.1250	553654.3125
N1784050962	1808526.8	22.4	0.3	29.0	22.5	32.0	563262.0625	884125.0000	546420.3125	548030.1875	553637.1250
N1784051095	1807467.6	22.4	0.3	29.2	22.5	32.3	562918.5000	884166.0625	546391.1875	548003.3125	553617.9375
N1784051228	1806403.4	22.4	0.3	29.5	22.5	32.6	563307.3750	884200.6250	546361.6875	547976.1250	553599.2500
N1807427023	208936.3	32.7	-0.6	159.2	24.4	137.5	507875.7500	875625.1250	501314.0938	503732.2500	513034.8125
N1858896258	600407.9	36.9	34.4	359.7	26.6	317.5	440398.1562	886395.4375	487943.7188	491621.4062	503397.8750
N1858896977	596710.5	35.5	33.9	359.6	26.6	319.1	454590.5625	886277.8750	494619.2500	498126.1250	509347.5625

**Table 25.** Brightness estimates from clear-filter images of Dione.

Filename	Range	Phase	Sub-S/C	Sub-S/C	Sub-Solar	Sub-Solar	$A_{\text{eff}}$	$A_{\text{phys}}$	$a_{\text{pred}}$	$a_{\text{pred}}$	$a_{\text{pred}}$
	(km)	(deg)	Latitude	Longitude	Latitude	Longitude	Value		k=1	k=0.75	k=0.50
			(deg)	(deg)	(deg)	(deg)	(km <sup>2</sup> )				
N1477563207	1170144.5	28.2	3.0	343.0	-23.6	333.3	370990.3125	995340.3750	592636.1250	595648.3750	605015.7500
N1490685593	809791.7	29.7	-0.3	165.6	-22.2	145.0	420229.0312	987021.1250	580514.4375	583542.4375	593330.8750
N1493443511	2022987.0	35.6	-16.2	59.5	-21.9	22.2	384033.1875	994090.6875	554967.2500	558834.2500	571424.5625
N1493490431	1483911.4	31.6	-21.4	127.9	-21.9	93.8	440784.8438	989768.0000	574031.2500	577404.6250	588149.5625
N1495082541	1947127.1	34.5	-15.8	32.5	-21.7	356.6	373174.8438	995271.3125	562407.0000	566208.2500	578319.3750
N1496541751	1899698.2	38.0	-17.9	97.9	-21.5	57.6	382418.9688	991109.1250	540685.9375	545129.3125	558951.5000
N1498185942	1845955.9	33.4	-17.6	75.2	-21.3	39.9	411062.7188	992851.3125	566026.3125	569668.1875	581332.3750
N1499867332	1303523.9	21.4	-21.9	102.0	-21.1	79.0	468760.2812	991185.3750	619325.9375	621271.0000	627294.8750
N1501604957	288094.3	37.3	-43.3	239.5	-20.9	203.5	317982.9375	992150.6875	543207.5000	547919.8750	561828.8750
N1501609726	273323.9	39.9	-41.3	251.5	-20.9	210.8	288696.3750	992566.5000	528932.3125	533965.6250	548955.6250
N1502914991	1869133.6	35.7	-17.7	75.0	-20.7	37.3	394480.3125	992874.8750	554019.0625	557983.9375	570690.9375
N1506008652	1337262.9	34.6	-0.3	94.7	-20.3	65.8	411185.1562	990455.3750	558488.0000	562471.2500	574799.9375
N1506043051	919843.0	36.8	-0.4	150.0	-20.3	118.3	400936.4375	987708.1875	544880.1875	548891.8750	561918.5625
N1506051828	846839.1	39.6	-0.4	166.7	-20.3	131.6	373850.3750	986984.1875	528447.3125	532833.4375	547051.1875

*Table 25 continued on next page*

**Table 25** (*continued*)

Filename	Range	Phase	Sub-S/C	Sub-S/C	Sub-Solar	Sub-Solar	$A_{\text{eff}}$	$A_{\text{phys}}$	$a_{\text{pred}}$	$a_{\text{pred}}$	$a_{\text{pred}}$
	(km)	(deg)	Latitude	Longitude	Latitude	Longitude	Value		k=1	k=0.75	k=0.50
			(deg)	(deg)	(deg)	(deg)	(km <sup>2</sup> )				
N1507717036	293406.1	21.9	-0.5	136.1	-20.1	146.0	529361.5000	988559.7500	614603.1250	616657.8125	622970.2500
N1514072486	655567.9	20.0	-0.5	91.6	-19.2	98.7	542196.5625	990477.1875	623476.6250	625234.3750	630682.1250
N1514076806	599824.7	21.2	-0.5	95.1	-19.2	105.3	474117.4062	990445.1875	619016.1250	620966.9375	626981.1875
N1514090211	435454.3	27.9	-0.6	104.5	-19.2	125.7	481039.1875	990247.3125	590981.4375	594019.4375	603254.8750
N1532405126	262241.2	30.3	6.8	299.4	-16.6	280.0	312744.2812	993844.2500	580596.1875	583907.9375	594227.8750
N1559169910	1823477.8	27.7	2.8	312.2	-12.2	335.6	363495.9375	994598.6250	594422.2500	597192.5625	606122.3750
N1564278522	2571333.8	30.9	0.1	162.4	-11.4	191.4	416955.0312	987129.8750	573560.6875	576980.0000	587579.1250
N1567746304	3195293.2	31.1	-3.2	38.6	-10.8	69.1	432631.8438	994956.8125	577110.0000	580753.8750	591715.7500
N1572293974	1865959.6	22.6	1.5	131.4	-10.0	150.9	513294.4375	988863.4375	611762.3125	614050.1250	620811.1250
N1572461561	2876342.0	25.0	1.7	23.4	-10.0	45.6	459496.1875	995271.9375	606250.3750	608928.2500	616887.3750
N1573329282	2549491.8	38.0	3.9	250.8	-9.8	286.3	252868.5156	990092.1875	540403.3125	544807.0625	558557.9375
N1574706112	1942190.4	23.9	6.9	204.8	-9.6	222.1	400248.5938	987519.3125	606075.4375	608308.1875	615440.2500
N1574925233	1722094.9	37.5	9.0	163.0	-9.6	195.7	360585.7188	987253.8750	539278.4375	543650.0000	557249.7500
N1576429623	1898161.0	38.0	18.2	298.3	-9.3	324.9	280827.6250	993996.8750	540896.2500	545286.5625	559135.2500
N1577179689	2384378.5	25.8	12.8	12.8	-9.2	26.6	438397.6875	995475.3125	603325.1250	606072.9375	614382.0625
N1578106537	304693.9	37.9	-25.2	33.3	-9.0	357.2	359710.7500	995511.3750	543492.0000	547867.9375	561634.0625
N1578108379	325606.5	36.1	-25.7	33.7	-9.0	0.0	373531.8750	995518.1875	553598.1250	557728.1875	570696.6250
N1578108472	326649.0	36.0	-25.7	33.7	-9.0	0.1	375209.8438	995518.1250	554096.2500	558213.6875	571141.6250
N1578108565	327690.3	35.9	-25.7	33.7	-9.0	0.3	375699.1875	995517.8750	554593.2500	558698.1250	571584.6875
N1578108658	328730.2	35.8	-25.8	33.8	-9.0	0.4	376476.9688	995517.5625	555089.1250	559181.5625	572027.8125
N1578108751	329768.6	35.7	-25.8	33.8	-9.0	0.6	377344.7188	995517.2500	555583.6875	559663.6875	572469.6250
N1579753287	2064658.9	31.7	21.4	333.5	-8.7	343.6	348140.4375	995534.7500	575841.5000	579426.1875	590504.3750
N1580393611	1304242.9	25.4	6.5	259.0	-8.6	238.5	337615.1875	990408.1875	602145.2500	604829.6250	612885.8750
N1581192726	210117.5	20.2	-21.6	358.5	-8.5	14.4	487487.4688	995732.9375	626206.4375	628095.7500	633734.1875
N1583753395	1672450.1	38.0	30.0	310.4	-8.0	311.8	278688.8438	995133.1250	541075.8750	545696.5625	559784.4375
N1583754475	1677033.9	37.9	29.9	311.8	-8.0	313.5	281202.7500	995186.1875	541453.3750	546063.0625	560123.0625
N1585073225	508056.2	28.6	-23.6	185.9	-7.8	161.1	443930.6562	987943.2500	584989.4375	588143.5000	597734.1250
N1588490669	1631241.4	21.0	3.7	340.0	-7.2	322.0	417211.5312	995316.3125	622349.1250	624392.5000	630434.6250
N1590793065	1103747.5	38.1	17.9	256.1	-6.8	226.7	269644.9688	990818.2500	538439.2500	543090.6875	557173.8125
N1592454837	1048199.9	39.4	-7.9	275.6	-6.5	235.9	251316.7656	991445.2500	532161.5000	536895.8750	551398.4375
N1593193982	1455349.2	31.7	7.3	309.4	-6.3	280.7	302771.9688	994482.4375	573613.0000	577268.6875	588446.1250
N1595042829	1056934.6	36.9	13.3	246.6	-6.0	214.9	286936.5938	990133.5625	544996.0625	549500.5000	563045.8750
N1595693030	989213.4	25.9	20.0	123.1	-5.9	124.5	497908.0312	989948.8750	599290.0000	602023.2500	610312.3750
N1596297444	1524967.9	27.9	14.7	343.2	-5.8	324.1	377125.7188	995484.2500	593782.6875	596911.7500	606282.3125
N1598251778	1273197.8	28.3	22.4	53.3	-5.4	58.6	455459.5312	994660.6875	590345.0625	593534.3750	603122.5000
N1598893602	1408063.2	33.2	20.6	336.6	-5.3	315.5	325258.0312	995557.0000	567956.7500	571935.3750	583865.9375
N1598930022	1324568.0	30.4	25.0	14.2	-5.3	10.8	396969.8125	995790.4375	582334.9375	585790.0000	596334.7500
N1599990954	873871.5	32.5	0.0	218.2	-5.1	186.1	362762.7188	988202.2500	566558.0625	570358.7500	581822.5625
N1599990987	874102.5	32.5	0.1	218.2	-5.1	186.1	363639.7812	988209.8750	566482.0000	570284.6875	581755.3750
N1599991735	879410.3	32.8	0.2	219.7	-5.1	187.3	360121.3750	988290.8750	564757.5000	568621.6875	580266.0000
N1599991769	879654.8	32.8	0.2	219.8	-5.1	187.3	359830.3438	988291.2500	564679.1250	568546.6875	580198.0000
N1599991803	879899.6	32.9	0.2	219.8	-5.1	187.4	359395.8125	988292.8750	564601.3125	568472.3125	580132.8125
N1599991837	880144.6	32.9	0.2	219.9	-5.1	187.4	359239.1875	988296.6875	564524.1875	568397.9375	580065.6250
N1600089171	1574746.2	24.6	10.9	353.9	-5.1	335.1	409796.7188	995471.0625	608700.8125	611265.5000	618979.1250
N1600692175	863539.6	29.9	13.3	197.2	-5.0	173.4	411527.2812	987450.1250	578458.3125	581801.0625	591997.8125
N1600693135	866454.8	30.5	13.5	199.2	-5.0	174.8	403225.5938	987531.3750	575899.0000	579334.1250	589798.0000
N1601985544	1583718.1	23.1	9.4	359.7	-4.8	341.4	428856.3125	995456.5625	615024.4375	617325.3750	624283.4375
N1602676149	1474464.1	31.5	16.2	336.6	-4.6	312.6	337726.2500	995446.0000	576060.2500	579800.4375	590966.4375
N1603020971	602365.4	38.6	-42.9	122.9	-4.6	117.7	392054.3750	991993.1875	536331.9375	541034.6875	555326.9375
N1622061567	1273818.4	34.7	12.7	329.8	-1.2	297.8	307475.9375	995263.5625	559331.7500	563589.9375	576289.8125
N1809886470	529120.2	24.4	0.2	334.2	24.5	332.6	406519.8125	995231.5625	609256.0625	611633.3125	619114.9375
N1809887696	519880.6	24.4	0.2	333.3	24.5	334.5	408513.1562	995225.8750	609389.6250	611748.6250	619202.6875
N1809889231	508575.9	24.8	0.2	332.2	24.5	336.8	407476.7812	995195.9375	607820.1875	610220.6875	617838.6250

**Table 26.** Brightness estimates from clear-filter images of Rhea

Filename	Range (km)	Phase (deg)	Sub-S/C	Sub-S/C	Sub-Solar	Sub-Solar	$A_{\text{eff}}$ Value	$A_{\text{phys}}$ (km <sup>2</sup> )	$a_{\text{pred}}$	$a_{\text{pred}}$	$a_{\text{pred}}$
			Latitude (deg)	Longitude (deg)	Latitude (deg)	Longitude (deg)			k=1	k=0.75	k=0.50
N1477220185	2585475.5	39.2	-8.8	76.4	-23.6	38.3	710596.1875	1835874.0000	988102.5625	996176.2500	1022431.0000
N1481511293	2012632.4	30.2	-3.6	58.0	-23.2	34.2	829956.0000	1839455.7500	1078401.8750	1084108.8750	1102722.0000
N1484528177	500340.0	34.8	3.7	318.7	-22.9	295.5	633058.1875	1841690.8750	1033522.5000	1041154.6250	1064504.7500
N1484528732	495890.5	34.7	3.7	318.9	-22.9	296.0	638173.2500	1841716.1250	1035086.8750	1042678.6250	1065899.0000
N1486953989	2366332.0	38.6	-1.8	45.3	-22.6	11.8	684924.6875	1841255.3750	998314.5625	1006207.2500	1031875.0000
N1488892945	1774114.6	29.4	-0.2	19.2	-22.4	359.3	774522.9375	1843294.6250	1088845.6250	1094685.0000	1112966.2500
N1488919155	1561799.4	24.0	-0.2	32.8	-22.4	23.4	888326.0625	1842469.8750	1132182.8750	1136421.3750	1149809.7500
N1488924761	1510984.0	23.1	-0.2	35.5	-22.4	28.5	907498.5625	1842268.6250	1137753.1250	1141781.3750	1154478.5000
N1490556712	1439026.4	31.2	-0.3	115.6	-22.2	92.9	838673.0000	1831451.3750	1065606.7500	1071885.0000	1091575.8750
N1506067445	1617571.4	33.7	-0.3	20.0	-20.3	352.3	709971.7500	1843247.8750	1050104.1250	1057106.6250	1079044.0000
N1507666541	1323310.0	23.0	-0.3	38.5	-20.1	26.5	912171.6250	1842000.7500	1138997.2500	1142901.5000	1155362.0000
N1519429236	930992.3	25.6	-0.5	89.1	-18.5	70.5	919022.9375	1832549.1250	1113097.2500	1117936.6250	1132885.1250
N1519487727	349646.8	26.7	-0.6	104.2	-18.5	124.3	922768.8125	1832014.6250	1103717.7500	1108978.5000	1124978.0000
N1519488890	340843.5	27.8	-0.6	103.8	-18.5	125.4	917186.8125	1832031.1250	1094825.1250	1100397.7500	1117353.2500
N1524910836	482137.0	22.7	-0.5	68.9	-17.7	84.0	978184.6250	1837440.1250	1135659.7500	1139679.7500	1152080.5000
N1549134967	1157387.2	38.2	-25.9	58.2	-13.9	96.9	734157.0000	1839544.8750	998041.6875	1006379.8125	1032253.1875
N1563980740	2061641.6	30.2	0.1	75.7	-11.4	103.8	852982.0625	1835942.8750	1074858.6250	1080973.5000	1099899.1250
N1564966606	3874277.2	35.8	0.2	258.8	-11.3	293.0	599306.3125	1832107.7500	1021538.0625	1029235.3750	1053045.3750
N1571996312	1280637.1	39.0	-1.1	332.2	-10.1	294.0	580197.0625	1842836.0000	992111.1250	1001236.0000	1028442.3750
N1572812618	3224843.2	24.2	2.4	305.7	-9.9	326.6	769510.7500	1840047.3750	1128428.5000	1132512.1250	1145867.1250
N1575050814	1308812.0	36.7	11.7	200.1	-9.5	230.1	613203.8750	1828508.5000	1010011.7500	1017660.8750	1041906.9375
N1575052974	1308992.9	36.1	11.7	202.7	-9.5	232.1	598835.9375	1828644.3750	1015325.8125	1022840.6875	1046665.0625
N1575193495	1699294.5	38.1	7.5	327.4	-9.5	1.6	625056.8750	1842463.2500	1005506.5625	1013434.8750	1038804.0000
N1577055968	1891043.1	22.2	9.8	290.4	-9.2	278.8	777649.1875	1837325.3750	1139040.3750	1142991.3750	1155050.0000
N1578719119	2256377.5	32.0	19.4	356.7	-8.9	12.0	732690.8750	1843497.1250	1065291.0000	1072028.7500	1092799.3750
N1579359444	1307401.2	30.8	6.0	269.6	-8.8	242.5	663718.3750	1832773.0000	1069172.0000	1075573.7500	1095152.5000
N1580699974	2271553.0	31.0	17.2	20.7	-8.5	38.2	790116.0000	1843081.1250	1072702.2500	1079392.0000	1099518.7500
N1581733181	1814352.9	30.8	21.6	278.2	-8.4	271.0	658524.4375	1835564.5000	1069424.5000	1075745.6250	1095266.8750
N1584377879	1060806.4	29.8	20.5	198.6	-7.9	189.2	737336.1250	1828964.2500	1073445.7500	1079598.0000	1098386.3750
N1585993691	1182167.6	38.5	2.2	276.4	-7.6	239.0	569937.4375	1834005.0000	993575.9375	1002031.6250	1028118.3125
N1587591022	1335788.0	39.3	-5.3	311.2	-7.3	271.7	568271.6875	1840807.1250	985639.8750	994257.0625	1021135.8750
N1587763884	1638259.0	24.4	13.7	58.2	-7.3	70.8	940582.2500	1839416.0000	1123590.3750	1128307.6250	1142481.3750
N1589214934	1479138.0	24.5	-7.9	353.6	-7.0	328.8	803413.2500	1843603.3750	1128964.5000	1133797.2500	1148070.6250
N1589414375	888519.9	30.8	23.7	150.3	-7.0	152.6	816640.8750	1829801.1250	1065728.7500	1072144.1250	1091771.6250
N1590791985	1757924.8	22.1	11.0	356.1	-6.8	342.8	844432.4375	1843602.2500	1147035.6250	1151024.3750	1163079.1250
N1591136687	1180182.6	39.9	-16.3	340.3	-6.7	300.7	577697.0000	1843140.6250	982936.0000	992370.5000	1020340.1875
N1592676958	1475150.1	38.4	15.9	312.3	-6.4	280.8	578492.5000	1840888.8750	995659.7500	1004319.2500	1030793.5625
N1594711972	497295.6	31.5	24.6	349.6	-6.1	356.9	731800.1875	1843304.6250	1070502.2500	1077030.1250	1097261.0000
N1597403261	1639217.0	27.8	-4.5	346.1	-5.6	318.2	739408.7500	1843467.5000	1101968.3750	1107869.2500	1125170.3750
N1598020836	601914.4	33.2	-17.0	199.3	-5.5	167.5	722057.3750	1828749.1250	1043090.1875	1050121.5000	1071751.2500
N1599496066	1179576.1	29.1	20.7	74.2	-5.2	87.5	867652.3125	1836816.1250	1084632.5000	1090483.1250	1108524.6250
N1599963463	634820.9	22.4	-7.4	180.9	-5.1	158.5	909405.4375	1827837.2500	1133118.1250	1136989.1250	1149011.0000
N1599964315	636131.7	22.9	-7.2	182.3	-5.1	159.3	897560.2500	1827836.1250	1129066.6250	1130989.1250	1145608.8750
N1599965167	637598.3	23.5	-6.9	183.6	-5.1	160.1	886272.3125	1827839.0000	1124933.5000	1129127.0000	1142130.2500
N1599966019	639220.2	24.1	-6.7	185.0	-5.1	160.8	874932.4375	1827849.0000	1120725.2500	1125081.7500	1138580.0000
N1599966871	640996.9	24.6	-6.4	186.3	-5.1	161.6	862931.3125	1827865.0000	1116448.1250	1120968.7500	1134965.1250
N1599967723	642927.2	25.2	-6.2	187.7	-5.1	162.4	853110.0000	1827884.8750	1112108.2500	1116793.2500	1131289.2500
N1599968575	645010.4	25.7	-5.9	189.1	-5.1	163.2	841671.1875	1827908.7500	1107712.6250	1112562.1250	1127556.6250
N1599969427	647245.1	26.3	-5.7	190.4	-5.1	164.0	830940.5000	1827939.5000	1103267.5000	1108281.6250	1123774.8750
N1599970279	649630.2	26.8	-5.4	191.7	-5.1	164.8	820494.5625	1827974.7500	1098779.7500	1103957.8750	1119948.3750
N1599971131	652164.2	27.4	-5.2	193.1	-5.1	165.6	810749.7500	1828014.1250	1094256.1250	1099597.5000	1116081.7500
N1599971983	654845.6	27.9	-4.9	194.4	-5.1	166.4	800540.1875	1828056.8750	1089703.1250	1095206.6250	1112181.2500
N1599972835	657672.8	28.5	-4.6	195.7	-5.1	167.1	790114.2500	1828105.8750	1085127.7500	1090792.2500	1108254.3750
N1599973687	660643.9	29.0	-4.4	197.0	-5.1	167.9	781185.4375	1828158.8750	1080536.2500	1086360.1250	1104303.3750
N1599974539	663757.1	29.5	-4.1	198.3	-5.1	168.7	769708.6875	1828215.0000	1075935.3750	1081917.1250	1100338.1250

Table 26 continued on next page

**Table 26** (*continued*)

Filename	Range	Phase	Sub-S/C	Sub-S/C	Sub-Solar	Sub-Solar	$A_{\text{eff}}$	$A_{\text{phys}}$	$a_{\text{pred}}$	$a_{\text{pred}}$	$a_{\text{pred}}$
	(km)	(deg)	Latitude	Longitude	Latitude	Longitude	Value		k=1	k=0.75	k=0.50
			(deg)	(deg)	(deg)	(deg)	(km <sup>2</sup> )				
N1599975391	667010.4	30.1	-3.9	199.6	-5.1	169.5	761611.6250	1828274.0000	1071331.5000	1077468.8750	1096360.0000
N1599976243	670401.9	30.6	-3.7	200.9	-5.1	170.3	751732.0625	1828338.0000	1066730.7500	1073021.7500	1092376.2500
N1599977095	673929.1	31.1	-3.4	202.2	-5.1	171.1	742521.3125	1828405.3750	1062139.1250	1068581.6250	1088393.8750
N1599977947	677590.1	31.6	-3.2	203.5	-5.1	171.9	732781.2500	1828475.1250	1057562.6250	1064153.8750	1084415.2500
N1599978799	681382.4	32.1	-2.9	204.8	-5.1	172.7	724024.6250	1828546.8750	1053007.1250	1059744.1250	1080445.5000
N1599979651	685303.6	32.6	-2.7	206.0	-5.1	173.4	714167.8125	1828622.5000	1048477.8125	1055358.6250	1076494.3750
N1599980503	689351.4	33.1	-2.5	207.3	-5.1	174.2	706533.6875	1828700.7500	1043980.1875	1051001.3750	1072560.5000
N1599981355	693523.1	33.5	-2.2	208.5	-5.1	175.0	698256.6875	1828780.3750	1039519.0625	1046677.4375	1068650.5000
N1599982207	697816.4	34.0	-2.0	209.7	-5.1	175.8	689402.7500	1828861.5000	1035099.3750	1042392.1875	1064770.5000
N1599983059	702228.5	34.4	-1.8	210.9	-5.1	176.6	682581.5000	1828945.1250	1030725.5625	1038149.5000	1060923.7500
N1599983911	706756.9	34.9	-1.5	212.2	-5.1	177.4	674640.0625	1829030.3750	1026401.9375	1033953.6250	1057113.5000
N1600090251	1484399.2	39.8	11.6	311.9	-5.1	275.6	565007.1250	1840858.5000	980168.4375	989051.5625	1016539.5000
N1603337413	1494478.4	23.2	18.6	28.8	-4.5	29.2	910338.1250	1842614.6250	1137894.5000	1142125.6250	1155046.3750
N1609569538	1425852.8	30.9	27.4	12.5	-3.4	15.0	768404.9375	1843205.0000	1075468.8750	1081894.5000	1101677.3750
N1610257504	1572974.6	38.1	6.4	326.3	-3.3	289.5	585658.8125	1842384.6250	1000578.5625	1009460.4375	1035964.8750
N1614797855	682792.8	29.0	16.7	177.5	-2.5	155.4	814970.5000	1828275.6250	1080486.0000	1086269.1250	1104199.5000
N1698203622	2693550.5	35.1	0.2	340.6	11.7	14.0	690165.1875	1843300.3750	1035975.6875	1043396.7500	1066575.6250
N1757514327	1565262.2	23.5	25.9	1.7	19.7	337.1	842704.7500	1843388.7500	1137337.3750	1141736.5000	1154959.1250
N1843190429	2157225.8	31.9	42.0	160.5	26.2	126.6	823925.3750	1831448.3750	1057577.1250	1064155.6250	1084617.0000

**Table 27.** Brightness estimates from color images of Aegaeon

Filename	Filter	Range	Phase	Sub-S/C	Sub-S/C	Sub-Solar	Sub-Solar	$A_{\text{eff}}$	$A_{\text{phys}}$	$a_{\text{pred}}$	$a_{\text{pred}}$	$a_{\text{pred}}$
		(km)	(deg)	Latitude	Longitude	Latitude	Longitude	Value		k=1	k=0.75	k=0.50
				(deg)	(deg)	(deg)	(deg)	(km <sup>2</sup> )				
N1643264167	CLR	14546.9	73.3	74.0	168.5	2.6	140.8	0.01090	0.5320	0.1032	0.1189	0.1437
N1643264273	CLR	14875.4	70.5	71.5	165.2	2.6	141.3	0.03011	0.5259	0.1053	0.1212	0.1461
N1643264379	CLR	15235.6	67.9	69.0	162.9	2.6	141.8	0.01150	0.5193	0.1071	0.1230	0.1479
N1643264504	CLR	15694.0	65.0	66.2	161.1	2.6	142.5	0.00276	0.5110	0.1088	0.1247	0.1494
N1643264609	RED	16121.3	62.6	63.9	160.1	2.6	143.0	0.01380	0.5034	0.1099	0.1257	0.1501
N1643264664	GRN	16352.0	61.4	62.7	159.6	2.6	143.3	0.01555	0.4994	0.1103	0.1260	0.1503
N1643264720	BL1	16590.4	60.2	61.6	159.3	2.6	143.6	0.01085	0.4953	0.1107	0.1263	0.1504
N1643264798	UV3	16902.0	58.8	60.2	158.9	2.6	144.0	0.00929	0.4901	0.1110	0.1265	0.1503
N1643264854	IR3	17195.7	57.5	59.0	158.7	2.6	144.3	0.01505	0.4853	0.1113	0.1266	0.1502
N1643264914	CLR	17482.6	56.4	57.9	158.5	2.6	144.6	0.01383	0.4807	0.1114	0.1266	0.1499
N1643265020	CLR	17998.3	54.4	56.0	158.3	2.6	145.2	0.01268	0.4727	0.1115	0.1264	0.1492
N1643265126	CLR	18532.2	52.6	54.2	158.2	2.6	145.7	0.01539	0.4648	0.1114	0.1260	0.1482
N1643265251	CLR	19177.2	50.6	52.2	158.2	2.6	146.3	0.00332	0.4556	0.1110	0.1252	0.1468
N1643265356	RED	19753.3	49.0	50.6	158.3	2.6	146.9	0.01544	0.4477	0.1105	0.1244	0.1454
N1643265411	GRN	20056.3	48.2	49.8	158.3	2.6	147.2	0.01478	0.4438	0.1102	0.1239	0.1446
N1643265467	BL1	20364.5	47.4	49.0	158.4	2.6	147.5	0.01311	0.4398	0.1098	0.1234	0.1437
N1643265545	UV3	20760.8	46.4	48.1	158.5	2.6	147.8	0.00951	0.4348	0.1094	0.1227	0.1426
N1643265601	IR3	21128.4	45.6	47.2	158.7	2.6	148.1	0.01748	0.4303	0.1089	0.1220	0.1415

**Table 28.** Brightness estimates from color images of Methone

Filename	Filter	Range (km)	Phase (deg)	Sub-S/C	Sub-S/C	Sub-Solar	Sub-Solar	$A_{\text{eff}}$	$A_{\text{phys}}$	$a_{\text{pred}}$	$a_{\text{pred}}$	$a_{\text{pred}}$
				Latitude	Longitude	Latitude	Longitude	Value		$k=1$	$k=0.75$	$k=0.50$
				(deg)	(deg)	(deg)	(deg)	(deg)	(km $^2$ )	(km $^2$ )	(km $^2$ )	(km $^2$ )
N1716192103	CLR	4454.4	63.1	-15.6	130.2	14.4	74.0	1.53738	6.5733	3.1004	3.0766	3.1407
N1716192136	UV3	4604.6	62.3	-15.1	129.6	14.4	74.2	1.33006	6.5866	3.1460	3.1221	3.1853
N1716192191	GRN	4868.9	60.9	-14.2	128.8	14.4	74.4	1.61003	6.6073	3.2183	3.1941	3.2558
N1716192224	IR1	5026.2	60.2	-13.7	128.3	14.4	74.5	1.69522	6.6183	3.2571	3.2328	3.2935
N1716192257	IR3	5181.9	59.5	-13.3	127.9	14.4	74.7	1.69304	6.6282	3.2928	3.2682	3.3281
N1716192290	CLR	5343.4	58.9	-12.9	127.5	14.4	74.8	1.72429	6.6377	3.3273	3.3025	3.3614
N1716192323	BL1	5500.6	58.3	-12.5	127.2	14.4	75.0	1.69781	6.6461	3.3585	3.3335	3.3915
N1716192356	RED	5662.6	57.7	-12.1	126.9	14.4	75.1	1.76546	6.6540	3.3885	3.3632	3.4203
N1716192389	IR2	5822.3	57.2	-11.7	126.6	14.4	75.2	1.81560	6.6611	3.4162	3.3907	3.4468
N1716192437	IR4	6033.7	56.5	-11.3	126.2	14.4	75.4	1.65345	6.6697	3.4502	3.4243	3.4792
N1716193897	UV3	13398.4	47.2	-4.7	124.9	14.4	81.4	1.83983	6.6747	3.8671	3.8182	3.8353
N1716193952	GRN	13682.8	47.0	-4.6	125.1	14.4	81.7	2.14004	6.6697	3.8706	3.8207	3.8364
N1716193985	IR1	13851.1	46.9	-4.5	125.1	14.4	81.8	2.21760	6.6667	3.8725	3.8219	3.8369
N1716194018	IR3	14016.6	46.9	-4.4	125.2	14.4	81.9	2.16507	6.6636	3.8742	3.8230	3.8372